Advances in Clinical and Experimental Medicine

MONTHLY ISSN 1899-5276 (PRINT) ISSN 2451-2680 (ONLINE) www.advances.umed.wroc.pl

2018, Vol. 27, No. 11 (November)

Impact Factor (IF) – 1.262
Ministry of Science and Higher Education – 15 pts.
Index Copernicus (ICV) – 155.19 pts.

Wroclaw Medical University

Advances
in Clinical and Experimental Medicine

ISSN 1899-5276 (PRINT) ISSN 2451-2680 (ONLINE) www.advances.umed.wroc.pl

MONTHLY 2018
Vol. 27, No. 11
(November)

Advances in Clinical and Experimental Medicine is a peer-reviewed open access journal published by Wroclaw Medical University. Its abbreviated title is Adv Clin Exp Med. Journal publishes original papers and reviews encompassing all aspects of medicine, including molecular biology, biochemistry, genetics, biotechnology, and other areas. It is published monthly, one volume per year.

Editorial Office
ul. Marcinkowskiego 2–6
50-368 Wrocław, Poland
Tel.: +48 71 784 12 05
E-mail: redakcja@umed.wroc.pl

Publisher
Wroclaw Medical University
Wybrzeże L. Pasteura 1
50-367 Wrocław, Poland

Online edition is the original version of the journal

Editorial Policy

Advances in Clinical and Experimental Medicine (Adv Clin Exp Med) is an independent multidisciplinary forum for exchange of scientific and clinical information, publishing original research and news encompassing all aspects of medicine, including molecular biology, biochemistry, genetics, biotechnology and other areas. During the review process, the Editorial Board conforms to the "Uniform Requirements for Manuscripts Submitted to Biomedical Journals: Writing and Editing for Biomedical Publication" approved by the International Committee of Medical Journal Editors (www.ICMJE.org/). The journal publishes (in English only) original papers and reviews. Short works considered original, novel and significant are given priority. Experimental studies must include a statement that the experimental protocol and informed consent procedure were in compliance with the Helsinki Convention and were approved by an ethics committee.

For all subscription-related queries please contact our Editorial Office:
redakcja@umed.wroc.pl

For more information visit the journal's website:
www.advances.umed.wroc.pl

Pursuant to the ordinance No. 134/XV R/2017 of the Rector of Wroclaw Medical University (as of December 28, 2017) from January 1, 2018 authors are required to pay a fee amounting to 700 euros for each manuscript accepted for publication in the journal Advances in Clinical and Experimental Medicine.

„Podniesienie poziomu naukowego i poziomu umiędzynarodowienia wydawanych czasopism naukowych oraz upowszechniania informacji o wynikach badań naukowych lub prac rozwojowych – zadanie finansowane w ramach umowy 784/p-DUN/2017 ze środków Ministra Nauki i Szkolnictwa Wyższego przeznaczonych na działalność upowszechniającą naukę".

Indexed in: MEDLINE, Science Citation Index Expanded, Journal Citation Reports/Science Edition, Scopus,
EMBASE/Excerpta Medica, Ulrich's™ International Periodicals Directory, Index Copernicus

Typographic design: Monika Kolęda, Piotr Gil
DTP: Wydawnictwo UMW, TYPOGRAF
Cover: Monika Kolęda
Printing and binding: EXDRUK

Advances
in Clinical and Experimental Medicine

MONTHLY 2018, Vol. 27, No. 11 (November)

ISSN 1899-5276 (PRINT)
ISSN 2451-2680 (ONLINE)
www.advances.umed.wroc.pl

Contents

Original papers

Comparative proteomics analysis of myocardium in mouse model of diabetic cardiomyopathy using the iTRAQ technique

Mingfeng Shao[B,D,F], Jing Chen[C,D,F], Suxia Zheng[A,D–F]

Department of Cardiology, Linyi People's Hospital, China

A – research concept and design; B – collection and/or assembly of data; C – data analysis and interpretation;
D – writing the article; E – critical revision of the article; F – final approval of the article

Advances in Clinical and Experimental Medicine, ISSN 1899-5276 (print), ISSN 2451-2680 (online) *Adv Clin Exp Med*. 2018;27(11):1469–1475

Address for correspondence
Suxia Zheng
E-mail: zhengsuxia110@126.com

Funding sources
None declared

Conflict of interest
None declared

Received on March 15, 2017
Reviewed on May 17, 2017
Accepted on June 7, 2017

Abstract

Background. Diabetic cardiomyopathy (DCM) is one of the most harmful diseases with high morbidity and mortality rates. However, the underlying pathological mechanism of the disorder still remains unclear.

Objectives. The purpose of our study was to identify differentially expressed proteins associated with DCM.

Material and methods. C57BLKS/J db/db (diabetes mellitus group – DM group) and db/m mice (normal control group – NC group) were acclimated in cages for 15 weeks. The general state was recorded. After 15 weeks, the heart tissues were used for histological examination. In addition, quantitative mass spectrometry using isobaric tags for relative and absolute quantitation (iTRAQ) was used to identify differentially expressed proteins in the heart tissues. SEQUEST software was used to identify proteins with data derived from liquid chromatography-tandem mass spectrometry (LC-MS/MS) spectra by searching ipi.MOUSE.v3.72.REVERSED.fasta database. Expert Protein Analysis System (ExPASy) was used to calculate the theoretical parameters. One upregulated protein (sorbin and SH3 domain containing 2 – Sorbs2) and 1 downregulated protein (myosin-3) was measured by western blot to validate the iTRAQ data.

Results. The mice in the NC group were active and grew well, while the mice in the DM group presented with obvious polydipsia, polyphagia and polyuria. The results of histological examination revealed that, compared to the NC group, the DM group showed significant myocardial hypertrophy and myofiber disarray accompanied by damaged nuclei. A total of 73 differentially expressed proteins were identified, including 44 upregulated and 29 downregulated proteins. Western blot analysis confirmed that the expression of Sorbs2 was significantly increased ($p < 0.01$), while the expression of myosin-3 was statistically decreased in the DM group compared to the NC group ($p < 0.05$).

Conclusions. These results suggest that DCM shows differences in its proteomics compared to normal controls. Our quantitative proteomic analysis may provide a new insight into the distinct molecular profile of DCM.

Key words: proteomics, diabetic cardiomyopathy, isobaric tag for relative and absolute quantitation

DOI
10.17219/acem/74539

Introduction

The number of patients with diabetes mellitus (DM) has been increasing worldwide at an alarming pace for the past 2 decades. These patients are predisposed to serious cardiovascular complications, including heart failure (HF), causing mortality and morbidity.[1] The development of diabetic cardiomyopathy (DCM) is a prominent contributing factor to HF.[2] The term DCM was first introduced by Rubler et al., and it is characterized by adverse structural and functional changes in the myocardium and coronary vasculature in the absence of coronary artery disease (CAD) and hypertension.[2–4] Among the diabetic population, the prevalence of DCM has been estimated between 30% and 60%.[5,6] Although remarkable progress has been made in recent years in the diagnosis and treatment of DCM, at present, there is no specific therapy for myocardial damage induced by DCM due to the unclear molecular etiologies. Therefore, it is urgent to understand the underlying pathological mechanism of DCM and then further improve the treatment strategy.

Many potential mechanisms have been proposed and studied, and the development and progression of DCM is involved in cellular and molecular perturbations.[7] It has been reported that fibrosis, inflammation, apoptotic and necrotic cell death, the activation of renin-angiotensin--aldosterone system (RAAS), increased fatty acid (FA) utilization, lipotoxicity, autophagy, and oxidative stress are the most important contributors to the onset and progression of DCM.[8–15] To gain new insights into the molecular mechanisms involved in the development and progression of DCM, we have performed proteomic profiling analysis of heart tissue samples from diabetic mice and normal mice to identify the differentially expressed proteins altered in diabetic hearts. Our proteomic profiling study suggests that heart tissue samples from diabetic mice exhibit significant differences in proteomics compared to normal controls. Our study might provide a new insight into the distinct molecular profile of DCM.

Material and methods

Animal testing

Seven-week-old male C57BLKS/J db/db mice (n = 8) and nondiabetic db/m littermates (n = 8) were purchased from the Model Animal Research Center of Nanjing University (China). All mice were housed in independent plastic cages in an air-conditioned room (room temperature 22–24°C, room humidity 50–60%) under a 12-hour light/12-hour dark cycle. They all received laboratory pellet chow and tap water ad libitum. All animal experimental protocols were performed according to the Principles of Laboratory Animal Care provided by the National Institutes of Health (NIH; Bethesda, USA) and approved by the Animal Ethics Committee at our University.

All animals were acclimated in the cages for 15 weeks before being euthanized. C57BLKS/J db/db mice were used as a DM group, while db/m mice were used as a normal control (NC) group. All the animals were weighed each week and the general state was recorded. Following 15 weeks of feeding, all mice were sacrificed and their hearts were immediately dissected. Heart tissue samples were fixed with 10% formalin for histological examination, or washed with normal saline (NS), and then they were kept at –80°C until further analysis.

Histological examination

For the histological examination, the tissue samples from both the DM and NC group were fixed with 10% formalin and embedded in paraffin, and 4-millimeter-thick sections were prepared. The sections were then stained with hematoxylin-eosin (H&E) and examined by light microscopy (Axioskop 40; Zeiss, Oberkochen, Germany).

Isobaric tags for relative and absolute quantitation proteomic analysis

The tissue samples (50 mg) from both the DM and NC group were prepared, homogenized in liquid nitrogen and lysed with 500 µL buffer containing 4% sodium dodecyl sulfonate (SDS), 100 mM dithiothreitol (DTT) and 150 mM Tris HCl. Then, the tissues were ultrasonically agitated and centrifuged. Total protein was extracted from the myocardium. Thereafter, the proteins were digested with trypsin, using the filter aided proteome preparation (FASP) protocol.[16] DNA concentration was measured using a NanoDrop 2000 spectrophotometer (Thermo Scientific, Waltham, USA). A total of 100 µg of peptides from each group were labeled with isobaric tags for relative and absolute quantitation (iTRAQ) reagents (Applied Biosystems, Foster City, USA) according to the manufacturer's instructions. Extracts from the NC group were labeled with reagent 114 and the ones from the DM group with reagent 117. Afterwards, the labeled samples were centrifuged at 1000 rpm for 30 s and incubated at room temperature for 1 h. Then, the samples were separated into 10 fractions, using Poly-Sulfoethyl A strong cation-exchange (SCX) columns (Poly LC, Murietta, USA).

Database search and bioinformatics analysis of differentially expressed proteins

Mass spectrometric analysis was carried out using a liquid chromatography-tandem mass spectrometry (LC-MS/MS) (Agilent Technologies, Palo Alto, USA) and an LTQ-Velos ion trap mass spectrometer (Thermo Finnigan Corp., San Jose, USA).[17] Protein searching was performed in the database of ipi.MOUSE.v3.72.REVERSED.fasta. and the filtration parameter in SEQUEST-HT (Proteome Discoverer 1.4 package; Thermo Scientific, Rockford, USA) was false

discovery rate (FDR) ≤0.01. Expert Protein Analysis System (ExPASy) (http://www.expasy.org) was used to calculate the molecular weight and isoelectric point (PI).

Western blotting analysis

After the protein concentrations had been determined, equal amounts of total protein were separated by SDS–polyacrylamide gel electrophoresis (PAGE) and transferred onto polyvinylidene difluoride membranes (PVDF; Bio-Rad, Chicago, USA). The membranes were then blocked with 5% nonfat dry milk in Tris-buffered saline-Tween (TBST) and probed with antibodies against sorbin and SH3 domain containing 2 (Sorbs2) (ab213616; Abcam Inc., Cambridge, USA), myosin-3 (Sigma-Aldrich, St. Louis, USA) or glyceraldehyde 3-phosphate dehydrogenase (GAPDH) (ab8245; Abcam Inc.) overnight at 4°C. Subsequently, the membranes were incubated with horseradish peroxidase (HRP)-conjugated secondary antibodies (Abcam Inc.) for 2 h and visualized by enhanced chemiluminescence (ECL; Thermo Scientific).

Statistical analysis

The data is presented as the mean ± standard deviation (SD). Student's t-test or one-way analysis of variance (ANOVA) was used to compare differences between the groups. Statistical analyses were performed using SPSS v. 19.0 (SPSS Inc., Chicago, USA). A p-value <0.05 was considered statistically significant.

Results

General observations

During the observation period, mice in the NC group were active, grew well, presented good mental condition, and had bright and smooth hair coat. On the other hand, mice in the DM group showed dull and shaggy hair coat, were less active, presented obvious polydipsia, polyphagia and polyuria, and gained substantially more weight than mice in the control group.

Histological observations

After the observation period, mice from both groups were sacrificed and their hearts were collected for histological examination. As indicated in Fig. 1A and 1B, we found that, compared to the NC group, the DM group showed significant myocardial hypertrophy and myofiber disarray accompanied by damaged nuclei.

iTRAQ proteomics profiling

We analyzed the myocardial protein profile of db/db and db/m mice using the iTRAQ approach. The myocardial protein from the NC group was labeled with reagent 114, which was considered as a control. The myocardial protein from the DM group was labeled with reagent 117. Frequency distribution histogram was constructed to analyze iTRAQ quantitative data. The ratio of each label was built by evaluating the logarithm (Log2). The group distance was set at 0.6, and the distribution ranged from –4.5 to 4.5. As shown in Fig. 2, we observed that the ratio was close to 1. This data was in line with the normal distribution, indicating the data was reliable.

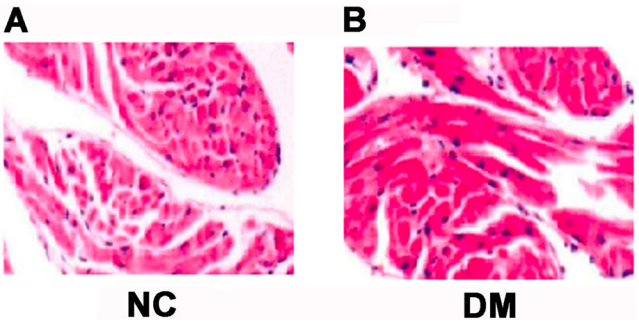

Fig. 1. Histological observation in 2 groups. After 10 weeks of feeding, heart tissue samples were obtained for histological examination. Compared to the NC group (A), the DM group (B) showed significant myocardial hypertrophy and myofiber disarray accompanied by damaged nuclei

NC – normal control; DM – diabetes mellitus.

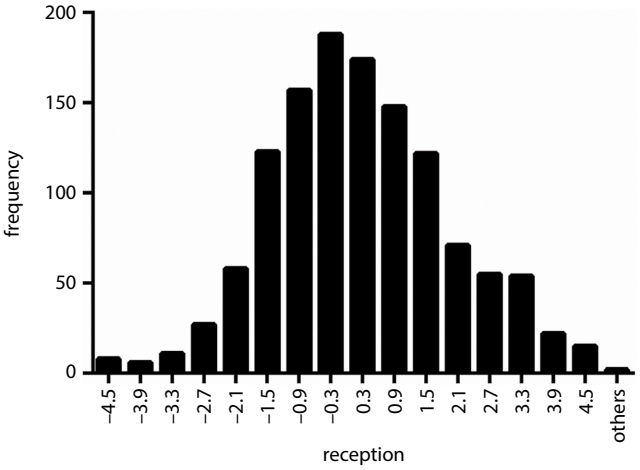

Fig. 2. Frequency distribution histogram of iTRAQ proteomics profiling. Frequency distribution histogram was constructed to analyze iTRAQ quantitative data. We found that the ratio was close to 1, indicating that the data was reliable

iTRAQ – isobaric tags for relative and absolute quantitation.

Mass spectrometric analysis

A total of 427 proteins were quantified by performing the iTRAQ-based experiments. Of these, 73 proteins were differentially expressed proteins (44 upregulated and 29 downregulated) in the DM group compared to the NC group (Fig. 3). After searching the ipi.MOUSE.v3.72.

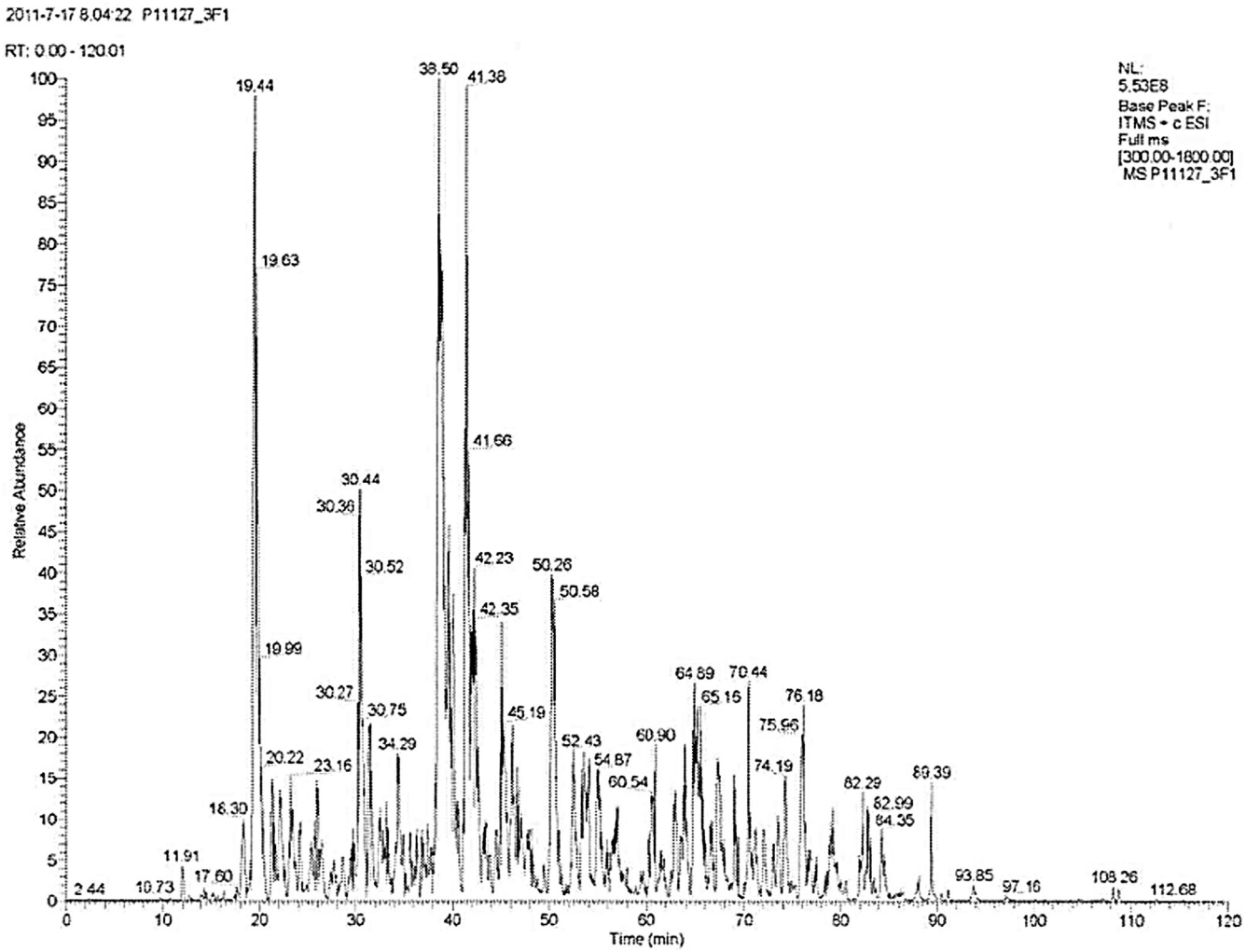

Fig. 3. Mass spectrometric analysis. A total of 73 differentially expressed proteins were identified (44 upregulated and 29 downregulated) in the DM group compared to the NC group

NC – normal control; DM – diabetes mellitus.

Table 1. Some of the differentially expressed proteins in 2 studied groups

Accession No.	Protein name	Molecular weight [Da]	PI	Protein expression rate (DM/NC)
IP100956780	sorbin and SH3 domain containing 2	78,155.37	9.42	19.67
IPI00880521	solute carrier family 13	14,485.73	6.62	15.33
IPI00128152	multidrug resistance protein	140,993.72	8.51	7.45
IP100885610	secretory carrier-associated membrane protein 3	38,458.31	7.55	5.78
IPI00131334	canon channel sperm-associated protein	78,705.89	6.80	5.53
IP100380895	myosin-3	223,791.03	5.62	0.19
IPI00323035	fibulin-5	50,193.55	4.55	0.29
IPI00130102	desmin	53,497.99	5.21	0.30
IPI04775849	alpha-actinin	59,897.83	5.69	0.35
1PI00116668	integrin-linked protein kinase	51,373.15	8.30	0.18

NC – normal control; DM – diabetes mellitus.

REVERSED.fasta. database and analyzing by SEQUEST-HT the information about proteins was identified. The top--ranked 5 most obviously increased and decreased expression rates were summarized in Table 1.

Validation of iTRAQ data

To validate the differentially expressed proteins identified by iTRAQ data, we selected 2 proteins for western blot analysis. We chose the highest protein expression rate

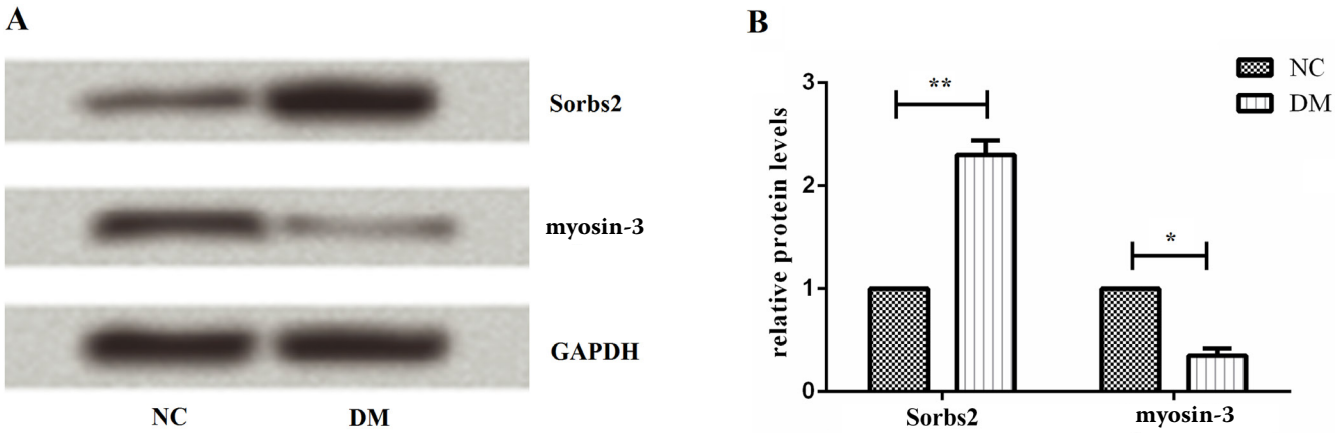

Fig. 4. Validation of iTRAQ data. We selected 2 proteins, Sorbs2 and myosin-3, to validate the differentially expressed proteins identified by iTRAQ data, using western blot analysis. Representative pictures of western blot (A) and quantitative analysis (B) showed that Sorbs2 was significantly increased in the DM group (p = 0.003), whereas myosin-3 was statistically decreased in the DM group compared to the NC group (p = 0.026). Data was shown as mean ±SD

iTRAQ – isobaric tags for relative and absolute quantitation; NC – normal control; DM – diabetes mellitus; Sorbs2 – sorbin and SH3 domain containing 2; GAPDH – glyceraldehyde 3-phosphate dehydrogenase; SD – standard deviation.

of upregulated and downregulated proteins, Sorbs2 and myosin-3. As shown in Fig. 4A, Sorbs2 was found to be significantly increased in the DM group (p = 0.003), whereas myosin-3 was statistically decreased in the DM group compared to the NC group (p = 0.026). Quantitative analysis showed the same results, which indicates that the results of iTRAQ data were reliable (Fig. 4B).

Discussion

In the present study, we used iTRAQ, a recently developed protein quantitation technique, combined with LC-MS/MS, to identify the protein profiles of the myocardium from both DM and normal heart tissues. We found that DCM shows different proteomics compared to normal individuals. Also, a total of 73 differentially expressed proteins (44 upregulated and 29 downregulated) were identified. In addition, we performed western blot to validate the results by measuring 2 reprehensive proteins.

Diabetic cardiomyopathy is a well-known specific cardiomyopathy which develops in patients with diabetes without coronary atherosclerosis and hypertension. It induces changes in cardiac structure/function, leading to significant clinical consequences, such as progressive HF and even cardiovascular death.[18] A prominent characteristic of the DCM is cardiac hypertrophy, which shows increased left ventricular (LV) mass and wall thickness accompanied by compromised systolic and diastolic function.[19,20] Numerous molecular mechanisms have been proposed to be responsible for the development of DCM.[21] For example, elevated FA utilization and lipotoxicity may contribute to mitochondrial dysfunction. Mitochondrial dysfunction and endoplasmic reticulum (ER) stress may promote apoptosis. In addition, oxidative stress, altered myocardial insulin signaling, increased advanced glycation end products (AGEs) signaling, impaired Ca^{2+} handling, and inflammation may accelerate increased pro-fibrotic genes expression or promote apoptosis. It is well-known that accurate and absolute protein quantification plays a critical role in better understanding the basic biological responses as well as revealing valuable biomarkers for the diagnosis, treatment and predicting the prognosis of diverse diseases.[22] In the last decades, protein quantification has become an important and significant component of modern MS-based proteomic research.[23,24] A number of quantification strategies have been developed and successfully applied. However, most of them are dependent on the incorporation of stable isotopes for the following MS sorting and quantification.[25,26] The recently established iTRAQ technique has been widely used as a comprehensive and efficient MS-based proteomic research tool for multiplexed protein quantification.[27,28] Isobaric tags for relative and absolute quantitation could compare the protein abundance by measuring the peak intensities of reporter ions released from iTRAQ-tagged peptides.[29] Hence, iTRAQ could be a potential method for studying quantitative proteomics.

In the present study, we used C57BLKS/J db/db mice and nondiabetic db/m littermates. Db/db mice are a well-characterized and widely used type 2 diabetic mouse model, which can show diabetic symptoms, such as hyperglycemia, obesity, insulin resistance (IR), and renal damage, occurring after 10–20 weeks of sustained hyperglycemia.[30] During the 15 weeks of feeding, we found that db/db mice gradually increased their water and food intake, indicative of developing diabetes. After 15 weeks of observation, the heart tissues were harvested to confirm the pathologic changes by using histological examination. As expected, significant myocardial hypertrophy and myofiber disarray accompanied by damaged nuclei were observed in db/db mice compared to the db/m mice, confirming myocardial damage. Thereafter, the proteomics of the myocardium

was quantitatively analyzed in both db/db mice and db/m mice, using the iTRAQ technique, to reveal differentially expressed proteins in the 2 groups. As a result, a total of 73 differentially expressed proteins – 44 upregulated and 29 downregulated – were identified. Some of the up- and downregulated proteins were shown in Table 1. Among them, we determined the expression of Sorbs2 and myosin-3 to confirm the reliability of iTRAQ. Sorbs2, also known as ArgBP2, is a protein encoded by the *Sorbs2* gene in humans.[31] It belongs to a small family of adaptor proteins having sorbin homology domains; Sorbs2 is highly expressed in cardiac muscle cells at sarcomeric Z-disc structures, as well as in other cells at actin stress fibers and the nucleus.[31,32] Sorbs2 is considered an adapter protein that plays a significant role in cytoskeletal organization, cell adhesion and signaling pathways.[33] A proteomic analysis of cardiac tissues from patients has suggested that Sorbs2 is released from injured cardiac tissue into the bloodstream upon lethal acute myocardial infarction (AMI).[34] An animal experiment also revealed that Sorbs2 was increased in the damaged heart tissues.[35] Similarly, our study found that Sorbs2 was highly expressed in the myocardium of db/db mice, implying a destroyed structure of the myocardium. Myosin is a ubiquitous eukaryotic contractile protein which converts chemical energy into mechanical energy by means of hydrolysis of adenosine triphosphate (ATP). Cardiac myosin has been reported to be changed in DM.[36,37] Myosin-3 is a protein that is encoded by the *MYH3* gene in humans.[38] Myosin-3 is a component of the signaling complex, which is required for the adaptation response, and functions as a plus-end directed motor.[39,40] However, no information is available on myosin-3 tissue expression. We first observed that myosin-3 is downregulated in DM compared to normal individuals. Thus, Sorbs2 and myosin-3 might serve as potential protein therapeutic targets for DCM. Still, the functions of other identified candidates, such as the solute carrier family 13 and integrin-linked protein kinase, remain to be further elucidated.

The novelty of this study lies in revealing a new insight into the molecular profile of DCM by using iTRAQ; part of the results was also confirmed by western blot. However, there are limitations of this study, which needs further development. Firstly, although we performed western blot to confirm our results, other experiments such as immunohistochemistry (IHC) or polymerase chain reaction (PCR) should be performed. Secondly, we only selected Sorbs2 and myosin-3 as testing factors in our study. Moreover, the potential mechanisms should be explored. Thirdly, the mouse model of DCM was used in the current study; human studies should also be conducted to verify the results of animal experiments.

In conclusion, the present study suggests that DCM shows protein differences in proteomics by the application of iTRAQ. The quantitative proteomic analysis might provide a new insight into the distinct molecular profile of DCM.

References

1. Danaei G, Finucane MM, Lu Y, et al. Global Burden of Metabolic Risk Factors of Chronic Diseases Collaborating Group (Blood Glucose). National, regional, and global trends in fasting plasma glucose and diabetes prevalence since 1980: Systematic analysis of health examination surveys and epidemiological studies with 370 country-years and 2.7 million participants. *Lancet*. 2011;378(9785):31–40.
2. Rubler S, Dlugash J, Yuceoglu YZ, Kumral T, Branwood AW, Grishman A. New type of cardiomyopathy associated with diabetic glomerulosclerosis. *Am J Cardiol*. 1972;30(6):595–602.
3. Boyer JK, Thanigaraj S, Schechtman KB, Pérez JE. Prevalence of ventricular diastolic dysfunction in asymptomatic, normotensive patients with diabetes mellitus. *Am J Cardiol*. 2004;93(7):870–875.
4. Mahgoub MA, Abd-Elfattah AS. Diabetes mellitus and cardiac function. *Mol Cell Biochem*. 1998;180(1–2):59–64.
5. Bonito PD, Cuomo S, Moio N, et al. Diastolic dysfunction in patients with non-insulin-dependent diabetes mellitus of short duration. *Diabet Med*. 1996;13(4):321–324.
6. Nicolino A, Longobardi G, Furgi G, et al. Left ventricular diastolic filling in diabetes mellitus with and without hypertension. *Am J Hypertens*. 1995;8(4 Pt 1):382–389.
7. Falcão-Pires I, Leite-Moreira AF. Diabetic cardiomyopathy: Understanding the molecular and cellular basis to progress in diagnosis and treatment. *Heart Fail Rev*. 2012;17(3):325–344.
8. Shimizu M, Umeda K, Sugihara N, et al. Collagen remodelling in myocardia of patients with diabetes. *J Clin Pathol*. 1993;46(1):32–36.
9. Westermann D, Rutschow S, Jäger S, et al. Contributions of inflammation and cardiac matrix metalloproteinase activity to cardiac failure in diabetic cardiomyopathy: The role of angiotensin type 1 receptor antagonism. *Diabetes*. 2007;56(3):641–646.
10. Chowdhry MF, Vohra HA, Galiñanes M. Diabetes increases apoptosis and necrosis in both ischemic and nonischemic human myocardium: Role of caspases and poly-adenosine diphosphate-ribose polymerase. *J Thorac Cardiovasc Surg*. 2007;134(1):124–131,131.e1–3.
11. Orea-Tejeda A, Colín-Ramírez E, Castillo-Martínez L, et al. Aldosterone receptor antagonists induce favorable cardiac remodeling in diastolic heart failure patients. *Rev Invest Clin*. 2007;59(2):103.
12. Bugger H, Boudina S, Hu XX, et al. Type 1 diabetic Akita mouse hearts are insulin sensitive but manifest structurally abnormal mitochondria that remain coupled despite increased uncoupling protein 3. *Diabetes*. 2008;57(11):2924–2932.
13. Chiu H-C, Kovacs A, Blanton RM, et al. Transgenic expression of fatty acid transport protein 1 in the heart causes lipotoxic cardiomyopathy. *Circ Res*. 2005;96(2):225–233.
14. Nakai A, Yamaguchi O, Takeda T, et al. The role of autophagy in cardiomyocytes in the basal state and in response to hemodynamic stress. *Nat Med*. 2007;13(5):619–624.
15. Seddon M, Looi YH, Shah AM. Oxidative stress and redox signalling in cardiac hypertrophy and heart failure. *Heart*. 2007;93(8):903–907.
16. Wiśniewski JR, Zougman A, Nagaraj N, Mann M. Universal sample preparation method for proteome analysis. *Nat Methods*. 2009;6(5):359–362.
17. Muschter S, Berthold T, Bhardwaj G, et al. Mass spectrometric phosphoproteome analysis of small-sized samples of human neutrophils. *Clin Chim Acta*. 2015;451(Pt B):199–207.
18. Scognamiglio R, Avogaro A, Negut C, Piccolotto R, de Kreutzenberg SV, Tiengo A. Early myocardial dysfunction in the diabetic heart: Current research and clinical applications. *Am J Cardiol*. 2004;93(8A):17–20.
19. Devereux RB, Roman MJ, Paranicas M, et al. Impact of diabetes on cardiac structure and function: The strong heart study. *Circulation*. 2000;101(19):2271–2276.
20. Lee M, Gardin JM, Lynch JC, et al. Diabetes mellitus and echocardiographic left ventricular function in free-living elderly men and women: The Cardiovascular Health Study. *Am Heart J*. 1997;133(1):36–43.
21. Bugger H, Abel ED. Molecular mechanisms of diabetic cardiomyopathy. *Diabetologia*. 2014;57(4):660–671.
22. Wang G, Wu WW, Zeng W, Chou C-L, Shen R-F. Label-free protein quantification using LC-coupled ion trap or FT mass spectrometry: Reproducibility, linearity, and application with complex proteomes. *J Proteome Res*. 2006;5(5):1214–1223.
23. Bantscheff M, Lemeer S, Savitski MM, Kuster B. Quantitative mass spectrometry in proteomics: Critical review update from 2007 to the present. *Anal Bioanal Chem*. 2012;404(4):939–965.

24. Heck AJ, Krijgsveld J. Mass spectrometry-based quantitative proteomics. *Expert Rev Proteomics*. 2004;1(3):317–326.
25. Couttas TA, Raftery MJ, Erce MA, Wilkins MR. Monitoring cytoplasmic protein complexes with blue native gel electrophoresis and stable isotope labelling with amino acids in cell culture: Analysis of changes in the 20S proteasome. *Electrophoresis*. 2011;32(14):1819–1823.
26. Albaum SP, Hahne H, Otto A, et al. A guide through the computational analysis of isotope-labeled mass spectrometry-based quantitative proteomics data: An application study. *Proteome Sci*. 2011;9:30.
27. Hu J, Qian J, Borisov O, et al. Optimized proteomic analysis of a mouse model of cerebellar dysfunction using amine-specific isobaric tags. *Proteomics*. 2006;6(15):4321–4334.
28. Gan CS, Chong PK, Pham TK, Wright PC. Technical, experimental, and biological variations in isobaric tags for relative and absolute quantitation (iTRAQ). *J Proteome Res*. 2007;6(2):821–827.
29. Pottiez G, Wiederin J, Fox HS, Ciborowski P. Comparison of 4-plex to 8-plex iTRAQ quantitative measurements of proteins in human plasma samples. *J Proteome Res*. 2012;11(7):3774–3781.
30. Herberg L, Coleman DL. Laboratory animals exhibiting obesity and diabetes syndromes. *Metabolism*. 1977;26(1):59–99.
31. Wang B, Golemis EA, Kruh GD. ArgBP2, a multiple Src homology 3 domain-containing, Arg/Abl-interacting protein, is phosphorylated in v-Abl-transformed cells and localized in stress fibers and cardiocyte Z-disks. *J Biol Chem*. 1997;272(28):17542–17550.
32. Sanger JM, Wang J, Gleason LM, et al. Arg/Abl-binding protein, a Z-body and Z-band protein, binds sarcomeric, costameric, and signaling molecules. *Cytoskeleton (Hoboken)*. 2010;67(12):808–823.
33. Kioka N. A novel adaptor protein family regulating cytoskeletal organization and signal transduction – Vinexin, CAP/ponsin, ArgBP2 [in Japanese]. *Seikagaku*. 2002;74(11):1356–1360.
34. Kakimoto Y, Ito S, Abiru H, et al. Sorbin and SH3 domain-containing protein 2 is released from infarcted heart in the very early phase: Proteomic analysis of cardiac tissues from patients. *J Am Heart Assoc*. 2013;2(6):e000565.
35. Liu Z, Huang J, Huo Y, et al. Identification of proteins implicated in the increased heart rate in ShenSongYangXin-treated bradycardia rabbits by iTRAQ-based quantitative proteomics. *Evid Based Complement Alternat Med*. 2015;2015:385953.
36. Dillmann WH. Diabetes mellitus induces changes in cardiac myosin of the rat. *Diabetes*. 1980;29(7):579–582.
37. Trost SU, Belke DD, Bluhm WF, Meyer M, Swanson E, Dillmann WH. Overexpression of the sarcoplasmic reticulum Ca^{2+}-ATPase improves myocardial contractility in diabetic cardiomyopathy. *Diabetes*. 2002; 51(4):1166–1171.
38. Bober E, Buchberger-Seidl A, Braun T, Singh S, Goedde HW, Arnold HH. Identification of three developmentally controlled isoforms of human myosin heavy chains. *Eur J Biochem*. 1990;189(1):55–65.
39. Bähler M. Are class III and class IX myosins motorized signalling molecules? *Biochim Biophys Acta*. 2000;1496(1):52–59.
40. Komaba S, Inoue A, Maruta S, Hosoya H, Ikebe M. Determination of human myosin III as a motor protein having a protein kinase activity. *J Biol Chem*. 2003;278(24):21352–21360.

Adipose tissue miRNA level variation through conjugated linoleic acid supplementation in diet-induced obese rats

Maryam Nazari[1,A,B,D], Alihossein Saberi[2,E,F], Majid Karandish[3,C,E], Mohammad Taha Jalali[4,C,F]

[1] Food (Salt) Safety Research Center, School of Nutrition and Food Sciences, Semnan University of Medical Sciences, Iran
[2] Department of Medical Genetics, Faculty of Medicine, Ahvaz Jundishapur University of Medical Sciences, Iran
[3] Nutrition and Metabolic Diseases Research Center, Ahvaz Jundishapur University of Medical Sciences, Iran
[4] Hyperlipidemia Research Center, Ahvaz Jundishapur University of Medical Sciences, Iran

A – research concept and design; B – collection and/or assembly of data; C – data analysis and interpretation;
D – writing the article; E – critical revision of the article; F – final approval of the article

Advances in Clinical and Experimental Medicine, ISSN 1899-5276 (print), ISSN 2451-2680 (online) *Adv Clin Exp Med*. 2018;27(11):1477–1482

Address for correspondence
Alihossein Saberi
E-mail: saberi-a@ajums.ac.ir

Funding sources
The study was supported by Ahvaz Jundishapur University of Medical Sciences, Iran (grant No. NRC 9204).

Conflict of interest
None declared

Acknowledgements
The authors would like to thank Dr. Azadeh Saki for her statistical advice.

Received on June 16, 2017
Reviewed on August 2, 2017
Accepted on July 24, 2018

Abstract

Background. Conjugated linoleic acid (CLA), which is an octadecadienoic acid isomer, is believed to play different positive physiological roles, such as lowering body fat. Due to some reported side effects of CLA, like lipodystrophy and impaired glucose metabolism, it is important to establish its safety by understanding detailed molecular mechanisms. One of these mechanisms may be the role of this dietary agent in modifying the function and activity of microRNAs (miRNAs).

Objectives. The aim of the study was to investigate how adipocyte miR-27a and miR-143 expression may be influenced by CLA in obese rats.

Material and methods. In this study, 24 male Wistar rats were randomly divided into normal-fat diet (NFD) and high-fat diet (HFD) groups. After 8 weeks, the rats were weighed and half of the diet-induced obese rats were randomly selected to receive 500 mg CLA per 1 kg body weight for 4 weeks. At the end of this period, epididymal fat was isolated to investigate the expression level of miRNAs by real-time polymerase chain reaction (RT-PCR).

Results. After 12 weeks, the obese rats in the HFD group, compared with rats in the NFD group, demonstrated a significant decrease in the expression of miR-27a ($p < 0.05$) and a significant increase in the expression of miR-143 ($p < 0.05$). In the group which had received CLA for a 4-week period, these events were reversed. Moreover, the rats in this group gained less weight than other rats in HFD groups, although the difference was not statistically significant.

Conclusions. In conclusion, this study demonstrated that CLA, as an anti-obesity agent, may minimize abnormal changes in miRNA expression in obesity. This suggests a new pathway for weight loss; however, further studies are needed.

Key words: obesity, microRNA, high-fat diet, conjugated linoleic acid

DOI
10.17219/acem/93728

The growing global prevalence of obesity, which is recognized as a disease by the American Medical Association, has had damaging effects on various aspects of life and has even increased mortality and morbidity rates as a result of cardiovascular diseases, cancers and metabolic syndrome.[1,2] On the one hand, various approaches such as increasing physical activity, diet therapy, surgery, and medication have demonstrated only partial success. On the other hand, several anti-obesity drugs have been withdrawn from the market because of their proven adverse effects.[3] Hence, an increasing demand for safe and effective anti-obesity drugs has arisen.

In this regard, it is necessary to consider regulatory mechanisms in order to find effective agents for obesity control. Recently, microRNAs (miRNAs) as epigenetic regulators in obesity have attracted considerable attention from researchers. The miRNAs are short-length, noncoding RNAs which, by pairing with the 3'-untranslated region (UTR) of their target mRNAs, control gene expression.

Besides the important roles of miRNAs in different processes such as proliferation, differentiation, apoptosis, growth, and development, it seems that several miRNAs are deregulated in animals and humans with obesity. However, there is insufficient evidence regarding the role of these small molecules in the metabolism of adipose tissue.[4,5] Among the numerous miRNAs existing in adipose tissue, a few of them are differentially expressed in obesity or demonstrate regional variance in their expression.[6]

Recently, some studies have shown that miRNA expression in adipose tissue may possibly affect the pathogenesis of diseases related to high-fat diets. Some miRNAs can be modified by epigenetic mechanisms when the diet composition is changed.[7–9] Thus, understanding the mechanisms by which miRNAs exert their potential roles in adipose tissue metabolism may possibly lead to the discovery of new paths in the development and treatment of obesity.[10] However, very few studies have addressed this issue and have considered the effect of different kinds of diet or dietary agents on miRNA variations.[11,12]

Therefore, a hypothesis can be put forward that investigating the use of pharmacological agents such as fat burners in obesity management can elucidate the probable mechanisms for their anti-obesity action.[13] One agent that is considered an anti-obesity drug is conjugated linoleic acid (CLA), which contains a linoleic acid isomer (C18:2, n-6).[14] A large proportion of the obese population is interested in CLA supplements, claiming body fat-lowering effects. Conjugated linoleic acid is considered a "natural" compound without dangerous side effects.[15] However, this fatty acid inhibits the entry of glucose into the adipocytes, and may lead to hyperinsulinemia and increases in inflammatory markers. Consequently, there are doubts regarding the exact mechanisms of action of CLA in adipocytes that result in the reduction of body fat, and regarding the safety of using this compound as a dietary supplement.[14]

From among numerous adipocyte miRNAs, miR-143 and miR-27, which are up- and downregulated (respectively) during adipocyte differentiation, were selected for further investigation.[16–18]

The expression of miR-143 was reported to be increased in mice fed a high-fat diet, which in turn caused hyperinsulinemia and impaired glucose tolerance. On the other hand, in mice with reduced miR-143 level or activity, undesirable blood glucose changes were modified, and consequently, this microRNA was regarded as a potential candidate to be targeted in type 2 diabetes as well as obesity treatment.[7] Furthermore, a high-fat diet was found to lead to reduced expression of miR-27a in concordance with amplified peroxisome proliferator-activated receptor γ (PPARγ) activity, which is a well-known transcription factor in adipocyte differentiation.[8,18] Therefore, recommendation of dietary agents that induce miR-27a or inhibit miR-143 seems to be logical to decelerate adipogenesis. Consequently, the aim of this study was to determine the variations in expression of these 2 miRNAs in adipose depots in the epididymis of rats fed a high-fat diet before and after CLA supplementation.

Material and methods

Animals and diet

Twenty-four 8-week-old male albino Wistar rats were obtained from the Animal Laboratory Unit of Ahvaz Jundishapur University of Medical Sciences (Iran). The rats, which weighed 150–200 g, were housed in groups of 2 per cage and maintained on a 12-hour light/dark cycle at 22°C with a relative humidity at 50 ±5%, and were fed a standard chow diet and tap water ad libitum. After a 1-week acclimation period, they were randomly allocated into 2 different diet groups: a normal-fat diet (NFD) for the entire experimental procedure (a semi-purified NFD), (n = 8) as the control group; and a high-fat diet (HFD) for the entire experimental procedure (a semi-purified HFD to induce obesity) (n = 16).

The basic diet in this study was a semi-purified form of the American Institute of Nutrition (AIN)-93M diet. The proportional compositions of the 2 diets are presented in Table 1.[19] Fresh portions were prepared twice a week and stored at 4°C. After the 8th week, the HFD group was randomly subdivided into 2 categories (n = 8 in each): a control group, which received HFD + 1 mL of corn oil per day for 4 weeks by oral gavage; and a CLA group, which received HFD + 500 mg per kg body weight of CLA (Tonalin® CLA; Natural Factors, Coquitlam, Canada, composed of a 75% mixture of c9, t11 and t10, c12 isomers in a 50:50 ratio) dissolved in 0.5 mL of corn oil (1 mL total) per day for 4 weeks by oral gavage.

During the course of the experiment, body weights were recorded weekly to verify the obesogenic effects of the HFD. At the 12th week, the animals were fasted for 10 h before

Table 1. Modified* American Institute of Nutrition diet composition

Ingredients in 1 kg of diet	Normal-fat diet [g]	High-fat diet [g]
Corn starch	465.6	237
Casein (>85% protein)	140	140
Dextrinized corn starch	155	78
Sucrose	100	50
Soybean oil	40	185
Margarine	0	185
Fiber	50	50
Mineral mix (AIN-93M-MX)	35	35
Vitamin mix (AIN-93-VX)	10	10
L-Cystine	1.8	3
Choline bitartrate	2.5	2.5
Tert-butylhydroquinone	0.008	0.01
Total energy [kcal]	3600	5350

*AIN-93M Purified Diet for Laboratory Rodents was modified.[19] Fiber was replaced by wheat bran in the formulation.

being sacrificed and then white adipose tissue (WAT) from epididymal fat was isolated and directly submerged in RNA later solution (RNA Stabilization Reagent; Qiagen, Hilden, Germany) to stabilize and keep cellular RNA in situ, and was kept at –80°C until analysis.

All the procedures carried out in this study involving animals were approved by the ethical committee for experimental animal care at Ahvaz Jundishapur University of Medical Sciences (NRC9204).

MicroRNA extraction from adipose tissue

To extract total miRNA from WAT taken from NFD- or HFD-fed rats, approx. 100 mg of tissue was homogenized in 1–2 mL of Qiazol (Qiagen) using a digital homogenizer (WiseTis Homogenizer HG-15D, Grafstal, Germany). Thereafter, miRNA isolation was carried out utilizing the RNeasy Mini Kit (Qiagen) according to the manufacturer's instructions. The concentration of extracted miRNA was measured using the NanoDrop Spectrophotometer 2000c (Thermo Fisher Scientific, Inc., Waltham, USA) and its integrity was confirmed by 2% agarose gel electrophoresis. The RNA samples were directly frozen and stored at –80°C.

MicroRNA quantification was initiated by reverse transcription of the RNA samples and then amplification by Power SYBR Green PCR Master Mix (Applied Biosystems, Foster City, USA) and specific primers. Reverse transcription and real-time polymerase chain reaction (RT-PCR) were carried out using a miScript Reverse Transcription Kit (Qiagen), miScript SYBR Green PCR Kit (Qiagen) and miScript Primer Assay (Qiagen) in accordance with the manufacturer's instructions. All the primers were manufactured by Qiagen (Hs_RNU6-2_11 Cat. No. MS00033740, RN_miR-143_1 Cat. No. MS00000420 and RN_miR-27a_1 Cat. No. MS00000147) and their sequences were not revealed.

MiR-27a and miR-143 levels were normalized to RNA U6. Real-time PCR was performed on a StepOne Real Time PCR System (Applied Biosystems). The RT-PCR thermal cycling included 15 min incubation at 95°C, followed by 40 cycles of a 3-stage temperature profile of 94°C for 15 s, 55°C for 30 s and finally 70°C for 30 s. All the samples were run in triplicate and the fold changes in the miRNA level were calculated by the comparative cycle threshold (Ct) method $2^{-\Delta\Delta Ct}$, where ΔCt = Ct miRNA – Ct U6 and ΔΔCt = ΔCt treated samples – ΔCt untreated controls.

Statistical analysis

The statistical analysis was performed using the Statistical Package for Social Sciences v. 18.0 (SPSS Inc., Chicago, USA) The results were expressed as means ± standard error of the mean (SEM). The normality and homogeneity of variances were tested with the Kolmogorov-Smirnov test. Student's t-test and a 1-way analysis of variance (ANOVA) followed by Fisher's least significant difference (LSD) test were employed to compare the mean differences between the groups. A p-value <0.05 was considered statistically significant.

Results

Effects of high-fat diet and normal-fat diet on weight gain

Body weights at the beginning were not different between the 2 groups (p-value >0.05). At the 8th week, the HFD-fed rats gained significantly more weight than the controls and developed the obese phenotype (Table 2).

Effects of conjugated linoleic acid on weight gain

Four-week treatment with CLA reduced the animals' weight gain throughout the treatment period; however, this effect was not statistically significant (Table 3).

Table 2. Effects of NFD and HFD on rats' weight gain over 8 weeks

Group	n	Baseline weight [g]	p-value	8-week weight [g]	p-value
NFD	8	169.66 ±8.91	0.67[a]	246.38 ±9.48	0.009[b]
HFD	16	173.00 ±4.02		296.43 ±5.36	

Values are expressed as means ± standard error of the mean (SEM). NFD – normal-fat diet; HFD – high-fat diet;
[a] insignificant weight difference between NFD and HFD at baseline; [b] significant weight difference between NFD and HFD at the 8th week.

Table 3. Effect of CLA on weight gain rate over 4 weeks in obese rats

Group	n	8-week weight [g]	12-week weight [g]	Weight gain [g]	p-value
NFD	8	246.38 ±6.48	264.62 ±8.03	18 (7.3%)	
HFD	8	300.50 ±13.16	336.43 ±15.10	35.9 (11.9%)	0.08[a]
CLA	8	288.38 ±7.60	312.68 ±9.60	24 (8.3%)	

Values are expressed as means ± standard error of the mean (SEM). NFD – normal-fat diet; HFD – high-fat diet; CLA – conjugated linoleic acid; [a] significant difference between CLA and control HFD in weight gain over 4 weeks.

Effects of high-fat diet on adipose tissue miR-143 and miR-27a expression levels

Parallel to the weight gain in HFD-fed rats, the expression levels of the miR-27a and miR-143 were altered in the adipose tissue of the obese rats compared to the NFD-fed rats. The HFD reduced miR-27a expression to 0.021-fold and increased miR-143 expression to 2.3-fold compared to the NFD-fed rats (Fig. 1).

Effects of conjugated linoleic acid on adipose tissue miR-143 and miR-27a expression levels

After 4 weeks, RT-PCR results showed that overexpression of miR-143 and downregulation of miR-27a in the adipose tissue induced by the HFD were weakened in the rats in the CLA group compared to the obese rats fed only a HFD. An increase in miR-27a expression to 2.26-fold was accompanied by a decrease in miR-143 to 0.42-fold following daily doses of 500 mg of CLA/kg of body weight (Fig. 1).

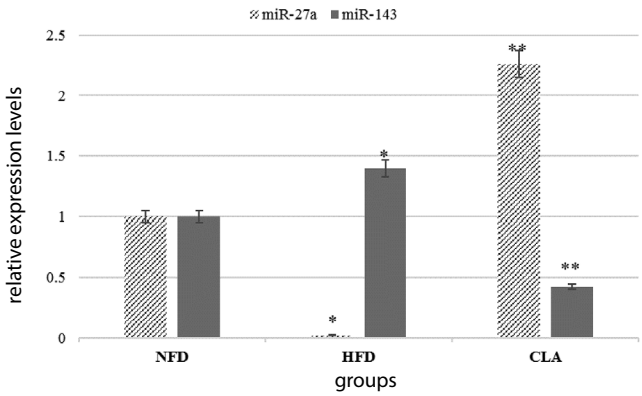

Fig. 1. Relative expression levels of miR-143 and miR-27a in the adipose tissue of rats fed a NFD or HFD in comparison with the CLA group. MicroRNA levels were normalized to U6 small nuclear RNA. The means ± standard error of the mean (SEM) of 8 rats in each group is shown.

* values with significant changes relative to the NFD group (* $p < 0.05$);
** values with significant changes relative to the HFD group (** $p < 0.05$);
NFD – normal-fat diet; HFD – high-fat diet; CLA – conjugated linoleic acid.

Discussion

Although CLA supplementation (in both animals and humans) has been found to bring about changes in body weight and some other beneficial effects in previous studies, the current results are very conflicting.

One of the main results of this study was the deceleration of the weight-gain trend in the CLA group in comparison with the HFD group. As shown in Table 3, the weight-gain rate in the HFD+CLA group was close to that of the NFD group (8.3% vs 7.3%); however, the final weight difference between the HFD group and the HFD+CLA group was not statistically significant. It seems that CLA does not diminish food intake in rodents (we did not measure food intake) and its effects are independent of the amount of fat in the diet, while some protein sources may change the effects of CLA on adipocyte fat content and the production of adipocytokine.[15] Despite the reduction in the fat content of CLA-fed animals reported in various studies, there was not much difference between the total body weights of the treated animals and the controls. As suggested by a few investigators, this happens mainly because of hepatomegaly and splenomegaly, which have been attributed to CLA supplementation.[20]

Furthermore, the weight changes in this study were judged only by body weight, while fat mass is a more sensitive index for evaluating obesity in animals. Woods et al. reported that rats fed a HFD for 10 weeks demonstrated a 10% increase in body weight. However, a 35–40% increase in body fat was detected compared with animals fed a NFD.[21] Another study has verified that a decrease in adipose mass was evident as early as after 1 week of feeding the animals CLA.[22]

It should be noted that regional differences in responsiveness to CLA have been reported. To determine cell proliferation response to CLA supplementation, it seems logical to expose animals to CLA during fetal growth, when most pre-adipocyte hyperplasia occurs.[22]

On the other hand, a few adverse effects of CLA have been reported, mainly due to the 10-trans, 12-cis isomer. For example, increased production of eicosanoids, pro-carcinogenic effects and negative alterations in glucose and lipoprotein metabolism have been attributed to CLA.[14,23] Its pro-oxidant effect enhances lipid hydroperoxide and lessens total antioxidant defenses, which leads to adverse effects on the lipid profile.[24] Thus, understanding the mechanism of action of CLA is vital for establishing an anti-obesity drug such as CLA.

In addition to determining the real impact of CLA on adiposity, it is necessary to ascertain the extent of the positive alterations obtained. Furthermore, it will be necessary to consider reciprocal interactions between dietary CLA and hormones such as leptin and insulin.[25]

As in most studies, a mixture of 2 major isomers (9-cis, 11-trans and 10-trans, 12-cis in equal proportions) was utilized in this study. In addition, a synthetic NFD was utilized to adjust the confounding effects of the control diet. In most other studies, a chow diet is used, although its basic composition is totally different from the experimental HFD and this is a noteworthy point.[26] Therefore, in this research, find the AIN-93 M diet was used as the basic diet and was formulated with different fat contents.

Since CLA has been reported to diminish fat deposition in animals, Parra et al. carried out a study to determine whether or not CLA administration affects the expression of miRNAs in the adipose tissue of mice. They found that miR-143 was downregulated in animals fed a standard-fat diet and treated with CLA,[27] which is in line with our results.

The association between abnormal miRNA expression and anomalies in adipogenesis alongside obesity may be a reason to target these molecules in obesity management. On the other hand, because the targets of miR-143 and miR-27a have not been identified, the association between the alterations in miRNAs brought about by CLA administration and fat accumulation needs further investigation.[27]

Supplementation with CLA in obese rats led to significant modifications in miR-27a and miR-143 expression in adipose tissue, suggesting probable pathways through which CLA mediates its biological effects in weight changes.

Esau et al. studied miRNA expression arrays in pre-adipocytes and demonstrated that miR-143 normally induces adipocyte differentiation and is overexpressed in obesity.[28] We obtained similar results. As in the present study, Takanabe et al. reported a 3.3-fold greater expression of adipose tissue miR-143 in obese mice; this was associated with overexpressions of PPARγ and activator-protein 2 (AP2), which are adipocyte differentiation markers.[17] Transcriptional factors (TF) such as C/EBP (α, β, δ), fatty acid synthase and fatty acid binding proteins genes can control adipocyte differentiation.[29] Similarly, *miR-143,* which mainly acts through *ERK5* (extracellular signal-regulated kinase 5) and *MAPK7,* can modulate the aforementioned TFs and control adipogenesis.[6,28,30]

In contrast, miR-27a in mature adipocytes of the obese mice was downregulated in comparison with lean mice.[18] A diet inducing non-alcoholic fatty liver disease (NAFLD) (high fat or high carbohydrate content) has been shown to decrease the expression of miR-27, -122, and -451, while upregulating miR-429, -200a and -200b expression in rat livers, which is consistent with our results in the HFD group.[7]

Investigating the protein and mRNA levels of key molecules and the expression levels of some genes related to adipogenesis or lipolysis, such as PPARγ, CEBPs and FAS, could be important and interesting. Since every single miRNA is able to control hundreds of target mRNAs, exploration of miRNA profile alteration is suggested; it was not possible for the researchers in the present study.

Conclusions

Complementary studies regarding the modification roles played by dietary agents or supplements in miRNA expression and other related genes are needed, not only to confirm the potential of miRNAs as novel prognostic metabolic biomarkers, but also to find new and more specific goals in obesity management, as well as the treatment of other metabolic disorders. However, we must bear in mind that studies evaluating the effects of nutrients on miRNA levels have mainly focused on the oncologic aspects and there are limited studies in line with ours.[12]

References

1. Padula WV, Allen RR, Nair KV. Determining the cost of obesity and its common comorbidities from a commercial claims database. *Clin Obes*. 2014;4(1):53–58.
2. Alexander R, Lodish H, Sun L. MicroRNAs in adipogenesis and as therapeutic targets for obesity. *Expert Opin Ther Targets*. 2011;15(5):623–636.
3. Kumar P, Bhandari U. Letter to the editor: Obesity Pharmacotherapy: Current Status. *EXCLI J*. 2015;14:290–293.
4. Ortega FJ, Moreno-Navarrete JM, Pardo G, et al. MiRNA expression profile of human subcutaneous adipose and during adipocyte differentiation. *PLOS ONE*. 2010;5(2):e9022.
5. Xie H, Sun L, Lodish HF. Targeting microRNAs in obesity. *Expert Opin Ther Targets*. 2009;13(10):1227–1238.
6. Arner P, Kulyté A. MicroRNA regulatory networks in human adipose tissue and obesity. *Nat Rev Endocrinol*. 2015;11(5):276–288.
7. García-Segura L, Pérez-Andrade M, Miranda-Ríos J. The emerging role of microRNAs in the regulation of gene expression by nutrients. *J Nutrigenet Nutrigenomics*. 2013;6(1):16–31.
8. Chartoumpekis DV, Zaravinos A, Ziros PG, et al. Differential expression of microRNAs in adipose tissue after long-term high-fat diet-induced obesity in mice. *PLOS One*. 2012;7(4):e34872.
9. Romao JM, Jin W, He M, McAllister T, Guan LL. Altered microRNA expression in bovine subcutaneous and visceral adipose tissues from cattle under different diet. *PLOS One*. 2012;7(7):e40605. doi:10.1371/journal.pone.0040605.
10. Williams MD, Mitchell GM. MicroRNAs in insulin resistance and obesity. *Exp Diabetes Res*. 2012;2012:484696. doi:10.1155/2012/484696.
11. McCann SE, Liu S, Wang D, et al. Reduction of dietary glycaemic load modifies the expression of microRNA potentially associated with energy balance and cancer pathways in pre-menopausal women. *Br J Nutr*. 2013;109(4):585–592.
12. Keller J, Ringseis R, Eder K. Supplemental carnitine affects the microRNA expression profile in skeletal muscle of obese Zucker rats. *BMC Genomics*. 2014;15(1):512. doi:10.1186/1471-2164-15-512.
13. Jeukendrup AE, Randell R. Fat burners: Nutrition supplements that increase fat metabolism. *Obes Rev*. 2011;12(10):841–851.
14. Lehnen TE, Ramos M, Camacho A, Marcadenti A, Lehnen AM. A review on effects of conjugated linoleic fatty acid (CLA) upon body composition and energetic metabolism. *J Int Soc Sports Nutr*. 2015. doi:10.1186/s12970-015-0097-4.
15. Silveira M-B, Carraro R, Monereo S, Tébar J. Conjugated linoleic acid (CLA) and obesity. *Public Health Nutr*. 2007;10(10A):1181–1186.
16. Sacco J, Adeli K. MicroRNAs: Emerging roles in lipid and lipoprotein metabolism. *Curr Opin Lipidol*. 2012;23(3):220–225.
17. Takanabe R, Ono K, Abe Y, et al. Up-regulated expression of microRNA-143 in association with obesity in adipose tissue of mice fed high-fat diet. *Biochem Biophys Res Commun*. 2008;376(4):728–732.
18. Kim SY, Kim Y, Lee HW, et al. miR-27a is a negative regulator of adipocyte differentiation via suppressing PPARγ expression. *Biochem Biophys Res Commun*. 2010;392(3):323–328.
19. Reeves PG, Nielsen FH, Fahey GC Jr. AIN-93 purified diets for laboratory rodents: Final report of the American Institute of Nutrition ad hoc writing committee on the reformulation of the AIN-76A rodent diet. *J Nutr*. 1993;123(11):1939–1951.

20. LaRosa PC, Miner J, Xia Y, Zhou Y, Kachman S, Fromm ME. Trans-10, cis-12 conjugated linoleic acid causes inflammation and delipidation of white adipose tissue in mice: A microarray and histological analysis. *Physiol Genomics.* 2006;27(3):282–294.
21. Woods SC, Seeley RJ, Rushing PA, D'Alessio D, Tso P. A controlled high-fat diet induces an obese syndrome in rats. *J Nutr.* 2003;133(4):1081–1087.
22. Chopra RJ. Synergistic conjucated linoleic acid (CLA) and carnitine combination. *Pat Appl Publ.* 2006;23:1–13.
23. Kopelman PG, Caterson ID. An overview of obesity management. In: Kopelman PG, Caterson ID, Dietz WH, eds. *Clinical Obesity in Adults and Children*. 3rd ed. Hoboken, USA: Wiley-Blackwell; 2010:267–274.
24. Diniz YS, Santos PP, Assalin HB, et al. Conjugated linoleic acid and cardiac health: Oxidative stress and energetic metabolism in standard and sucrose-rich diets. *Eur J Pharmacol.* 2008;579(1–3):318–325.
25. Visscher TLS, Snijder MB, Seidell JC. Epidemiology: Definition and classification of obesity. In: Kopelman PG, Caterson ID, Dietz WH, eds. *Clinical Obesity in Adults and Children.* 3rd ed. Hoboken, USA: Wiley-Blackwell; 2010:3–14.
26. Warden CH, Fisler JS. Comparisons of diets used in animal models of high fat feeding. *Cell Metab.* 2009;7(4):277.
27. Parra P, Serra F, Palou A. Expression of adipose microRNAs is sensitive to dietary conjugated linoleic acid treatment in mice. *PLOS ONE.* 2010;5(9):e13005. doi:10.1371/journal.pone.0013005.
28. Esau C, Kang X, Peralta E, et al. MicroRNA-143 regulates adipocyte differentiation. *J Biol Chem.* 2004;279(50):52361–52365.
29. Lin Q, Gao Z, Alarcon RM, Ye J, Yun Z. A role of miR-27 in the regulation of adipogenesis. *FEBS J.* 2009;276(8):2348–2358.
30. McGregor R, Choi M. microRNAs in the regulation of adipogenesis and obesity. *Curr Mol Med.* 2011;11(4):304–316.

The impact of sitagliptin, inhibitor of dipeptidyl peptidase-4 (DPP-4), on the ADMA-DDAH-NO pathway in ischemic and reperfused rat livers

Małgorzata Trocha[1,A–D,F], Beata Nowak[1,C,E], Anna Merwid-Ląd[1,D], Andrzej Szuba[2,3,C], Piotr Dzięgiel[4,5,E], Małgorzata Pieśniewska[1,B], Agnieszka Gomułkiewicz[4,B], Jerzy Wiśniewski[6,C], Tomasz Piasecki[7,B], Magdalena Gziut[1,D], Adam Szeląg[1,E,F], Tomasz Sozański[1,C,E]

[1] Department of Pharmacology, Faculty of Medicine, Wroclaw Medical University, Poland
[2] Department of Internal Medicine, 4th Military Hospital with Policlinic, Wrocław, Poland
[3] Department of Internal Nursing, Faculty of Health Sciences, Wroclaw Medical University, Poland
[4] Department of Histology and Embryology, Faculty of Medicine, Wroclaw Medical University, Poland
[5] Department of Histology and Embryology, Poznan University of Medical Sciences, Poland
[6] Department of Medical Biochemistry, Faculty of Medicine, Wroclaw Medical University, Poland
[7] Department of Epizootiology and Clinic of Bird and Exotic Animals, Wroclaw University of Environmental and Life Sciences, Poland

A – research concept and design; B – collection and/or assembly of data; C – data analysis and interpretation;
D – writing the article; E – critical revision of the article; F – final approval of the article

Advances in Clinical and Experimental Medicine, ISSN 1899-5276 (print), ISSN 2451-2680 (online) *Adv Clin Exp Med.* 2018;27(11):1483–1490

Address for correspondence
Małgorzata Trocha
E-mail: malgorzata.trocha@umed.wroc.pl

Funding sources
The study was financially supported by Wroclaw Medical University statutory research funding (ST-555).

Conflict of interest
None declared

Received on April 24, 2017
Reviewed on May 24, 2017
Accepted on June 25, 2017

DOI
10.17219/acem/75499

Abstract

Background. A correlation between the level of asymmetric dimethylarginine (ADMA) – the inhibitor of the nitric oxide (NO) synthesis – and the liver function and survival after a liver transplantation has been reported.

Objectives. The aim of this study was to evaluate the effect of sitagliptin – the inhibitor of dipeptidyl peptidase-4 (DPP-4) – on the NO-ADMA-dimethylarginine dimethylaminohydrolase (DDAH) pathway in rat livers subjected to ischemia/reperfusion (IR).

Material and methods. The rats received sitagliptin (5 mg/kg, per os – p.o.) (groups: S – livers not subjected to IR procedure, and SIR – livers subjected to IR procedure) or a saline solution (groups: C – livers not subjected to IR procedure, and CIR – livers subjected to IR procedure) for 14 days; following this, livers in the SIR and CIR groups were subjected to ischemia (60 min) and reperfusion (24 h). Aminotransferases were measured before the surgery; additionally, the arginine (ARG), ADMA and symmetric dimethylarginine (SDMA) levels were estimated just before ischemia and during reperfusion (at 0.5 h, 4 h and 24 h). After IR, citrulline, the DDAH activity, mRNA for type 1 DDAH (*DDAH1*), and arginine methyltransferase type 1 (*PRMT1*) were determined.

Results. The increase in the initial level of ARG/ADMA0 (A/A) ratio in group S compared to group C verged on statistical significance. At 0.5 h and 4 h of reperfusion, the highest concentration of ADMA was found in group CIR. At those time points, the ARG level and the A/A ratio were decreased in groups CIR and SIR as compared to groups C and S, respectively. The alanine transaminase (ALT) activity was lower in the sitagliptin-treated group than in the non-treated one. The DDAH and citrulline levels were reduced in group CIR as compared to group C, but were greater in group SIR as compared to group S. The *PRMT1* mRNA expression was higher in groups CIR and SIR, compared to groups C and S, respectively.

Conclusions. The increased A/A ratio suggests a protective effect of sitagliptin on livers not subjected to IR. Changes in the DDAH activity and the *PRMT1* mRNA expression also imply the protective activity of sitagliptin during IR.

Key words: liver, rat, ischemia/reperfusion, asymmetric dimethylarginine, sitagliptin

Introduction

Nitric oxide (NO), synthetized from arginine (ARG), is an essential factor regulating relaxation and dilatation of hepatic stellate cells, and hence, sinusoid blood flow.[1–3] Endothelial NO synthase (eNOS) is responsible for both the basal production of NO and, when larger amounts of NO are required, the production for its inducible form – iNOS. At a higher concentration, NO reacts with superoxide, forming peroxinitrite, which augments cell injury.[3,4] Numerous individual factors influence the NO concentration, including the levels of eNOS cofactors – the reduced form of nicotinamide adenine dinucleotide phosphate (NADPH) and tetrahydropterin, oxygen support, the ARG level, the argininase activity, and the concentration of methylated derivatives of ARG, including asymmetric and symmetric dimethylarginine (ADMA, SDMA) and N-monomethyl-L-arginine (L-NMMA), known as endogenous inhibitors of NOS. The regulation of the ADMA synthesis by arginine methyltransferases (PRMTs), and its degradation by dimethylarginine dimethylaminohydrolase (DDAH) to dimethylamine and citrulline are also highly important.[5]

Liver injury during a partial hepatectomy or a transplantation is initially caused by ischemia and aggravated by reperfusion of hepatic parenchyma. Generally, reperfusion can be divided into 2 phases. During the first 3–6 h of renewed blood flow, the generation of reactive oxygen species (ROS) and NO, and the activation of T cells and Kupffer cells can be observed; following this, the neutrophil infiltration, leading to the cytokine, chemokine and ROS production, is seen within the next 18–24 h.[6,7] Asymmetric dimethylarginine, released during reperfusion, is one of the factors inhibiting the synthesis of NO. Vasoconstriction, considered a consequence of the imbalance between NO and endothelin, has been postulated to form the basis of disturbed liver function in ischemia/reperfusion (IR).[8,9] Notwithstanding the upregulated protein degradation with the relaxation of free methylarginines, impaired degradation of the latter has also been observed in such conditions.Furthermore, as the correlation between the level of ADMA and the liver function and survival after a liver transplantation has been reported, the identification of substances decreasing the ADMA level and the elucidation of the mechanism of their influence on the NO level appears crucial.[5]

Sitagliptin is an oral hypoglycemic drug proficient in inhibiting dipeptidyl peptidase-4 (DPP-4) – an enzyme involved in the metabolism of incretins, such as glucagon-like peptide-1 (GLP-1).[10] Although sitagliptin is a relatively new drug, introduced to European Pharmacopeia in 2007, individual cases of its antioxidative and anti-inflammatory action have been reported, including the inhibition of the DPP-4 activity, which reduced IR injury in mice after a lung transplantation.[11–13]

The aim of the current work was to investigate the effect of sitagliptin on ARG and its derivatives as well as the activity of DDAH, *DDAH1* and *PRMT1* mRNA – enzymes involved in the production and degradation of ADMA, in rat livers subjected and not subjected to IR. The experiment was carried out on healthy rodents to eliminate the influence of harmful factors, extraneous to IR, on the liver function.

Material and methods

Animals

Thirty-six Wistar male rats were included in this study. Animals were housed in individual chambers with a 12:12 h light-dark cycle. The temperature was maintained at 21–23°C. The experiment protocol was approved by the Local Ethics Commission for Experiments on Animals (No. 80/2012 of December 5, 2012).

Chemicals

Sitagliptin (Januvia – tablets, 100 mg; MSD sp. z o.o., Warszawa, Poland), heparin (Heparinum WZF – ampoules, 25,000 U/5 mL; Polfa Warszawa S.A., Warszawa, Poland), ketamine hydrochloride (Bioketan; Vetoquinol Biowet, Gorzów Wielkopolski, Poland), medetomidine hydrochloride (Domitor – ampoules, 1 mg/mL; Orion Pharma, Espoo, Finland), 0.9% sodium chloride solution (Polpharma S.A., Starogard Gdański, Poland), and Ringer's solution (Polfa Lublin S.A., Lublin, Poland) were used in the study.

Experimental design

Following acclimatization, animals were divided randomly into 4 groups: groups C (n = 9) and S (n = 8) – the livers were not subjected to IR procedure, and groups CIR (n = 9) and SIR (n = 10) – the livers undergoing IR procedure. Rat livers from groups S and SIR received sitagliptin intragastrically (5 mg/kg) once a day for 14 days, prior to the surgical procedure. To determine the initial levels of ARG derivatives and activities of aminotransferases – alanine transaminase (ALT) and aspartate transaminase (AST) – blood samples were obtained from the tail vein after the drug treatment.

Preparation of the liver ischemia/reperfusion injury model

Following the administration of medetomidine (0.1 mg/kg intramuscularly – i.m.) and ketamine (7 mg/kg i.m.) anesthesia, the animals underwent a midline laparotomy. In the CIR and SIR groups, the ischemia of median and left lateral liver lobes was achieved by occluding the branches of the portal vein and hepatic artery with a microvascular clip. After ischemia (60 min), the clip was removed and reperfusion was started (24 h). At 0.5 h, 4 h and 24 h

of reperfusion, samples of blood were collected to mark the ADMA, SDMA and ARG levels. The citrulline concentration was measured at 24 h of reperfusion. Once the experiment was terminated, the livers were weighted and ischemic lobes were isolated. In the C and S groups, the animals underwent the same surgical procedure as in the ischemic groups, but after a laparotomy, the branches of the portal vein and hepatic artery were not occluded.

A portion of the obtained liver lobes was placed in the RNAlater RNA Stabilization Reagent (Qiagen, Hilden, Germany) and used for the real-time polymerase chain reaction (PCR); the remaining liver tissues were homogenized and the supernatant was collected.[14]

Blood enzymes, arginine and its derivatives, and citrulline

The activity of DDAH was determined spectrophotometrically (Marcel S350 PRO; Marcel sp. z o.o., Zielonka, Poland), using the method based on the L-citrulline production rate, described in our previous study.[15] Briefly, 1 mM of ADMA was added to each sample of the homogenate with a phosphate buffer (pH 6.5), and then incubated for 45 min at 37°C. The reaction was stopped with 4% sulfosalicylic acid and the samples were centrifuged. Following this, diacetic monooxime in 5% acetic acid mixed with antipyrine in 50% sulfuric acid was added to the samples. L-citrulline was determined following the incubation at 60°C and cooling on ice. The DDAH activity was presented as μm of L-citrulline/gram of protein/min at 37°C.

The concentrations of amide derivative ARG, citrulline, ADMA, and SDMA were measured simultaneously by high-performance liquid chromatography (HPLC) with mass spectrometry detection.[16] All the separations were performed with the HPLC system Agilent Technologies 1260 Infinity (Agilent Technologies, Santa Clara, USA). The Acquity UPLC HSS T3 50 × 1.0 mm, 1.8 μm column from Waters (Milliford, USA) was used throughout the chromatographic separation. A 0.22-micrometer membrane inline filter from Waters was installed to protect the analytical column. The volume of injection was 2 μL. Gradient elution was performed using 0.1% formic acid in water (A) and 0.1% formic acid in methanol (B) at a flow rate of 0.2 mL/min. The overall time of the method was 14.5 min and consisted of 7 steps: from 0 min to 1 min, 10% B; from 1 min to 6 min, 10–35% B; from 6 min to 7 min, 35–60% B; from 7 min to 7.5 min, 60–90% B; from 8 min to 8.5 min, 90–100% B. All the separations were conducted at 60°C.

The level of protein in liver homogenates and the activity of aminotransferases in serum were determined in a certified laboratory.

Real-time polymerase chain reaction

Total RNA was extracted from the studied tissues using the RNeasy Mini Kit (Qiagen) as described in the protocol. Reverse transcription of mRNA to cDNA was performed using the QuantiTect Reverse Transcription Kit (Qiagen). The expression of *DDAH1* and *PRMT1* mRNA was evaluated by the real-time PCR in the 7900HT Fast Real-Time PCR System (Applied Biosystems, Carlsbad, USA). Glyceraldehyde-3-phosphate dehydrogenase (*GAPDH*) was used as a reference gene. The real-time PCR was performed using the TaqMan Gene Expression Master Mix, and specific primers and TaqMan probes: Rn 00574200_m1 for *DDAH1*, Rn 00821202_g1 for *PRMT1* and Rn 99999916_m1 for *GAPDH* (Applied Biosystems). All the reactions were performed in triplicates in standardized thermal cycling conditions, including the polymerase activation at 50°C for 2 min, denaturation at 94°C for 10 min and 40 cycles of denaturation at 94°C for 15 s, followed by annealing and synthesis at 60°C for 1 min. Relative quantity (RQ) of *DDAH1* and *PRMT1* mRNA was calculated using the 2-ΔΔCt method.

Statistical analysis

Data was expressed as mean ± standard deviation (SD). The two-way analysis of variance (ANOVA) was used to analyze the impact of sitagliptin and IR on the activity of DDAH and the mRNA expression for DDAH and PRMT. The one-way ANOVA was used to determine the effect of the sitagliptin administration on the initial values of aminotransferases. The analysis of variance with repeats was used for the statistical analysis of the influence of the drug and the time of reperfusion on the ARG, ADMA and SDMA levels, and the ARG/ADMA (A/A) ratio. Specific comparisons were made with the contrast analysis. Hypotheses were considered positively verified at $p < 0.05$.

Results

Asymmetric dimethylarginine, symmetric dimethylarginine, arginine, and the arginine/ /asymmetric dimethylarginine ratio

After the sitagliptin administration, no significant differences between all the groups in the ADMA0, ARG0 and SDMA0 levels were found (Fig. 1). The observed increase in the A/A0 ratio in group S, as compared to group C, was not statistically significant, but it was close to the significance threshold (S vs C; $p = 0.07$).

At 0.5 h and 4 h of reperfusion, the highest ADMA concentration was found in group CIR and the lowest in group S (after 0.5 h: CIR0.5 vs S0.5; $p < 0.05$, and after 4 h: CIR4 vs S4; $p < 0.01$). Similar differences were noted in the SDMA levels after 0.5 h of reperfusion (CIR0.5 vs S0.5; $p < 0.05$). After 4 h of reperfusion, the ADMA level was also significantly higher in groups that underwent IR (CIR4 vs C4 and SIR4 v. S4; $p < 0.05$ in both comparisons) (Fig. 1A,1B).

At 0.5 h and 4 h of reperfusion, both the level of ARG and the A/A ratio were the highest in group S and the

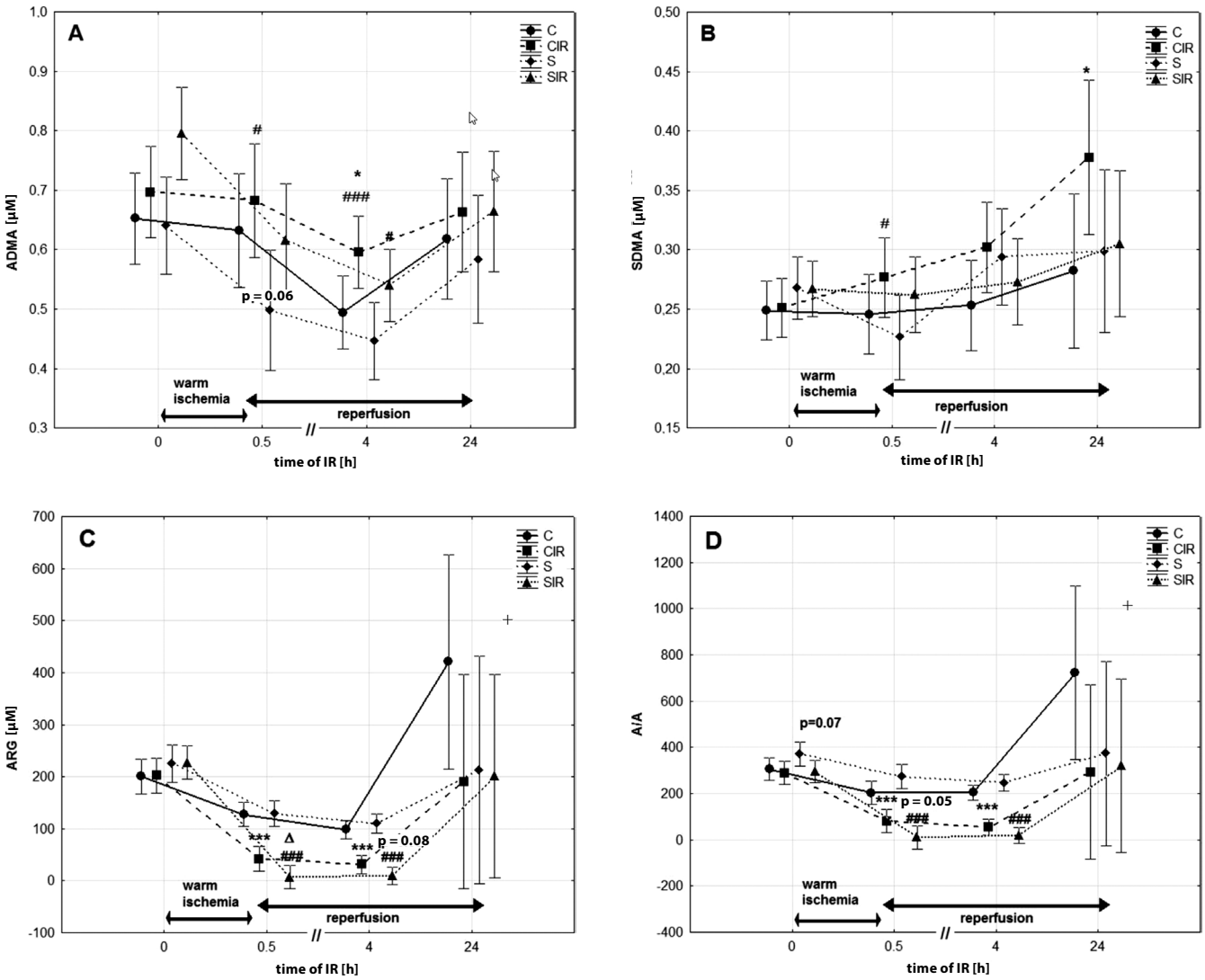

Fig. 1. The influence of IR and the sitagliptin treatment on the levels of ADMA (A), SDMA (B), ARG (C), and the A/A ratio (D)

Values are presented as mean ± standard deviation (SD); ADMA – asymmetric dimethylarginine; SDMA – symmetric dimethylarginine; A/A – arginine/asymmetric dimethylarginine; group C – non-treated and not subjected to IR; group CIR – non-treated and subjected to IR; group S – sitagliptin-treated and not subjected to IR; group SIR – sitagliptin-treated and subjected to IR; IR – ischemia/reperfusion; specific comparisons: * $p < 0.05$ and *** $p < 0.005$ (compared to C); # $p < 0.05$ and ### $p < 0.005$ (compared to S); Δ $p < 0.05$ (compared to CIR).

lowest in group SIR. Furthermore, at those reperfusion time points, in groups CIR and SIR, the concentration of ARG was significantly lower as compared to groups C and S, respectively (CIR0.5 vs C0.5 and SIR0.5 vs S0.5, as well as CIR4 vs C4 and SIR4 vs S4; $p < 0.005$ in all comparisons). Similarly, the level of the A/A ratio was also significantly lower in groups that underwent IR (CIR0.5 vs C0.5 and SIR0.5 vs S0.5, as well as CIR4 vs C4 and SIR4 vs S4; $p < 0.005$ in all comparisons). At 0.5 h of reperfusion, the concentration of ARG was significantly lower in group SIR than in group CIR (SIR0.5 vs CIR0.5; $p < 0.05$). The level of the A/A ratio did not reach significance, but it was close to the significance threshold (SIR0.5 vs CIR0.5; $p = 0.05$). Similarly, at 4 h of reperfusion, the difference in the concentration of ARG was near the threshold of statistical significance (SIR4 vs CIR4; $p = 0.08$) (Fig. 1C,1D)

At 24 h of reperfusion, the levels of the 3 examined parameters (ADMA, ARG and the A/A ratio) were restored to baseline values. At this time, SDMA was significantly higher in group CIR than in group C (CIR24 vs C24; $p < 0.05$) (Fig. 1).

Biochemical analyses

The activity of dimethylarginine dimethylaminohydrolase

The activity of DDAH in liver homogenates was lower in group S as compared to group C (S vs C; $p < 0.005$). In IR conditions, the DDAH activity decreased in group CIR as compared to group C (CIR vs C; $p < 0.01$); in contrast, in drug-treated groups, it was significantly increased in group SIR compared to group S (SIR vs S; $p < 0.05$) (Fig. 2A).

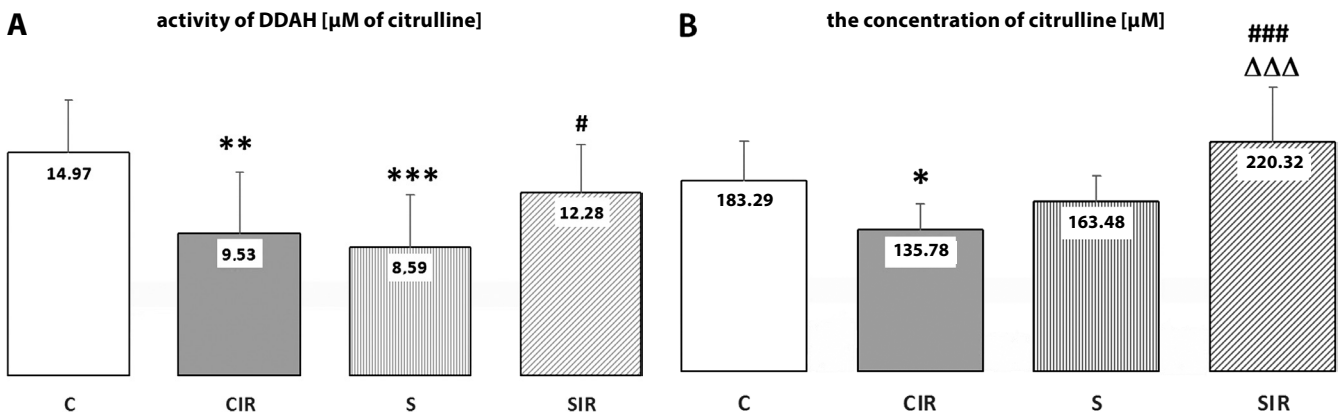

Fig. 2. The influence of IR and the sitagliptin treatment on the DDAH activity (A) and the citrulline concentration (B)

Values are presented as mean ± standard deviation (SD); DDAH – dimethylarginine dimethylaminohydrolase; group C – non-treated and not subjected to IR; group CIR – non-treated and subjected to IR; group S – sitagliptin-treated and not subjected to IR; group SIR – sitagliptin-treated and subjected to IR; IR – ischemia/reperfusion; specific comparisons: * $p < 0.05$, ** $p < 0.01$, *** $p < 0.005$ (compared to C); # $p < 0.05$ and ### $p < 0.005$ (compared to S); ΔΔΔ $p < 0.005$ (compared to CIR).

Citrulline

After 24 h of reperfusion, the concentration of citrulline decreased in group CIR compared to group C (CIR vs C; $p < 0.05$); however, in drug-treated groups, it was significantly increased in group SIR as compared to groups S and CIR (SIR vs S and SIR vs CIR; $p < 0.005$) (Fig. 2B).

Aminotransferases

After 2 weeks of the sitagliptin administration, the activity of ALT was significantly lower in group S than in group C (S vs C; $p < 0.05$). No significant changes in the AST activity were observed in all the examined groups (Table 1).

Table 1. The values of the ALT and AST activity after 2 weeks of treatment with sitagliptin at a dose of 5 mg/kg intragastrically (groups S and SIR) or with a saline solution (groups C and CIR)

Groups	ALT [U/L]	AST [U/L]
	mean ±SD	mean ±SD
C (n = 9)	66.89 ±20.14	175.11 ±104.08
CIR (n = 9)	88.67 ±55.14	178.78 ±93.88
S (n = 8)	46.00* ±8.09	206.75 ±51.87
SIR (n = 10)	62.80 ±10.61	186.90 ±26.54

IR – ischemia/reperfusion; ALT – alanine transaminase; AST – aspartate transaminase; SD – standard deviation; * $p < 0.05$ (compared to C).

The dimethylarginine dimethylaminohydrolase and arginine methyltransferase mRNA expression

The *DDAH1* mRNA expression was observed to be the lowest in group S and the highest in group C, but the differences were not statistically significant. The *PRMT1* mRNA expression was higher in groups CIR and SIR as compared to groups C and S, respectively (CIR vs C and SIR vs S; $p < 0.005$) (Fig. 3A,3B).

Discussion

Despite significant progress in available therapies, an organ transplantation often remains the only option of treatment for many patients. An important limitation of this method is the damage suffered by the transplanted organs following ischemia, and particularly during the

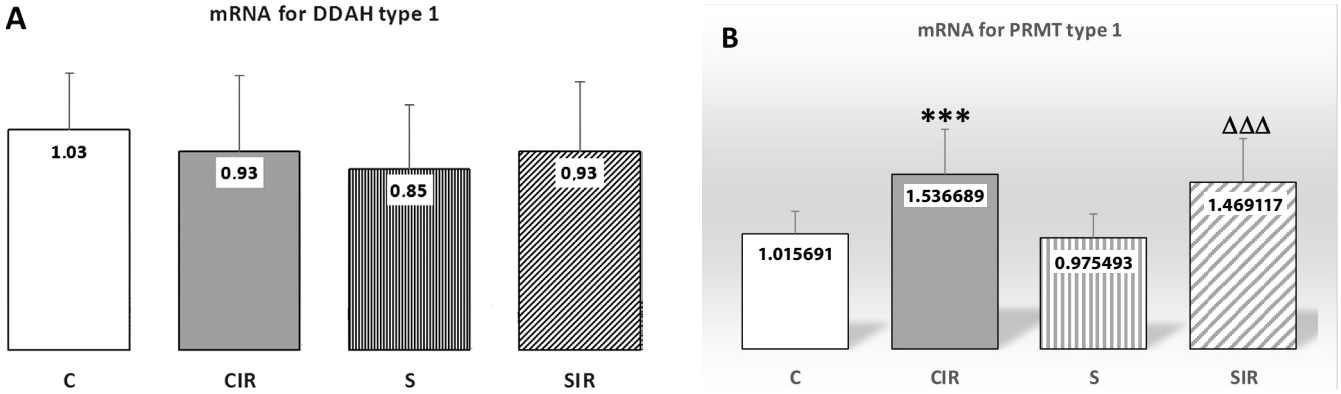

Fig. 3. The influence of IR and the sitagliptin treatment on the relative expression of *PRMT1* (A) and *DDAH1* (B) mRNA

Data is expressed as a percentage of control values and as mean ± standard deviation (SD); *PRMT1* – arginine methyltransferase type 1; *DDAH1* – dimethylarginine dimethylaminohydrolase type 1; group C – non-treated and not subjected to IR; group CIR – non-treated and subjected to IR; group S – sitagliptin-treated and not subjected to IR; group SIR – sitagliptin-treated and subjected to IR; IR – ischemia/reperfusion; specific comparisons: *** $p < 0.005$ (compared to C); ΔΔΔ $p < 0.005$ (compared to S).

subsequent reperfusion. Consequently, numerous studies have focused on the elucidation of novel substances with a protective activity under these conditions, or novel, advantageous properties of already known, chronically administrated substances. For that reason, the present study set out to clarify the activity of hypoglycemic drug – sitagliptin – in a liver undergoing IR. The key conclusions are as follows:

– in the group treated with sitagliptin, not subjected to IR, an increase in the level of the A/A ratio measured just before the surgery, as compared to the untreated group, verged on statistical significance, the DDAH activity was significantly lowered and the mRNA expression for *DDAH1* was slightly lowered as compared to the untreated group, while the ALT activity was significantly lower in the drug-treated group than in the untreated group;

– in the drug-treated and subjected to IR group, the ARG level and the A/A ratio were significantly decreased compared to the group non-subjected to IR and also to the untreated group subjected to IR, the ADMA level was higher as compared to the treated group without IR, while the levels of DDAH and citrulline were higher than in the drug-treated non-IR group;

– in the untreated groups subjected to IR, the ADMA and SDMA concentrations measured during reperfusion were the highest among all the groups, the ARG level and the A/A ratio were significantly decreased as compared to the group non-subjected to IR, the levels of DDAH and citrulline were increased and the *PRMT1* mRNA expression was increased as compared to the group without IR.

Asymmetric dimethylarginine inhibits the activity of all isoforms of NOS. Symmetric dimethylarginine does not have a direct impact on NO synthases, but may also downregulate their activity, acting as a competitor of the ARG transport through the cell membrane by the cationic amino acid transporter (CAT) y+ system.[17] In various pathological conditions (e.g., hypercholesterolemia, hyperglycemia, hyperhomocysteinemia, arterial hypertension, diabetes, and cardiac failure), the ADMA and SDMA levels increase, causing a reduction in the NO production and the dysfunction of endothelium.[4,18] Increased ADMA levels are also associated with liver damage during IR.[8] In patients with severely impaired liver function after a major hepatic resection, an increased level of ADMA was observed during the postoperative period.[19] In our work, the ADMA level during reperfusion was the highest in the untreated group subjected to IR, and was significantly higher than in the non-IR group. At 0.5 h of reperfusion, the SDMA level was the highest, which may be an additional reason for the inhibition of the NO production. Following 24 h of reperfusion, the concentrations of both methylarginines were similar in all the groups, which indicated that the observed changes were relatively reversible and that monitoring changes in those parameters during the experiment was more valuable than a single measurement at the end of reperfusion.

The level of ARG, being the main substrate for NOS, may also influence the bioavailability of NO.[20] In the case of ARG deficiency, eNOS assumes the uncoupled form and catalyzes a reaction with molecular oxygen instead of ARG, leading to the production of peroxide instead of NO.[21] The balance between the ADMA and ARG level is crucial and the ARG activity depends on the initial level of ADMA. In the case of hypercholesterolemia, the normalization of the endothelium-dependent relaxation after the ARG administration was observed only in patients with increased ADMA levels.[22,23] As reported by other researchers, and in accordance with our previous experiments, in both ischemic groups, the ARG level and the A/A ratio decreased during reperfusion.[24–26]

Asymmetric dimethylarginine is metabolized to citrulline and dimethylamine in a reaction catalyzed by DDAH.[4] Therefore, the reduced DDAH activity in the untreated group subjected to IR may be at least partially responsible for increased ADMA levels in our experiment. The citrulline concentration was significantly lowered, in line with the lowered DDAH activity. In pathological conditions, such as stress, ischemic heart disease, diabetes, fasting, or infections, an increased concentration of ADMA may also be a result of increased protein degradation.[27,28] Under IR injury, the protein methylation is upregulated to remove altered proteins.[27] The dimethylation of ARG in an asymmetric and symmetric configuration is a reaction catalyzed by PRMTs.[29] It has been reported that under conditions of hypertension or diabetes, the expression of *PRMT1* mRNA increases.[30] We also observed an increased mRNA expression for *PRMT1* in ischemic livers, which suggests extensive protein degradation under IR. In order to deepen this knowledge, our work should be complemented by a determination of the PRMT activity and its enzymatic protein level.

In rats not subjected to IR, the protective effect of sitagliptin could be seen in terms of the A/A ratio; when measured just before the surgery, it was higher in the treated group. The protective effect of sitagliptin may be, as in other studies, more evident in rats with diabetes than in healthy animals.[11,12] The ADMA level measured during the surgery was lower in the drug-treated non-ischemic group than in the untreated one. Similarly to the response to a decreased ADMA level, the DDAH activity after the surgery was lower in the drug-treated group compared to the untreated one, which was confirmed by a slightly lowered expression of *DDAH1* mRNA. This observation may suggest that sitagliptin is able to protect livers subjected to some degree of gentle manipulation during the surgery.

Based on previous experiments, in which the inhibition of the DPP-4 activity significantly reduced IR injury,[31,32] and also on literature data suggesting that sitagliptin protects the kidneys from IR injury mainly by inhibiting oxidative stress and the inflammatory reaction, we expected evident effects of sitagliptin on rat livers in IR

conditions.[11,12] The DDAH activity and the citrulline concentration significantly increased and were higher as compared to the non-ischemic group, probably as a response to a higher concentration of ADMA. The ARG level and the A/A ratio were significantly lower than in the non-ischemic group. The latter parameters were also lower than in untreated rats subjected to IR. This unexpected effect may question the protective effect of sitagliptin in IR conditions. The phenomenon may be explained by a need to reduce the concentration of NO, produced in large quantities under IR, and to augment cell injury.[33] In other works, sitagliptin or exenatide lowered an increased level of NO in diabetic rats undergoing renal IR.[11,34] Certainly, this issue needs to be clarified in further studies.

Only a few cases of hepatotoxicity of sitagliptin have been reported so far.[35,36] Conversely, reports on the beneficial effects of this drug on the liver, reflected by a slight decrease in transaminases, have also been published.[37,38] Sitagliptin or exenatide exerted a protective effect on the livers also in animals with IR renal injury.[11,34] In our research, no harmful effects of sitagliptin on the liver function were observed. Although the period of drug administration was rather short and the drug was given in small doses, the results suggest that rat livers were rather improved after the treatment, which was reflected by the lower ALT activity in the group receiving sitagliptin than in the untreated one.

The use of a partial liver ischemia model is one of the limitations of this work. The principal disadvantage is increased blood flow in non-ischemic part of the liver during induced ischemia of the median and left lateral lobe. Due to the collateral blood supply, the exchange of oxygen from the perfused to the ischemic part of the liver may take place. Therefore, differences in the examined parameters were not so evident. It is also worth noting that the livers used in this experiment were derived from healthy animals, and to our knowledge, the effect of sitagliptin in healthy animals is different from that in hypoglycemic ones. However, hyperglycemia is an additional factor contributing to the NO system and the results attained in the work on rats with induced diabetes are more evident. It is also difficult to compare the results obtained in healthy animals to those in diabetic ones.

In conclusion, a slight protective effect of sitagliptin on the ADMA-DDAH-NO pathway in rat livers not subjected to IR was shown in our study. A more evident impact was seen under IR conditions. Probably, the protective effect of sitagliptin is at least partly independent of the main hypoglycemic action of the drug – a fact that we also tried to demonstrate in this work. The results of the present work should be confirmed in future studies, involving other key factors taking part in the development of IR injury. The mechanism of action of sitagliptin during IR may be more complex and may be also associated with anti-inflammatory and antioxidant properties of the drug.[11,34]

References

1. Maslak E, Gregorius A, Chlopicki S. Liver sinusoidal endothelial cells (LSECs) function and NAFLD: NO-based therapy targeted to the liver. *Pharmacol Rep*. 2015;67(4):689–694.
2. Langer DA, Shah VA. A gas, an amino acid, and an imposter: The story of nitric oxide, L-arginine, and ADMA in portal hypertension. *Hepatology*. 2005;42(6):1255–1257.
3. Mòdol T, Natal C, Pérez de Obanos MP, et al. Apoptosis of hepatic stellate cells mediated by specific protein nitration. *Biochem Pharmacol*. 2011;81(3):451–458.
4. Buttery LD, Springall DR, Chester AH, et al. Inducible nitric oxide synthase is present within human atherosclerotic lesions and promotes the formation and activity of peroxynitrite. *Lab Invest*. 1996; 75(1):77–85.
5. Tran CT, Leiper JM, Vallance P. The DDAH/ADMA/NOS pathway. *Atheroscler Suppl*. 2003;4(4):33–40.
6. Fan C, Zwacka RM, Engelhardt JF. Therapeutic approaches for ischemia/reperfusion injury in the liver. *J Mol Med*. 1999;77(8):577–596.
7. Hines IN, Harada H, Flores S, Gao B, McCord JM, Grisham MB. Endothelial nitric oxide synthase protects the post-ischemic liver: Potential interactions with superoxide. *Biomed Pharmacother*. 2005;59(4): 183–189.
8. Martin-Sanz P, Olmedilla L, Dulin E, et al. Presence of methylated arginine derivatives in orthotopic human liver transplantation: Relevance for liver function. *Liver Transpl*. 2003;9(1):40–48.
9. Vallance P, Leiper J. Cardiovascular biology of the asymmetric dimethylarginine: Dimethylarginine dimethylaminohydrolase pathway. *Arterioscler Thromb Vasc Biol*. 2004;24(6):1023–1030.
10. Deacon CF. Dipeptidyl peptidase 4 inhibition with sitagliptin: A new therapy for type 2 diabetes. *Expert Opin Investig Drugs*. 2007;16(4): 533–545.
11. Vaghasiya J, Sheth N, Bhalodia Y, Manek R. Sitagliptin protects renal ischemia reperfusion induced renal damage in diabetes. *Regulatory Peptides*. 2011;166(1–3):48–54.
12. Chen YT, Tsai TH, Yang CC, et al. Exendin-4 and sitagliptin protect kidney from ischemia-reperfusion injury through suppressing oxidative stress and inflammatory reaction. *J Transl Med*. 2013;11:270–289.
13. Wolfgang J, Ingrid DM, Veerle M, et al. Inhibition of CD26/DPP IV attenuates ischemia/reprfuson injury in orthotopic mouse lung transplants: The pivotal role of vasoactive intestinal peptide. *Peptides*. 2010;31:585–591.
14. Morales AI, Vicente-Sanchez C, Jerkic M, et al. Effect of quercetin on metallothionein, nitric oxide synthase and cyclooxygenase-2 expression on experimental chronic cadmium nephrotoxicity in rats. *Toxicol Appl Pharmacol*. 2006;210(1–2):128–135.
15. Trocha M, Merwid-Ląd A, Chlebda-Sieragowska E, et al. Age-related changes in ADMA-DDAH NO pathway in rat liver subjected to partial ischemia followed by global reperfusion. *Exp Gerontol*. 2014;50:45–51.
16. Wiśniewski J, Fleszar MG, Piechowicz J, et al. A novel mass spectrometry-based method for simultaneous determination of asymmetric and symmetric dimethylarginine, l-arginine and l-citrulline optimized for LC-MS-TOF and LC-MS/MS. *Biomed Chromatogr*. 2017;31:1–11. doi: 10.1002/bmc.3994
17. Bode-Böger SM, Scalera F, Kielstein JT, et al. Symmetrical dimethylarginine: A new combined parameter for renal function and extent of coronary artery disease. *J Am Soc Nephrol*. 2006;17(4):1128–1134.
18. Gore MO, Lüneburg N, Schwedhelm E, et al. Symmetrical dimethylarginine predicts mortality in the general population: Observations from the Dallas heart study. *Arterioscler Thromb Vasc Biol*. 2013; 33(11):2682–2688.
19. Nijveldt RJ, Teerlink T, Siroen MP, et al. Elevation of asymmetric dimethylarginine (ADMA) in patients developing hepatic failure after major hepatectomy. *JPEN J Parenter Enteral Nutr*. 2004;28(6):382–387.
20. Lorin J, Zeller M, Guilland JC, Cottin Y, Vergely C, Rochette L. Arginine and nitric oxide synthase: Regulatory mechanisms and cardiovascular aspects. *Mol Nutr Food Res*. 2014;58(1):101–116.
21. Nguyen MC, Park JT, Jeon YG, et al. Arginase inhibition restores peroxynitrite-induced endothelial dysfunction via L-arginine-dependent endothelial nitric oxide synthase phosphorylation. *Yonsei Med J*. 2016;57(6):1329–1338.
22. Pope AJ, Karuppiah K, Cardounel AJ. Role of the PRMT-DDAH-ADMA axis in the regulation of endothelial nitric oxide production. *Pharmacol Res*. 2009;60(6):461–465.

23. Hornig B, Arakawa N, Böger RH, Bode-Böger SM, Frölich JC, Drexler H. Plasma levels of ADMA are increased and inversely related to endothelium-mediated vasodilation in patients with chronic heart failure: A new predictor of endothelial dysfunction? *Circulation*. 1998; 98(Suppl 1):318.
24. Dimitrow PP, Undas A, Bober M, Tracz W, Dubiel JS. Plasma biomarkers of endothelial dysfunction in patients with hypertrophic cardiomyopathy. *Pharmacol Rep*. 2007;59(6):715–720.
25. Trocha M, Merwid-Ląd A, Sozański T, et al. Influence of ezetimibe on ADMA-DDAH-NO pathway in rat liver subjected to partial ischemia followed by global reperfusion. *Pharmacol Rep*. 2013;65(1): 122–133.
26. Trocha M, Merwid-Ląd A, Szuba A, et al. Effect of simvastatin on nitric oxide synthases (eNOS, iNOS) and arginine and its derivatives (ADMA, SDMA) in ischemia/reperfusion injury in rat liver. *Pharmacol Rep*. 2010;62(2):343–351.
27. Tran CT, Leiper JM, Vallance P. The DDAH/ADMA/NOS pathway. *Atheroscler Suppl.* 2003;4(4):33–40.
28. Ferrigno A, Di Pasqua LG, Berardo C, Richelmi P, Vairetti M. Liver plays a central role in asymmetric dimethylarginine-mediated organ injury. *World J Gastroenterol*. 2015;21(17):5131–5137.
29. Maas R. Pharmacotherapies and their influence on asymmetric dimethylargine (ADMA). *Vasc Med*. 2005;10(Suppl 1):S49–S57.
30. Matsuguma K, Ueda S, Yamagishi S, et al. Molecular mechanism for elevation of asymmetric dimethylarginine and its role for hypertension in chronic kidney disease. *J Am Soc Nephrol*. 2006;17(8): 2176–2183.
31. Zhai W, Cardell M, De Meester I, et al. Ischemia/reperfusion injury: The role of CD 28/dipeptidyl-peptidase-IV-inhibition in lung transplantation. *Transplant Proc*. 2006;38(10):3369–3371.
32. Chang MW, Chen CH, Chen YC, at al. Sitagliptin protects rat kidneys from acute ischemia-reperfusion injury via upregulation of GLP-1 and GLP-1 receptors. *Acta Pharmacol Sin*. 2015;36(1):119–130.
33. Trocha M, Merwid-Ląd A, Szuba A, Sozański T, Magdalan J, Szeląg A. Asymmetric dimethylarginine synthesis and degradation under physiological and pathological conditions. *Adv Clin Exp Med*. 2010; 19(2):223–243.
34. Vaghasiya JD, Sheth NR, Bhalodia YS, Jivani NP. Exaggerated liver injury induced by renal ischemia reperfusion in diabetes: Effect of exenatide. *Saudi J Gastroenterol*. 2010;16(3):174–180.
35. Toyoda-Akui M, Yokomori H, Kaneko F, et al. A case of drug-induced hepatic injury associated with sitagliptin. *Intern Med*. 2011;50(9): 1015–1020.
36. Gross BN, Cross LB, Foard J, Wood Y. Elevated hepatic enzymes potentially associated with sitagliptin. *Ann Pharmacother*. 2010;44(2): 394–395.
37. Raz I, Hanefel M, Xu L, Caria C, Williams-Herman D, Khatami H. Efficacy and safety of the dipeptidyl peptidase-4 inhibitor sitagliptin as monotherapy in patients with type 2 diabetes mellitus. *Diabetologia*. 2006;49(11):2564–2571.
38. Nauck MA, Meininger G, Sheng D, Terranella L, Stein PP. Efficacy and safety of the dipeptidyl peptidase-4 inhibitor, sitagliptin, compared with the sulfonylurea, glipizide, in patients with type 2 diabetes inadequately controlled on metformin alone: A randomized, double-blind, non-inferiority trial. *Diabetes Obes Metab*. 2007;9(2):194–205.

The effect of caveolin-1 knockdown on interleukin-1β-induced chemokine (C-C motif) ligand 2 expression in synovial fluid-derived fibroblast-like synoviocytes from patients with rheumatoid arthritis

Dorota Trzybulska[1,A–F], Anna Olewicz-Gawlik[2,A,C–F], Jan Sikora[3,C–F], Magdalena Frydrychowicz[3,B–F], Agata Kolecka-Bednarczyk[3,A,C,E,F], Mariusz Kaczmarek[3,C,E,F], Paweł Hrycaj[3,4,A,C–F]

[1] Department of Rheumatology and Clinical Immunology, Poznan University of Medical Sciences, Poland
[2] Department of Infectious Diseases, Poznan University of Medical Sciences, Poland
[3] Department of Immunology, Poznan University of Medical Sciences, Poland
[4] Department of Rheumatology, Municipal Hospital, Kościan, Poland

A – research concept and design; B – collection and/or assembly of data; C – data analysis and interpretation; D – writing the article; E – critical revision of the article; F – final approval of the article

Advances in Clinical and Experimental Medicine, ISSN 1899-5276 (print), ISSN 2451-2680 (online) *Adv Clin Exp Med*. 2018;27(11):1491–1497

Address for correspondence
Dorota Trzybulska
E-mail: trzybulskadorota@gmail.com

Funding sources
None declared

Conflict of interest
None declared

Received on January 25, 2017
Reviewed on June 18, 2017
Accepted on June 30, 2017

Abstract

Background. Rheumatoid arthritis (RA) is a chronic autoimmune disease leading to destructive changes in peripheral joints and their irreversible deformity. The influx of chemoattractant-mediated inflammatory cells to the joints is one of the main features of RA.

Objectives. The aim of this study was to investigate the effect of a knockdown of caveolin-1 (*CAV1*), a known regulator of multiple cell signaling pathways, on chemokine (C-C motif) ligand 2/monocyte chemoattractant protein-1 (*CCL2/MCP-1*) expression in synovial fluid-derived fibroblast-like synoviocytes (sfd-FLSs) obtained from patients with RA.

Material and methods. Primary cell cultures of sfd-FLSs were established from RA synovial fluids. Cells were transiently transfected with small interfering RNA (siRNA) specific for *CAV1*, and then incubated with interleukin (IL)-1β to induce *CCL2* expression. The expression levels of *CAV1* and *CCL2* were assessed at transcript level, using quantitative polymerase chain reaction (qPCR) and at protein level by enzyme-linked immunosorbent assay (ELISA) and western blotting analysis.

Results. A transient *CAV1* knockdown in sfd-FLSs resulted in a decrease in the IL-1β-induced *CCL2* mRNA expression level vs non-transfected cells and cells transfected with non-targeting siRNA. The concentration of secreted CCL2 was not affected significantly.

Conclusions. Our study demonstrates that *CCL2* expression in sfd-FLSs is CAV1-dependent, but only at transcript level. As the function of *CAV1* has not been unequivocally determined, more studies are needed to confirm the role of *CAV1* in inflammatory processes related to RA.

Key words: rheumatoid arthritis, caveolin-1, C-C chemokine ligand 2/monocyte chemoattractant protein-1, synoviocytes

DOI
10.17219/acem/75611

Introduction

Rheumatoid arthritis (RA) is a chronic autoimmune disease resulting in destructive changes in peripheral joints, and subsequently in their irreversible deformity. Rheumatoid arthritis pathogenesis is extremely complex and, despite the identification of many compelling contributory factors, it has not been fully explained.[1]

In RA, cells constituting the intimal lining layer of the synovium proliferate in an uncontrolled manner and form pannus tissue.[2] There are 2 predominant cell types participating in synovial hyperplasia. Type A synoviocytes are terminally differentiated cells with little capacity to proliferate and uneven distribution in the synovial membrane; they activate synoviocytes type B, also called fibroblast-like synoviocytes (FLSs), by producing pro-inflammatory cytokines, chemokines and growth factors.[2,3] Fibroblast-like synoviocytes represent a specialized type of cells and their implication in RA pathogenesis is considered in terms of 2 aspects: destructive changes in joints and chronic inflammation.[2–6] Fibroblast-like synoviocytes present in pannus tissue secrete matrix metalloproteinases, cathepsins and aggrecanases, destroying cartilage which, in consequence, leads to bone resorption.[6] Fibroblast-like synoviocytes promote the influx of chemoattractant-mediated inflammatory cells into the joint cavity in response to the joint milieu, factors such as interleukin (IL)-1β or tumor necrosis factor alpha (TNFα), which is one of the main features of RA.[4,6–8] Secreted C-C chemokine ligand 2 (CCL2) chiefly induces monocytes migrating into the joints, where they differentiate into exudate macrophages, but it can also affect T cells, natural killer cells and basophils.[5] Activated monocytes/macrophages play an important role in the maintenance of inflammation in RA by producing pro-inflammatory cytokines and mediators responsible for the development of synovitis. Therefore, the inhibition of their multi-step migration, driven by a chemoattractant gradient toward the sites of inflammation, is of therapeutic value.[2,9]

Together, the processes in joints perpetuate RA development by recruiting and retaining inflammatory cells, pannus hyperplasia and bone damage. It is believed that effective therapy to restore the balance between pro- and anti-inflammatory cytokines should aim not only at individual cytokines but also at signaling molecules responsible for their production.[10] Thus, the key issue is to find a crucial molecular process which would enable us to control the course of RA. Caveolin-1 (CAV1), expressed in 2 isoforms (α and β), is one of the major structural components of caveolae and has a number of signaling functions.[11,12] This protein contains a scaffolding domain in the position 82–101, which, by binding to signaling molecules (e.g., Src kinases, endothelial nitric oxide synthase 3, G protein α subunits, or protein kinase C), is able to negatively regulate cell signaling.[11,13–15] On the other hand, CAV1α has the ability to positively regulate signal transduction intracellularly through phosphorylation on tyrosine-14 (Tyr14), which can happen in response to cellular stress, growth factors or stimulation with hormones.[16,17]

Regarding inflammatory disorders, *CAV1* could either prevent or induce inflammation, depending on cellular context.[11,18–21] In this study, we decided to investigate the impact of *CAV1* on *CCL2* expression in synovial fluid-derived fibroblast-like synoviocytes (sfd-FLSs) obtained from patients with RA.

Material and methods

Patients

The protocol for this study was approved by the Bioethics Committee of Poznan University of Medical Sciences (Poland). Synovial fluids were aspirated for therapeutic reasons from inflammatory knee joint effusions from 3 RA patients (2 women/1 man; age: 48–52 years, disease duration: 1.5–20.5 years) fulfilling both the 1987 American College of Rheumatology (ACR)[22] and the 2010 American College of Rheumatology/European League Against Rheumatism (ACR/EULAR) classification criteria.[23] Written informed consent was obtained from every patient before any study procedure was carried out.

Cell culture

Primary cell cultures of sfd-FLSs, which could be an alternative to FLSs derived from tissues after surgery,[24] were established from RA synovial fluids based on the procedure described by Scanu et al.[25] To summarize briefly, fluids were collected in tubes containing ethylenediaminetetraacetic acid (EDTA), diluted twice with sterile phosphate-buffered saline (PBS) and centrifuged at 1500 rpm for 10 min at room temperature. Pellets were suspended in a complete Dulbecco's Modified Eagle's medium (DMEM) (Sigma, St. Louis, USA) with 10% fetal bovine serum (Biochrom AG, Berlin, Germany) and antibiotic-antimycotic containing 10000 units/mL of penicillin G, 10 mg/mL of streptomycin sulfate and 25 µg/mL of amphotericin B (ABAM; Sigma). The cells were placed into T-25 flasks and incubated under standard conditions (37°C, 5% CO_2 in a humidified atmosphere). After 24 h, non-adherent cells were washed out and fresh DMEM was added to the cells. The medium was changed twice a week. Cells from passages 3–10 were used for the study. Synovial fluid-derived fibroblast-like synoviocytes were checked for the presence of macrophages by flow cytometry. The cells were stained with the following antibodies: phycoerythrin-conjugated CD14 (clone MΦP9, 345785; BD, Franklin Lakes, USA), allophycocyanin/Cy7-conjugated CD45 (clone 2D-1, 348815; BD) and allophycocyanin-conjugated CD163 (clone 215927, FAB1607A; R&D Systems, Minneapolis, USA) for 20 min. Next, 500 µL of fluorescence-activated cell sorting (FACS)-lysing solution (BD) was added in a proportion

of 1:10 and incubated for 10 min, protected from light and at room temperature. The cells were washed twice with PBS by centrifugation at 1200 g for 4 min, suspended in 500 µL of PBS, and then subjected to flow cytometry on FACSCanto II (BD). A total of 30,000 events per sample were acquired. The results were analyzed with FACSDiva software (BD Biosciences, Franklin Lakes, USA). Cultured cells did not show markers characteristic for macrophages.

A dose-response study of IL-1β on *CCL2* expression in sfd-FLSs

As FLSs lose their primary phenotype with increasing passage number and become quiescent by passage 3, they require exposure to IL-1β to restore their ability to produce chemokines.[2] To determine the most effective IL-1β dose inducing *CCL2* expression, FLSs were seeded on 6-well plates (1×10^5 cells/well) and serum starved for 24 h. After that, the cells were washed with PBS and treated with different doses of IL-1β (Sigma) (0.1 ng/mL, 1 ng/mL, 5 ng/mL, and 10 ng/mL) diluted in serum-free Opti-Minimal Essential Medium (MEM) (Gibco; Life Technologies, Carlsbad, USA) or left untreated. The conditioned media were collected and frozen immediately after a 2-hour incubation. The cells were washed with PBS, lysed with TRIzol (Sigma) and stored at –70°C for further RNA extraction.

Optimization of transfection conditions

Transfection conditions were optimized for 1×10^5 cells/well with 0.2% and 0.4% v/v concentrations of Lipofectamine2000 (Life Technologies) by using BLOCK-iT™ Fluorescent Oligo (Life Technologies, Carlsbad, USA) and Opti-MEM. Small interfering RNA (siRNA) uptake was assessed under a fluorescent microscope. Intensive fluorescence was visible at a minimal final concentration of labeled siRNA (10 nM) and 0.2% v/v Lipofectamine2000, which indicated high transfection efficiency (not shown). Such conditions were tested for *CAV1*-siRNA and control siRNA at final concentrations of 10 nM, 50 nM and 100 nM. All the transfections were performed according to the protocols provided by the manufacturer. Cell viability was assesses by the trypan blue exclusion test (Sigma).

Experiment protocol

The cells were seeded on 6-well plates (1×10^5 cells/well) in antibiotic- and serum-free DMEM 24 h before transfection. Next, they were washed with Opti-MEM and transiently transfected with siRNA specific for *CAV1* or control siRNA (at a final concentration of 50 nM) (sc-29241 and sc-37007; Santa Cruz Biotechnology, Dallas, USA) in 2.5 mL of Opti-MEM by using 0.2% v/v Lipofecta-mine2000, or left untreated. Additionally, to check transfection efficiency, each time the cells were transfected with fluorescein labeled siRNAs BLOCK-iT™ and the uptake of siRNA was assessed under a fluorescent microscope. Based on information from the previous report and preliminary stages of this study, the cells were re-transfected after 48 h to counteract excessive *CAV1* expression under the influence of IL-1β activity.[26] Next, they were stimulated for 2 h with 1 ng/mL IL-1β diluted in Opti-MEM to induce *CCL2* expression. Simultaneously, control incubations with non-transfected cells and without IL-1β induction were conducted. After incubation, supernatants were collected and frozen immediately at –70°C. The cells were washed with cold PBS and lysed using TRIzol for RNA extraction or an radioimmunoprecipitation assay (RIPA) buffer (Sigma) for protein isolation. Three independent experiments were conducted on cells obtained from 3 RA synovial fluids.

Total RNA extraction and cDNA synthesis

Total cellular RNA extraction was performed using TRIzol. The concentration and purity of RNA were measured using a NanoDrop1000 spectrophotometer (Thermo Scientific, Waltham, USA). Total RNA in a dose of 0.5 µg was reverse-transcribed into complementary DNA (cDNA) using a QuantiTect® Reverse Transcription Kit (Qiagen, Hilden, Germany) in accordance with the protocol provided by the manufacturer.

Quantitative real-time polymerase chain reaction

The primers used in this study (Table 1) were synthesized by DNA Sequencing and Oligonucleotides Synthesis Laboratory (Institute of Biochemistry and Biophysics, the Polish Academy of Sciences, Warszawa, Poland; www.oligo.pl). Quantitative polymerase chain reactions

Table 1. Primers used for real-time PCR

Gene name (symbol)	Accession No. (NCBI)	Sequences of primers 5'→3' (exon numbers)	Product length [bp]
Porphobilinogen deaminase (*PBGD*)	NM_000190	GCCAAGGACCAGGACATC (11) TCAGGTACAGTTGCCCATC (12/13)	160
Chemokine (C-C motif) ligand 2 (*CCL2*)	NM_002982	AGAAGAATCACCAGCAGCAAGT (2) GGAATCCTGAACCCACTTC (3)	102
Caveolin-1 (*CAV1*)	NM_001753	GACCCTAAACACCTCAAC (2) AACCAGTATTTCGTCACAG (3)	134

PCR – polymerase chain reaction; NCBI – National Center for Biotechnology.

(qPCRs) were carried out on a Corbett Rotor-Gene 6000 with Rotor-Gene 6000 Series Software 1.7 (Corbett Life Science, Sydney, Australia), employing a QuantiFast SYBR® Green PCR Kit (Qiagen). To determine the relative mRNA levels of the genes studied, standard curves were generated using a mix of randomly pooled cDNA samples in six 0.6-fold dilution series of cDNA. The thermal cycling conditions were as follows: denaturation at 95°C for 5 min, followed by 45 cycles of 95°C for 5 s and 60°C for 30 s and melting curve creation: 65–97°C. The levels of *CCL2* and *CAV1* mRNA were normalized to porphobilinogen deaminase (*PBGD*) mRNA levels. The results are expressed in arbitrary units as a ratio of the studied gene level to reference gene level. The reactions were done in triplicate.

Sodium dodecyl sulfate–polyacrylamide gel electrophoresis and western blotting analysis

Equal amounts of protein (20 µg) were boiled for 10 min in Laemmli buffer, and then separated in 12% sodium dodecyl sulfate (SDS) polyacrylamide gel. Proteins from gel were transferred onto a polyvinylidene difluoride (PVDF) membrane using the Mini Semi-dry Blotting System (EPS-BIO, Chennai, India). The blots were cut into 2 pieces so as to identify CAV1 (~22 kDa) and β-actin (~43 kDa), and blocked with 5% w/v skimmed milk dissolved in Tris-buffered saline with Tween 20 (TBS-T). Pieces with lower-molecular-weight proteins were probed with a primary antibody for CAV1 (AP16383PU-N; Acris Antibodies, Herford, Germany) diluted 1:5,000 in 2% skimmed milk in TBS-T for 2 h. Afterwards, this was washed with TBS-T and incubated for 1 h with a horseradish peroxidase (HRP)-conjugated secondary donkey anti-goat antibody (sc-2033; Santa Cruz Biotechnology) diluted 1:20,000 in 2% skimmed milk in TBS-T. The second piece of membrane was incubated with a HRP-conjugated polyclonal anti-β-actin antibody (sc-1616; Santa Cruz Biotechnology). The proteins were visualized as bands using the SuperSignal West Femto Maximum Sensitivity Substrate (Thermo Scientific, Rockford, USA) by exposing the membrane to X-ray film. The proteins fold change was quantified using ImageJ software v. 1.47 (NIH, Bethesda, USA). The band intensities for CAV1 were normalized to β-actin as a loading control. The CAV/β-actin ratio for the control siRNA was assumed to be 1.

Enzyme-linked immunosorbent assay

Concentrations of secreted CCL2 were determined using a commercially available enzyme-linked immunosorbent assay (ELISA) kit for recombinant human CCL2/monocyte chemoattractant protein-1 (MCP-1) (R&D) in accordance with the manufacturer's protocol. The absorbance was measured with an ELISA plate reader ELx800 (Bio-Tek Instruments, Inc., Winooski, USA) using KC Junior analysis software (Bio-Tek Instruments, Inc.). The mean minimum detectable dose of CCL2 was 1.7 pg/mL.

Statistical analysis

The calculations were carried out with Microsoft Excel 2010 and GraphPad Prism v. 6.0 (GraphPad Software, La Jolla, USA). The data was analyzed by a two-way analysis of variance (ANOVA) followed by Šidák's test, a one-way ANOVA followed by Tukey's honest significant difference (HSD) test or, when compared to a single control, by Dunnett's test. The results are expressed as means ± standard deviation (SD). The differences were considered to be statistically significant at $p < 0.05$.

Results

IL-1β induces *CCL2* expression in sfd-FLSs, but not in a concentration-dependent manner

A statistically significant increase in *CCL2* expression both at transcript and protein level was seen after a 2-h incubation. Interleukin-1β at a concentration of 1 ng/mL was used for further incubations. The data revealed a non-linear relationship between an increasing IL-1β concentration and *CCL2* expression in sfd-FLSs (Fig. 1).

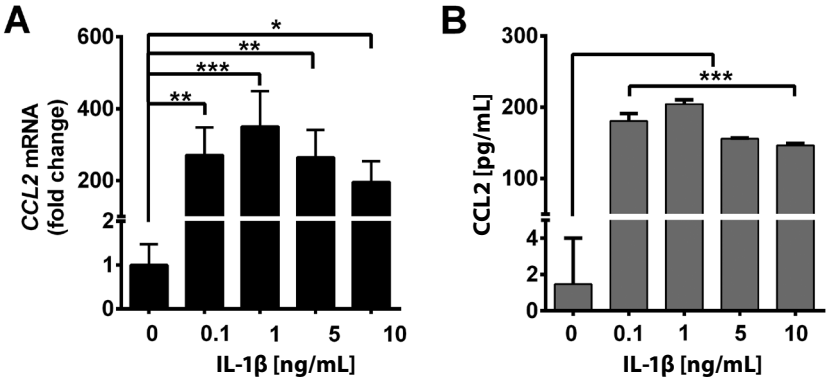

Fig. 1. The effect of IL-1β on the expression and production of *CCL2* in sfd-FLSs

Twenty-four hours before the experiment 1×10^5 cells/well were seeded on 6-well plates in DMEM without serum. The next day, the cells were incubated for 2 h with indicated concentrations of IL-1β. The relative *CCL2* transcript levels were measured using qPCR with *PBGD* as an internal reference gene. A) The CCL2 concentrations in conditioned medium were measured using ELISA. B) The graph bars show data as means ±SD from 3 individual experiments; the differences between the means were analyzed by the one-way ANOVA followed by Dunnett's test; * $p < 0.05$; ** $p < 0.01$; *** $p < 0.001$.

IL-β – interleukin-1β; *CCL2* – chemokine (C-C motif) ligand 2; sfd-FLSs – synovial fluid-derived fibroblast-like synoviocytes; DMEM – Dulbecco's Modified Eagle's Medium; qPCR – quantitative polymerase chain reaction; *PBGD* – porphobilinogen deaminase; ELISA – enzyme-linked immunosorbent assay.

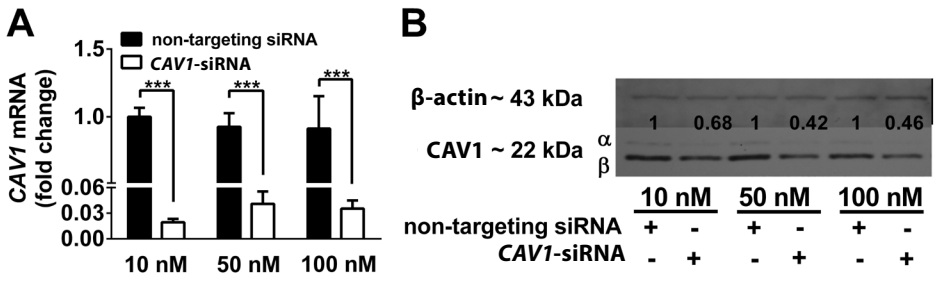

Fig. 2. Small interfering RNA (siRNA)-mediated knockdown of *CAV1* expression in sfd-FLSs

Synovial fluid-derived fibroblast-like synoviocytes were transfected with *CAV1*-siRNA and control siRNA with indicated final concentrations. A – the relative *CAV1* transcript level was assessed by qPCR with *PBGD* as an internal reference gene. The results are presented as a fold decrease of *CAV1* expression compared with non-targeting siRNA at 48 h after transfection. The graph bars show data as means ±SD from 3 individual experiments; the differences between the means were analyzed by the two-way ANOVA followed by Šídák's test; *** $p < 0.001$. B – The *CAV1* knockdown was assessed by western blotting analysis (both isoforms were visible after longer exposure to X-ray film). Cell lysates were prepared as described in the "Material and methods" section. Equal amounts of proteins were subjected to SDS–PAGE, blotted into a PVDF membrane and incubated with anti-CAV1 and anti-β-actin antibodies. The band intensities for CAV1 were normalized to β-actin as a loading control. The CAV1/β-actin ratio for the control siRNA was assumed to be 1.

CAV1 – caveolin-1; sfd-FLSs – synovial fluid-derived fibroblast-like synoviocytes; qPCR – quantitative polymerase chain reaction; *PBGD* – porphobilinogen deaminase; SDS–PAGE – sodium dodecyl sulfate–polyacrylamide gel electrophoresis; PVDF – polyvinylidene difluoride.

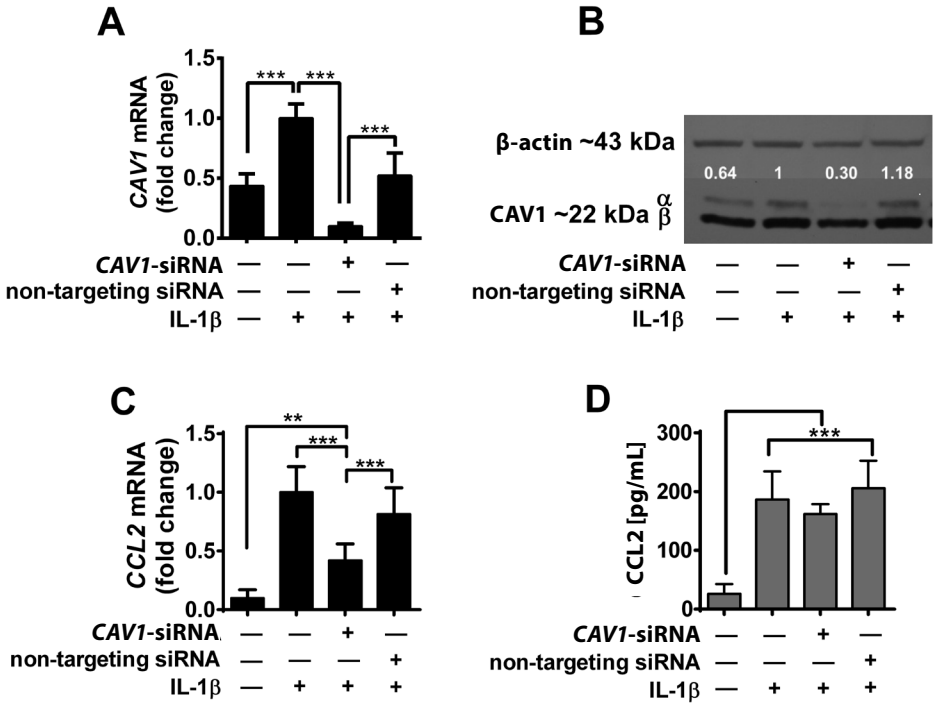

Fig. 3. *CAV1* knockdown efficacy and effect on *CCL2* expression in sfd-FLSs

Twenty-four hour before the experiment, 1×10^5 cells/well were seeded on 6-well plates in DMEM without serum. The following day, the cells were transfected with *CAV1*-siRNA, control siRNA or non-transfected. After 48 h, the cells were re-transfected and incubated with IL-1β to induce *CCL2* expression. The *CCL2* and *CAV1* transcript levels were measured using qPCR with *PBGD* as an internal reference gene (A and C). The *CAV1* knockdown was assessed by western blotting analysis (both isoforms were visible after longer exposure with predominant β isoform). The band intensities for CAV1 were normalized to β-actin as a loading control. The CAV1/β-actin ratio for the control siRNA was assumed to be 1 (B). The concentrations of CCL2 in conditioned media were measured using ELISA (D). The graph bars show data as means ±SD from 3 independent experiments conducted on sfd-FLSs obtained from each patient; the differences were tested by the one-way ANOVA followed by Tukey's HSD test; ** $p > 0.01$; *** $p < 0.001$.

CAV1 – caveolin-1; *CCL2* – chemokine (C-C motif) ligand 2; sfd-FLSs – synovial fluid-derived fibroblast-like synoviocytes; DMEM – Dulbecco's Modified Eagle's Medium; IL-β – interleukin-1β; qPCR – quantitative polymerase chain reaction; *PBGD* – porphobilinogen deaminase; ELISA – enzyme-linked immunosorbent assay.

CAV1 knockdown in sfd-FLSs impairs *CCL2* transcription

Transfection with siRNA did not affect sfd-FLSs viability. As CAV1 is a long-lived protein, transcript level did not correspond with protein level after transfections.[27] For further transfections, 50 nM siRNA was chosen (Fig. 2). A longer exposure (for 1 min) of the PVDF membrane blot to X-ray film revealed both *CAV1* isoforms with predominant β isoform.

The CAV1 level was transiently knocked down by about 70% in comparison with cells transfected with control

siRNA or non-transfected cells. Incubation with IL-1β caused an increase in *CAV1* expression, which is in line with the previous report (Fig. 3A,3B).[26] Transcription of *CCL2* in cells transfected with *CAV1*-siRNA was significantly suppressed (approx. 2-fold) in comparison with non-transfected cells and cells transfected with control siRNA (Fig. 3C). The *CAV1* knockdown caused no significant change in the concentration of secreted CCL2 in comparison with cells transfected with control siRNA and non-transfected cells (Fig. 3D).

Discussion

Many chemoattractants overproduced by cells residing in the synovium enhance leukocyte migration into the joints, which is the main characteristic of RA. The activation of FLSs is believed to be the key process promoting inflammation and joint damage in RA.[5] In this study, we checked whether the knockdown of *CAV1*, a regulator of intracellular signal transduction, affects *CCL2* expression in sfd-FLSs obtained from RA synovial fluid.[14] Our results showed that under the study conditions, the *CAV1* knockdown significantly impaired IL-1β-induced *CCL2* expression, but only at transcript level. To date, there have been no similar reports on associations between *CAV1* and chemoattractants in cells important for RA development.

Majkova et al. showed that the *CAV1* knockdown almost completely prevented *CCL2* expression induced by 3,3',4,4'-tetrachlorobiphenyl (PCB77) in endothelial cells.[28] These results were also confirmed in vivo on LDL-R$^{-/-}$/Cav1$^{-/-}$ mice. A similar expression pattern was observed at both the transcript and protein level for IL-6 – another important molecule stimulating immune responses. Their results suggested that *CAV1* can be a common regulator of inflammatory responses caused by toxic properties of PCB77. It was also presented that PCB77-induced *CCL2* expression depends on p38 mitogen-activated protein kinases (MAPK) and c-Jun amino-terminal kinase (JNK). They suggested that functional caveolae are essential in order to regulate *CCL2* expression.[28]

Li et al. reported that *CAV1* expression may enhance inflammation by an increased leukocyte influx. In their study on retinitis in Cav1$^{-/-}$ mice, the levels of CCL2, CXCL1, IL-6, and IL-1β, which are downstream effectors of the Toll-like receptor (TLR)-4 signaling pathway, were reduced.[29] It is highly possible that *CAV1* could also be responsible for the expression of pro-inflammatory molecules also in FLSs. TLR-2, -3 and -4 are predominant and the most functional TLRs in this cell type.[29] An inflamed joint and its milieu are the source of different potential TLR ligands and CAV1 may be one of these proteins which efficiently enhance TLR4 signaling, followed by the production of pro-inflammatory cytokines.[30] Another point of importance is that CAV1 phosphorylation on Tyr14 induces its interaction with TLR4 and leads to nuclear factor kappa-light-chain-enhancer of activated B cells (NF-κB) activation.[31]

Lv et al. reported that the overexpression of CAV1 in mouse lung alveolar type-1 cells enhances the phosphorylation and expression of p38 MAPK and NF-κB, which induce the expression of inflammatory cytokines such as IL-6 and TNF-α. Thereby, it was additionally proven that *CAV1* could be an important activator of inflammation.[32]

Based on molecular studies on the promoter region of *CCL2*, some cis-regulatory elements and trans-acting factors involved in *CCL2* expression were identified. It was shown that 2 NF-κB-binding sites located 2.6 kb from the transcription initiation site are pivotal to *CCL2* expression in response to stimuli such as IL-1β and TNF-α.[33,34] This fact together with the study by Garrean et al. and studies mentioned above point to the importance of CAV1 in NF-κB activation, which could partially explain the inhibition of *CCL2* expression at transcript level in sfd-FLSs with diminished CAV1 expression.[35]

Studies showing the pro-inflammatory character of *CAV1* are not consistent with the results presented by Gardner et al.[36] In a study on the hepatotoxic activity of paracetamol, they revealed an elevated expression of *CCL2* in the liver obtained from Cav1$^{-/-}$ mice. In this case, this was linked to the "positive" effect of monocyte influx, leading to repairing processes mediated by macrophages with an anti-inflammatory phenotype.[36]

Looking at all the research conducted on animal models, it can be concluded that *CCL2* expression is *CAV1*-dependent, but only to a certain extent. Our results suggest that CCL2 secretion by sfd-FLSs obtained from RA patients could be regulated at the posttranslational level. It would be worth seeing if the disproportions between CCL2 transcript and protein levels could be a result of the activity of some regulators controlled by the particular CAV1 isoform. This is due to the fact that only α isoform has a complete sequence and undergoes phosphorylation on Tyr14, which facilitates binding both inductors and effector proteins in signaling pathways.[37] Kogo et al. suggested that the ratio of the 2 isoforms may vary depending on the cell type.[38] We found that CAV1β (lacking N-terminal 31 amino acids) is predominant in sfd-FLSs.[39] Therefore, it seems that the functional diversity of both isoforms should be considered when interpreting the role of *CAV1* in a specific molecular context.

As some stimuli may act differently on various cell types, *CCL2* expression could also vary among different cells and for different kinds of stimuli, and, as was shown in our study, the secreted CCL2 level does not always correspond with its transcript level, especially in cells with an impaired *CAV1* expression.[35] Here, it should be also noted that in vivo, the final level of a particular cytokine is very often an effect of complex, reciprocal synergistic and antagonistic associations between other cytokines. Additionally, understanding epigenetic mechanisms (DNA methylation and histone modifications as well as regulation by small non-coding RNAs) can be helpful in current studies on the pathogenesis of RA. A recent study by Li et al. presented that targeting *CAV1* by restoring the

microRNA-192 levels in FLSs led to their apoptosis and the inhibition of cell proliferation,[40] and possibly by regulating the expression of other relevant genes in a direct (chemokine (C-X-C motif) ligand 2; source: miRDB-an online database (http://www.mirdb.org/cgi-bin/search.cgi?searchType=miRNA&searchBox=hsa-miR-192-5p&full=1) or indirect way. To summarize, the normalization of pathological processes in RA, preferably by aiming at one pivotal factor, is highly desirable but, so far, unattainable.

Conclusions

Our results show a significant role of *CAV1* in *CCL2* transcription induction in RA sfd-FLSs under the influence of IL-1β. However, processes involving *CAV1* still require more profound research into a broader spectrum of cytokines in auto-inflammatory disorders.

References

1. Bax M, van Heemst J, Huizinga TW, Toes RE. Genetics of rheumatoid arthritis: What have we learned? *Immunogenetics*. 2011;63(8):459–466.
2. Bartok B, Firestein GS. Fibroblast-like synoviocytes: Key effector cells in rheumatoid arthritis. *Immunol Rev.* 2010;233(1):233–255.
3. Iwanaga T, Shikichi M, Kitamura H, Yanase H, Nozawa-Inoue K. Morphology and functional roles of synoviocytes in the joint. *Arch Histol Cytol.* 2000;63(1):17–31.
4. Filer A. The fibroblast as a therapeutic target in rheumatoid arthritis. *Curr Opin Pharmacol.* 2013;13(3):413–419.
5. Iwamoto T, Okamoto H, Toyama Y, Momohara S. Molecular aspects of rheumatoid arthritis: Chemokines in the joints of patients. *FEBS J.* 2008;275(18):4448–4455.
6. Juarez M, Filer A, Buckley CD. Fibroblasts as therapeutic targets in rheumatoid arthritis and cancer. *Swiss Med Wkly.* 2012;142:w13529.
7. Bottini N, Firestein GS. Duality of fibroblast-like synoviocytes in RA: Passive responders and imprinted aggressors. *Nat Rev Rheumatol.* 2013;9(1):24–33.
8. Harigai M, Hara M, Yoshimura T, Leonard EJ, Inoue K, Kashiwazaki S. Monocyte chemoattractant protein-1 (MCP-1) in inflammatory joint diseases and its involvement in the cytokine network of rheumatoid synovium. *Clin Immunol Immunopathol.* 1993;69(1):83–91.
9. Thurlings RM, Wijbrandts CA, Bennink RJ, et al. Monocyte scintigraphy in rheumatoid arthritis: The dynamics of monocyte migration in immune-mediated inflammatory disease. *PLoS ONE.* 2009;4(11):e7865.
10. Jorgensen C, Apparailly F. Prospects for gene therapy in inflammatory arthritis. *Best Pract Res Clin Rheumatol.* 2010;24(4):541–552.
11. Fujimoto T, Kogo H, Nomura R, Une T. Isoforms of caveolin-1 and caveolar structure. *J Cell Sci.* 2000;113(19):3509–3517.
12. Anderson RG. The caveolae membrane system. *Annu Rev Biochem.* 1998;67:199–225.
13. Torres VA, Tapia JC, Rodríguez DA, et al. Caveolin-1 controls cell proliferation and cell death by suppressing expression of the inhibitor of apoptosis protein survivin. *J Cell Sci.* 2006;119(9):1812–1823.
14. Boscher C, Nabi IR. Caveolin-1: Role in cell signaling. *Adv Exp Med Biol.* 2012;729:29–50.
15. Luanpitpong S, Talbott SJ, Rojanasakul Y, et al. Regulation of lung cancer cell migration and invasion by reactive oxygen species and caveolin-1. *J Biol Chem.* 2010;285(50):38832–38840.
16. Head BP, Insel PA. Do caveolins regulate cells by actions outside of caveolae? *Trends Cell Biol.* 2006;17(2):51–57.
17. Kimura A, Mora S, Shigematsu S, Pessin JE, Saltiel AR. The insulin receptor catalyzes the tyrosine phosphorylation of caveolin-1. *J Biol Chem.* 2002;277(33):30153–30158.
18. Wang XM, Kim HP, Nakahira K, Ryter SW, Choi AM. The heme oxygenase-1/carbon monoxide pathway suppresses TLR4 signaling by regulating the interaction of TLR4 with caveolin-1. *J Immunol.* 2009;182(6):3809–3818.
19. Catalán V, Gómez-Ambrosi J, Rodríguez A, et al. Expression of caveolin-1 in human adipose tissue is upregulated in obesity and obesity-associated type 2 diabetes mellitus and related to inflammation. *Clin Endocrinol (Oxf).* 2008;68(2):213–219.
20. Zhang PX, Murray TS, Villella VR, et al. Reduced caveolin-1 promotes hyperinflammation due to abnormal heme oxygenase-1 localization in lipopolysaccharide-challenged macrophages with dysfunctional cystic fibrosis transmembrane conductance regulator. *J Immunol.* 2013;190(10):5196–5206.
21. Takizawa N, Sawada S, Chosa N, Ishisaki A, Naruishi K. Secreted caveolin-1 enhances periodontal inflammation by targeting gingival fibroblasts. *Biomed Res.* 2013;34(1):1–11.
22. Arnett FC, Edworthy SM, Bloch DA, et al. The American Rheumatism Association 1987 revised criteria for the classification of rheumatoid arthritis. *Arthritis Rheum.* 1988;31(3):315–324.
23. Aletaha D, Neogi T, Silman AJ, et al. 2010 Rheumatoid arthritis classification criteria: an American College of Rheumatology/European League Against Rheumatism collaborative initiative. *Arthritis Rheum.* 2010;62(9):2569–2581.
24. Stebulis JA, Rossetti RG, Atez FJ, Zurier RB. Fibroblast-like synovial cells derived from synovial fluid. *J Rheumatol.* 2005;32(2):301–306.
25. Scanu A, Oliviero F, Braghetto L, et al. Synoviocyte cultures from synovial fluid. *Reumatismo.* 2007;59(1):66–70.
26. Baugé C, Girard N, Leclercq S, Galéra P, Boumédiene K. Regulatory mechanism of transforming growth factor beta receptor type II degradation by interleukin-1 in primary chondrocytes. *Biochim Biophys Acta.* 2012;1823(5):983–986.
27. Hayer A, Stoeber M, Ritz D, Engel S, Meyer HH, Helenius A. Caveolin-1 is ubiquitinated and targeted to intralumenal vesicles in endolysosomes for degradation. *J Cell Biol.* 2010;191(3):615–629.
28. Majkova Z, Smart E, Toborek M, Hennig B. Up-regulation of endothelial monocyte chemoattractant protein-1 by coplanar PCB77 is caveolin-1-dependent. *Toxicol Appl Pharmacol.* 2009;237(1):1–7.
29. Li X, Gu X, Boyce TM, Zheng M, et al. Caveolin-1 increases proinflammatory chemoattractants and blood-retinal barrier breakdown but decreases leukocyte recruitment in inflammation. *Invest Ophthalmol Vis Sci.* 2014;55(10):6224–6234.
30. Mirza MK, Yuan J, Gao XP, et al. Caveolin-1 deficiency dampens Toll-like receptor 4 signaling through eNOS activation. *Am J Pathol.* 2010;176(5):2344–2351.
31. Jiao H, Zhang Y, Yan Z, et al. Caveolin-1 Tyr14 phosphorylation induces interaction with TLR4 in endothelial cells and mediates MyD88-dependent signaling and sepsis-induced lung inflammation. *J Immunol.* 2013;191(12):6191–6199.
32. Lv XJ, Li YY, Zhang YJ, Mao M, Qian GS. Over-expression of caveolin-1 aggravate LPS-induced inflammatory response in AT-1 cells via up-regulation of cPLA2/p38 MAPK. *Inflamm Res.* 2010;59(7):531–541.
33. Yadav A, Saini V, Arora S. MCP-1: Chemoattractant with a role beyond immunity: A review. *Clin Chim Acta.* 2010;411(21–22):1570–1579.
34. Ueda A, Okuda K, Ohno S, et al. NF-kappa B and Sp1 regulate transcription of the human monocyte chemoattractant protein-1 gene. *J Immunol.* 1994;153(5):2052–2063.
35. Garrean S, Gao XP, Brovkovych V, et al. Caveolin-1 regulates NF-kappaB activation and lung inflammatory response to sepsis induced by lipopolysaccharide. *J Immunol.* 2006;177(7):4853–4860.
36. Gardner CR, Gray JP, Joseph LB, et al. Potential role of caveolin-1 in acetaminophen-induced hepatotoxicity. *Toxicol Appl Pharmacol.* 2010;245(1):36–46.
37. Li S, Seitz R, Lisanti MP. Phosphorylation of caveolin by src tyrosine kinases. The alpha-isoform of caveolin is selectively phosphorylated by v-Src in vivo. *J Biol Chem.* 1996;271(7):3863–3868.
38. Kogo H, Aiba T, Fujimoto T. Cell type-specific occurrence of caveolin-1alpha and -1beta in the lung caused by expression of distinct mRNAs. *J Biol Chem.* 2004;279:25574–25578.
39. Scherer PE, Tang Z, Chun M, Sargiacomo M, Lodish HF, Lisanti MP. Caveolin isoforms differ in their N-terminal protein sequence and subcellular distribution: Identification and epitope mapping of an isoform-specific monoclonal antibody probe. *J Biol Chem.* 1995;270(27):16395–16401.
40. Li S, Jin Z, Lu X. MicroRNA-192 suppresses cell proliferation and induces apoptosis in human rheumatoid arthritis fibroblast-like synoviocytes by downregulating caveolin 1. *Mol Cell Biochem.* 2017;432(1–2):123–130.

CYP2D6 basic genotyping as a potential tool to improve the antiemetic efficacy of ondansetron in prophylaxis of postoperative nausea and vomiting

Przemysław A. Niewiński[1,A,D], Robert Wojciechowski[2,B], Marek Śliwiński[2,B], Magdalena E. Hurkacz[1,B,C,F], Krystyna Głowacka[1,B], Krystyna Orzechowska-Juzwenko[1,A,E], Anna K. Wiela-Hojeńska[1,A,E,F]

[1] Department of Clinical Pharmacology, Faculty of Pharmacy with Division of Laboratory Diagnostics, Wroclaw Medical University, Poland
[2] Department of Anesthesiology and Intensive Therapy, Faculty of Medicine, Wroclaw Medical University, Poland

A – research concept and design; B – collection and/or assembly of data; C – data analysis and interpretation; D – writing the article; E – critical revision of the article; F – final approval of the article

Advances in Clinical and Experimental Medicine, ISSN 1899-5276 (print), ISSN 2451-2680 (online) *Adv Clin Exp Med*. 2018;27(11):1499–1503

Address for correspondence
Magdalena E. Hurkacz
E-mail: magdalena.hurkacz@umed.wroc.pl

Funding sources
None declared

Conflict of interest
None declared

Received on October 18, 2016
Reviewed on February 21, 2017
Accepted on March 13, 2017

Abstract

Background. Postoperative nausea and vomiting (PONV) is a common complication after anesthesia and surgery. Ondansetron is one of the most widely used drugs in the prophylaxis of PONV and is extensively metabolized in humans. In vitro metabolism studies have shown that ondansetron is a substrate for human hepatic cytochrome P450 enzymes. The cytochrome P450 (human hepatic cytochrome (CYP)) 2D6 inhibitor quinidine reduced in vitro hydroxylation of ondansetron, which indicates the important role of CYP2D6 in ondansetron metabolism. Genotyping these alleles allows the prediction of the extensive metabolizer (EM) and poor metabolizer (PM) phenotypes with approx. 90–96% accuracy.

Objectives. The aim of our study was to evaluate whether the pharmacological prevention of PONV with ondansetron depends on the most common *CYP2D6* alleles (*CYP2D6*1*, **3*, **4*, **5*, and *NxN* (multiplication gene)).

Material and methods. Genotyping for the defective *CYP2D6*3*, *CYP2D6*4* and *CYP2D6*5* alleles among 93 surgical female patients was performed by polymerase chain reaction amplification and restriction fragment length polymorphism (PCR-RFLP).

Results. The genetically defined EMs and ultrarapid metabolizers (UMs) of CYP2D6 had a statistically significant ($p < 0.02$) higher frequency of nausea and vomiting after strumectomy (33.3%) than intermediate metabolizers (IMs) (10.3%) and PMs (0%). The relative risk (odds ratio (OR)) of PONV occurrence was 5 times higher for EMs/UMs than IMs/PMs.

Conclusions. Our results suggest that PONV treatment with ondansetron could be improved by basic, widely available and inexpensive PCR-RFLP genetic tests.

Key words: CYP2D6, ondansetron, postoperative nausea and vomiting

DOI
10.17219/acem/69451

Introduction

Postoperative nausea and vomiting (PONV) is a common complication after anesthesia and surgery. Pain, nausea and vomiting are frequently listed by patients as their most pressing perioperative concerns. With the change in emphasis from inpatient hospitals to outpatient hospitals and office-based medical/surgical settings, there has been an increased interest in the problem of PONV. The etiology and consequences of PONV are complex and multifactorial, with patient-, medicine-, and surgery-related factors; the important predictors are female gender, a history of PONV and a history of motion sickness. The vomiting center can be triggered by the activation of dopamine, serotonin (type 3), histamine (type 1), and muscarinic cholinergic receptors in the chemoreceptor trigger zone and the nucleus tractus solitarius, as well as acetylcholine receptors in the vestibular apparatus, vagal afferents from the periphery and the endocrine environment. Currently, the overall incidence of PONV is estimated to be 25–30%.[1–3]

Ondansetron is one of the most widely used drugs in the prophylaxis of PONV.[4] While its mechanism of action has not been fully characterized, ondansetron is not a dopamine-receptor antagonist. Serotonin receptors of 5-HT3 type are present both peripherally on vagal nerve terminals and centrally in the chemoreceptor trigger zone of the area postrema. It is not certain whether ondansetron's antiemetic action is mediated centrally, peripherally or in both sites. Approximately 95% of ondansetron is extensively metabolized in humans: only 5% of a radiolabeled dose is recovered from the urine in the form of the parent compound. The primary metabolic pathway is hydroxylation on the indole ring, followed by subsequent glucuronide or sulfate conjugation. Although some non-conjugated metabolites have pharmacological activity, these are not found in plasma at concentrations likely to significantly contribute to the biological activity of ondansetron.[5,6]

In vitro metabolism studies have shown that ondansetron is a substrate for human hepatic cytochrome (CYP) P450 enzymes, including CYP1A2, CYP2D6, CYP3A4, and CYP2E1. According to Fisher et al. as well as Janicki and Sugino, the CYP2D6 inhibitor quinidine reduced the in vitro hydroxylation of ondansetron, which indicates the important role of CYP2D6 in ondansetron metabolism.[5,7,9] The in vitro study by Sanwald et al. confirmed that ondansetron is both CYP2D6- and CYP2E1-dependent.[8]

The enzymes belonging to the cytochrome P450 family, especially CYP2D6, have an important role in the metabolism of over 25% of drugs.[9,10] Tricyclic antidepressants, neuroleptics, cardiologic drugs, and opioids in particular show wide interindividual and interethnic variability in both therapeutic efficacy and adverse effects.[11–14] The polymorphism of CYP2D6 is relatively well-known and more than 20 mutations of the *CYP2D6* gene have been described. *CYP2D6*3* (formerly A-mutation), *CYP2D6*4* (formerly B-mutation) and *CYP2D6*5* (gene deletion, formerly D-mutation) are the most common non-functional *CYP2D6* alleles.[15] Therefore, the genotyping of these alleles allows the prediction of the extensive metabolizer (EM) and poor metabolizer (PM) phenotypes with about 90–96% accuracy.[16,17]

Objectives

The aim of our study was to evaluate whether the efficacy of antiemetic treatment with ondansetron is influenced by mutations of the most common *CYP2D6* genotype, hypothesizing that extensive metabolizers of this drug are at risk of being undertreated. This study sought to investigate whether the efficacy of antiemetic treatment with ondansetron could be improved by adjusting for the most common *CYP2D6* genotype, using basic, widely available and inexpensive (less than $100) polymerase chain reaction (PCR), and polymerase chain reaction amplification and restriction fragment length polymorphism (PCR-RFLP) tests.

Material and methods

Subjects

The study was performed on a group of 93 women with thyroid diseases (neutral struma nodosa and struma nodosa toxica), hospitalized for thyroid gland surgery (strumectomy). They were patients of the 1st Department of Surgery, Wroclaw Medical University, Poland. Their ages ranged from 18 to 84 years, with a mean of 49.85 years (standard deviation (SD): 14.41). None had significant renal, hepatic or cardiovascular disease, insulin-dependent diabetes, chronic obstructive pulmonary disease, or cerebral vascular accident. Patients were excluded if any potential CYP2D6 inhibitor, such as other agents metabolized by isoenzyme CYP2D6, i.e., beta-adrenergic blocking agents, tricyclic antidepressants, antiarrhythmic Ic class drugs, debrisoquine, codeine, or dextromethorphan, had been administered 14 days prior to surgery.

Informed consent was obtained in every case. The protocol for the study was approved by the Bioethics Committee of the Wroclaw Medical University, Poland.

Study design

Ondansetron was administered to patients orally in doses of 8 mg before surgery, for the prevention of PONV.

Genotyping methods

DNA was arranged from leukocytes extracted from peripheral blood. Genotyping for the defective *CYP2D6*3*, *CYP2D6*4* and *CYP2D6*5* alleles (a single base-pair deletion in exon 5 for *CYP2D6*3*, G1934 to A point mutation for *CYP2D6*4*, and a gene deletion for *CYP2D6*5*) was performed by PCR-RFLP method, based on the method

described by Smith et al.[18] For the *CYP2D6*3* mutation, PCR was performed using the primers E – GATGAGCTGCTAACTGAGCCC and F – CCGAGAGCATACTCGGGAC. For the *CYP2D6*4* mutation, PCR was performed using the primers C –GCCTTCGCCAACCACTCCG and D – AAATCCTGCTCTTCCGAGGC.

The PCR amplification product (after verification by electrophoresis in 2% agarose gel) was identified by the RFLP method. The restriction enzymes BstNI (for *CYP2D6*4* mutation) and HpaII (for *CYP2D6*3* mutation) were used. The separation of restriction products was performed by electrophoresis in 3% agarose gel with the addition of ethidium bromide. The results were observed under UV light and recorded in a graphic form.

A lack of *CYP2D6* amplification, suggesting *CYP2D6* gene deletion, was confirmed by an external laboratory (Research Institute of Medicinal Plants, Poznań, Poland).

Alleles not carrying *CYP2D6*3*, *CYP2D6*4* or *CYP2D6*5* were classified as *CYP2D6*1* (wild-type) alleles using this method. Dominant homozygotes with 2 wild-type alleles (*wt/wt – CYP2D6*l/CYP2D6*1*) were classified as CYP2D6 EMs. Heterozygotes with 1 wild-type allele (*wt – CYP2D6*1*) and 1 *CYP2D6*3*, *CYP2D6*4* or *CYP2D6*5* allele were classified as *CYP2D6* intermediate metabolizers (IMs). Recessive homozygotes, carrying 2 alleles with a mutation (*CYP2D6*3* or *CYP2D6*4*) were classified as CYP2D6 PMs.

To identify individuals carrying multiple *CYP2D6* genes (*CYP2D6*NxN*), *CYP2D6* multiplication assays were performed according to the method of Lovlie et al., modified by Steijns and van der Weide.[19,20] Expand Long-PCR was carried out using an Expand Long Template PCR System kit (Hoffmann-La Roche, Basel, Switzerland). With the primer combination of CYP-17f (5′-TCCCCCACTGACCCAACTCT-3′) and CYP-32r (5′-CACGTGCAGGGCACCTAGAT-3′), a 3.6-kb PCR fragment amplified from the *CYP2D6-CYP2D6* region was observed in subjects having multiple alleles of the *CYP2D6* gene.

The number of nausea and vomiting episodes was counted, and PONV intensity was evaluated with the Postoperative Nausea and Emetic Scale (PNES) (Table 1) during the first 5 h after surgery.

The PNES results were calculated immediately after surgery (0 h), during the 1st hour (1 h) and during the next 4 h (5 h).

Table 1. The Postoperative Nausea and Emetic Scale (PNES)

Postoperative Nausea and Emetic Scale (PNES)		Value [points]
Nausea	absent	0
	slight	1
	medium	2
	heavy	3
Vomiting	1 episode	4
	2–3 episodes	5
	4 or more episodes	6

Statistical analysis

The statistical analysis of the results was performed using the χ^2 test, with or without Yates's correction, and the Fisher's exact test. For the statistical analysis of the antiemetic efficacy of ondansetron among different *CYP2D6* genotype groups, the relative risk (odds ratio (OR)) was calculated. The pharmacoeconomic value of genotyping was determined by calculating the Number Needed to Diagnose (NND): the number of people who should be screened in order to prevent 1 adverse end point.

Statistical software used included STATISTICA v. 10 and 12 (StatSoft Inc., Tulsa, USA) and RelRisk v. 0.8 (author's own software, Wrocław, Poland).

Results

The frequency of the *CYP2D6*1*, *CYP2D6*3*, *CYP2D6*4*, and *CYP2D6*NxN* alleles among the 93 genotyped patients was 79.0%, 1.1%, 18.8%, and 1.1%, respectively. Fifty-nine patients (63.4%) were homozygous for the wild-type *CYP2D6* allele (*CYP2D6*1/*1*) and were classified as EMs. One woman (1.1%) was a carrier of *CYP2D6* multiplication (*CYP2D6*1/NxN*) and was classified as an ultrarapid metabolizer (UM). Among 29 heterozygous women (31.2%) predicted to be IMs, 27 individuals (29.0%) carried the *CYP2D6*1/*4* genotype (B-mutation), while 2 (2.2%) carried the *CYP2D6*1/*3* genotype (A-mutation). A group of 4 carriers of *CYP2D6*-deficient genes (4.3%) were homozygous individuals carrying 2 nonfunctional B alleles (*CYP2D6*4/*4* genotype).

Out of all 93 patients, 23 (24.7%) experienced nausea and vomiting. Sixty subjects genetically defined as EMs and UMs of CYP2D6 had statistically significant higher frequency of nausea and vomiting (Yates corrected $\chi^2 = 5.48$, $p < 0.02$, Fisher's exact test $p < 0.011$) than IMs and PMs. As many as 20 of the 60 EMs and UMs (33.3%) experienced PONV, while only 3 of the 29 IMs (10.3%) and none of the 4 PMs (0%) reported this condition (Fig. 1).

Moreover, PONV intensity (measured by the PNES) was higher among EMs and UMs (mean PNES value = 3.97) than among IMs and PMs (mean PNES value = 0.19). Detailed information regarding the frequency and intensity of PONV immediately after surgery (0 h), during the 1st hour (1 h) and during the next 4 h (5 h) is shown in Table 2.

The relative risk (OR) of PONV occurrence was 5 times higher (confidence interval (CI) = 1.36–18.39, $p < 0.02$) for EMs and UMs than for IMs and PMs. The relative risk was especially higher immediately after surgery (OR = 4.18, CI = 1.02–10.47, $p < 0.04$), compared with the 1st hour (OR = 2.29, CI = 0.60–8.77, non-significant (NS)) or the period of 1–5 h after surgical treatment (OR = 3.30, CI = 0.382–28.59, NS).

The NND – the number of people who should be screened in order to prevent 1 episode of PONV – was 3.35 (CI = 2.35–20.85), which suggests a relatively high pharmacoeconomic value for *CYP2D6* genotyping.

Table 2. Postoperative nausea and vomiting (PONV) frequency and intensity (measured by the Postoperative Nausea and Emetic Scale [PNES]) in patients during the 1st 5 h after surgical treatment

Genotype	0 h after surgery		1 h after surgery		5 h after surgery	
	number of episodes	mean PNES points	number of episodes	mean PNES points	number of episodes	mean PNES points
UMs and EMs (n = 60)	17	5.10	11	4.70	5	2.1
IMs (n = 29)	3	0.26	2	0.20	1	0.1
PMs (n = 4)	0	0	0	0	0	0

UMs – ultrarapid metabolizers; EMs – extensive metabolizers; IMs – intermediate metabolizers; PMs – poor metabolizers.

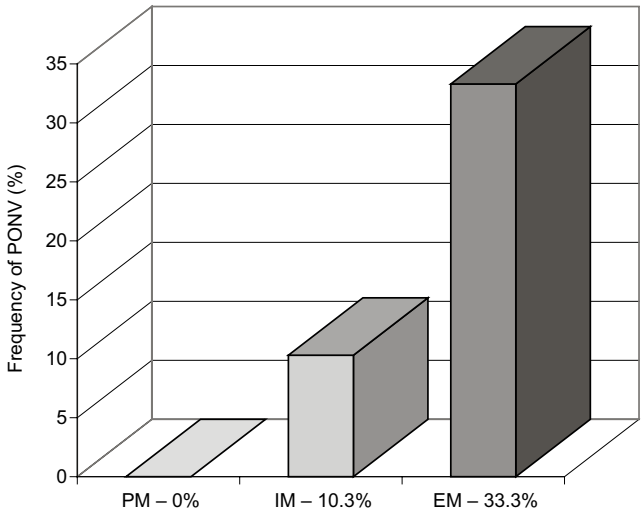

Fig. 1. Percentage of postoperative nausea and vomiting (PONV) episodes among poor metabolizers (PMs), intermediate metabolizers (IMs) and extensive metabolizers (EMs) treated with ondansetron

Discussion

The evaluation of the metabolic polymorphism of *CYP2D6* and the frequency of PONV among surgical patients treated with ondansetron has rarely been reported until now. The antiemetic efficacy of ondansetron has only been studied during cancer chemotherapy. Our results are parallel to the results of Kaiser et al., who analyzed the effects of antiemetic treatment with ondansetron and tropisetron during cancer chemotherapy and revealed that genetically defined UMs of *CYP2D6* had a higher frequency of vomiting within the first 4 h ($p < 0.001$) and within the period of 5–24 h ($p < 0.03$) after treatment than all the other patients; the tendency for nausea was similar.[21] The results of both studies confirm conclusions of Fisher et al. and Dixon et al. from in vitro studies, endorsing the key role of *CYP2D6* in the metabolism of ondansetron, despite the doubts of Ashforth et al.[5,22,23] The latter questioned the importance of *CYP2D6* phenotype in the in vivo metabolism of ondansetron by showing that there was no significant difference in area under curve (AUC), maximal concentration (C_{max}), clearance (CL), or half-life time ($t_{1/2}$) between the 6 PMs and the 6 EMs.[23]

The involvement of the *CYP2D6* system in the sensitivity to PONV was further confirmed by Wesmiller et al. and Dong et al.[24–26] Patients who were classified as PMs had fewer PONV episodes and higher pain scores. These findings suggest variability in *CYP2D6*'s impact on susceptibility to PONV.[27]

Janicki and Sugino suggested that genotyping for *CYP2D6* UM polymorphisms (gene multiplications) for PONV or other medications "currently may be prohibitively costly and inconvenient" because "only a small proportion of Caucasians carry the *CYP2D6* allele duplication and hence are at risk for PONV treatment failure".[28,29] The frequency of the UM genotype varies by population, ranging from 1% to 8% among Caucasians.[14,26] Basic, inexpensive genotyping for *CYP2D6*NxN*, *CYP2D6*3*, *CYP2D6*4*, and *CYP2D6*5*, definitely the most common mutations among Caucasians, could be useful for dividing patients into 2 subpopulations. The combined group of EMs and the rare UMs (66% of the Caucasian population) requires higher doses of ondansetron. The combined group of IMs and PMs (34%) could be treated with standard doses. The NND is low (3.35), which suggests a relatively high (in comparison with other tests) pharmacoeconomic value for basic *CYP2D6* analysis.[30] We suggest that this approach is quite affordable and could be clinically useful.

Our results, and those of other studies, strongly suggest that antiemetic treatment with ondansetron could be improved by adjusting the drug dosage according to the patient's *CYP2D6* genotype, by using a basic, inexpensive and widely available PCR-RFLP test.

Conclusions

The antiemetic efficacy of ondansetron in PONV after strumectomy is associated with *CYP2D6* metabolism, determined by genotyping for the *CYP2D6*1*, *CYP2D6*3*, *CYP2D6*4*, *CYP2D6*5*, and *CYP2D6*NxN* alleles.

Genetically defined *CYP2D6 EMs* and UMs present a statistically significant higher risk of PONV than IMs and PMs.

Postoperative nausea and vomiting treatment with ondansetron could be improved by adjusting the drug dosage based on *CYP2D6* genotyping, using simple, inexpensive and widely available PCR and PCR-RFLP tests.

References

1. Golembiewski JA, O'Brien D. A systematic approach to the management of postoperative nausea and vomiting. *J Perianesth Nurs*. 2002;17(6):364–376.
2. Kovac AL. Prevention and treatment of postoperative nausea and vomiting. *Drugs*. 2000;59(2):213–243.
3. Horn CC, Wallisch WJ, Homanics GE, Williams JP. Pathophysiological and neurochemical mechanisms of postoperative nausea and vomiting. *Eur J Pharmacol*. 2014;722:55–66.
4. Vrabel M. Is ondansetron more effective than granisetron for chemotherapy-induced nausea and vomiting? A review of comparative trials. *Clin J Oncol Nurs*. 2007;11(6):809–813.
5. Fischer V, Vickers AE, Heitz F, et al. The polymorphic cytochrome P-4502D6 is involved in the metabolism of both 5-hydroxytryptamine antagonists, tropisetron and ondansetron. *Drug Metab Dispos*. 1994; 22(2):269–274.
6. Lewis DFV, Ito Y, Eddershaw PJ, et al. An evaluation of ondansetron binding interactions with human cytochrome P450 enzymes *CYP3A4* and *CYP2D6*. *Drug Metab Lett*. 2010;4(1):25–30.
7. Sugino S, Janicki PK. Pharmacogenetics of chemotherapy-induced nausea and vomiting. *Pharmacogenomics*. 2015;16(2):149–160.
8. Sanwald P, David M, Dow J. Characterization of the cytochrome P450 enzymes involved in the in vitro metabolism of dolasetron. Comparison with other indole-containing 5-HT3 antagonists. *Drug Metab Dispos*. 1996;24(5):602–609.
9. Hocum BT, White JR, Heck JW, et al. Cytochrome P-450 gene and drug interaction analysis in patients referred for pharmacogenetic testing. *Am J Health Syst Pharm*. 2016;73(2):61–67.
10. Belle DJ, Singh H. Genetic factors in drug metabolism. *Am Fam Physician*. 2008;77(11):1553–1560.
11. Abaji R, Krajinovic M. Current perspective on pediatric pharmacogenomics. *Expert Opin Drug Metab Toxicol*. 2016;12(4):363–365.
12. Zanger UM, Raimundo S, Eichelbaum M. Cytochrome P450 2D6: Overview and update on pharmacology, genetics, biochemistry. *Naunyn Schmiedebergs Arch Pharmacol*. 2004;369(1):23–37.
13. He ZX, Chen XW, Zhou ZW, Zhou SF. Impact of physiological, pathological and environmental factors on the expression and activity of human cytochrome P450 2D6 and implications in precision medicine. *Drug Metab Rev*. 2015;47(4):470–519.
14. Gardiner SJ, Begg EJ. Pharmacogenetics, drug-metabolizing enzymes, and clinical practice. *Pharmacol Rev*. 2006;58(3):521–590.
15. Daly AK, Brockmöller J, Broly F, et al. Nomenclature for human *CYP2D6* alleles. *Pharmacogenetics*. 1996;6(3):193–201.
16. Dahl ML, Johansson I, Palmertz MP, at al. Analysis of the *CYP2D6* gene in relation to debrisoquine and desipramine hydroxylation in a Swedish population. *Clin Pharmacol Ther*. 1992;51(1):12–17.
17. Sachse C, Brockmöller J, Bauer S, Roots I. Cytochrome P450 2D6 variants in Caucasian population: Allele frequencies and phenotyping consequences. *Am J Hum Genet*. 1997;60(2):284–295.
18. Smith C, Gough A, Leigh P, et al. Debrisoquine hydroxylase gene polymorphism and susceptibility to Parkinson's disease. *Lancet*. 1992;339 (8806):1375–1377.
19. Lovlie R, Daly AK, Molven A, et al. Ultrarapid metabolizers of debrisoquine: Characterization and PCR-based detection of alleles with duplication of the *CYP2D6* gene. *FEBS Lett*. 1996;392(1):30–34.
20. Steijns LSW, van der Weide J. Ultrarapid drug metabolism: PCR-based detection of *CYP2D6* gene duplication. *Clin Chem*. 1998;44(5):914–917.
21. Kaiser R, Sezer O, Papies A, et al. Patient-tailored antiemetic treatment with 5-hydroxytryptamine type 3 receptor antagonists according to cytochrome P-450 2D6 genotypes. *J Clin Oncol*. 2002;20(12): 2805–2811.
22. Dixon CM, Colthup PV, Serabjit-Singh CJ, et al. Multiple forms of cytochrome P450 are involved in the metabolism of ondansetron in humans. *Drug Metab Dispos*. 1995;23(11):1225–1230.
23. Ashforth EI, Palmer JL, Bye A, Bedding A. The pharmacokinetics of ondansetron after intravenous injection in healthy volunteers phenotyped as poor or extensive metabolizers of debrisoquine. *Br J Clin Pharmacol*. 1994;37(4):389–391.
24. Wesmiller SW, Conley Y, Sereika S, et al. Postoperative nausea and vomiting among women with breast cancer: A genetic analysis of selected polymorphisms of genes of the serotonin pathway. *Biology and Control of Nausea and Vomiting 2013 Online Abstracts*. http://internationalvomitingconference.org/Program-book.pdf. Pittsburgh, PA: University of Pittsburgh; 2013:63. Accessed 20 January, 2015.
25. Wesmiller SW, Henker RA, Sereika SM, et al. The association of *CYP2D6* genotype and postoperative nausea and vomiting in orthopedic trauma patients. *Biol Res Nurs*. 2013;15(4):382–389.
26. Dong H, Lu SJ, Zhang R, Liu DD, Zhang YZ, Song CY. Effect of the *CYP2D6* gene polymorphism on postoperative analgesia of tramadol in Han nationality nephrectomy patients. *Eur J Clin Pharmacol*. 2015;71(6):681–686.
27. Bell GC, Caudle KE, Whirl-Carrillo M, et al. Clinical Pharmacogenetics Implementation Consortium (CPIC) guideline for *CYP2D6* genotype and use of ondansetron and tropisetron. *Clin Pharmacol Ther*. 2017;102(2):213–218.
28. Janicki PK. Cytochrome P450 2D6 metabolism and 5-hydroxytryptamine type 3 receptor antagonists for postoperative nausea and vomiting. *Med Sci Monit*. 2005;11(10):322–328.
29. Janicki PK, Sugino S. Genetic factors associated with pharmacotherapy and background sensitivity to postoperative and chemotherapy-induced nausea and vomiting. *Exp Brain Res*. 2014;232(8):2613–2625.
30. Plumpton CO, Roberts D, Pirmohamed M, Hughes DA. A systematic review of economic evaluations of pharmacogenetic testing for prevention of adverse drug reactions. *Pharmacoeconomics*. 2016;34(8): 771–793.

Loganic acid and anthocyanins from cornelian cherry (*Cornus mas* L.) fruits modulate diet-induced atherosclerosis and redox status in rabbits

Tomasz Sozański[1,A–F], Alicja Z. Kucharska[2,B–F], Stanisław Dzimira[3,B,C,E,F], Jan Magdalan[1,B,C,E,F], Dorota Szumny[1,C,E,F], Agnieszka Matuszewska[1,C,E,F], Beata Nowak[1,C,E,F], Narcyz Piórecki[4,5,B,E,F], Adam Szeląg[1,C,E,F], Małgorzata Trocha[1,C,E,F]

[1] Department of Pharmacology, Wroclaw Medical University, Poland
[2] Department of Fruit, Vegetable and Plant Nutraceutical Technology, Wrocław University of Environmental and Life Sciences, Poland
[3] Department of Pathology, Wrocław University of Environmental and Life Sciences, Poland
[4] Arboretum and Institute of Physiography in Bolestraszyce, Poland
[5] Department of Tourism and Recreation, University of Rzeszów, Poland

A – research concept and design; B – collection and/or assembly of data; C – data analysis and interpretation; D – writing the article; E – critical revision of the article; F – final approval of the article

Advances in Clinical and Experimental Medicine, ISSN 1899-5276 (print), ISSN 2451-2680 (online) *Adv Clin Exp Med*. 2018;27(11):1505–1513

Address for correspondence
Tomasz Sozański
E-mail: tsoz@wp.pl

Funding sources
The study was financially supported by the statutory means of Wroclaw Medical University (ST.A080.17.035).

Conflict of interest
None declared

Received on March 6, 2017
Reviewed on May 31, 2017
Accepted on June 8, 2017

Abstract

Background. Cornelian cherry (*Cornus mas* L.) is a plant growing in southeast Europe, in the past used in folk medicine. There are many previous publications showing the preventive effects of (poly)phenolic compounds, especially anthocyanins, on cardiovascular diseases, but there is a lack of studies comparing the effects of (poly)phenolics and other constituents of fruits.

Objectives. We have attempted to determine if iridoids and anthocyanins from cornelian cherry fruits may affect the formation of atherosclerotic plaques in the aorta as well as lipid peroxidation and oxidative stress in the livers of cholesterol-fed rabbits.

Material and methods. Fractions of iridoids and anthocyanins were analyzed using the high-performance liquid chromatography (HPLC) and liquid chromatography-mass spectrometry (LC-MS) methods. Loganic acid (20 mg/kg bw.) and a mixture of anthocyanins (10 mg/kg bw.) were administered orally for 60 days to rabbits fed with 1% cholesterol. Histopathological samples of the aortas and the livers were stained with hematoxylin and eosin. Lipid peroxidation (malondialdehyde – MDA) and redox status (glutathione – GSH, glutathione peroxidase – Gpx and superoxide dismutase – SOD) were analyzed using spectrophotometrical methods.

Results. Both loganic acid (an iridoid) and a mixture of anthocyanins diminished the formation of atherosclerotic plaques in the aorta. Both substances also diminished lipid peroxidation, measured as a decrease of MDA, and attenuated oxidative stress, measured as an increase of GSH in the livers depleted by cholesterol feeding. Unexpectedly, cholesterol feeding decreased the Gpx activity in the liver, which was reversed by both investigated substances.

Conclusions. We have shown that both iridoids and anthocyanins help prevent fed-induced atherosclerosis, and the consumption of fruits rich in these substances may elicit beneficial effects on the cardiovascular system.

Key words: atherosclerosis, glutathione, anthocyanins, cornelian cherry, loganic acid

DOI
10.17219/acem/74638

Introduction

Cardiovascular diseases are the leading causes of morbidity and mortality in both developing and developed countries.[1] Oxidative stress and subsequent lipid peroxidation contribute to the development and progression of atherogenesis and other tissue damage.[2,3] They also interact with other factors, like proinflammatory cytokines or substances the affecting nitric oxide (NO) synthesis, contributing to vascular pathologies from endothelial dysfunction to clinical symptoms of cardiovascular diseases.[4]

It is also widely accepted that diet, especially a diet consisting of large amounts of fruits and vegetables, may prevent the development and progression of cardiovascular diseases.[5,6] There are many studies on both humans and animals showing the preventive effects of (poly)phenolic compounds – flavonoids, and especially their subclass – anthocyanins, on atherosclerosis and cardiovascular diseases.[7–9] In contrast, we have not found any surveys comparing the effects and interactions of different constituents of plants, particularly fruits, on the risk factors and symptoms of cardiovascular diseases. Moreover, there are only a few studies comparing the potency of various flavonoids on high-fat diet-induced changes.[10] In recent decades there has been increasing interest in iridoids, a wide group of plant constituents with possible pleiotropic effects on human metabolism.[11] Although both anthocyanins or iridoids are common constituents of plants, only a few edible fruits contain pronounced amounts of iridoids or both substances. In the present study, we focused on cornelian cherry (*Cornus mas* L.), a plant growing or cultivated in Europe and southwest Asia, and cultivated in North America; widely consumed in some countries and, in the past, used in folk medicine. In our previous studies we proved that the European cultivar of cornelian cherry contains large amounts of iridoids – mainly loganic acid – and anthocyanins. We also showed the preventive effects of whole fruits on diet-induced atherosclerosis in animals, through the activation of peroxisome proliferator-activated receptors alpha (PPARα).[12,13] In another study, using the same model of diet-induced atherosclerosis we showed that isolated loganic acid and anthocyanins decreased dyslipidemia, increased the expression of both PPARα and peroxisome proliferator-activated receptors gamma (PPARγ) in the liver, and decreased the intima thickness and the intima/media ratio in the thoracic aortas.[14]

The aim of the present investigation was to compare the effects of loganic acid and anthocyanins isolated from cornelian cherry on the formation of atherosclerosis in the thoracic and abdominal aorta, measured by histopathological examination, as well as on lipid peroxidation and redox state in the liver, measured as the malondialdehyde (MDA), glutathione (GSH), glutathione peroxidase (Gpx), and superoxide dismutase (SOD) levels.

Material and methods

Plant material and the preparation of samples of loganic acid and anthocyanins

Cornelian cherry fruits were harvested in the Arboretum and Institute of Physiography in Bolestraszyce, Poland. The plant material was verified by Prof. Jakub Dolatowski, the voucher specimen (BDPA 3 967) is stored at the Herbarium of the Arboretum and Institute of Physiography in Bolestraszyce. Loganic acid and a mixture of anthocyanins were prepared in the Department of Fruit, Vegetable and Plant Nutraceutical Technology at Wrocław University of Environmental and Life Science (Poland), according to Kucharska et al.'s instructions with minor modifications.[13]

Juice from cornelian cherry fruits was purified using an Amberlite XAD-16 resin column (Rohm and Haas, Chauny Cedex, France). Iridoid and anthocyanin compounds present in the juice were eluted with ethanol/water/acetic acid (80:19.9:0.1, v/v/v). Purified compounds were concentrated, using a Rotavapor rotary evaporator (Büchi, Flawil, Switzerland) in a water bath at 40°C, and then dried in an SPT-200 vacuum dryer (ZUT Colector, Kraków, Poland) (40°C, 00.094 MPa). Dried compounds were fractionated by polyamide column chromatography (150 mm × 30 mm) (Macherey-Nagel-CC 6.6, Düren, Germany), using ethanol/water/acetic acid (50:49.5:0.5, v/v/v) as the eluent. As a result of separation, we obtained loganic acid and anthocyanins. The former was monitored at 254 nm, while the latter – at 520 nm (Fig. 1). Next, the resulting fractions were concentrated with a Rotavapor rotary evaporator, and then dried in an SPT-200 vacuum dryer (40°C, 0.094 MPa). The fractions were analyzed using the high-performance liquid chromatography (HPLC) (Fig.1) and liquid chromatography-mass spectrometry (LC-MS) methods.

Table 1. Schedule of animal feeding and administering test substances

Control group P	Regular feed + saline p.o.
Experimental group CHOL	regular feed with the addition of 1% cholesterol + saline p.o.
Experimental group CHOL+LA	regular feed with the addition of 1% cholesterol + loganic acid 20 mg/kg bw. p.o
Experimental group CHOL+ANT	regular feed with the addition of 1% cholesterol + anthocyanins 10 mg/kg bw. p.o.

p.o. – taken orally.

The in vivo study

This research was conducted in accordance with the National Institutes of Health (NIH) Guide for the Care and Use of Laboratory Animals and Directive 2010/63/EU, and was approved by the Local Ethical Committee on Animal Research at the Institute of Immunology and Experimental Therapy, Polish Academy of Sciences in Wrocław (Poland).

Chemicals

Loganic acid and anthocyanins were prepared as described above. Cholesterol was purchased from POCH (Gliwice, Poland).

Animals and treatment

Forty mature New Zealand rabbits aged 8–12 months were used in the study. The animals were housed in individual chambers with a temperature maintained at 21––23°C under a 12:12 h light-dark cycle. During the experiment, the rabbits had free access to water and received the same daily portion of feed (40 g/kg bw.). After 4 weeks of acclimatization, the animals were divided by block randomization into 4 groups of 10 animals each. For 60 consecutive days of the experiment, the animals in group P ingested standard feed. The other groups – CHOL, CHOL+LA and CHOL+ANT – received the same feed + 1% cholesterol. Once daily, in the morning, the following test substances were administered orally to the rabbits: groups P and CHOL – normal saline solution (negative and positive control), group CHOL+LA – loganic acid at a dose of 20 mg/kg bw. and group CHOL+ANT – a mixture of anthocyanins at a dose of 10 mg/kg bw. (Table 1).

On the 0^{th} and 60^{th} days of study, blood samples were collected from each animal from the marginal vein of the ear, or the saphenous vein. On the 60^{th} day, the animals were euthanized with terminal anesthesia, using morbital (1 mL containing 133.3 mg of sodium pentobarbital and 26.7 mg of pentobarbital), administered intraperitoneally (ip.) at a dose of 2 mL/kg bw. The organs were collected – the livers for the measurements of lipid peroxidation and oxido-redox state parameters, and the aortas for histopathological assessment.

Biomarkers associated with oxido-redox state in the liver

All parameters in the liver were assessed spectrophotometrically. The MDA level was assayed using the BIOXYTECH-MDA-586 kit (OxisResearch, Portland, USA) and expressed as μM/g of tissue. The GSH concentration was assayed using the BIOXYTECH GSH-400 kit (OxisResearch) and expressed as mM/mg of tissue. The SOD activity was measured using the Ransod kit (Randox Laboratories, Crumlin, UK) and expressed as U/mg of protein. The GPx activity was measured using the GPx-340 kit (Randox Laboratories) and expressed as U/mg of protein.

Histopathological evaluations

Postmortem thoracic and abdominal aorta and liver samples were collected for histological examinations. Tissue sections were fixed in a 7% buffered formalin solution, embedded in paraffin, cut into 4 μm thick slices, and stained by means of the hematoxylin and eosin method. The samples were blindly examined by an experienced pathomorphologist.

Statistical analysis

Histopathological results were expressed as the number (percentage) of animals presenting the same degree of changes. The χ^2 test of independence was used to study the qualitative data. The results of all the other data were expressed as mean ±standard deviation (mean ±SD). The normality of all continuous variables was verified by the Shapiro-Wilk test. Statistical comparisons of histopathological data were performed using the Kruskall-Wallis test, followed by the Dunn test

Table 2. Histopathological changes in the thoracic and abdominal aorta in rabbits in experimental groups – hematoxylin and eosin (HE) staining

Thoracic aorta	Group			
	P n = 10	CHOL** n = 10	CHOL+LA# n = 10	CHOL+ANT# n = 10
–	10 (100.0%)	1 (10.0%)	8 (80.0%)	9 (90.0%)
+	0 (0.0%)	5 (50.0%)	2 (20.0%)	1 (10.0%)
++	0 (0.0%)	2 (20.0%)	0 (0.0%)	0 (0.0%)
+++	0 (0.0%)	1 (10.0%)	0 (0.0%)	0 (0.0%)
++++	0 (0.0%)	1 (10.0%)	0 (0.0%)	0 (0.0%)
Abdominal aorta	**Group**			
	P n = 10	CHOL*** n = 10	CHOL+LA*Δ n = 10	CHOL+ANT n = 10
–	10 (100.0%)	1 (10.0%)	5 (50.0%)	8 (80.0%)
+	0 (0.0%)	5 (50.0%)	5 (50.0%)	0 (0.0%)
++	0 (0.0%)	3 (30.0%)	0 (0.0%)	2 (20.0%)
++++	0 (0.0%)	1 (10.0%)	0 (0.0%)	0 (0.0%)

Scoring: / – / no visible endothelium damage; / + / a few assembled foam cells occupying no more than 10% of the artery circumference; / ++ / 2 or more collections of atheromatous plaques; / +++ / atheromatous plaques occupying more than 2/3 of the artery circumference and of thickness accounting for about 50% of the artery wall thickness; / ++++ / massive atheromatous plaques occupying all the artery circumference and of thickness exceeding 50% of the artery thickness. P – standard feed and vehicle-treated rabbits; CHOL – cholesterol-treated rabbits, CHOL+LA – rabbits treated with cholesterol + loganic acid 20 mg/kg bw.; CHOL+ANT – rabbits treated with cholesterol + anthocyanins 10 mg/kg bw. Values are presented as number and percentiles. Specific comparisons (the χ^2 test): * $p < 0.05$ vs P; ** $p < 0.01$ vs P; *** $p < 0.001$ vs P; # $p < 0.05$ vs CHOL; Δ $p < 0.05$ vs CHOL+ANT.

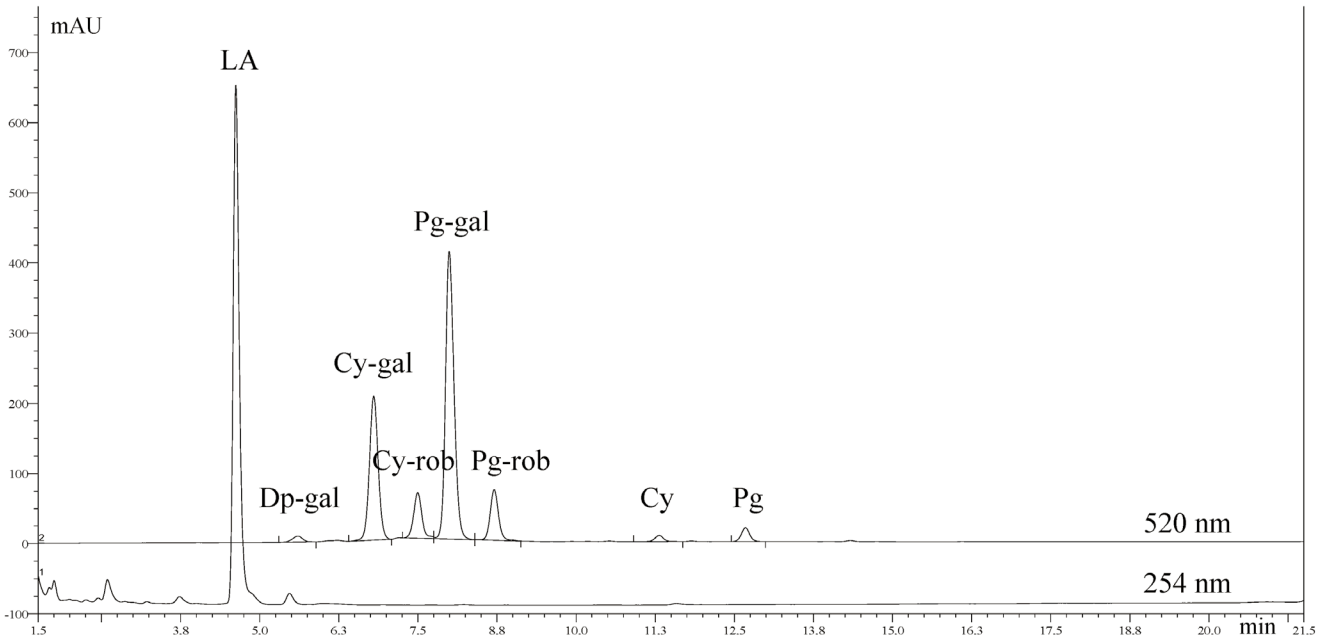

Fig. 1. High-performance liquid chromatography-diode-array detection (HPLC-DAD) chromatograms of iridoid (254 nm) and anthocyanins (520 nm) fractions from cornelian cherry (*Cornus mas* L.) fruits

LA – loganic acid; Dp-gal – delphinidin 3-O-galactoside; Cy-gal – cyanidin 3-O-galactoside; Cy-rob – cyanidin 3-O-robinobioside; Pg-gal – pelargonidin 3-O-galactoside; Pg-rob – pelargonidin 3-O-robinobioside; Cy – cyanidin; Pg – pelargonidin; mAU – milli absorbance units.

for multiple comparisons. Other data was analyzed using the analysis of variance (ANOVA), followed by a post-hoc least significant difference (LSD) test. The p-values <0.05 were considered statistically significant.

Results

We compared the impact of orally administered cornelian cherry constituents, an iridoid – loganic acid and anthocyanins, on dietary-induced hyperlipidemia in rabbits.

Both the thoracic and abdominal aortas in the control P group presented no atheromatous changes, whereas cholesterol-fed rabbits developed characteristic atheromatous lesions. There were plaques of different thickness, comprising lipid-loaded foam cells, lymphocytes, fibrin, and disintegrated cells with debris in the extracellular matrix. There were also visible mild proliferations of myocytes and the exudation in the subendothelial layer consisting of amorphous proteins and glycosaminoglycans. In a few cases, there were microclots on the tunica intima, composed of red blood cells and thrombocytes, occasionally incorporated into the arterial walls when surrounded by endothelium. Both loganic acid and anthocyanins prevented or significantly decreased the development of atheromatous changes (Table 2). In the thoracic aorta, in the CHOL+LA and CHOL+ANT groups, no lesions were noted in 80% and 90% of the rabbits, respectively. The remaining animals developed only mild changes with a few collections of assembled foam cells. The length of those changes did not exceed 10% of the circumference of the artery. In the abdominal aorta, in the CHOL+LA and CHOL+ANT groups, no lesions were noted in 50% and 80% of the rabbits, respectively. In the remaining 50% of the animals in the CHOL+LA group, only mild changes were observed, as described above. In only 20% of the rabbits in the CHOL+ANT group, some atheromatous changes were noted, although they were moderate, with 2 or more plaques. Representative pictures showing histological cross-sections of the thoracic and abdominal aortas are presented in Fig. 2.

The cholesterol-enriched diet induced moderate fatty degeneration in the livers compared to the control group. Neither anthocyanins nor loganic acid significantly decreased those changes (data not presented).

Lipid peroxidation in the livers was measured by the MDA concentrations, and redox status by both enzymatic and non-enzymatic oxidative markers.

The MDA concentration in the CHOL group increased significantly in comparison to the control group. The addition of either anthocyanins or loganic acid significantly decreased lipid peroxidation. The MDA levels in the CHOL+ANT and CHOL+LA groups were comparable to each other and lower compared to the CHOL group, although they were still higher than in the group P. Simvastatin treatment completely reversed the increased MDA level caused by administering cholesterol (Fig. 3A).

Cholesterol-rich feeding significantly depleted the concentration of GSH. Both anthocyanins and loganic acid significantly increased the GSH level in comparison

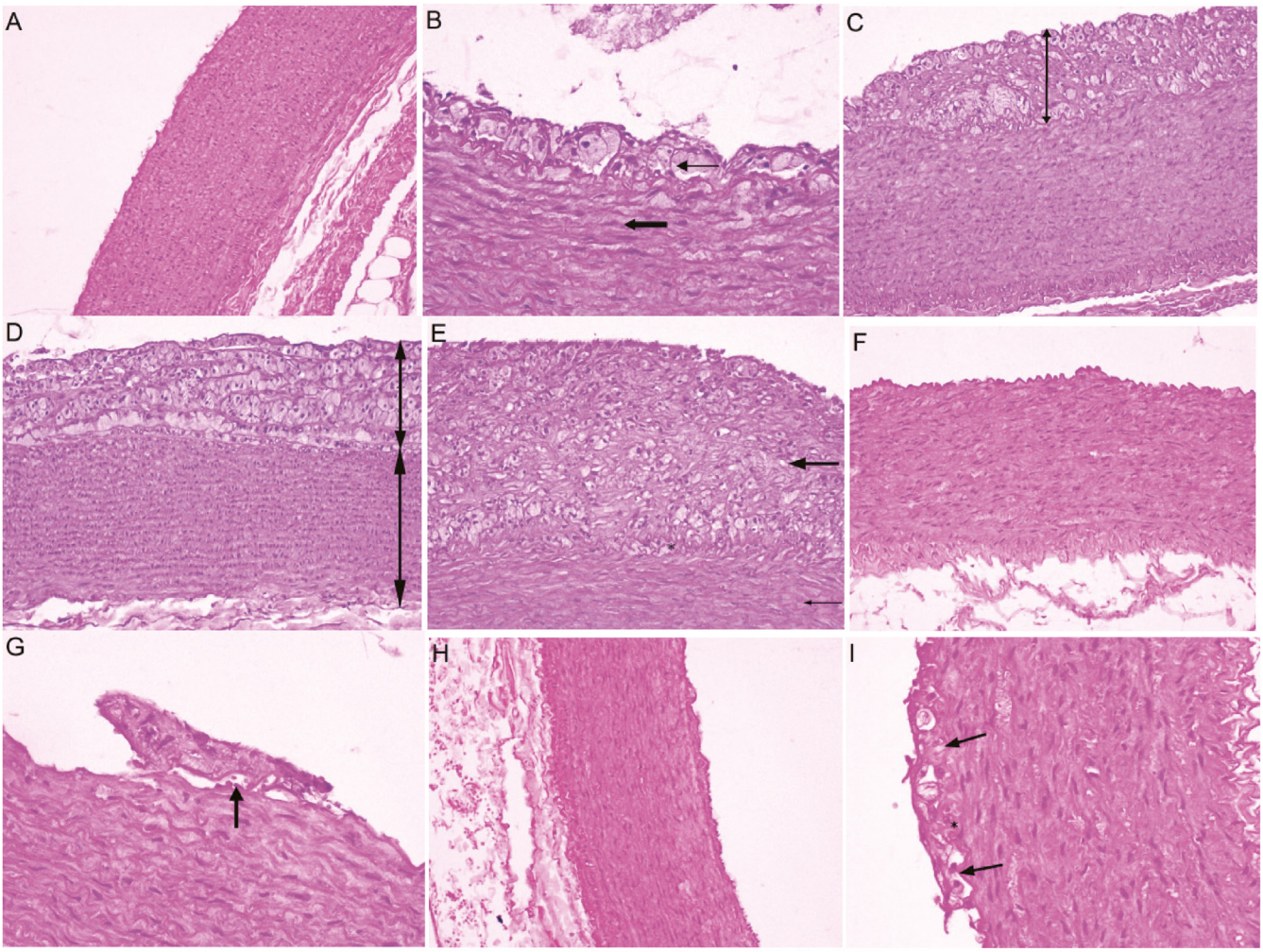

Fig. 2. Representative photos showing histological cross-sections of the aortas with hematoxylin and eosin (HE) staining

A – control group (rabbit No. 7). Normal endothelium and media of the thoracic aorta; changes classified as (–); HE staining, magnification ×100. B – CHOL group (rabbit No. 18). A few assembled foam cells (thin arrow) on the endothelium of the abdominal aorta (thick arrow); changes classified as (+); HE staining, magnification ×200. C – CHOL group (rabbit No. 19). A layer of atheromatous plaque (arrow) located on the endothelium of the thoracic aorta, composed of foam cells, a few lymphocytes and disintegrated cell debris; changes classified as (++); HE staining, magnification ×100. D – CHOL group (rabbit No. 17). A thick layer of atheromatous plaque on the thoracic aorta endothelium, composed of numerous foam cells, a few lymphocytes and disintegrated cell debris; arrows indicate the thickness of the atheromatous plaque and the vessel; changes classified as (+++); HE staining, magnification ×100. E – group CHOL (rabbit No. 14). A very thick layer of atheromatous plaque (thick arrow) on the abdominal aorta endothelium (thin arrow), composed of numerous foam cells, a few lymphocytes, myocytes, and disintegrated cell debris; changes classified as (++++); HE staining, magnification ×100; * the border between the vessel and the plaque. F – CHOL+LA group (rabbit No. 21). Normal endothelium and media of the thoracic aorta; changes classified as (–); HE staining, magnification ×100. G – CHOL+LA group (rabbit No. 26). Slightly detached endothelium (arrow) of the abdominal aorta; changes classified as (+); HE staining, magnification ×200. H – CHOL+ANT group (rabbit No. 31). Normal endothelium and media of the thoracic aorta; changes classified as (–); HE staining, magnification ×100. I – CHOL+ANT group (rabbit No. 39) Slightly detached endothelium (arrows) of the thoracic aorta; changes classified as (+); HE staining, magnification ×200; * the border between the vessel and the plaque.

to the CHOL group; anthocyanins completely and significantly reversed the GSH depletion caused by cholesterol, although the loganic acid effect was weaker. The GSH level in the CHOL+LA group was lower than in the CHOL group, but still higher than in the P group. Simvastatin completely prevented a decrease in the GSH concentration (Fig. 3B).

The GPx concentration in the CHOL group decreased compared to the control group, while the addition of either anthocyanins or loganic acid increased GPx activities to levels comparable to the control group (Fig. 3C).

SOD activities in the cholesterol-treated group increased significantly as compared to the control group. The addition of neither anthocyanins nor loganic acid modulated these cholesterol-evoked changes. SOD activities in the CHOL+ANT and CHOL+LA groups were significantly higher compared to the control group, and comparable to the CHOL group (Fig. 3D).

Discussion

The most important finding of our study is that both iridoids and anthocyanins from the same plant may prevent atherosclerosis and redox stress. The key results are

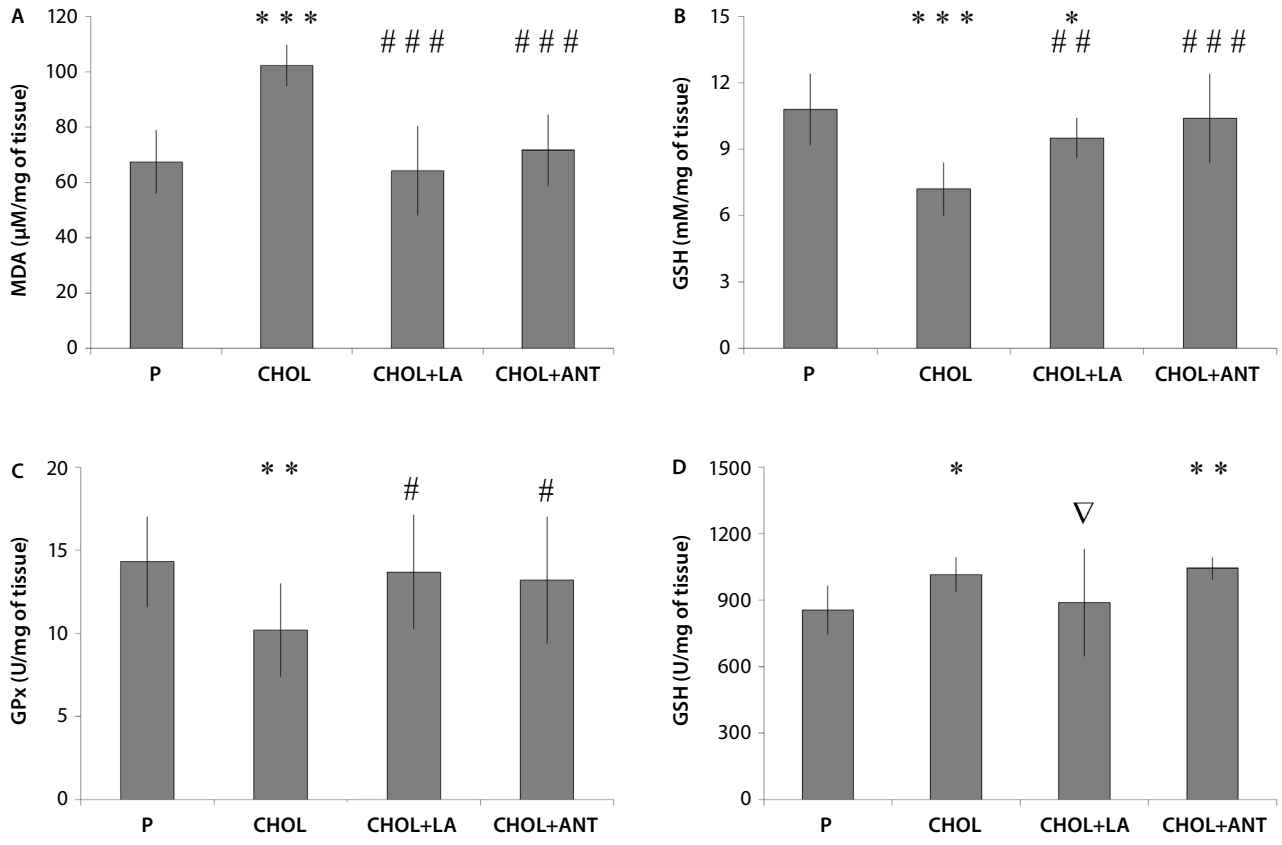

Fig. 3. The malondialdehyde (MDA) concentrations (A), glutathione (GSH) concentrations (B), glutathione peroxidase (GPx) activities (C), and superoxide dismutase (SOD) activities (D) in the liver

P – standard feed and vehicle-treated rabbits; CHOL – cholesterol-treated rabbits; CHOL+LA – rabbits treated with cholesterol + loganic acid 20 mg/kg bw.; CHOL+ANT – rabbits treated with cholesterol + anthocyanins 10 mg/kg bw.; values are presented as mean ±SD. Specific comparisons: * $p < 0.05$ vs P; ** $p < 0.01$ vs P; *** $p < 0.001$ vs P; # $p < 0.05$ vs CHOL; ## $p < 0.01$ vs CHOL; ### $p < 0.001$ vs CHOL; Δ $p < 0.05$ vs CHOL+ANT.

that both loganic acid, which belongs to a class of iridoids, and anthocyanins isolated from cornelian cherry fruits decreased the formation of atherosclerosis in the thoracic and, to a lesser extent, in the abdominal aorta of cholesterol-fed animals, while both substances decreased lipid peroxidation and oxidative stress in the liver.

Our finding that anthocyanins prevent atherosclerosis is consistent with numerous previous observations. Most of the available data attributes the cardiovascular benefits of fruits mainly to their (poly)phenolic fractions. A subclass of those, anthocyanins, abounds in cornelian cherry fruits.[13,15] They are regarded as potent substances preventing atherosclerosis and cardiovascular diseases.[8] Previous studies have found a higher content of anthocyanins in cornelian cherry fruits compared to other native or cultivated small fruits, such as raspberries, blackberries, red currants, and gooseberries,[15,16] although the total content of anthocyanins may differ significantly among cultivars.[17]

Atherosclerosis is a complex pathological condition that engages various pathways, such as lipid oxidation and accumulation in the arteries, inflammation, redox stress, and NO depletion. Drugs and natural products used nowadays in the treatment of dyslipidemia, like 3-hydroxy-3-methyl glutaryl coenzyme A (HMG-CoA) reductase inhibitors (statins), fibric acid derivatives, bile acid-binding resins, and phytosterols, have quite different mechanisms of action. We hypothesize that fruits may also affect lipid metabolism and atherogenesis through their different constituents and through different mechanisms. Beyond the (poly)phenolic fraction, other constituents of plants generally regarded as contributing to the prevention of dyslipidemia and atherosclerosis are mono- and polyunsaturated fatty acids, soluble fiber, vegetable proteins, and phytosterols.[18] Nevertheless, they are not found in substantial amounts in fruits.

As described in the Introduction, cornelian cherry fruits contain large amounts of anthocyanins, but are also abundant in iridoids. To the best of our knowledge, there is inadequate data comparing the biological effects and possible interactions between anthocyanins and iridoids, though those substances are present in the daily diet of western populations. In our previous studies, we detailed the constituents of cornelian cherry and proved that administering whole lyophilisated fruits diminished atherosclerosis through the same cholesterol-fed rabbit model we used in the present study.[12,14,19] Subsequently, we found that both isolated loganic acid and anthocyanins contributed to the prevention of atherosclerosis, decreasing dislipidemia as well as decreasing the intima

thickness and the intima/media ratio in the thoracic aorta of cholesterol-fed rabbits. We also revealed that both substances, especially anthocyanins, increased the expression of PPARs, while only iridoids possessed anti-inflammatory effects.[13] At present, we completed a detailed evaluation of the formation of atherosclerosis in both the thoracic and abdominal aorta as well as the assessment of redox status in the livers, and proved that loganic acid contributes to the benefits we observed previously.

Iridoids that we investigated, including loganic acid, are a wide group of cyclopentan[c]pyran monoterpenoids, metabolites found in plants and animals. Previous studies have shown their potent biological effects, mainly their anti-inflammatory qualities.[11] However, their preventive effects on diet-induced atherosclerosis, especially the possible mechanisms of action contributing to those effects, are not fully understood. This may be important, because some fruits, like those described in our studies – cornelian cherry, but also other members of the *Cornus* genus, especially the Asiatic *Cornus officinalis* L., and a few other fruits, contain large amounts of both anthocyanins and iridoids, although their qualitative and qualitative composition is different.[14,20] The beneficial effects of iridoids on lipid metabolism and diabetes, with the modulation of PPARα and sterol regulatory-element binding protein expression, were described regarding *Cornus officinalis* L., which grows mainly in Asia and has been used for years in traditional Chinese and Japanese medicine.[21–23] However, *Cornus officinalis* L. contains different iridoids than the European cornelian cherry we investigated, mainly loganin and morroniside. The positive effects on lipids and atherosclerosis were also proven for other iridoids isolated from various plants.[24–26] Nevertheless, knowledge about the effects of loganic acid we found in cornelian cherry on living systems, especially on atherogenesis, is poor.

In addition to the impact of loganic acid and anthocyanins on atherosclerosis, we also investigated their effects on lipid peroxidation and redox parameters in the liver. As we mentioned in the Introduction, there is a general conviction that oxidative stress plays a significant role in the pathogenesis of atherosclerotic vascular disease, proven by several in vitro and animal studies.[2,3,27] Oxidative stress causes direct damage to molecules, lipid peroxidation, and affects inflammation (e.g., by the stimulation of inflammatory genes transcription), at the same time causing vascular dysfunction through the endothelial nitric oxide synthase (eNOS) depletion.[4,28]

We found that both loganic acid and anthocyanins exerted a preventive effect on lipid peroxidation through an impact on the MDA level, and that both substances restored depleted GSH levels in the liver. The effects of anthocyanins shown in the present study are consistent with previous in vitro and in vivo studies, in which both cornelian cherry and isolated anthocyanins showed antioxidant capacities.[17,29,30] That observation seems to be supported by human studies that showed direct correlations between single anthocyanins intake and postprandial increases in serum antioxidant capacity.[29] However, that increase was only temporary and probably cannot explain the impact of anthocyanins on atherosclerosis development.

There are also publications attributing antioxidant effects to iridoids.[31] As we also described above, iridoids are a large group of substances that exert several effects on living systems, including substantial anti-inflammatory effects that may influence oxidative stress.[11] Loganic acid and other iridoids also showed antiglycation activity, decreasing the production of advanced glycation end products (AGE), the elevation of which may be triggered by oxidative stress.[32] However, we did not find any previous studies examining the direct effects of loganic acid on redox status.

Taking into account the doses of substances used in our experiment, human equivalent doses (HEDs) may be determined. According to the Food and Drug Administration, Center for Drug Evaluation and Research guidelines,[33,34] HEDs of loganic acid and anthocyanins are 6.48 mg/kg bw. per day and 3.24 mg/kg bw. per day, respectively. For the human body weighing 100 kg, HED of loganic acid is 648 mg/day and of anthocyanins – 324 mg/day. Estimated HEDs enable the creation of phytopharmaceuticals in solid dosage forms, such as capsules or tablets, as well as in liquid forms (both substances are soluble in water and in alcohol solutions). Moreover, taking into consideration the amount of loganic acid and anthocyanins in lyophilisated fruits, cornelian cherries may be used as a functional food. Daily HEDs of loganic acid and anthocyanins found in whole lyophilisated fruits (without a pit) are approx. 79 g and 137.4 g, respectively (for a 100 kg man).

Based on our present and previous studies, possible indications for cornelian cherry and its isolated constituents include dyslipidemia and atherosclerosis.[12,14,19] Whole dried or lyophilisated fruits may be used as a functional food in patients treated with a diet and lifestyle modifications alone. Isolated components or extracts may be used as phytopharmaceuticals in patients treated with statins. In our previous studies, we proved that both whole fruits and isolated constituents of cornelian cherry upregulated the expression of PPARα in the liver. PPARα is a transcriptional factor responsible for fatty acid catabolism via the activation of their beta-oxidation.[12,14] We may speculate that due to a possibly different mechanism of pharmacological actions of cornelian cherry and its components and of statins, they may exert additive or synergistic effects.

Anthocyanins and iridoids are regarded as generally safe. Moreover, cornelian cherry fruits containing high amounts of those substances are considered edible and have been used in cuisine for hundreds of years. In our present and previous experiments, we have observed no adverse effects of 2-month-long oral administration of loganic acid, anthocyanins or whole lyophilisated fruits. Substances isolated from cornelian cherry used in our study, were not modified and, as stated above, their amounts may be consumed daily in dried or lyophilisated form by the general population.

Here, the limitations of our study should be noted. Although we showed the preventive effects of the investigated substances on both atherosclerosis and oxidative stress, the assessment of a direct correlation is difficult, because there are many other factors influencing atherogenesis that we did not investigate. Moreover, although many in vitro and in vivo studies support the importance of redox modulation in tissues, their effects on clinical outcomes are unclear. Results of many human clinical trials involving the use of antioxidant vitamins are highly ambiguous.[35] Analyzing the changes in redox status, we should ask if the observed changes in lipid peroxidation and redox state are the direct results of the treatment and contribute to the positive effects on lipids and atherosclerosis. Alternatively, the antioxidant effects of the investigated substances may only be secondary changes related to other mechanisms – like the PPAR pathway or anti-inflammatory effects – subsequently diminishing redox triggering factors. This possibility remains a puzzle in several risk factors contributing to the development of atherosclerosis.

Conclusions

In conclusion, we have shown that different constituents – anthocyanins and iridoid loganic acid – of the same cornelian cherry plant showed the similar beneficial effects on holesterol-fed induced atherosclerosis. Anthocyanins and loganic acid diminished the formation of atherosclerotic plaques in the thoracic and, to a lesser extent, in the abdominal aorta, as well as diminished lipid peroxidation and reversed cholesterol-induced depletion of GSH in the liver. The results of our study indicate some potential benefits of consuming fruits containing both anthocyanins and iridoids that prevent cardiovascular diseases. Those results may also be applied in future attempts to produce phytopharmaceuticals containing those substances.

References:

1. Townsend N, Nichols M, Scarborough P, Rayner M. Cardiovascular disease in Europe: Epidemiological update. *Eur Heart J*. 2015;36(40):2696–2705.
2. He F, Zuo L. Redox roles of reactive oxygen species in cardiovascular diseases. *Int J Mol Sci*. 2015;16(11):27770–27780.
3. Daiber A, Di Lisa F, Oelze M, et al. Crosstalk of mitochondria with NADPH oxidase via reactive oxygen and nitrogen species signaling and its role for vascular function [published online on December 9, 2015]. *Br J Pharmacol*. 2015. doi:10.1111/bph.13403
4. Daiber A, Mader M, Stamm P, et al. Oxidative stress and vascular function. *Cell Membranes and Free Radical Research*. 2013;5(1):221–232.
5. Henkin Y, Kovsan J, Gepner Y, Shai I. Diets and morbid tissues: History counts, present counts. *Br J Nutr*. 2015;113(Suppl 2):S11–18.
6. Stefler D, Malyutina S, Kubinova R, et al. Mediterranean diet score and total and cardiovascular mortality in Eastern Europe: the HAPIEE study. *Eur J Nutr*. 2017;56(1):421–429.
7. Tsuda T. Dietary anthocyanin-rich plants: Biochemical basis and recent progress in health benefits studies. *Mol Nutr Food Res*. 2012;56(1):159–170.
8. Cassidy A, Mukamal KJ, Liu L, Franz M, Eliassen AH, Rimm EB. High anthocyanin intake is associated with a reduced risk of myocardial infarction in young and middle-aged women. *Circulation*. 2013;127(2):188–196.
9. Rangel-Huerta OD, Pastor-Villaescusa B, Aguilera CM, Gil A. Systematic review of the efficacy of bioactive compounds in cardiovascular disease: Phenolic compounds. *Nutrients*. 2015;7(7):5177–5216.
10. Hoek-van den Hil EF, van Schothorst EM, van der Stelt I, et al. Direct comparison of metabolic health effects of the flavonoids quercetin, hesperetin, epicatechin, apigenin and anthocyanins in high-fat-diet-fed mice. *Genes and Nutrition*. 2015;10(4):469.
11. Viljoen A, Mncwangi N, Vermaak I. Anti-inflammatory iridoids of botanical origin. *Curr Med Chem*. 2012;19(14):2104–2127.
12. Sozański T, Kucharska AZ, Szumny A, et al. The protective effect of the *Cornus mas* fruits (cornelian cherry) on hypertriglyceridemia and atherosclerosis through PPARα activation in hypercholesterolemic rabbits. *Phytomedicine*. 2014;21(13):1774–1784.
13. Kucharska AZ, Szumny A, Sokół-Łętowska A, Piórecki N, Klymenko SV. Iridoids and anthocyanins in cornelian cherry (*Cornus mas* L.) cultivars. *J Food Comp Anal*. 2015;40:95–102.
14. Sozański T, Kucharska AZ, Rapak A, et al. Iridoid-loganic acid versus anthocyanins from the *Cornus mas* fruits (cornelian cherry): Common and different effects on diet-induced atherosclerosis, PPARs expression and inflammation. *Atherosclerosis*. 2016;254:151–160.
15. Pantelidis GE, Vasilakakis M, Manganaris GA, Diamantidis G. Antioxidant capacity, phenol, anthocyanin and ascorbic acid contents in raspberries, blackberries, red currants, gooseberries and cornelian cherries. *Food Chem*. 2007;102:777–783.
16. Vareed SK, Reddy MK, Schutzki RE, Nair MG. Anthocyanins in *Cornus alternifolia, Cornus controversa, Cornus kousa* and *Cornus florida* fruits with health benefits. *Life Sci*. 2006;78(7):777–784.
17. Popović BM, Stajner D, Slavko K, Sandra B. Antioxidant capacity of cornelian cherry (*Cornus mas* L.): Comparison between permanganate reducing antioxidant capacity and other antioxidant methods. *Food Chem*. 2012;134(2):734–741.
18. Rosa COB, dos Santos CA, Leite JI, Caldas AP, Bressan J. Impact of nutrients and food components on dyslipidemias: What is the evidence? *Adv Nutr*. 2015;6(6):703–711.
19. Sozański T, Kucharska AZ, Szumny D, et al. Cornelian cherry consumption increases the L-arginine/ADMA ratio, lowers ADMA and SDMA levels in the plasma, and enhances the aorta glutathione level in rabbits fed a high-cholesterol diet. *J Funct Foods*. 2017;34:189–196.
20. Du WF, Cai H, Wang MY, Ding X, Yang H, Cai BC. Simultaneous determination of six active components in crude and processed *Fructus Corni* by high performance liquid chromatography. *J Pharm Biomed Anal*. 2008;48(1):194–197.
21. Park CH, Yamabe N, Noh JS, Kang KS, Tanaka T, Yokozawa T. The beneficial effects of morroniside on the inflammatory response and lipid metabolism in the liver of db/db mice. *Biol Pharm Bull*. 2009;32(10):1734–740.
22. Park CH, Noh JS, Tanaka T, Yokozawa T. Effects of morroniside isolated from *Corni Fructus* on renal lipids and inflammation in type 2 diabetic mice. *J Pharm Pharmacol*. 2010;62(3):374–380.
23. Yamabe N, Noh JS, Park CH, et al. Evaluation of loganin, iridoid glycoside from *Corni Fructus*, on hepatic and renal glucolipotoxicity and inflammation in type 2 diabetic db/db mice. *Eur J Pharmacol*. 2010;648(1-3):179–187.
24. Liao P, Liu L, Wang B, Li W, Fang X, Guan S. Baicalin and geniposide attenuate atherosclerosis involving lipids regulation and immunoregulation in ApoE-/- mice. *Eur J Pharmacol*. 2014;740:488–495.
25. Liu JY, Zhang DJ. Amelioration by catalpol of atherosclerotic lesions in hypercholesterolemic rabbits. *Planta Med*. 2015;81(3):175–184.
26. Gao Y, Chen ZY, Liang X, Wei SF. Anti-atherosclerotic effect of geniposidic acid in a rabbit model and related cellular mechanisms. *Pharm Biol*. 2015;53(2):280–285.
27. Kang DH, Kang SW. Targeting cellular antioxidant enzymes for treating atherosclerotic vascular disease. *Biomol Ther (Seoul)*. 2013;21(2):89–96. doi:10.4062/biomolther. 2013.015
28. Aboonabi A, Singh I. Chemopreventive role of anthocyanins in atherosclerosis via activation of Nrf2-ARE as an indicator and modulator of redox. *Biomed Pharmacother*. 2015;72:30–36.
29. Mazza G, Kay CD, Cottrell T, Holub BJ. Absorption of anthocyanins from blueberries and serum antioxidant status in human subjects. *J Agric Food Chem*. 2002;50(26):7731–7737.
30. Rafieian-Kopaei M, Asgary A, Adelnia M, et al. The effects of cornelian cherry on atherosclerosis and atherogenic factors in hypercholesterolemic rabbits. *J Med Plants Res*. 2011;5:2670–2676.

31. Barreto RS, Albuquerque-Júnior RL, Araújo AA, et al. A systematic review of the wound-healing effects of monoterpenes and iridoid derivatives. *Molecules*. 2014;19(1):846–862.
32. West BJ, Uwaya A, Isami F, Deng S, Nakajima S, Jensen CJ. Antiglycation activity of iridoids and their food sources. *Int J Food Sci*. 2014;2014:276950. doi:10.1155/2014/276950
33. U.S. Department of Health and Human Services, Food and Drug Administration, Center for Drug Evaluation and Research (CDER). Guidance for Industry. Estimating the Maximum Safe Starting Dose in Initial Clinical Trials for Therapeutics in Adult Healthy Volunteers. Chapter V. Step 2: Human equivalent dose calculation. Published by the Annual Review of Pharmacology and Toxicology, July 2005. https://www.fda.gov/downloads/drugs/guidances/ucm078932.pdf. Accessed April 16, 2016.
34. Nair AB, Jacob S. A simple practice guide for dose conversion between animals and human. *J Basic Clin Pharm*. 2016;7(2):27–31.
35. Vogiatzi G, Tousoulis D, Stefanadis C. The role of oxidative stress in atherosclerosis. *Hellenic J Cardiol*. 2009;50(5):402–409.

Obesity without comorbidity may also lead to non-thyroidal illness syndrome

Şakir Ö. Keşkek[A,C–F], Özlem Kurşun[A,B], Gülay Ortoğlu[B,E], Mehmet Bankir[A,E], Zeynep Tüzün[B], Tayyibe Saler[D,F]

Department of Internal Medicine, Numune Training and Research Hospital, Adana, Turkey

A – research concept and design; B – collection and/or assembly of data; C – data analysis and interpretation; D – writing the article; E – critical revision of the article; F – final approval of the article

Advances in Clinical and Experimental Medicine, ISSN 1899-5276 (print), ISSN 2451-2680 (online) *Adv Clin Exp Med*. 2018;27(11):1515–1520

Address for correspondence
Şakir Keşkek
E-mail: drkeskek@yahoo.com

Funding sources
None declared

Conflict of interest
None declared

Received on October 27, 2016
Reviewed on December 1, 2016
Accepted on April 5, 2017

Abstract

Background. Obesity mediates a series of operations in the body by increasing the production of proinflammatory cytokines. Cytokines play an important role in the development of non-thyroidal illness syndrome (NTIS).

Objectives. The aim of this study was to investigate the association between obesity and NTIS.

Material and methods. A total of 423 subjects were included. The study group was comprised of 219 obese patients without any comorbid disease and the control group was comprised of 204 healthy subjects. Body mass index (BMI), thyroid hormone levels, high-sensitivity C-reactive protein (hs-CRP) levels, erythrocyte sedimentation rate (ESR), complete blood count, and other biochemical parameters were measured. Frequencies of NTIS were calculated. MedCalc v. 12.5 software program (MedCalc, Ostend, Belgium) was used for statistical analysis.

Results. Groups were statistically different according to BMI ($p < 0.001$). The mean BMIs of the study and the control group were 34.6 ± 5.0 kg/m^2 and 22.6 ± 1.8 kg/m^2, respectively. Obese patients had higher serum hs-CRP levels, ESR and white blood cells (WBC) levels (0.99 ± 3.17 mg/L vs 0.39 ± 1.09 mg/L; 17.2 ± 10.6 mm/h vs 12.6 ± 8.0 mm/h; 7.8 ± 2.1 10^3/μL vs 6.9 ± 1.5 10^3/μL, respectively; $p < 0.001$). There were 21 (9.5%) obese patients with NTIS, while there were none NTIS cases in the control group. The difference was statistically significant ($p < 0.001$). There was a strong association between obesity and NTIS (odds ratio (OR) = 44.2, 95% confidence interval (CI) = 2.66–736.3; $p = 0.0082$).

Conclusions. Inflammation, which is strongly associated with adipose tissue, may lead to NTIS in obese patients without any comorbid disease.

Key words: obesity, high-sensitivity C-reactive protein, erythrocyte sedimentation rate, white blood cell, non-thyroidal illness syndrome

DOI
10.17219/acem/70226

Introduction

Obesity has a high prevalence throughout the world. The World Health Organization (WHO) reported that more than 1.9 billion adults were overweight in 2014. Obesity has become an important public health problem because of its related complications. It can lead to diabetes mellitus, hypertension, cardiovascular disease, and other chronic disorders.[1–3] Multiple etiological factors have been connected to the genesis of obesity, of which genetic susceptibility, high calorie intake, lifestyle, and psychiatric illness are important.[1–4]

The production of cytokines, chemokines and coagulation proteins increase in the case of obesity due to the increased adipose tissue, which is an endocrine organ. This condition brings about several reactions in the body.[5,6] These pathophysiological reactions can stimulate endoplasmic reticulum stress and inflammation in various cells. Inflammation and lipotoxicity play an important role in the progression of chronic diseases associated with obesity.[7]

Abnormalities in thyroid hormone levels in the absence of underlying thyroid disease can be found in the case of acute or severe disease. Illness results in profound changes in thyroid hormone metabolism called the sick euthyroid syndrome or non-thyroidal illness syndrome (NTIS). Although the etiologic mechanism of NTIS is not well-known, there are several theories regarding the disease. The 1st theory concerns the difference between the effects of type I and type II deiodinase, which are mediated by inflammatory cytokines; the 2nd theory focuses on decreased hypothalamus and pituitary response to thyroid hormones; the 3rd theory concerns lower levels of T4 binding protein and cellular uptake.[8]

According to the previous studies, obesity is an inflammatory disease and inflammation has negative effects on thyroid metabolism.[5–7] The aim of the current study was to investigate the association between obesity and NTIS in obese patients without any comorbid disease.

Material and methods

This cross-sectional cohort study was carried out in Numune Training and Research Hospital, Adana, Turkey, from December 2013 to May 2015. Approval for the study protocol was granted by the hospital institutional review board (approval No: ANEAH.EK 2013/60) and the study was conducted in accordance with the Declaration of Helsinki, as revised in 2008. Informed consent was obtained from all participants before enrollment. All applications were concordant with the Good Clinical Practice standards.

A total of 423 subjects of both genders were enrolled. The study group comprised 219 obese patients without any comorbid disease and the control group comprised 204 healthy subjects. Patients with a diagnosis of any acute or chronic disease, and patients with a history of thyroid diseases (primary, secondary or autoimmune) were excluded. Pregnant or breastfeeding women were also excluded.

Biochemical tests were performed, and body mass index (BMI) and blood pressure were measured. Blood pressure of patients was measured after 10 min of rest with calibrated sphygmomanometers (Erka, Bad Tölz, Germany) at least 2 times. Body mass index was calculated by weight [kg]/height [m^2].

A venous blood sample for biochemical tests was collected in the morning following overnight fasting. Fasting glucose, serum lipids, creatinine, aspartate aminotransferase (AST), alanine aminotransferase (ALT), insulin, insulin resistance, thyrotropin (thyroid stimulating hormone – TSH), free triiodothyronine (FT3), free thyroxine (FT4), erythrocyte sedimentation rate (ESR), and high-sensitivity C-reactive protein (hs-CRP) levels were measured. A complete blood count was performed. The levels of TSH, FT3, FT4, and insulin were measured by the Abbott Architect i2000 SR analyzer system (Abbott Laboratories, Abbot Park, USA). Fasting glucose, triglyceride, low-density lipoprotein (LDL) and high-density lipoprotein (HDL) levels were analyzed with an automatic analyzer (Roche C-501; Roche, Tokyo, Japan) by using the hexokinase method (glucose) and the homogeneous colorimetric enzyme test (triglyceride, LDL and HDL). Other biochemical values (creatinine, AST and ALT) were analyzed with Beckman Coulter Synchron LX 20 (Beckman Coulter, Brea, USA), using commercially available kits (original Beckman Coulter reagents). Complete blood counts were measured with Sysmex XE 2100i (Sysmex, Kobe, Japan) by fluorescence flow cytometry. Erythrocyte sedimentation rates were measured using the Westergren method with Sed Rate Screener 100 (Greiner Bio-One GmbH, Kremsmünster, Austria). The level of hs-CRP was analyzed using the immunoturbidimetric method with Roche Integra 400 (Roche). Insulin resistance (homeostasis model assessment of insulin resistance – HOMA-IR) was calculated according to the fasting insulin × fasting glucose/405 formulas.

Patients with a BMI higher than 30 kg/m^2 were defined as obese. Non-thyroidal illness syndrome was diagnosed when free FT3 levels were below the normal range, and/or FT4 levels were within the normal or low values, and TSH levels were within the normal or low values.[9]

Statistical analyses were performed using the MedCalc v. 12.5 software program (MedCalc, Ostend, Belgium). Categorical measurements were reported as number and percentage. Quantitative measurements were reported as mean ± standard deviation (SD). The Kolmogorov-Smirnov test was used to show normal distribution of quantitative measurements. The χ^2 test was used to compare categorical (gender) measures and frequency of thyroid dysfunction between the groups. The t-test or the Mann-Whitney U test were used for comparison of biochemical tests and thyroid hormone concentrations between the 2 groups. Pearson's correlation coefficient was used

to analyze the degree of association between 2 variables. A log transformation was used for the variables that were not normally distributed. The odds ratio (OR) was used to analyze the degree of association between NTIS and obesity. An overall p-value <0.05 was considered a statistically significant result.

Results

The mean age of the study group (obese patients) and control group (healthy patients) was 38.6 ±10.9 years and 37.2 ±12.1 years, respectively. There were 163 (74.4%) women and 56 (25.6%) men in the study group, and 139 (68.1%) women and 65 (31.9%) men in the control group. There was no statistically significant difference in the age and gender distribution in the 2 groups (p = 0.065 and p = 0.153, respectively) (Table 1). The mean BMI of the obese patients was 34.6 ±5.0 kg/m^2, while it was 22.6 ±1.8 kg/m^2 in healthy subjects. The groups were statistically different regarding BMI (p < 0.001) (Table 1).

The groups were comparable in terms of blood glucose, triglyceride, HDL, LDL, AST, ALT, and creatinine levels, as well as systolic blood pressure (SBP) and diastolic blood pressure (DBP) (p > 0.05, for each) (Table 1). The mean serum insulin level (16.3 ±14.4 μU/mL vs 10.9 ±7.5 μU/mL; p < 0.001) and HOMA-IR (3.4 ±2.0 vs 2.4 ±1.7; p < 0.001) were high in obese patients (Table 1).

The mean serum hs-CRP levels of the study and control groups were 0.99 ±3.17 mg/L and 0.39 ±1.09 mg/L, respectively. There was a statistically significant difference between the groups regarding the hs-CRP level (p < 0.001) (Table 2). The levels of ESR and white blood cells (WBC) were higher in obese patients. The mean ESR level was 17.2 ±10.6 mm/h in obese patients, while it was 12.6 ±8.0 mm/h in healthy subjects (p < 0.001). The mean level of WBC was 7.8 ±2.1 10^3/μL in obese patients, while it was 6.9 ±1.5 10^3/μL in healthy subjects (p < 0.001) (Table 2).

The groups were comparable regarding the thyroid hormone levels (TSH, FT3 and FT4) (p > 0.05, for each). There were 21 (9.5%) obese patients with NTIS, while there were none NTIS cases in the control group. The difference was statistically significant (p < 0.001) (Table 3).

Obese patients with NTIS (n = 21) had higher hs-CRP levels and ESR compared to obese patients without NTIS (n = 198). The level of hs-CRP and ESR in obese subjects with NTIS were 2.58 ±8.3 mg/L and 23.3 ±16.2 mm/h, respectively, while they were 0.81 ±1.9 mg/L and 16.6 ±9.7 mm/h, respectively, in obese subjects without NTIS (p = 0.015 and p = 0.005, respectively) (Table 4).

Table 1. Demographic and clinical properties of the groups

Variables	Obese group (n = 219)	Healthy group (n = 204)	p-value
Age [years]	38.6 ±10.9	37.2 ±12.1	0.065
Female	163 (74.4)	139 (68.1)	0.153
BMI [kg/m^2]	34.6 ±5.0	22.6 ±1.8	<0.001
Glucose [mg/dL]	91.6 ±6.5	90.7 ±6.4	0.145
Insulin [μU/mL]	16.3 ±14.4	10.9 ±7.5	<0.001
HOMA-IR	3.4 ±2.0	2.4 ±1.7	<0.001
Triglyceride [mg/dL]	133.1 ±47.5	126.9 ±57.8	0.082
HDL [mg/dL]	44.9 ±14.6	47.3 ±12.1	0.064
LDL [mg/dL]	124.5 ±34.0	117.3 ±26.0	0.144
SBP [mm Hg]	118.0 ±10.1	117.6 ±7.4	0.654
DBP [mm Hg]	72.3 ±5.7	71.9 ±5.1	0.520
ALT [IU/L]	19.2 ±9.6	18.5 ±8.9	0.095
AST [IU/L]	20.2 ±11.3	18.6 ±10.6	0.115
Creatinine [mg/dL]	0.76 ±0.22	0.74 ±0.24	0.660

Data is presented as mean ± standard deviation (SD) or as n (%).
BMI – body mass index; HOMA-IR – homeostasis model assessment of insulin resistance; LDL – low-density lipoprotein, HDL – high-density lipoprotein, AST – aspartate aminotransferase, ALT –alanine aminotransferase; SBP – systolic blood pressure; DBP – diastolic blood pressure.

Table 2. WBC, ESR and hs-CRP levels of the groups

Variables	Obese group (n = 219)	Healthy group (n = 204)	p-value
WBC [10^3/μL]	7.8 ±2.1	6.9 ±1.5	<0.001
ESR [mm/h]	17.2 ±10.6	12.6 ±8.0	<0.001
hs-CRP [mg/L]	0.99 ±3.17	0.39 ±1.09	<0.001

Data is presented as mean ± standard deviation (SD). WBC – white blood cells; ESR – erythrocyte sedimentation rate; hs-CRP – high-sensitivity C-reactive protein.

Table 3. Thyroid hormone levels and frequency of NTIS of the groups

Variables	Obese group (n = 219)	Healthy group (n = 204)	p-value
FT3 [pg/mL]	3.1 ±0.58	3.2 ±0.35	0.090
FT4 [ng/dL]	1.17 ±0.3	1.11 ±0.21	0.095
TSH [mcIU/mL]	1.96 ±1.0	1.78 ±0.88	0.127
Frequency of NTIS	21 (9.5)	0 (0)	<0.001

Data is presented as mean ± standard deviation (SD) or as n (%).
NTIS – non-thyroidal illness syndrome; FT3 – free triiodothyronine; FT4 – free thyroxine; TSH – thyroid-stimulating hormone.

Table 4. Comparison of obese patients according to NTIS

Variables	Obese patients NTIS (+)	Obese patients NTIS (–)	p-value
WBC [10^3/μL]	7.7 ±2.2	7.8 ±2.0	0.483
ESR [mm/h]	23.3 ±16.2	16.6 ±9.7	0.005
hs-CRP [mg/L]	2.58 ±8.3	0.81 ±1.9	0.015

Data is presented as mean ± standard deviation (SD). NTIS – non-thyroidal illness syndrome; WBC – white blood cells; ESR – erythrocyte sedimentation rate; hs-CRP – high-sensitivity C-reactive protein.

Table 5. Correlations of hs-CRP with BMI, FT3 and HOMA-IR

Variables	BMI	FT3	HOMA-IR
hs-CRP	r = 0.416 p < 0.01	r = –0.176 p = 0.009	r = 0.170 p = 0.011

hs-CRP – high-sensitivity C-reactive protein; BMI – body mass index; FT3 – free triiodothyronine; HOMA-IR – homeostasis model assessment of insulin resistance.

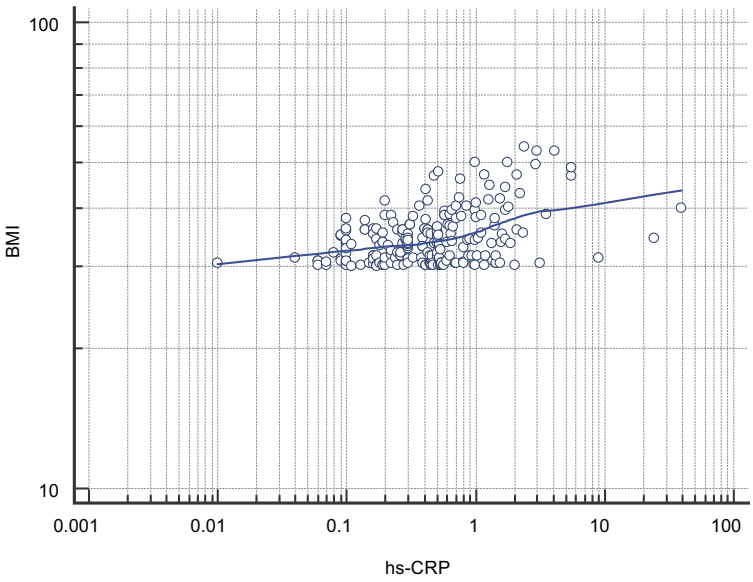

Fig. 1. Correlation between hs-CRP and BMI

In a scatter diagram, the correlation between hs-CRP and BMI has been shown graphically. The horizontal axis defines hs-CRP and the vertical axis defines BMI.

BMI – body mass index; hs-CRP – high-sensitivity C-reactive protein.

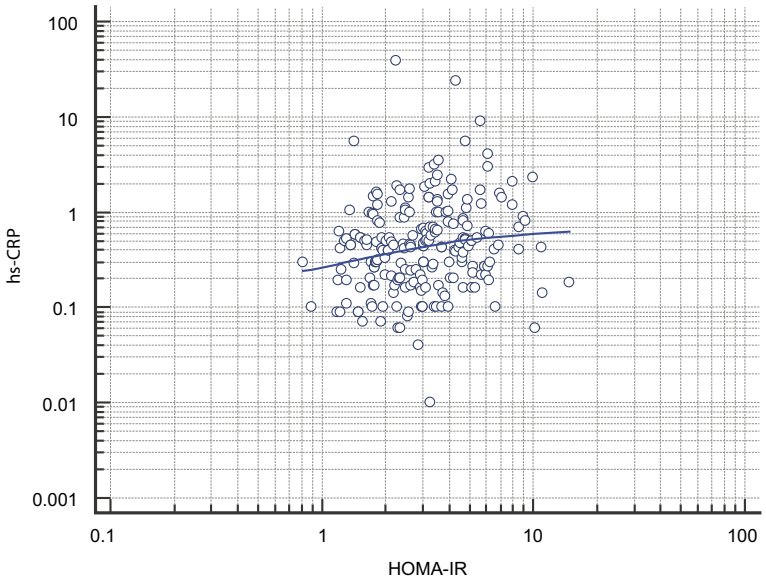

Fig. 2. Correlation between hs-CRP and HOMA-IR

In a scatter diagram, the correlation between hs-CRP and HOMA-IR has been shown graphically. The vertical axis defines hs-CRP and the horizontal axis defines HOMA-IR.

hs-CRP – high-sensitivity C-reactive protein; HOMA-IR – homeostasis model assessment of insulin resistance.

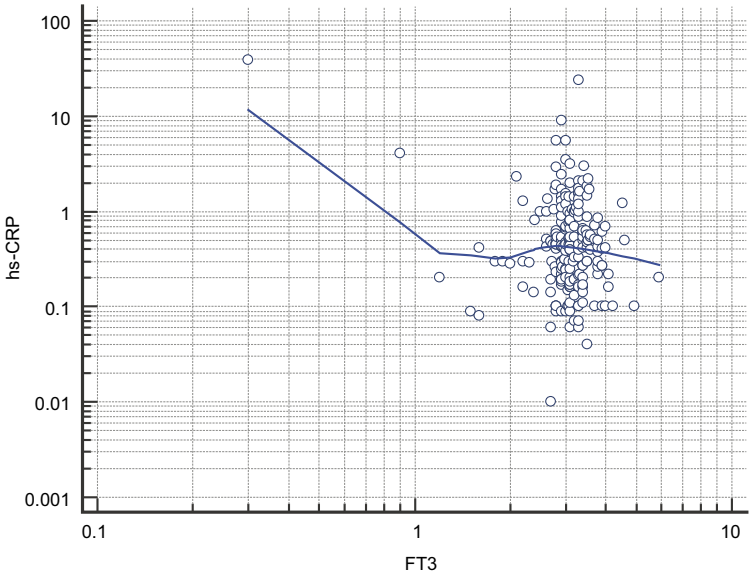

Fig. 3. Correlation between hs-CRP and FT3

In a scatter diagram, the correlation between hs-CRP and FT3 has been shown graphically. The vertical axis defines hs-CRP and the horizontal axis defines FT3.

hs-CRP – high-sensitivity C-reactive protein; FT3 – free triiodothyronine.

A positive correlation was found between hs-CRP level and BMI (r = 0.416; p < 0.01) (Table 5, Fig. 1), and between hs-CRP level and HOMA-IR (r = 0.170; p = 0.011) (Table 5, Fig. 2) in the study group, according to Pearson's correlation analyses. Additionally, a negative correlation was found between hs-CRP and FT3 levels (r = −0.176; p = 0.009) (Table 5, Fig. 3). There was a strong association between obesity and NTIS (OR = 44.2; confidence interval (CI) = 95% 2.66–736.3; p = 0.0082).

Discussion

A high frequency of NTIS in obese patients was found in this study. Moreover, a potent association between NTIS and obesity was also shown. Non-thyroidal illness syndrome is an abnormality of thyroid hormone concentration observed in a wide variety of acute or severe diseases without underlying thyroid illness. Inhibition of hepatic enzyme and deiodinases mediated by inflammatory cytokines strongly contributes to the development of NTIS.[10,11]

Obesity degenerates tissue functions and increases the development of a number of diseases, such as high blood pressure, atherosclerosis, diabetes, and non-alcoholic fatty liver disease.[1,2,12] On the other hand, obesity is also an inflammatory disease. Expression and secretion of proinflammatory cytokines, such as tumor necrosis factor alpha (TNF-α), monocyte chemoattractant protein 1 (MCP1), interleukin 6 (IL-6), CRP, and plasminogen activator inhibitor type 1 (PAI-1) are increased by the adipose tissue of obese individuals.[13–15] As evidence of inflammation, we found high levels of hs-CRP, ESR and WBC in obese individuals. We also showed a significant correlation between hs-CRP and BMI. In accordance with this link, Ramírez Alvarado and Sánchez Roitz reported that serum levels of CRP, and therefore subclinical inflammation, seemed to be associated with high rates of anthropometric measures in the South American population.[16]

Genes involved in the production and release of T4 and T3 are severely affected by high concentrations of pro-inflammatory cytokines.[17] Therefore, cytokines play an important role in the development of NTIS. Interleukin 6 was found to be negatively correlated with serum T3 concentrations in hospitalized patients.[18] Davies et al. reported an association between elevated serum IL-6 concentrations and changes in circulating thyroid hormones in NTIS, secondary to several medical conditions.[19] Tumor necrosis factor alpha was found to be a mediator of several disorders leading to hypothalamic-pituitary dysfunction. Research of the effects of administering TNF-α and IL-1β to animals and humans showed their possible role in the pathogenesis of NTIS, with each cytokine stimulating critical illness and changes of low serum T3.[20–23] Further reinforcing this link, Tognini et al. reported an inverse correlation between FT3 and hs-CRP levels in 301 critically ill patients.[24] In the current study, we found higher levels of hs-CRP in obese patients with NTIS. Additionally, we showed an inverse correlation between hs-CRP and serum FT3.

Chronic inflammation plays a significant role in the pathophysiologic mechanism of insulin resistance. Increased secretion of TNF-α from the adipose tissue of obese individuals has been reported previously.[5,25,26] Additionally, insulin resistance was found to be associated with TNF-α levels.[5,25] Tumor necrosis factor alpha promotes inflammation and suppresses insulin sensitivity in insulin target cells. Elevated plasma TNF-α level may be an important mediator of insulin resistance by impairing insulin signaling.[5,25,26] Furthermore, CRP, which is an acute phase reactant and an inflammatory signal, is commonly elevated in the case of insulin resistant disorders.[27] In this study, high serum insulin levels and HOMA-IR index were shown in obese subjects. Moreover, a significant positive correlation was shown between hs-CRP level and HOMA-IR. Low levels of anti-inflammatory and antidiabetic adiponectins have also been shown in obese subjects previously.[28] In accordance with this link, Menon et al. examined the effects of surgically removing visceral adipose tissue in Ames dwarf mice. They concluded that the altered profile of adipokines secreted by visceral fat might play a key role in increased insulin sensitivity.[29] Similarly, Masternak et al. investigated the effects of visceral fat removal in normal and growth hormone receptor-resistant mice. They reported that visceral fat removal had a beneficial effect on insulin sensitivity in normal mice.[30] The results of the current study are supported by studies carried out by both Menon et al. and Masternak et al.[29,30]

Our study had also some limitations. Firstly, it could have been beneficial if reverse triiodothyronine (rT3) had been measured in obese patients with NTIS. Secondly, well-balanced diets and regular exercise are important components of the overall approach to treating obesity. We suggested well-balanced diets and regular exercise for all patients. However, we did not check the patients after weight loss for NTIS.

On the other hand, we have some powerful points. Firstly, according to the power analyses (80%), the sample size of the current study was sufficient for clear results. Secondly, the extensive exclusion criteria is another strong point. The obese individuals in this study had no disease other than obesity. According to our best knowledge, this is the first study that investigates NTIS in obese patients without any comorbid disease.

Conclusions

In conclusion, NTIS can be found in obese patients without any comorbid disease. Obesity can degenerate tissue functions due to the increased expression and secretion of proinflammatory cytokines. Abnormalities in thyroid hormone levels in the absence of underlying thyroid disease can be found in the case of severe diseases.

Inflammation, which is strongly associated with obesity, can lead to NTIS in these patients. Finally, obese patients without any comorbidity should be evaluated for NTIS before treating thyroid dysfunctions.

References

1. World Health Organization. Obesity and overweight. http://www.who.int/mediacentre/factsheets/fs311/en//. Accessed December 2, 2017.
2. Visscher TL, Seidell JC. The public health impact of obesity. *Annu Rev Public Health*. 2001;22:355–375.
3. Rippey FF. Thrombosis and embolism. In: *General Pathology*. Johannesburg, South Africa: Witwatersrand University Press; 2003:103–109.
4. Rang HP, Dale MM, Ritter JM, Moore PK. *Pharmacology*. New Delhi, India: Churchill Livingstone; 2006:394–403.
5. Hotamisligil GS, Arner P, Caro JF, Atkinson RL, Spiegelman BM. Increased adipose tissue expression of tumor necrosis factor-alpha in human obesity and insulin resistance. *J Clin Invest*. 1995;95(5):2409–2415. doi: 10.1172/JCI117936
6. Mathieu P, Poirier P, Pibarot P, Lemieux I, Després JP. Visceral obesity: The link among inflammation, hypertension, and cardiovascular disease. *Hypertension*. 2009;53(4):577–584.
7. Hotamisligil GS. Role of endoplasmic reticulum stress and c-Jun NH2-terminal kinase pathways in inflammation and origin of obesity and diabetes. *Diabetes*. 2005;54(Suppl 2):S73–S78.
8. De Groot LJ. Non-thyroidal illness syndrome is a manifestation of hypothalamic-pituitary dysfunction, and in view of current evidence, should be treated with appropriate replacement therapies. *Crit Care Clin*. 2006;22(1):57–86.
9. Adler SM, Wartofsky L. The nonthyroidal illness syndrome. *Endocrinol Metab Clin North Am*. 2007;36(3):657–672.
10. Demers LM, Spencer C. The thyroid. Pathophysiology and thyroid testing. In: Burtis CA, Ashwood ER, Bruns DE, eds. *Tietz Textbook of Clinical Chemistry and Molecular Diagnostics*. 4th ed. St. Louis, MO: Elsevier; 2006.
11. McIver B, Gorman CA. Euthyroid sick syndrome: An overview. *Thyroid*. 1997;7(1):125–132.
12. Flegal KM, Graubard BI, Williamson DF, Gail M. Cause-specific excess deaths associated with underweight, overweight, and obesity. *JAMA*. 2007;298(17):2028–2037.
13. Mohamed-Ali V, Goodrick S, Rawesh A, et al. Subcutaneous adipose tissue releases interleukin-6, but not tumor necrosis factor-alpha, in vivo. *J Clin Endocrinol Metab*. 1997;82(12):4196–4200.
14. Fried SK, Bunkin DA, Greenberg AS. Omental and subcutaneous adipose tissues of obese subjects release interleukin-6: Depot difference and regulation by glucocorticoid. *J Clin Endocrinol Metab*. 1998;83(3):847–850.
15. Visser M, Bouter LM, McQuillan GM, Wener MH, Harris T. Elevated C-reactive protein levels in overweight and obese adults. *JAMA*. 1999;282(22):2131–2135.
16. Ramírez Alvarado MM, Sánchez Roitz C. Relation of serum levels of C-reactive protein to anthropometric measurements: A systematic review of studies in South America [in Spanish]. *Nutr Hosp*. 2012;27(4):971–977.
17. Bartalena L, Brogioni S, Grasso L, Velluzzi F, Martino E. Relationship of the increased serum interleukin-6 concentration to changes of thyroid function in nonthyroidal illness. *J Endocrinol Invest*. 1994;17(4):269–274.
18. Boelen A, Platvoet-Ter Schiphorst MC, Wiersinga WM. Association between serum interleukin-6 and serum 3,5,3'-triiodothyronine in nonthyroidal illness. *J Clin Endocrinol Metab*. 1993;77(6):1695–1699.
19. Davies PH, Black EG, Sheppard MC, Franklyn JA. Relation between serum interleukin-6 and thyroid hormone concentrations in 270 hospital in-patients with non-thyroidal illness. *Clin Endocrinol*. 1996;44(2):199–205.
20. Rasmussen AK. Cytokine actions on the thyroid gland. *Dan Med Bull*. 2000;47(2):94–114.
21. Ozawa M, Sato K, Han DC, Kawakami M, Tsushima T, Shizume K. Effects of tumor necrosis factor-alpha on thyroid hormone metabolism in mice. *Endocrinology*. 1988;123(3):1461–1467.
22. van der Poll T, Romijn JA, Wiersinga WM, Sauerwein HP. Tumor necrosis factor: A putative mediator of the sick euthyroid syndrome. *J Clin Endocrinol Metab*. 1991;71(6):1567–1572.
23. Hermus AR, Sweep CG. Cytokines and the hypothalamic–pituitary–adrenal axis. *J Steroid Biochem Mol Biol*. 1990;37(6):867–871.
24. Tognini S, Marchini F, Dardano A, et al. Non-thyroidal illness syndrome and short-term survival in a hospitalised older population. *Age Ageing*. 2010;39(1):46–50.
25. Hotamisligil GS, Shargill NS, Spiegelman BM. Adipose expression of tumor necrosis factor alpha: Direct role in obesity-linked insulin resistance. *Science*. 1993;259(5091):87–91.
26. Visser M, Bouter LM, McQuillan GM, Wener MH, Harris TB. Elevated C-reactive protein levels in overweight and obese adults. *JAMA*. 1999;282(22):2131–2135.
27. Sartipy P, Loskutoff DJ. Monocyte chemoattractant protein 1 in obesity and insulin resistance. *Proc Natl Acad Sci U S A*. 2003;100(12):7265–7270.
28. El-Wakkad A, Hassan N-M, Sibaii H, El-Zayat SR. Proinflammatory, anti-inflammatory cytokines and adipokines in students with central obesity. *Cytokine*. 2013;61(2):682–687.
29. Menon V, Zhi X, Hossain T, et al. The contribution of visceral fat to improved insulin signaling in Ames dwarf mice. *Aging Cell*. 2014;13(3):497–506.
30. Masternak MM, Bartke A, Wang F, et al. Metabolic effects of intra-abdominal fat in GHRKO mice. *Aging Cell*. 2012;11(1):73–81.

Standard values of the upper body posture in male adults

Daniela Ohlendorf[1,A–D], Frederic Adjami[2,B,C,E], Benjamin Scharnweber[3,B,C,E], Johannes Schulze[1,D–F], Hanns Ackermann[4,C,E], Gerhard M. Oremek[1,E,F], Stefan Kopp[2,E,F], David A. Groneberg[1,A,E,F]

[1] Institute of Occupational Medicine, Social Medicine and Environmental Medicine, Faculty of Medical Science, Goethe University Frankfurt, Germany
[2] Department of Orthodontics, School of Dentistry, Faculty of Medical Science, Goethe University Frankfurt, Germany
[3] Department of Prosthetics, School of Dentistry, Faculty of Medical Science, Goethe University Frankfurt, Germany
[4] Institute of Biostatistics and Mathematical Modeling, Faculty of Medical Science, Goethe University Frankfurt, Germany

A – research concept and design; B – collection and/or assembly of data; C – data analysis and interpretation;
D – writing the article; E – critical revision of the article; F – final approval of the article

Advances in Clinical and Experimental Medicine, ISSN 1899-5276 (print), ISSN 2451-2680 (online) *Adv Clin Exp Med*. 2018;27(11):1521–1528

Address for correspondence
Daniela Ohlendorf
E-mail: ohlendorf@med.uni-frankfurt.de

Funding sources
None declared

Conflict of interest
None declared

Received on January 19, 2017
Reviewed on March 23, 2017
Accepted on April 25, 2017

Abstract

Background. Interactions within the musculoskeletal system have been investigated and confirmed in numerous studies.

Objectives. Since there are no standard values for the posture of healthy persons, this study attempts to define reference values for the upper body posture in healthy men.

Material and methods. A 3-dimensional back scan was performed to quantify the upper back posture while habitually standing. Tolerance regions for habitual posture were calculated, including the upper and lower limit for 95% of all values. Furthermore, the left and right limit of the confidence interval (CI) was carried out. Group differences were tested by using the t-test or the Wilcoxon-Mann-Whitney U test.

Results. Height, weight and body mass index (BMI) of the participants were comparable to those of the average young German males. The spinal column was marginally twisted to the right. The spinal curves, defined by the thoracic or lumbar flexion angle, and the kyphosis and lordosis angle, indicated that the angle in the thoracic spine area was larger than that in the lumbar region. Consequently, a more kyphotic posture was observed in the sagittal plane. The habitual posture was slightly scoliotic, with a rotational component (scapular depression left, right scapula marginally located more dorsally, high state of pelvic left, iliac left further rotated posteriorly and simultaneously tilted further ventrally). No significant difference between right and left-handed persons could be proven.

Conclusions. Video raster stereography is a suitable method to measure the 3-dimensional back surface. Using this method for healthy young men, we observed that they had an almost ideally balanced posture with minimal ventral body inclination and a marginal scoliotic deviation. The normal values allow a better comparison of data between different studies of body posture.

Key words: standard value, tolerance value, confidence interval, back scan, male subjects

DOI
10.17219/acem/70669

Introduction

Interactions between the temporomandibular joints and the spine, pelvis or the lower limbs have been investigated and the values confirmed in numerous studies.[1–6] This leads to an interdisciplinary treatment of diseases and to a holistic approach to health disorders or diseases.

This has been particularly shown in studies concerning the correlation of dental findings with body posture. Korbmacher et al. proved a correlation between asymmetrical posture in the cervical spine and jaw asymmetry as well as shoulder and pelvis asymmetry (leg length discrepancy) in children.[7] Similarly, Saccucci et al. described the association of scoliosis with lateral crossbite or a midline shift.[8] The relationship between a drooping posture and prognathism was already presented by Wachsman in 1960.[9] Also, Lippold et al. demonstrated significant correlations, but they pointed out that the changes did not follow any systematics with respect to orthopedic findings and dental occlusion in the sagittal plane (Angle's classes).[10]

In patients without subjective cervical, spine and pelvic complaints, Fink et al. indicated an altered passive range of motion and functional limitations of the shoulder, compared to subjects with temporomandibular disorders (TMD).[11,12] The latter also described increasing joint disc changes and muscle tension in the shoulder, back and pelvic area. Saito et al. also related the posture (plantar arch, lower extremities, pelvis, shoulder and head posture) and temporomandibular joint changes.[5] When patients with the anterior displacement of the articular disc were compared to a control group without disc displacement, changes were observed in the pelvic, thoracic, lumbar spine, and head position. The authors emphasized that no conclusions could be drawn in terms of cause and effect, but rather the analysis of posture should include more than 1 component in the prevention and management of temporomandibular joint changes. In all studies, correlations were made between body posture and dental findings by comparing different patient groups or by pre–post intervention comparison.

Up to now, there have been no standard or reference values for patients in particular; reference values could indicate changes in the posture before treatment and validate changes associated with any dental treatments. Also, classifications, e.g., of the severity of posture deviations, are only possible with standard or reference values. The comparison between the current posture and standard values could provide a description of preexisting changes. These "deviations" could be quantified, e.g., in the form of (parametric or non-parametric) percentiles, similar to the Z- or T-scores of bone density.[13]

The optimal physiological posture is the result of the functional interaction of all body segments, including the head, thorax, spine, and pelvis. When standing or moving, all muscles are used to balance the body. Ideally, the perpendicular line of the body's center of gravity crosses the center of the support surface between the feet, also termed "center of pressure" (CoP). Both feet carry the body weight equally.[14] Seen from the lateral plane, this vector optimally crosses the external auditory canal, the dens, the anatomical-functional spine transitions, the gravity center at the 2nd sacral vertebra, and then through the hip and knee to the ankle. Any deviation from this optimum leads to disbalance of the weight-bearing structures with a local overload of the musculoskeletal system.[14,15] This change of the body posture can be measured, e.g., by a 3-dimensional back scan.

Since standard values for the posture of healthy persons are lacking, this study tries to define reference values for the upper body posture in healthy men. These values can be used to categorize the results of other studies and to define tolerance ranges. The back of male subjects in a prone posture was measured by a 3-dimensional back scanner (video scanning stereography); it measured the back geometry between the 7th cervical vertebra and the gluteal cleft. Additional measurements, e.g., of the distance between selected points or angle measurements, are possible. This back scanner has been used in several studies to correlate the upper body static and dental findings.[16–19]

Material and methods

Subjects

A total of 102 male volunteers 18–35 years old (mean age 25.4 ±3.6 years) were included in the study. Their body weight ranged from 57 to 108 kg (mean 77.2 ±10.0 kg), their height from 1.54 to 2.02 m (mean 1.81 ±0.07 m) and the body mass index (BMI) from 18.8 to 30.5 kg/m² (mean 23.6 ±2.3 kg/m²). According to the WHO weight classification,[20] 77.4% of the participants had a normal BMI (18.5–24.9 kg/m²), 20.6% were pre-obese (BMI: 25–29.9 kg/m²) and 2% of subjects had obesity I° (BMI: 30–34.9 kg/m²).

All subjects were healthy and free of complaints regarding the musculoskeletal system. Subjects with disorder symptoms in the temporomandibular system were excluded using a questionnaire.[21]

Briefly, 91.2% of the subjects reported to be right-handed and 8.8% were left-handed. 72.4% of the participants were students, 27.6% were employees in different occupations (dentist, military musicians, professional athletes, office workers).

All subjects volunteered to participate in the investigations. They were informed about the study design before giving written informed consent. The study was in accordance with the 1964 Helsinki Declaration and its later amendments, and was approved by the local medical ethics committee of the Faculty of Medical Science, Goethe University Frankfurt, Germany (approval No. 307/12).

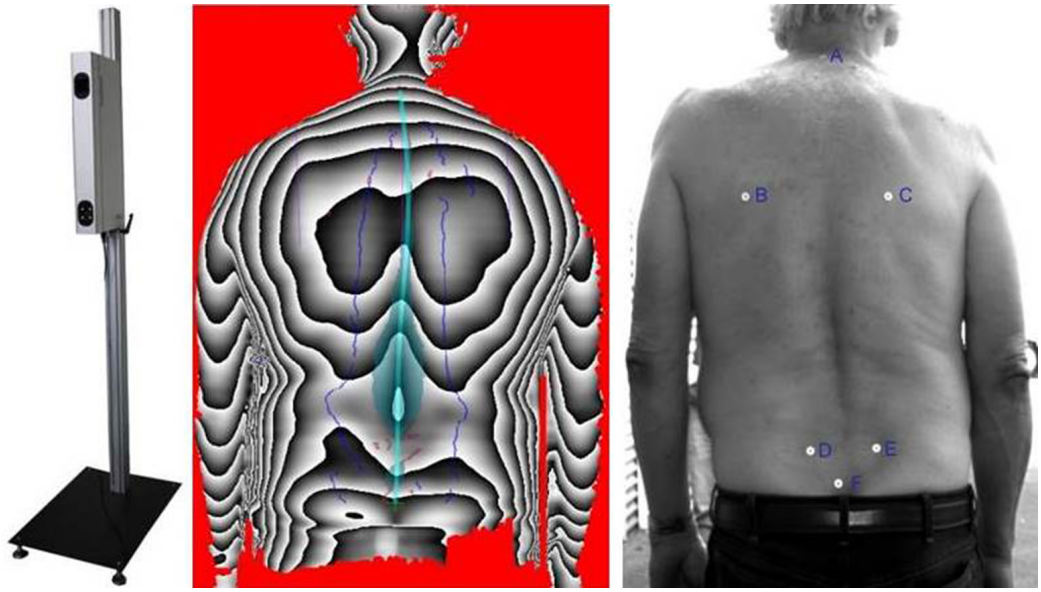

Fig. 1. Back scanner MiniRot Kombi (ABW GmbH, Frickenhausen, Germany); 3-dimensional phase picture of the back and marker position on the back

A – vertebra prominens (7th cervical vertebra); B – lower scapular angle left; C – lower scapular angle right; D – spina iliaca posterior superior (SIPS) left; E – spina iliaca posterior superior (SIPS) right; F – sacrum-point (cranial beginning of the gluteal cleft).

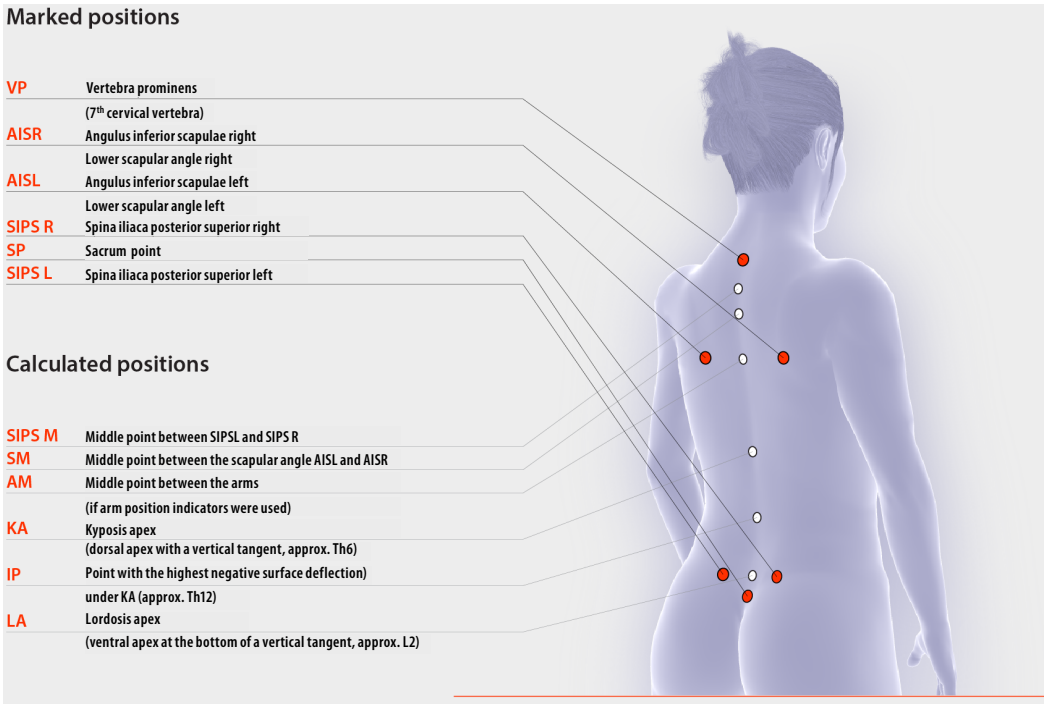

Fig. 2. Marked and calculated positions of the back scan

Measurement system

A 3-dimensional back scan was performed to quantify the upper back posture of a subject standing (Fig. 1). The scan was taken with the MiniRot Kombi system (ABW GmbH, Frickenhausen, Germany), using a projector that projects a zebra pattern on the back, which was videographed. This system represented the back surface in 3 dimensions.

Rotation movements in the shoulder and pelvic area, but also the shape of the spine (lordotic or kyphotic posture as well as a sense of a scoliosis posture), were calculated.

An LCD camera captured the stripe pattern from a defined angle (this angle is determined by the permanent installation of the camera and the projector in the unit). Thus, the back surface was represented as a phase picture, which was analyzed by an integrated software program. To calibrate the phase picture, all test persons were marked at 6 defined anatomical locations as indicated in Fig. 2. Thus, always 2 markers allowed a direct detection of an angle for the spine, the shoulder and the pelvic area (Fig. 2).

A back scan of 2 s identified and measured the 6 surface markers, including the calculation and representation of the 3-dimensional coordinates in a phase picture. During a movement sequence, 15 photos were shot. The maximal picture frequency of the MiniRot Kombi system is more than 50 fps with a spatial resolution of 1/100 mm. The calculation of the 3-dimensional coordinates of the

back surface is possible with triangulation techniques. The system error is specified as <1 mm (manufacturer's information), while the reproducibility is limited by the calculations of the upper body posture being made from the markers directly on the skin (<0.5 mm). Artifacts may occur due to different patient placements in front of the scanner and have to be avoided, i.e., for each scan the marker location has to be standardized.

Body scans

The subjects stood barefoot in habitual body and jaw posture, about 90 cm in front of the back scanner. Their arms were hanging loosely; the subjects looked horizontally at the opposite wall. To measure this position, 3 repeated measurements were taken within 2 min.

Evaluation of parameters

To quantify the parameters from the back scan, the 3-dimensional phase picture of the back was split into 3 components: spine with markers on the 7th cervical vertebra (C7) and the 3rd lumbar vertebra (L3), shoulder with markers at the top of the scapula, and pelvis with the markers on the left and right spina iliaca posterior superior (SIPS). The marker position is shown in Fig. 2. A list and explanation of the spine parameters are shown in Table 1, those of the pelvis parameters in Table 2, and Table 3 contains the shoulder parameters.

Statistical evaluation

With the initial Kolmogorov-Smirnov test, the normal distribution can only partly be rejected, so that either parametrical tolerance regions or non-parametrical tolerance

Table 1. Detailed list and explanation of the spine parameters

Spine parameter	
Trunk length D [mm]	spatial distance between the markers VP and DM
Trunk length S [mm]	spatial distance between the markers VP and SP
Sagittal trunk decline [°]	inclination of the trunk length D marked line from the perpendicular to the sagittal plane tilt anteriorly, flexion (negative values) tilt dorsally, extension (positive values)
Frontal trunk decline [°]	inclination of the trunk length D marked line from the perpendicular to the frontal plane tilt anteriorly (negative values) = possible lordosis tilt dorsally (positive values) = possible kyphosis
Axis decline [°]	deviation of the line of the area marked by the trunk length D line of the 90° rotated distance DL–DR → decline between the upper body and the pelvis
Thoracic bending angle [°]	deviation of the distance VP–KA from the perpendicular
Lumbar bending angle [°]	deviation of the distance KA–LA from the perpendicular
SD of lateral deviation [mm]	root mean square deviation of the median line of the distance VP–DM
Maximal lateral deviation [mm]	maximum deviation of the median line of the distance VP–DM negative values = deviation to the left positive values = deviation to the right
SD of rotation [°]	root mean square deviation of surface rotation of the median line (torsion of the spinous processes of the spine)
Maximal rotation [°]	maximum positive or negative surface rotation of the median line
Kyphosis angle [°]	angle measured in the sagittal plane between the upper IP of the spine at the thoracolumbar and the IP at VP
Lordosis angle [°]	angle between the inflection point at DM and the thoracolumbar inflection point IP

SIPS – spina iliaca posterior superior; VP – vertebra prominens; DM – middle between dimple (= SIPS) left and dimple (= SIPS) right; SP – sacrum point; DL–DR = distance between dimple (= SIPS) left and dimple (= SIPS) right; KA – kyphosis apex; LA – lordosis apex; IP – inflection point (point of the greatest negative surface decline); SD – standard deviation.

Table 2. Detailed list and explanation of the pelvis parameters

Pelvis parameter	
Pelvis distance [mm]	spatial distance between SIPS L and SIPS R
Pelvis height [°] and [mm]	decline of the connecting line between SIPS L and SIPS R to the horizontal in the frontal plane
Pelvis torsion [°]	angle between the surface normal at the 2 dimples SIPS L and SIPS R negative differential angle = normal at point SIPS L is stronger upward as at point SIPS R positive difference angle = normal at point SIPS L is stronger downward as at point SIPS R
Pelvis rotation (°)	rotation of the distance SIPS L–SIPS R in the transversal plane

SIPS L – spina iliaca posterior superior left; SIPS R – spina iliaca posterior superior right.

regions were calculated, defined by the upper and lower limit for 95% of all values (= ±2σ values). These values are results that are found in about 95% of the examined subjects. Within this tolerance range, all values have to be considered normal, so that the tolerance ranges estimate the central part of 95% of the measured subject population.

Furthermore, the two-sided 95% confidence interval (CI) was calculated; it indicates the possible range for the mean or median value depending on the distribution quality and shows the accuracy of these values. For testing group differences, the t-test or the Wilcoxon-Mann-Whitney U test was used. The evaluation of the data was carried out using Bias v. 11.0 (Epsilon Verlag, Darmstadt, Germany).

Results

The constitutional parameters of body height, body weight and BMI were not normally distributed. The median of body weight was 76.0 kg (tolerance range: 59.4–98.9 kg; CI = 74–78 kg). For the body height, a median of 1.82 m was calculated with a tolerance range between 1.64 and 2.00 m and a CI of 1.80–1.83 m. For the BMI, a median of 23.1 kg/m² was calculated, with a corresponding tolerance range from 19.4 to 29.6 kg/m² and a CI from 22.6 to 23.8 kg/m².

To exclude the influence of handedness on all spine parameters, they were tested in advance using the t-test or the Wilcoxon-Mann-Whitney U test. Not all parameters were significant ($p \geq 0.05$).

The posture of an average healthy male was calculated based on the back scan readings. In Table 4 the spine parameters are listed as mean or median values, including tolerance range and CIs. On average, the subjects were slightly inclined in anterior line of 3.66° (tolerance range: from 8.35° ventrally to 1.05° dorsally; CI from 4.12° to the right to 3.20° to the left).

Laterally, a minimal deviation of 0.33° to the right of the frontal trunk decline was observed. The CI (0.00–0.67°) includes the perpendicular position, the tolerance range ranged from –1,79° to the left to 2.33° to the right. Compensatory, the axial deviation (as the inclination between the upper body and the pelvis) was in the mean value slightly tilted to the left (–0.34°), with a tolerance range of ±4° and a CI <1° (–0.78° and 0.11°, respectively). This

Table 3. Detailed list and explanation of the shoulder parameters

Shoulder parameter	
Scapular distance [mm]	distance between lower scapular angle left (AISL) and lower scapular angle right (AISR)
Scapular height [°]	height difference between the points AISL and AISR positive value = AISR higher than AISL negative value = AISR deeper than AISL
Scapular rotation [°]	rotation of the distance DL–DR in the transversal plane
Scapular angle left [°]/scapula angle right [°]	best fit straight line on the shoulders to the horizontal; the center point of the regression line is set vertically above AISL/AISR the greater the angle, the more caudally located the shoulder

AISL – angulus inferior scapulae left; AISR – angulus inferior scapulae right; SIPS – spina iliaca posterior superior; DL–DR – distance between dimple (= SIPS) left and dimple (= SIPS) right.

Table 4. Spine parameters: mean value, median, tolerance ranges (upper and lower limit), confidence intervals (CIs) (left and right limit)

Spine parameter	Mean value/ median	Tolerance range lower limit	Tolerance range upper limit	CI left limit	CI right limit
Trunk length D [mm]	478.42	423.19	533.66	473.03	483.82
Trunk length S [mm]	528.44	470.63	586.25	522.80	534.08
Sagittal trunk decline [°]	–3.66	–8.35	1.05	–4.12	–3.20
Frontal trunk decline [°]	0.33*	–1.79*	2.33*	0.00*	0.67*
Axis decline [°]	–0.34	–4.87	4.20	–0.78	0.11
Thoracic bending angle [°]	16.34	9.62	23.07	15.69	17.00
Lumbar bending angle [°]	10.10	3.63	16.58	9.47	10.74
SD of the lateral deviation [mm]	3.83*	1.33*	10.12*	3.33*	4.00*
Maximal lateral deviation [mm]	–3.16*	–15.92*	13.31*	–5.00*	0.67*
SD rotation [°]	3.67*	1.54*	9.71*	3.00*	4.00*
Maximal rotation [°]	–4.17	–16.46*	12.58*	–6.00*	1.67*
Kyphosis angle [°]	45.85	27.24	64.46	44.03	47.67
Lordosis angle [°]	30.67*	9.83*	47.75*	29.33*	32.00*

SD – standard deviation; * non-parametrical values.

implied that there were no obvious differences in the inclination between the upper and lower body (Tables 1–3).

The thoracic bending angle was calculated from the distance between the vertebra prominens and the kyphosis apex, and indicated the deviation from the perpendicular line. The median angle was 16.24°, confirming the expected thoracic kyphosis. Here, wider variations were indicated by a tolerance range varying by 7° and a CI varying by 0.6°. Similar variations of the tolerance range and the CIs were seen in the lumbar region with a flection angle on average 10.10° (tolerance range: 3.63–16.58°; CI = 9.47–10.74°). The lumbar bending angle describes the deviation of the distance between the lordosis- and kyphosis apex.

Measurement of the standard deviation (SD) of the lateral deviation showed a right-sided inclination of the median line by 3.83° when connecting the points vertebra prominens (VP) and the center of the pelvic markers. Both the tolerance range (1.33–10.12°) as well as the CI (3.33–4°) indicated a right-sided deviation.

The SD of the rotation of the spinal column is a marker of the spinal torsion, considering the direction of the spinous processes of vertebrae. A negative value describes a rotation to the left and a positive value to the right. The median rotation was 3.67°, with a tolerance range between 1.54 and 9.71°, and a CI between 3 and 4°. Consequently, on average a right-sided spinal rotation was found.

The next 2 parameters, the kyphosis and lordosis angle, had a mean or a median of 45.85° and 30.67°, respectively, with a substantial tolerance range of approx. ±19° and a CI of about ±1.5°.

Shoulder parameters are good indicators for upper body posture; in Table 5 parameters for shoulder position are compiled, including values for the tolerance ranges and the CIs.

The lower spine parameters of the scapula were additionally measured from the fixed markers; the scapula distance value as an indicator of the variability of the upper body was 179.23 mm, with a tolerance range of 130.24–228.22 mm and a CI = 174.45–184.01 mm. The scapular height (deviation from the horizontal line) refers to a slightly lower left shoulder blade (3°), whereas the upper and lower limit of the tolerance range were 22.67° and 15.29°, respectively. In contrast, the limit of the tolerance range was the data of the CI in the negative range, so the left shoulder blade was always located more caudally.

The rotation of the shoulder markers illustrated a minimally more dorsally located right shoulder (0.52°), with a tolerance range of –5.90–6.94° and a CI of –0.10–1.15°. Only minor differences between the left and right shoulder blade angle show that the right shoulder was located 3° (median) more caudally.

The pelvic position anchors the body and is also influenced by the feet length (differences). Table 6 compiles the parameters found for the pelvis, measured by the back scanner. The distance for the fixed markers on the SIPS refers to the pelvic width, which is on average 93.68 mm (tolerance range: 71.34–116.01 mm; CI = 91.50–95.86 mm).

The deviation of the pelvic height (in degrees) identifies the horizontal plane and deviations from it. Both differences in pelvic height (in mm) and deviations from the horizontal line (in degrees) indicate a slightly higher position of the left pelvic side (Tables 1–3).

The same applies to the pelvis torsion and rotation, so that the iliac left is further rotated posteriorly and simultaneously tilted further ventrally (mean pelvis torsion: –0.43°; mean pelvic rotation: –0.86°).

Table 5. Shoulder parameters: mean value, median, tolerance ranges (upper and lower limit), confidence intervals (CIs) (left and right limit)

Shoulder parameter	Mean value/median	Tolerance range lower limit	Tolerance range upper limit	CI left limit	CI right limit
Scapular distance [mm]	179.23	130.24	228.22	174.45	184.01
Scapular height [°]	–3.00*	–22.67	15.29	–4.33	–0.67
Scapular rotation [°]	0.52	–5.90	6.94	–0.10	1.15
Scapular angle left [°]	26.00*	–29.75	44.92	24.67	27.00
Scapula angle right [°]	29.00*	–31.12	48.79	27.67	29.67

* non-parametrical values.

Table 6. Pelvis parameters: mean value, median, tolerance ranges (upper and lower limit), confidence intervals (CIs) (left and right limit)

Pelvis parameter	Mean value/median	Tolerance range lower limit	Tolerance range upper limit	CI left limit	CI right limit
Pelvis distance [mm]	93.68	71.34	116.01	91.50	95.86
Pelvis height [°]	–0.77	–5.27	3.73	–1.21	–0.33
Pelvis height [mm]	–1.24	–8.61	6.13	–1.96	–0.52
Pelvis torsion [°]	–0.43	–10.83	9.97	–1.45	0.58
Pelvis rotation [°]	–0.86	–8.06	6.33	–1.56	–0.16

* non-parametrical values.

Discussion

This paper presents normal values (tolerance range and CI) for body posture of healthy young males. All participants were young, healthy men, both students and employees.

Height, weight and BMI of the participants are comparable to those of the average young German males.[22] Mensink et al. measured over 700 adults from the general German population, who were 1.02 cm smaller, 2.4 kg heavier, and thus also had by 0.9 kg/m² higher BMI, within the CI of the presented values.[22] Similar findings were reported by the German Federal Statistical Office in 2011 for the survey year of 2009.[23]

Standard values from a homogeneous group of subjects eliminate constitutional, habitual and degenerative changes that increase both the tolerance range and CI.[24–27] This prevents comparisons of studies in which such factors may have an influence on the habitual posture. A similar approach, using a homogenous group of healthy individuals for comparison purposes, was used in the definition of osteoporosis by bone density, where healthy, 30-year-old males were selected.[28,29] Sex and age differences are known factors in bone density, as well as other factors, like TMD and temporomandibular dysfunctions. Possible reasons have been postulated in hormone levels,[24] pain perception[25,27] and connective tissue properties.[26]

Among the participants of this study, 77% had a normal BMI, about 15% higher than Mensink et al. found for 18–29-year-old men.[22] Since these authors investigated the relation of overweight with social status, this selection may have been a confounder in their results. The German Federal Statistical Office did not collect such data. The differences in BMI may also be explained with the selection of the participants from the school of dentistry, which indicates a higher social status.

The values of the back scan indicated a characteristic posture. Only small deviations from an ideal perpendicular position were noted; the lateral deviation and rotation of the spine were very small; the ventral trunk tilted marginally to the right side, with a compensatory lumbar left tilt. All values included exact perpendicular position in the CI. The spinous processes of the spinal column were marginally twisted to the right (SD of the rotation), too (Table 4). The spinal curves, defined by the thoracic or lumbar flexion angle, and the kyphosis and lordosis angle, indicated that the angle in the thoracic spine area is larger than that in the lumbar region (Table 4) and, consequently, a more kyphotic posture in the sagittal plane could be observed. The posture was slightly scoliotic, with rotation component (scapular depression left, right scapula marginally located more dorsally, high state of pelvic left, iliac left further rotated posteriorly and simultaneously tilted further ventrally). The influence of handedness could be excluded in the parameters. However, it must be considered that no balance between left- and right-handed subjects could be seen, since the majority of the study participants reported to be right-handed (91.2%). Whether there is an influence of the dominating leg or of one's preferred chewing side on the posture of the present investigation, cannot be answered.[30–33] An appropriate test method for determining these components should be used in further studies on the same topic.

The 3-dimensional back scan is a fast, non-contact method to calculate body posture and movement. This method is suitable for measuring pathological body postures, like attitude pathologies, scoliosis, kyphosis, leg length differences, and functional movement disorders. Sensitivity and specificity of the video raster stereographic survey is 98% and 84%, respectively. The data proportion of false-positive values is 13.9%.[34] Furthermore, Drerup and Hierholzer showed a strong correlation between the system of raster stereography and radiological angles with a correlation coefficient of 0.8–0.93.[35,36] Hübner found a highly variable perpendicular deflection as well as kyphosis and lordosis angles; however, that study used a system from a different manufacturer.[37] The data differences indicate the need for calibrating values when comparing kinematic values obtained with different technical systems.

All participants were encouraged to assume the same posture to prevent differences in position, which could influence vertebral and surface rotations.[38] To reduce motion artifacts, multiple measurements were carried out, and the average values from 2-minute measurements were used for the analysis. Another possible influence factor is the accuracy of the anatomical marker fixation. Drerup and Hierholzer found a 1-millimeter variation of the lumbar spine dimple.[39]

Measuring exactly the back surface in overweight subjects is described by Asamoah et al.[34] They observed a significantly lower correlation between video raster stereography and X-ray measurements with a correlation coefficient of 0.56. Furthermore, they mentioned that the constitution had an impact on the accuracy of the data, but without quantifiable factors. Since in the present study 77% of the participants were of normal weight, this artifact was less relevant. It cannot be conclusively confirmed whether the back geometry of the remaining volunteers with an increased BMI was detected accurately with the system.

The system used in the present study allows for correction with manually placed markers. Correcting the measurements in this way after scanning resulted in deviations of up to ±5 mm, as quantified in a study with a different back scanner.[40] In order to quantify the precision of the markers on a subject, the back side anatomical landmarks were positioned 12 times on the back of 1 individual under the same conditions (unpublished results). The markers could be placed with a standard deviation of 0.91%. Thus, a maximal error from marking and data evaluation of 2% can be safely assumed.

Video raster stereography is a suitable method to measure the 3-dimensional back surface. Using this method for healthy young men ensures that they have an almost ideally balanced posture, with minimal ventral body inclination and a marginal scoliotic deviation. The normal values allow a comparison of other control and patient data.

References

1. Hairston LE, Blanton PL. An electromyographic study of mandibular position in response to changes in body position. *J Prosthet Dent.* 1983;49(2):271–275.
2. Leiva M, Miralles R, Palazzi C, et al. Effects of laterotrusive occlusal scheme and body position on bilateral sternocleidomastoid EMG activity. *Cranio.* 2003;21(2):99–109.
3. Miralles R, Gutierrez C, Zucchino G, et al. Body position and jaw posture effects on supra- and infrahyoid electromyographic activity in humans. *Cranio.* 2006;24(2):98–103.
4. Palazzi C, Miralles R, Soto MA, Santander H, Zuniga C, Moya H. Body position effects on EMG activity of sternocleidomastoid and masseter muscles in patients with myogenic cranio-cervical-mandibular dysfunction. *Cranio.* 1996;14(3):200–209.
5. Saito ET, Akashi PM, Sacco Ide C. Global body posture evaluation in patients with temporomandibular joint disorder. *Clinics (Sao Paulo).* 2009;64(1):35–39.
6. Van't Spijker A, Creugers NH, Bronkhorst EM, Kreulen CM. Body position and occlusal contacts in lateral excursions: A pilot study. *Int J Prosthodont*. 2011;24(2):133–136.
7. Korbmacher H, Koch L, Eggers-Stroeder G, Kahl-Nieke B. Associations between orthopaedic disturbances and unilateral crossbite in children with asymmetry of the upper cervical spine. *Eur J Orthod*. 2007;29(1):100–104.
8. Saccucci M, Tettamanti L, Mummolo S, Polimeni A, Festa F, Tecco S. Scoliosis and dental occlusion: A review of the literature. *Scoliosis*. 2011;6:15. doi: 10.1186/1748-7161-6-15
9. Wachsman K. Über den Zusammenhang der Gebißanomalien mit Krümmungen der Wirbelsäule und schlaffer Körperhaltung. *Fortschr Kieferorthop.* 1960;21(4):449–453.
10. Lippold C, Ehmer U, Van Den Boos L. Beziehungen zwischen kieferorthopädischen und orthopädischen Befunden. *Manuelle Medizin*. 2000;38:346–350.
11. Fink M, Tschernitschek H, Stiesch-Scholz M. Asymptomatic cervical spine dysfunction (CSD) in patients with internal derangement of the temporomandibular joint. *Cranio.* 2002;20(3):192–197.
12. Fink M, Wahling K, Stiesch-Scholz M, Tschernitschek H. The functional relationship between the craniomandibular system, cervical spine, and the sacroiliac joint: A preliminary investigation. *Cranio*. 2003;21(3):202–208.
13. Bazzocchi A, Ponti F, Diano D, et al. Trabecular bone score in healthy ageing. *Br J Radiol.* 2015;88(1052):20140865. doi: 10.1259/bjr.20140865
14. Perry J, Burnfield JM. *Gait Analysis*. Thorofare, NJ: Slack Incorporated; 2010.
15. Götz-Neumann K. *Gehen Verstehen*: *Ganganalyse in der Physiotherapie*. Stuttgart, Germany: Thieme Verlag; 2011.
16. Marini I, Alessandri Bonetti G, Bortolotti F, Bartolucci ML, Gatto MR, Michelotti A. Effects of experimental insoles on body posture, mandibular kinematics and masticatory muscles activity: A pilot study in healthy volunteers. *J Electromyogr Kinesiol.* 2015;25(3):531–539.
17. Marini I, Gatto MR, Bartolucci ML, Bortolotti F, Alessandri Bonetti G, Michelotti A. Effects of experimental occlusal interference on body posture: An optoelectronic stereophotogrammetric analysis. *J Oral Rehabil.* 2013;40(7):509–518.
18. Nobili A, Adversi R. Relationship between posture and occlusion: A clinical and experimental investigation. *Cranio.* 1996;14(4):274–285.
19. Sinko K, Grohs JG, Millesi-Schobel G, et al. Dysgnathia, orthognathic surgery and spinal posture. *Int J Oral Maxillofac Surg.* 2006;35(4):312–317.
20. Obesity: Preventing and managing the global epidemic. Report of a WHO Consultation (WHO Technical Report Series 894). http://www.who.int/nutrition/publications/obesity/WHO_TRS_894/en/. Published 2000. Accessed January 1, 2017.
21. Kopp S. Okklusale und klinisch funktionelle Befunde im cranio-mandibulären System bei Kindern und Jugendlichen. Friedrich-Schiller-Universität Jena; 2005.
22. Mensink GBM, Schienkewitz A, Haftenberger M, Lampert T, Ziese T, Scheidt-Nave C. Übergewicht und Adipositas in Deutschland. *Bundesgesundheitsblatt.* 2013;56:786–794.
23. Statistiches Bundesamt. Mikrozensus – Fragen zur Gesundheit – Körpermaße der Bevölkerung. https://www.destatis.de/DE/Publikationen/Thematisch/Gesundheit/Gesundheitszustand/Koerpermasse5239003139004.pdf?__blob=publicationFile. Published 2013. Accessed January 12, 2017.
24. Abubaker AO, Raslan WF, Sotereanos GC. Estrogen and progesterone receptors in temporomandibular joint discs of symptomatic and asymptomatic persons: A preliminary study. *J Oral Maxillofac Surg.* 1993;51(10):1096–1100.
25. Bush FM, Harkins SW, Harrington WG, Price DD. Analysis of gender effects on pain perception and symptom presentation in temporomandibular pain. *Pain.* 1993;53(1):73–80.
26. Conti PC, Ferreira PM, Pegoraro LF, Conti JV, Salvador MC. A cross-sectional study of prevalence and etiology of signs and symptoms of temporomandibular disorders in high school and university students. *J Orofac Pain.* 1996;10(3):254–262.
27. Nordstrom G, Eriksson S. Longitudinal changes in craniomandibular dysfunction in an elderly population in northern Sweden. *Acta Odontol Scand.* 1994;52(5):271–279.
28. Kanis JA, Melton LJ, Christiansen C, Johnston CC, Khaltaev N. The diagnosis of osteoporosis. *J Bone Miner Res.* 1994;9(8):1137–1141.
29. Kanis JA; WHO Study Group. Assessment of fracture risk and its application to screening for postmenopausal osteoporosis: Synopsis of a WHO report. *Osteoporos Int.* 1994;4(6):368–381.
30. Fischer K. *Rechts-Links-Probleme in Sport und Training. Studien zur angewandten Lateralitätsforschung*. Schorndorf, Germany: Hofmann Verlag; 1988.
31. Paphangkorakit J, Chaiyapanya N, Sriladlao P, Pimsupa S. Determination of chewing efficiency using muscle work. *Arch Oral Biol.* 2008;53(6):533–537.
32. Martinez-Gomis J, Lujan-Climent M, Palau S, Bizar J, Salsench J, Peraire M. Relationship between chewing side preference and handedness and lateral asymmetry of peripheral factors. *Arch Oral Biol.* 2009;54(2):101–107.
33. Ratnasari A, Hasegawa K, Oki K, et al. Manifestation of preferred chewing side for hard food on TMJ disc displacement side. *J Oral Rehabil*. 2011;38(1):12–17.
34. Asamoah V, Mellerowicz H, Venus J, Klockner C. Measuring the surface of the back. Value in diagnosis of spinal diseases. *Orthopade.* 2000;29(6):480–489.
35. Drerup B. Improvements in measuring vertebral rotation from the projections of the pedicles. *J Biomech.* 1985;18(5):369–378.
36. Drerup B, Hierholzer E. Objective determination of anatomical landmarks on the body surface: Measurement of the vertebra prominens from surface curvature. *J Biomech.* 1985;18(6):467–474.
37. Hübner J. *Handbook Formetric III*. Schlangenbad, Germany: Diers International GmbH; 2007.
38. Hierholzer E. *Objektive Analyse der Rückenform von Skoliosepatienten.* Stuttgart, Germany: Gustav Fischer Verlag; 1993.
39. Drerup B, Hierholzer E. Automatic localization of anatomical landmarks on the back surface and construction of a body-fixed coordinate system. *J Biomech.* 1987;20(10):961–970.
40. Diers H. Optische Wirbelsäulen- und Haltungsvermessung. *Orthopädie Technik.* 2008;38:479–484.

Determination of the concentration of cathepsin B by SPRI biosensor in children with appendicitis, and its correlation with proteasomes

Ewa Matuszczak[1,A–D], Marta Komarowska[1,B], Marzena Tylicka[2,B,C], Wojciech Dębek[1,E,F], Ewa Gorodkiewicz[3,F], Anna Tokarzewicz[3,B], Anna Sankiewicz[3,B], Adam Hermanowicz[1,F]

[1] Department of Pediatric Surgery, Medical University of Bialystok, Poland
[2] Department of Biophysics, Medical University of Bialystok, Poland
[3] Department of Electrochemistry, Institute of Chemistry, University of Bialystok, Poland

A – research concept and design; B – collection and/or assembly of data; C – data analysis and interpretation; D – writing the article; E – critical revision of the article; F – final approval of the article

Advances in Clinical and Experimental Medicine, ISSN 1899-5276 (print), ISSN 2451-2680 (online) *Adv Clin Exp Med*. 2018;27(11):1529–1534

Address for correspondence
Ewa Matuszczak
E-mail: ewamat@tlen.pl

Funding sources
None declared

Conflict of interest
None declared

Received on December 31, 2016
Reviewed on March 6, 2017
Accepted on April 27, 2017

Abstract

Background. Cathepsin B (CatB) belongs to a family of lysosomal cysteine proteases and plays an important role in intracellular proteolysis.

Objectives. The concentration of CatB and 20S proteasome was evaluated in the serum of children with appendicitis, before and after surgery, on a basis of an innovative method for determining biomolecules concentration – surface plasmon resonance imaging (SPRI) biosensor.

Material and methods. Forty-two children with acute appendicitis, who were treated at the Department of Pediatric Surgery (Medical University of Bialystok, Poland), were randomly included into the study (age: 5–17 years, mean age: 11.5 ±1 year). There were 15 girls and 27 boys in the study group. Eighteen healthy, age-matched subjects, admitted for planned surgeries, served as controls. Exclusion criteria were the following: severe preexisting infections, immunological or cardiovascular diseases that required long-term medication, and complicated cases of appendicitis with perforation of the appendix and/or peritonitis.

Results. The CatB concentrations in the blood plasma of patients with acute appendicitis were elevated before surgery, they were the highest 24 h after surgery, and were above the range of concentrations measured in controls; the difference was statistically significant. The CatB concentration measured 72 h after the operation was decreased, but still did not reach the normal range when compared with the concentration measured in controls ($p < 0.05$).

Conclusions. Cathepsin B concentration may reflect the metabolic response to acute state of inflammation, surgical intervention in the abdominal cavity and the process of gradual ebbing of the inflammation. The method of operation – classic open appendectomy or laparoscopic appendectomy – does not influence the general trend in the CatB concentration in children with appendicitis. There is a strong positive correlation between the CatB and 20S proteasome concentrations 24 h after surgery. The SPRI method can be successfully used for determining the concentration of active forms of enzymes presented in lysosomes in the diagnosis of inflammatory conditions in the abdominal cavity.

Key words: appendicitis, inflammation, proteasomes, cathepsin B, surface plasmon resonance imaging biosensor

DOI
10.17219/acem/70811

Introduction

Cathepsins are a family of acidic endopeptidases, the activity of which is restricted to the lysosomal compartment under physiological conditions.[1] Cathepsins take part in protein turnover by degrading unneeded proteins into amino acids.[1] Various pathologic stresses, such as global cerebral ischemia, induce the release of cathepsins into the cytoplasm, where they perform their proteolytic function and can promote direct cell degradation.[1–3] Cathepsin B (CatB) directly activates caspase-11 and/or caspase-1 pathways, e.g., in focal cerebral ischemia, and confirms that apoptosis, necrosis and autophagia are interrelated mechanisms that can act in synergy and lead to cell death in acute pathologic conditions.[1] Cathepsin B is also responsible for nuclear factor kappa-light-chain-enhancer of activated B cells (NF-κB) activation through autophagy degradation of inhibitor of κBα (IκBα) in microglia and macrophages.[4] The inhibition of CatB can rescue cells from tumor necrosis factor (TNF)-induced apoptosis.[5] The inhibition of cathepsins leads to significant neuroprotection, because treatment with a specific CatB inhibitor significantly reduces infarct volumes.[1]

Elevated levels of CatB in fibroblasts are typically observed in many chronic inflammatory diseases, including rheumatoid arthritis as well as periodontitis, because CatB promotes inflammation involved in the production of mature interleukin 1β (IL-1β).[4,6–8] Interleukin 1β is a potent pro-inflammatory cytokine that is crucial for host-defense responses to infection and injury.[9] Lysosomal membrane rupture and CatB activity are important for the activation of the NLRP3 inflammasome in response to some stimuli, where the inhibition of CatB attenuates IL-1β release.[10,11] Cathepsin B also degrades collagens in fibroblasts and leads to tissue destruction.[4,12]

Proteasome is generally considered a dominating component in protein degradation pathway.[13] Through degrading regulatory proteins or their inhibitors, proteasome regulates many cellular transduction pathways. The ubiquitin-proteasome pathway also offers extremely high substrate specificity and the ability to quickly alter the rate of proteolysis.[13] Extracellular proteasomes have been found to circulate in the plasma of patients suffering from a variety of inflammatory, autoimmune and neoplastic diseases.[14–21] In various pathologic conditions, the concentration of circulating proteasomes correlates with disease activity.[14–21] The release of proteasome in the serum may be a result of membrane disruption. Endothelial cells, vascular smooth muscle cells and tubular epithelial cells all release proteasome-active vesicles when injured in vitro.[14] A study by Ito et al. demonstrated that extracellular 20S proteasome not only is released from cells, but also plays a functional role in physiological processes.[13]

Using the surface plasmon resonance imaging (SPRI) biosensor, we wanted to determine the concentration of CatB in the diagnostics of inflammatory condition located in the abdominal cavity and its correlation with 20S proteasome.

Material and methods

Forty-two children with acute appendicitis, who were treated at the Department of Pediatric Surgery of Medical University of Białystok, Poland, between 2013 and 2014, were randomly included into the study (age 5–17 years, mean age 11.5 ±1 year). There were 15 girls and 27 boys in the study group. Twenty-six children were subjected to laparoscopic appendectomy, while 16 children were subjected to classic open appendectomy. Eighteen healthy, age-matched subjects, admitted for planned surgeries, served as controls. Exclusion criteria were: severe preexisting infections, immunological or cardiovascular diseases that required long-term medication, and complicated cases of appendicitis with perforation of the appendix and/or peritonitis. All parents of our patients gave written informed consent for both a clinical and biochemical follow-up. We did not note any postoperative complications in our patients after appendectomy. All patients were discharged home on the 3rd day after surgery in good general state.

Venous blood samples (1–2 mL) were drawn on admission, 24 h after the appendectomy and 72 h after the appendectomy. Blood samples were collected in ethylenediaminetetraacetic acid (EDTA) tubes; the plasma was prepared according to standard protocols and was stored at –80°C. After all blood samples were collected and patient data recorded, the CatB and 20S proteasome concentrations were assessed using SPRI by the investigators blinded to other data.[22]

Procedure of cathepsin B and 20S proteasome determination

The CatB and 20S proteasome concentration was determined using the SPRI biosensor. The exact description of the methodology of measurements and biosensor design was set out in previous papers.[22] Gold chips were manufactured as described in other papers.[23–25] The gold surface of the chip was covered with photopolymer and hydrophobic paint.

Biosensor preparation

Chips were rinsed with ethanol and water, and then dried under a stream of nitrogen. They were then immersed in 20 mM of cysteamine ethanolic solutions for 2 h and, after rinsing with ethanol and water, dried again under a stream of nitrogen.[16]

Surface plasmon resonance imaging measurements

Surface plasmon resonance imaging for the protein biosensor array was performed as described in another study.[23]

Plasma samples from healthy children admitted for planned surgeries (n = 18) and from our patients after

appendectomy (n = 42) were diluted 2-fold with phosphate-buffered saline (PBS) (Biomed-Lublin, Lublin, Poland) and transferred onto the sensor surface for 10 min. The volume of the sample applied on each measuring field was 2 µL. The SPRI technique allows sensitive determination of proteins using highly specific enzyme-inhibitor interactions. An immobilized cystatin C (potent inhibitor of lysosomal proteinases) was purchased from Sigma-Aldrich (St. Louis, USA) and used for the CatB entrapment on the biosensor surface. The biosensor construction and optimization of measurement conditions used were previously described.[23] Briefly, plasma samples were placed directly on the prepared biosensor for ~10 min to allow interaction with the inhibitor (cystatin C). The biosensor was washed with water and HBS-ES buffer solution, pH = 7.4 (0.01 M 4-(2-hydroxyethyl)piperazine-1-ethanesulfonic acid, 0.15 M sodium chloride, 0.005% Tween 20, 3 mM EDTA) (all Biomed-Lublin, Lublin, Poland) to remove unbound molecules from the surface. The SPRI signal was measured twice on the basis of registered images, following the immobilization of cystatin C, and then following the interaction with CatB from the samples. The signal, which is proportional to coupled biomolecules, was obtained by calculating the difference between the signal prior to and following the interaction with biomolecules. The concentration was determined using the calibration curves of the SPRI signal depending on the concentration of CatB (Calbiochem; Merck, Warszawa, Poland).

Statistics

The Mann-Whitney U test and the Kruskal-Wallis H test with Dunn's post hoc correction to control for multiple testing were used to compare differences between groups. Statistical analyses were calculated with the STATISTICA PL (StatSoft Inc., Tulsa, USA) v. 10.0 program. A two-tailed $p < 0.05$ was considered significant. Correlations were examined by linear regression (r) using the Spearman's test. We presented median concentrations of CatB and 20S proteasome in children with appendicitis before surgery, as well as 24 h and 72 h after the appendectomy.

Results

The CatB concentrations in the blood plasma of patients with acute appendicitis were elevated before surgery, they were the highest 24 h after surgery, and were above the range of concentrations measured in controls, with the difference being statistically significant. The CatB concentrations measured 72 h after the operation were low, but still did not reach the normal range when compared with the concentrations measured in controls ($p < 0.05$) (Fig. 1).

The 20S proteasome concentrations in the blood plasma of patients with acute appendicitis were the highest before surgery, and were above the range of concentrations measured in controls, with the difference being statistically significant. The 20S proteasome concentrations measured 24 h and 72 h after the operation slowly decreased over time, and still did not reach the normal range when compared with the concentrations measured in controls ($p < 0.05$) (Fig. 2). There was no statistical difference between the CatB and 20S proteasome concentrations in children operated on laparoscopically and in children after classic appendectomy (data not shown). There was a strong positive correlation between the CatB and 20S proteasome concentrations 24 h after the surgical intervention ($r = 0.5871$; $p = 0.00004$) (Fig. 3). Both proteasomal and lysosomal systems are responsible for proteolysis, which is more intensive under pathologic conditions, and,

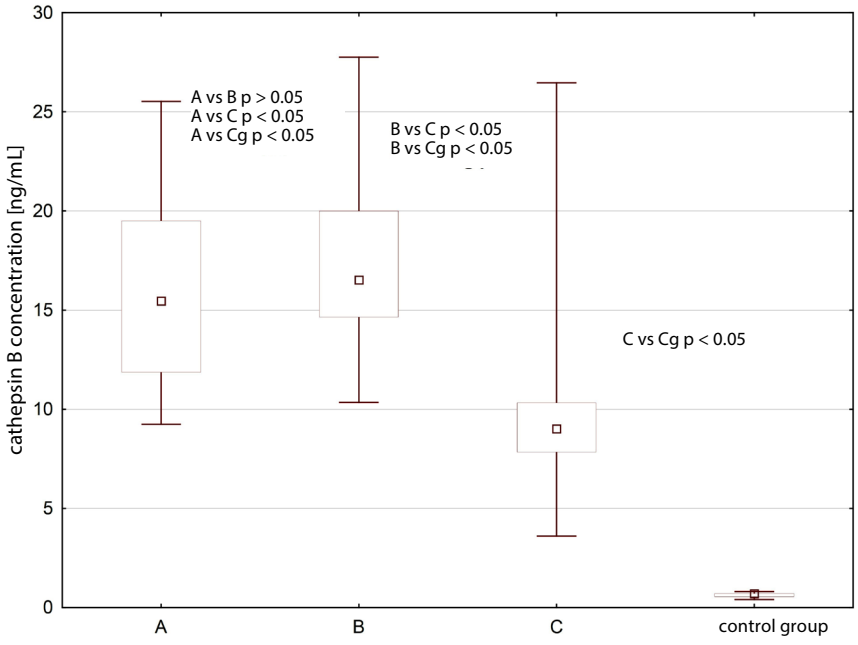

Fig. 1. Cathepsin B concentration in the plasma of children with acute appendicitis before (A), 24 h after (B) and 72 h after (C) appendicitis surgery, and in control group (Cg)

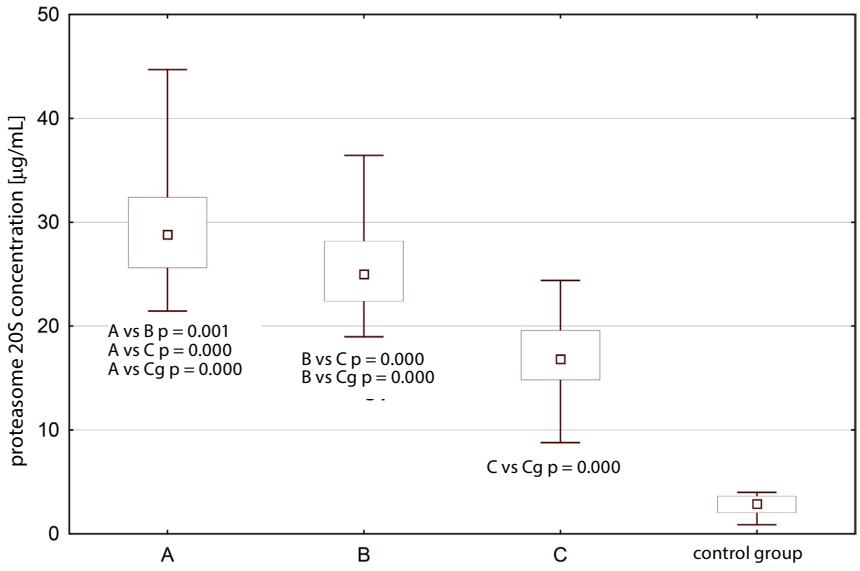

Fig. 2. Proteasome 20S concentration in the plasma of children with acute appendicitis before (A), 24 h after (B) and 72 h after (C) appendicitis surgery, and in control group (Cg)

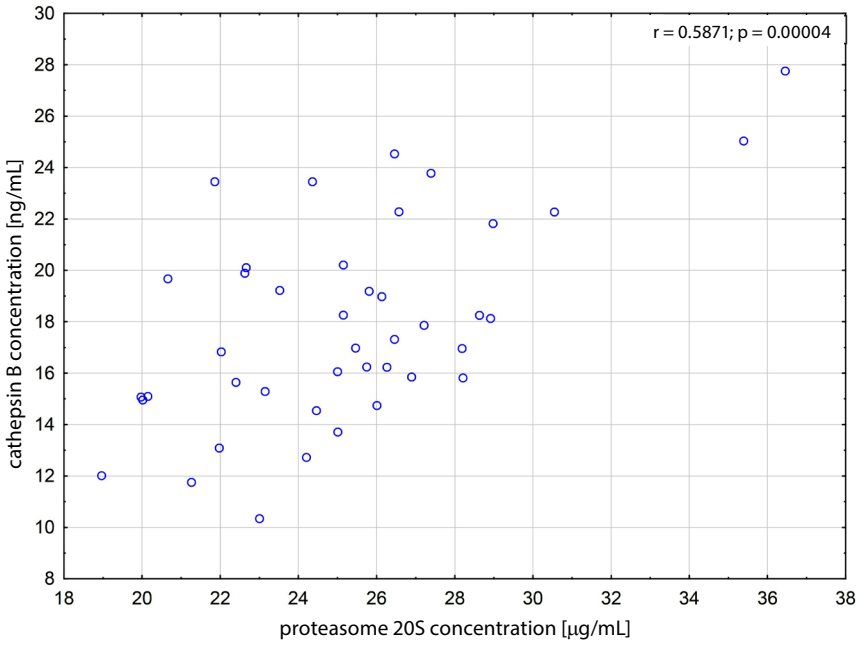

Fig. 3. Positive correlation between cathepsin B and 20S proteasome concentrations in the blood of children 24 h after appendectomy

in this case, was induced by inflammation and enhanced by surgical intervention. There were no such correlations before and 72 h after the surgery ($p > 0.05$).

Discussion

Appendicitis is caused by a blockage of the hollow portion of the appendix, most commonly by a calcified "stone" made of feces, but also by inflamed lymphoid tissue from a viral infection, parasites or tumors. This blockage leads to increased pressure in the lumen of the appendix, decreased blood flow in the appendiceal wall and bacterial growth inside the appendix, causing inflammation. The combination of inflammation, reduced blood flow to the appendix and distention of the appendix causes tissue injury and tissue death.

Protein degradation occurs in response to the activation of intracellular signaling pathways that increase the activity of the ubiquitin-proteasome, calcium-induced calpains and apoptotic regulators, such as caspase-3.[27,28] Various pathologic stresses induce the release of cathepsins – acidic endopeptidases, the activity of which is restricted to the lysosomal compartment – into the cytoplasm, where they perform their proteolytic function and can promote direct cell degradation.[1,3]

Cathepsin B is released from lysosomes after the activation of specific apoptotic inducers, such as death receptors of the TNF family, transforming growth factor-beta 1 (TGF-β1), p53, and sphingosine, as well as during oxidative stress and starvation. Sphingosine induces lysosomal permeabilization in a CatB-dependent manner.[1,5]

In our study, we found that the CatB concentrations in the blood plasma of patients with acute appendicitis were

elevated before surgery, they were the highest 24 h after surgery, and 72 h after the surgical intervention they were still above the range of concentrations measured in controls. This reflects the metabolic response to acute state of inflammation, surgical intervention and the process of gradual ebbing of the inflammation. We can conclude that lysosomal proteolysis connected with CatB activity was induced by inflammation and exacerbated by surgical intervention. Positive correlation between the CatB and proteasome concentrations 24 h after surgical intervention indicates higher destruction of cells and higher release of their content into the blood.

Apparently, the method of operation – classic open appendectomy or laparoscopic appendectomy – did not influence the general trend in the CatB and 20S proteasome concentrations in the blood of children with appendicitis. We may hypothesize that the resection of the appendix itself, regardless of the method of the operation, is the most influential factor in the process of reducing the inflammation resulting from acute appendicitis.

Cathepsin B regulates collagen expression by fibroblasts via prolonging toll-like receptor 2 (TLR2)/NF-κB activation during chronic inflammation and oxidative stress.[4] It is involved in degrading the intracellular and extracellular collagen produced by fibroblasts, thereby influencing the mechanisms of delayed tissue repair during chronic inflammation. Collagen type III and type IV in fibroblasts are important in wound healing and tissue remodeling.[4] Considering the role of CatB in collagen expression, CatB-specific inhibitors may be a useful approach for improving inflammation-delayed connective tissue repair, such as that found in dermatitis and periodontitis.[4]

Cathepsin B was also hypothesized to be involved in the generation of chronic pain.[29] It was demonstrated to be involved in the production of IL-1β, which is a key pain-related molecule.[29] The role of CatB in inflammatory pain suggests that CatB-specific inhibitors may represent a useful new strategy for treating inflammation-associated pain, such as arthritic pain and postoperative pain.[29]

Cathepsin B expression is greatly upregulated in traumatic brain injury (TBI) animal models, as well as in trauma patients. Knockout of the CatB gene in TBI mice results in substantial improvements of TBI-caused deficits in behavior, pathology and biomarkers, as well as improvements in related injury models.[30] During the process of TBI-induced injury, CatB likely escapes the lysosome, its normal subcellular location, into the cytoplasm or extracellular space. Cathepsin B in the extracellular space can induce neuronal cell apoptotic death. Non-brain polytrauma patients show increases in plasma CatB activity during the 1st day after trauma, which subsequently falls to moderately elevated levels by the 3rd day and remains roughly at that level for up to 2 weeks.[30] Importantly, the increase in plasma CatB activity correlates with the severity of injury.[30–32] Deleting or inhibiting CatB improves outcomes in injury models related to TBI, including epilepsy, aneurysm, ischemia, pain, surgical trauma, spinal cord trauma, infectious disease, and neurodegeneration.[30]

Cathepsin B is also a candidate target for inhibiting hepatocyte apoptosis in liver diseases.[33] Both genetic and pharmacologic inactivation of CatB reduces liver injury, inflammation and hepatic fibrogenesis during cholestasis.[24] Cathepsin B-mediated liver injury not only causes apoptosis, but also stimulates the production of proinflammatory chemokines.[33] Furthermore, inhibiting CatB catalytic activity with selective protease inhibitors, such as R-3032, might be a potential therapeutic option for cholestatic liver injury, inflammation and fibrosis.[33]

Cathepsin B is a potential drug target for several diseases, including various cancers, pancreatitis, liver fibrosis, rheumatoid arthritis, viral Ebola, bacterial *Streptococcus pneumoniae* meningitis, TBI, and parasitic *Trypanosoma cruzi* infections.[4,30,34–43] We strongly believe that further studies on CatB and its relation with inflammation located in the abdominal cavity and surgical interventions may bring future clinical implications.

Conclusions

Cathepsin B concentration may reflect the metabolic response to acute state of inflammation, surgical intervention in the abdominal cavity and the process of gradual ebbing of inflammation. The method of operation – classic open appendectomy or laparoscopic appendectomy – does not influence the general trend in the CatB concentration in children with appendicitis. There is a strong positive correlation between the CatB and 20S proteasome concentrations 24 h after surgery. Biosensors with SPRI as a detecting method can be successfully used for determining the concentration of active forms of enzymes presented in lysosomes in the diagnostics of inflammatory condition in the abdominal cavity.

References

1. Benchoua A, Braudeau J, Reis A, Couriaud C, Onténiente B. Activation of proinflammatory caspases by cathepsin B in focal cerebral ischemia. *J Cereb Blood Flow Metab*. 2004;24(11):1272–1279.
2. Uchiyama Y. Autophagic cell death and its execution by lysosomal cathepsins. *Arch Histol Cytol*. 2001;64(3):233–246.
3. Boya P, Andreau K, Poncet D, et al. Lysosomal membrane permeabilization induces cell death in a mitochondrion-dependent fashion. *J Exp Med*. 2003;197(10):1323–1334.
4. Li X, Wu Z, Ni J, et al. Cathepsin B regulates collagen expression by fibroblasts via prolonging TLR2/NF-κB activation. *Oxid Med Cell Longev*. 2016:7894247. doi: 10.1155/2016/7894247
5. Foghsgaard L, Wissing D, Mauch D, et al. Cathepsin B acts as a dominant execution protease in tumor cell apoptosis induced by tumor necrosis factor. *J Cell Biol*. 2001;153(5):999–1010.
6. Terada K, Yamada J, Hayashi Y, et al. Involvement of cathepsin B in the processing and secretion of interleukin-1β in chromogranin a-stimulated microglia. *Glia*. 2010;58(1):114–124.
7. Sun L, Wu Z, Hayashi Y, et al. Microglial cathepsin B contributes to the initiation of peripheral inflammation-induced chronic pain. *J Neurosci*. 2012;32(33):11330–11342.
8. Wu Z, Sun L, Hashioka S, et al. Differential pathways for interleukin-1β production activated by chromogranin A and amyloid β in microglia. *Neurobiol Aging*. 2013;34(12):2715–2725.

9. Dinarello CA. Biologic basis for interleukin-1 in disease. *Blood*. 1996; 87(6):2095–2147.
10. Hornung V, Bauernfeind F, Halle A, Samstad EO, Kono H, Rock KL. Silica crystals and aluminum salts activate the NALP3 inflammasome through phagosomal destabilization. *Nat Immunol*. 2008;9(8):847–856.
11. Halle A, Hornung V, Petzold GC, Stewart CR, Monks BG, Reinheckel T. The NALP3 inflammasome is involved in the innate immune response to amyloid-beta. *Nat Immunol*. 2008;9(8):857–865.
12. Geraghty P, Rogan MP, Greene CM, et al. Neutrophil elastase up-regulates cathepsin B and matrix metalloprotease-2 expression. *J Immunol*. 2007;178(9):5871–5878.
13. Ito WD, Lund N, Zhang Z, et al. Activation of cell surface bound 20S proteasome inhibits vascular cell growth and arteriogenesis. *Biomed Res Int*. 2015:719316. doi: 10.1155/2015/719316
14. Dieudé M, Bell C, Turgeon J, et al. The 20S proteasome core, active within apoptotic exosome-like vesicles, induces autoantibody production and accelerates rejection. *Sci Transl Med*. 2015;7(318):318–200. doi: 10.1126/scitranslmed.aac9816
15. Majetschak M, Perez M, Sorell LT, Lam J, Maldonado ME, Hoffman RW. Circulating 20S proteasome levels in patients with mixed connective tissue disease and systemic lupus erythematosus. *Clin Vaccine Immunol*. 2008;15(9):1489–1493.
16. Henry L, Lavabre-Bertrand T, Douche T, et al. Diagnostic value and prognostic significance of plasmatic proteasome level in patients with melanoma. *Exp Dermatol*. 2010;19:1054–1059.
17. Jakob C, Egerer K, Liebisch P, et al. Circulating proteasome levels are an independent prognostic factor for survival in multiple myeloma. *Blood*. 2007;109(5):2100–2105.
18. Matuszczak E, Tylicka M, Dębek W, Hermanowicz A, Ostrowska H. The comparison of C-proteasome activity in the plasma of children after burn injury, mild head injury and blunt abdominal trauma. *Adv Med Sci*. 2015;60(2):253–258.
19. Tylicka M, Matuszczak E, Dębek W, Hermanowicz A, Ostrowska H. Circulating proteasome activity following mild head injury in children. *Childs Nerv Syst*. 2014;30(7):1191–1196.
20. Matuszczak E, Tylicka M, Dębek W, Hermanowicz A, Ostrowska H. Correlation between circulating proteasome activity, total protein and c-reactive protein levels following burn in children. *Burns*. 2014;40(5): 842–847.
21. Sixt SU, Dahlmann B. Extracellular, circulating proteasomes and ubiquitin – incidence and relevance. *Biochim Biophys Acta*. 2008;1782(12): 817–823.
22. Sankiewicz A, Laudański P, Romanowicz L, et al. Development of surface plasmon resonance imaging biosensors for detection of ubiquitin carboxyl-terminal hydrolase L1. *Anal Biochem*. 2015;469:4–11.
23. Gorodkiewicz E. Surface plasmon resonance imaging sensor for cathepsin determination based in immobilized cystatin. *Protein Pept Lett*. 2009;16(11):1379–1385.
24. Gorodkiewicz E, Sieńczyk M, Regulska E, et al. Surface plasmon resonance imaging biosensor for cathepsin G based on a potent inhibitor: Development and applications. *Anal Bochem*. 2012;423:218–223.
25. Gorodkiewicz E, Sankiewicz A, Laudański P. Surface plasmon resonance imaging biosensors for aromatase based on a potent inhibitor and a specific antibody: Sensor development and application for biological material. *Cent Eur J Chem*. 2014;12(5):557–567.
26. Johnsson B, Lofas S, Lindquist G. Immobilization of proteins to a carboxymethyldextran-modified gold surface for biospecific interaction analysis in surface plasmon resonance sensors. *Anal Biochem*. 1991;198:268–277.
27. Jeschke MG, Gauglitz GG, Kulp GA, et al. Long-term persistance of the pathophysiologic response to severe burn injury. *PLoS ONE*. 2011;6(7): e21245. doi: 10.1371/journal.pone.0021245
28. Porter C, Herndon DN, Sidossis LS, et al. The impact of severe burns on skeletal muscle mitochondrial function. *Burns*. 2013;39(6):1039–1047.
29. Sun L, Wu Z, Hayashi Y, et al. Microglial cathepsin B contributes to the initiation of peripheral inflammation-induced chronic pain. *J Neurosci*. 2012;32(33):11330–11342.
30. Hook G, Jacobsen JS, Grabstein K, Kindy M, Hook V. Cathepsin B is a new drug target for traumatic brain injury therapeutics: Evidence for E64d as a promising lead drug candidate. *Front Neurol*. 2015;6:178. doi: 10.3389/fneur.2015.00178
31. Assfalg-Machleidt I, Jochum M, Nast-Kolb D, et al. Cathepsin B-indicator for the release of lysosomal cysteine proteinases in severe trauma and inflammation. *Biol Chem Hoppe Seyler*. 1990;371(Suppl): 211–222.
32. Jochum M, Machleidt W, Fritz H. Phagocyte proteinases in multiple trauma and sepsis: Pathomechanisms and related therapeutic approaches. In: Neugebauer EA, Holaday JW, eds. *Handbook of Mediators in Septic Shock*. Boca Raton, FL: CRC Press; 1993:335–361.
33. Canbay A, Guicciardi ME, Higuchi H, et al. Cathepsin B inactivation attenuates hepatic injury and fibrosis during cholestasis. *J Clin Invest*. 2003;112(2):152–159.
34. Gondi CS, Rao JS. Cathepsin B as a cancer target. *Expert Opin Ther Targets*. 2013;17(3):281–291.
35. Palermo C, Joyce JA. Cysteine cathepsin proteases as pharmacological targets in cancer. *Trends Pharmacol Sci*. 2008;29(1):22–28.
36. Kos J, Mitrovic A, Mirkovic B. The current stage of cathepsin B inhibitors as potential anticancer agents. *Future Med Chem*. 2014;6(11): 1355–1371.
37. Cha IS, Kwon J, Mun JY, et al. Cathepsins in the kidney of olive flounder, *Paralichthys olivaceus*, and their responses to bacterial infection. *Dev Comp Immunol*. 2012;38(4):538–544.
38. Canbay A, Feldstein AE, Higuchi H, et al. Kupffer cell engulfment of apoptotic bodies stimulates death ligand and cytokine expression. *Hepatology*. 2003;38(5):1188–1198.
39. Cunnane G, Fitzgerald O, Beeton C, Cawston TE, Bresnihan B. Early joint erosions and serum levels of matrix metalloproteinase 1, matrix metalloproteinase 3, and tissue inhibitor of metalloproteinases 1 in rheumatoid arthritis. *Arthritis Rheum*. 2001;44(10):2263–2274.
40. Mishiro T, Nakano S, Takahara S, et al. Relationship between cathepsin B and thrombin in rheumatoid arthritis. *J Rheumatol*. 2004;31(7): 1265–1273.
41. Baici A, Müntener K, Willimann A, Zwicky R. Regulation of human cathepsin B by alternative mRNA splicing: Homeostasis, fatal errors and cell death. *Biol Chem*. 2006;387(8):1017–1021.
42. Feng Y, Ni L, Wang Q. Administration of cathepsin B inhibitor CA-074Me reduces inflammation and apoptosis in polymyositis. *J Dermatol Sci*. 2013;72(2):158–167.
43. Bien S, Ritter CA, Gratz M, et al. Nuclear factor-κB mediates up-regulation of cathepsin B by doxorubicin in tumor cells. *Mol Pharmacol*. 2004;65(5):1092–1102.

Enamel defects and dental caries among children attending primary schools in Poznań, Poland

Justyna Opydo-Szymaczek[A–F], Karolina Gerreth[B,C,E,F], Maria Borysewicz-Lewicka[A,C,E,F], Tamara Pawlaczyk-Kamieńska[B,C,E,F], Natalia Torlińska-Walkowiak[B,C,E,F], Renata Śniatała[B,C,E,F]

Department of Pediatric Dentistry, Poznan University of Medical Sciences, Poland

A – research concept and design; B – collection and/or assembly of data; C – data analysis and interpretation; D – writing the article; E – critical revision of the article; F – final approval of the article

Advances in Clinical and Experimental Medicine, ISSN 1899-5276 (print), ISSN 2451-2680 (online) *Adv Clin Exp Med*. 2018;27(11):1535–1540

Address for correspondence
Justyna Opydo-Szymaczek
E-mail: jopydo@ump.edu.pl

Funding sources
Dental examinations were carried out as a part of dental screening financed from the Poznań City Council's budget.

Conflict of interest
None declared

Acknowledgements
The authors would like to thank the children who participated in the study, the staff of primary schools in Poznań and the staff of the Department of Pediatric Dentistry (Poznan University of Medical Sciences, Poland) who assisted in the project.

Received on April 18, 2017
Reviewed on May 7, 2017
Accepted on May 15, 2017

Abstract

Background. Both positive and negative associations between developmental enamel defects (DED) and dental caries have been reported in the literature.

Objectives. The aim of this study was to assess the prevalence of DED of permanent dentition and its association with dental caries in schoolchildren living in Poznań (Wielkopolskie Voivodeship, Poland).

Material and methods. A total of 2,522 6th grade children and 3,112 1st grade children were examined. Developmental enamel defects were described using the modified Developmental Defects of Enamel Index. Dental caries experience was assessed in accordance with the number of decayed, missing and filled teeth (DMFT).

Results. The study revealed 475 children (9.6%) to have at least 1 enamel defect of permanent dentition. In 6th-graders, statistical analysis confirmed significant differences between DMFT, DT (decayed teeth) and FT (filled teeth) numbers of various DED groups with subjects affected by diffuse opacities having generally the lowest caries indices and subjects with enamel hypoplasia and/or demarcated opacities having the highest caries indices. In both age groups, dental caries prevalence was statistically significantly higher in subjects with hypoplasia and/or demarcated opacities as compared to subjects without DED or with diffuse opacities ($p < 0.05$).

Conclusions. The prevalence of DED in the examined population was low and comparable to those reported in regions without fluoridated water. The study confirmed that children affected by diffuse enamel opacities were less susceptible to dental caries, while demarcated opacities and hypoplasia should be considered important dental caries risk factors.

Key words: dental caries, tooth abnormalities, enamel hypoplasia, dental fluorosis

DOI
10.17219/acem/73794

Introduction

Scientific research has demonstrated that ameloblasts, which are secretory cells that produce tooth enamel, are highly sensitive to changes in their environment. Since enamel is formed only during a certain period of tooth development, dysfunction of ameloblasts may lead to permanent morphological consequences, namely, developmental enamel defects (DED). Defective formation of the enamel matrix results in hypoplasia, a quantitative defect, presented as a reduced thickness of enamel. Defective calcification of an otherwise normal fully developed organic enamel matrix produces qualitatively defective enamel (hypomineralization). Clinically, enamel with hypomineralization has normal thickness, but changed translucency, which is presented as white, yellow, or brown diffuse, or demarcated opacities. Diffuse opacities spread over the enamel surface without a clearly defined margin, while demarcated opacities have distinct boundaries with the adjacent normal enamel.[1–4]

A very wide spectrum of etiological factors, including genetic, systemic, local, and environmental factors, may lead to the development of DED. Defects caused by genetic factors form a separate entity, usually affecting both the primary and permanent teeth. They are less common than those resulting from acquired causes. As far as environmental factors are concerned, fluoride exposure has been reported to be the main determinant of the prevalence of DED in the given population.[1,4] Several studies have also shown that teeth are very sensitive to the effects of dioxins, which arrest the degradation and removal of enamel matrix proteins.[5,6] Other etiological factors of DED include various metabolic disturbances, prematurity, irradiation, fever, infections, nutritional deficiencies, and direct traumas to cells, which lead to unfavorable changes in the environment of enamel-forming cells.[1,3,5]

Developmental enamel defects with a similar appearance are not necessarily caused by similar agents and the same insult can produce different defects depending on the stage of tooth development.[1] However, some types of DED are usually linked to specific etiological factors. The etiology of the diffuse opacities is generally thought to be associated with excessive fluoride exposure during tooth development.[2,7] Demarcated opacities and hypoplasia are related to systemic conditions influencing teeth development, such as infections, antibiotic therapy, nutritional deficiencies, low birth weight, and exposure to dioxins.[3,4,8,9] Also, the common causes of localized hypomineralization or hypoplasia in permanent dentition are chronic periapical infections and traumatic injuries within deciduous predecessors.[10,11]

Developmental enamel defects have a significant impact on oral health, compromising esthetics, increasing tooth sensitivity and altering occlusal functions. In addition, many studies have highlighted the possibility of some types of DED being important risk factors for caries and erosions of the hard dental tissues.[12–16] Enamel hypoplasia and demarcated opacities have been frequently reported to increase dental caries experience, due to the irregular, retentive surfaces leading to plaque accumulation and higher acid solubility of the affected enamel, respectively.[12,13,16]

Data concerning prevalence of enamel defects in Poland is sparse, since children are not routinely screened for DED in Polish national epidemiological surveys.

The aim of the present study was to assess the prevalence of various types of DED in permanent dentition and its association with dental caries in the population of Polish children living in the city of Poznań (Wielkopolskie Voivodeship, Poland).

Material and methods

The Ethical Committee of Poznan University of Medical Sciences granted its approval for this study (Resolution No. 466/10). The study involved the assessment of DED prevalence and dental caries experience in the city of Poznań (Wielkopolskie Voivodeship, Poland) and was a part of dental screening financed from the Poznań City Council's budget. Prior to the study, the parents of all children had received a letter about the examination and had been asked to give consent for their children participation in the investigation.

Schoolchildren of grades 1 and 6 (5–8-year-olds and 11–15-year-olds) were examined for DED and dental caries. Of the overall number of 8,165 1st- and 6th-grade children attending 81 public primary schools in Poznań, Poland, 5,634 children from 75 schools could enter the study. The remaining pupils were either not present on the day of the examination, or the school director or parents had not signed the consent for examination.

A total of 2,522 6th-grade children (1,343 girls and 1,179 boys) and 3,112 1st-grade children (1,572 girls and 1,540 boys) were examined, with 705 excluded, as they did not have permanent 1st molars fully erupted, leading to the final sample size of 4,929 children.

The mean age of the younger subjects was 6.9 ±0.4 years (± standard deviation (SD); range 5–8 years), while the mean age of the older subjects was 12.02 ±0.22 years (± SD; range 11–15 years).

According to the information from the Sanitary Inspection, the natural level of fluoride in the tap water in Poznań in 1995–2005, measured at various points of the water mains, ranged from 0.3 to 0.9 mg/L.

In Poland, parents and their children are subject to compulsory national health insurance. Professional oral health care for children is covered by this insurance. Since 2003 all primary schoolchildren have been included in the school program of supervised brushing with 1.25% fluoride gel (6 times per year).

Dental examinations were conducted in classrooms at the beginning of 2010 by 7 calibrated dentists from the

Department of Pediatric Dentistry of Poznan University of Medical Sciences. Subjects were examined under the following conditions: the child was seated in a chair, and an examiner stood in front of the chair with a headlamp, a mouth mirror and a WHO probe.

Developmental enamel defects were examined using the modified Developmental Defects of Enamel Index for screening surveys, recording the categories of demarcated and diffuse opacities and hypoplasia.[2] Teeth were inspected wet without previous professional cleaning. The status of the subject was defined according to the most severe defect seen in the subject. If a subject showed teeth with diffuse and demarcated opacities, they were designated as having demarcated opacities. Having teeth with opacities and teeth with hypoplasia was designated as having enamel hypoplasia. The prevalence of DED was determined by the inclusion of any individual who has been found to have at least 1 tooth affected by the condition.

The dental caries experience was assessed in accordance with the number of decayed (DT), missing (MT) and filled teeth (FT) calculated for all permanent teeth as the number decayed, missing and filled teeth (DMFT). Caries prevalence was calculated as a percentage of individuals with DMFT >0.

Caries diagnosis was carried out by visual and tactile examination, using an artificial light, a mouth mirror and a blunt dental probe. Active caries was recorded as present when the respective lesion showed an unmistakable cavity, undermined enamel or a detectably softened area. A probe was used to confirm the visual evidence of caries. Areas with visual evidence of demineralization, presenting no soft surface, were considered sound. A dental explorer was used for detecting the cavities on the proximal surfaces. Apart from that, if caries in dentine was visualized as a loss of translucency producing a shadow in a calculus-free and stain-free proximal surface, it was recorded as proximal decay, too. A tooth filled due to decay was recorded when a tooth had at least 1 permanent restoration placed to treat caries. Fissure sealants were not included in the FT component of the DMFT. The MT component was recorded when a tooth had been extracted due to caries complications (verified by interview).

Prior to the examination, a calibration exercise was conducted between examiners on a group of 30 patients, apart from the main study. The inter- and intra-examiner concordances assessed with Cohen's kappa coefficient were all above 0.75.

Data analysis was performed with STATISTICA v. 12 (StatSoft Inc., Tulsa, USA) for Windows 10, assuming $p < 0.05$ as the level of statistical significance.

Statistical significance for differences between proportions was assessed using the χ^2 test.

After performing the Shapiro-Wilk normality test, a non-parametric Kruskal-Wallis analysis of variance (ANOVA) was used to assess any differences in the mean DMFT, and its DT, MT and FT components of different DED groups. If a statistical difference was detected, post hoc non-parametric multiple comparisons of mean ranks procedures were used to compare individual pairs of means. In order to compare the risk of having caries between different DED groups, the odds ratio (OR) was calculated.

Results

Table 1 shows the prevalence of various types of DED as well as the effects of gender and age on the prevalence of enamel defects.

Out of the 4,929 children in the study, 475 children (9.6%) had at least 1 enamel defect of permanent dentition. Overall, the prevalence of DED in the older group was statistically significantly higher as compared to prevalence of DED in younger children ($p = 0.0000$). The presence of DED was not significantly associated with gender ($p > 0.05$).

No cases of generalized enamel defects, suggestive of genetically determined amelogenesis imperfecta, were detected in this study.

The prevalence of enamel hypoplasia was statistically significantly lower as compared to the prevalence of both types of opacities ($p < 0.001$). The percentage of subjects having diffuse and demarcated opacity was similar (3.7 vs 4.0, respectively).

Table 2 summarizes dental caries indices in 2 age groups according to different DED variables. Statistically significant differences were detected in both age groups. In the younger group, Kruskall-Wallis ANOVA detected statistically significant differences between DMFT, DT and FT

Table 1. Number of subjects (n) with hypoplasia, demarcated opacities and diffuse opacities in both age groups and both genders

Type of DED	Hypoplasia		Demarcated opacity		Diffuse opacity		Without DED		χ^2 test (subjects with DED vs subjects without DED)
Subjects	n	%	n	%	n	%	n	%	p-value
1st-graders	46	1.9	64	2.7	73	3.0	2,224	92.4	0.0000
6th-graders	48	1.9	135	5.4	109	4.3	2,230	88.4	
Females	48	1.9	110	4.3	102	4.0	2,318	89.9	0.2639
Males	46	2.0	89	3.8	80	3.4	2,136	90.9	
Total	94[a]	1.9	199	4.0	182	3.7	4,454	90.4	

DED – developmental enamel defects; [a] $p = 0.0000$ as compared to subjects with demarcated opacity or diffuse opacity.

numbers in groups affected by different types of DED ($p < 0.0001$; $p = 0.0001$; $p = 0.0181$, respectively). Post hoc non-parametric multiple comparisons of mean ranks confirmed this statistically significant difference only for DMFT of subjects affected by demarcated opacities and/or hypoplasia, as compared to subjects without DED. In 6th-graders, post hoc tests confirmed statistically significant differences between DMFT, DT and FT numbers of various DED groups with subjects affected by diffuse opacities having generally the lowest caries indices and subjects with enamel hypoplasia and/or demarcated opacity having the highest caries indices.

In both age groups, dental caries prevalence was statistically significantly higher in subjects with hypoplasia and/or demarcated opacity as compared to subjects without DED or with diffuse opacities ($p < 0.05$).

Estimation of the OR showed that children with demarcated or hypoplastic defects had several folds higher risk of having caries compared with those without DED (OR = 2.83 for 1st-graders, OR = 2.51 for 6th-graders) or those who had diffuse opacities (OR = 2.31 for 1st-graders and OR = 4.24 for 6th-graders). Older subjects without DED had a higher risk of having caries as compared to those with diffuse opacities (OR = 1.69).

Discussion

The overall prevalence of DED in permanent dentition (9.6% of the affected subjects) is at the lower end of the findings from other studies carried out in areas with and without fluoridated drinking water. Similar rates of prevalence were observed in children residing in low fluoride area of Naples (Italy) and Campeche (Mexico) (9.8% and 7.5%, respectively), while much higher figures were reported during a multicenter epidemiological study (from 43% in Greece to 70% in the Netherlands) and in a population of 14-year-old boys in Saudi Arabia (75%).[17–20]

Examinations of 1st-grade and 6th-grade children in the Śrem Commune (Wielkopolskie Voivodeship, Poland), where the level of fluoride in the drinking water ranges from 0.1 to 0.4 mg/L, revealed 25.7% of the subjects to have at least 1 permanent 1st molar or incisor affected by DED.[21]

Prevalence rates of DED in areas with water fluoridation ranged from 26.1% for residents of the city of Araraquara, Brazil, up to 92.1% for children in Hong Kong.[22–23]

Researchers examining fluoridated communities reported a higher prevalence of diffuse defects, which should be attributed to the higher fluoride exposure of children during critical periods of enamel formation. In the study by Arrow et al. (2008), 47% of 7-year-old schoolchildren from the fluoridated region of Western Australia had permanent 1st molars affected by white diffuse opacities and in the study by Milsom et al. (1996), 40% of 8–9-year-olds from fluoridated Cheshire (UK) had diffuse defects on the permanent incisors.[24–25]

In Poland, drinking water is not artificially fluoridated. In most of the country, fluoride concentration in drinking water is below 0.3 mg/L, although in some localities it exceeds 1.0 mg/L.[26] Fluoride content in the water of the city of Poznań in 1995–2005 ranged from 0.3 to 0.9 mg/L,

Table 2. Dental caries prevalence (%) of permanent dentition, DMFT numbers in various DED groups of younger and older subjects

	Subjects without DED	Subjects with demarcated opacities or hypoplasia	Subjects with diffuse opacities	p-value (non-parametric Kruskal-Wallis ANOVA)
1st-grade children				
N	2,224	110	73	
DMFT	0.17 ±0.59	0.38 ±0.80[a]	0.18 ±0.51	0.0000
DT	0.11 ±0.45	0.28 ±0.73	0.03 ±0.16	0.0001
MT	0.00 ±0.00	0.00 ±0.00	0.00 ±0.00	NA
FT	0.06 ±0.35	0.10 ±0.41	0.15 ±0.49	0.0181
Caries prevalence	10.30	24.55[b]	12.33	NA
6th-grade children				
N	2,230	183	109	
DMFT	1.50 ±1.78	2.15 ±1.88[c]	1.04 ±1.47[d]	0.0000
DT	0.56 ±1.17	0.67 ±1.25	0.14 ±0.37[e]	0.0002
MT	0.02 ±0.16	0.03 ±0.21	0.02 ±0.19	0.4352
FT	0.91 ±1.36	1.45 ±1.65[f]	0.88 ±1.43	0.0000
Caries prevalence	57.94[h]	77.60[g]	44.95	NA

ANOVA – analysis of variance; OR – odds ratio; DED – developmental enamel defects; N – number of subjects; DMFT – number of decayed, missing and filled teeth; DT – number of decayed teeth; MT – number of missing teeth; FT – number of filled teeth; [a] $p = 0.0371$ as compared to subjects without DED; [b] $p = 0.0000$ as compared to subjects without DED (OR = 2.83), $p = 0.0418$ as compared to subjects with diffuse opacities (OR = 2.31); [c] $p = 0.0000$ as compared to subjects without DED and subjects with diffuse opacities; [d] $p = 0.0216$ as compared to subjects without DED, $p = 0.0000$ as compared to subjects with demarcated opacities or hypoplasia; [e] $p = 0.0087$ as compared to subjects without DED, $p = 0.0048$ as compared to subjects with demarcated opacities or hypoplasia; [f] $p = 0.0000$ as compared to subjects without DED, $p = 0.0015$ as compared to subjects with diffuse opacities; [g] $p = 0.0000$ as compared to subjects without DED (OR = 2.51) and subjects with diffuse opacities (OR = 4.24); [h] $p = 0.0075$ (OR = 1.69) as compared to subjects with diffuse opacities; NA – not applicable; OR – odds ratio.

which is close to WHO recommendations on the optimal fluoride level in the drinking water (0.5–1.0 mg/L).[27] Apart from drinking water, the most common source of fluoride in Poland is toothpaste with an age-related concentrations between 250 and 1500 mg/L. Dietary fluoride supplements are available only on prescription and intended for use by children living in nonfluoridated areas.

In the present study, the prevalence of diffuse opacities (3.7%) was lower as compared to those reported in the drinking water of other communities with similar fluoride content, which suggests that total fluoride exposure of most examined children did not exceed limits above which fluorosis may develop. However, children in this study were examined at schools, under headlamp lighting and without previous cleaning of the teeth, which could significantly affect the number of detected anomalies. It must be remembered that wide variations of reported values of DED prevalence in the literature might be attributed to the differences in the study conditions, as well as the use of various terminologies and diagnostic criteria to describe the enamel defects. The diagnosis of DED can be influenced by the type of light source used for the examination, brushing or drying of teeth before the examination, additional photographs taken, as well as examination of only a particular group of teeth or the whole dentition.[15,18]

As far as the environmental risk factors of demarcated opacities are concerned, studies of Alaluusua et al. have shown that polychlorinated dibenzo-*p*-dioxins and dibenzofurans in mother's milk may cause hypomineralization defects in the child's permanent 1st molar teeth, while other studies did not confirm this association.[5,28] Nevertheless, Jaraczewska et al. proved that the levels of dioxin-like compounds in the human milk samples from Wielkopolskie Voivodeship are lower than those reported in other European countries.[29]

Regarding gender, studies are in conflict as to whether boys or girls are more affected by DED.[21,30,31] Our present study failed to demonstrate any significant difference in the prevalence of DED between girls and boys.

Differences in the prevalence of DED in both age groups could be explained from the biological point of view: given that as age increases, more permanent teeth erupt, the probability of finding teeth with DED also increases. On the other hand, in the older group, some enamel defects might be masked by dental caries and large restorations.[18,21]

As far as dental caries risk factors are concerned, the results of the majority of studies have so far been consistent in showing a positive relationship between caries and hypoplasia and/or demarcated enamel opacities, and results of the present study concur with these previous findings.[13,16,30,32] With regard to diffuse opacities, epidemiological surveys revealed controversial results on their association with dental caries. According to many studies, caries prevalence tends to be reduced with increasing fluoride exposure during dentition development and fluoride-opacities are accompanied by lower dental caries prevalence.[17,33–36] However, an opposite trend was also reported.[37] The results of the current study revealed that in an older group of the subjects, diffuse opacities were associated with significantly lower dental caries prevalence and intensity.

The limitations of the study include: involvement of all children who had permission for examination (not only lifetime residents of Poznań), examination of teeth without previous cleaning (which might have affected examiners' ability to detect abnormalities), and assigning subjects to particular group of DED on the basis of the most severe defect seen in the permanent dentition of the subject (lack of information about teeth and surfaces affected by DED).

However, the results clearly indicate that fluoride exposure of the majority of examined children did not exceed limits above which visible enamel fluorosis may develop. Moreover, children affected by diffuse enamel opacities turned out to be less susceptible to dental caries, while demarcated opacities and hypoplasia significantly increased the risk of caries.

It must be remembered that the determination of risk and protective factors for dental caries development in Polish children is important, since dental caries indices in the Polish children are at the high end of those reported for other European countries.[38]

Conclusions

The prevalence of DED in examined population was comparable to those reported in regions without fluoridated water. The study confirmed that children affected by diffuse enamel opacities were less susceptible to dental caries, while demarcated opacities and hypoplasia should be considered important dental caries risk factors. The findings emphasize the need for continuous promotion of the proper use of fluorides, as well as intensification of dental caries prevention in patients affected by caries-prone enamel defects.

References

1. Anthonappa NM, Robert PP. Enamel defects in the permanent dentition: Prevalence and etiology. In: Drummond BK, Kilpatrick N, eds. *Book Planning and Care for Children and Adolescents with Dental Enamel Defects Etiology, Research and Contemporary Management*. 1st ed. Berlin and Heidelberg, Germany: Springer-Verlag; 2015:15–30.
2. Clarkson J, O'Mullane D. A modified DDE index for use in epidemiological studies of enamel defects. *J Dent Res*. 1989;68:445–450.
3. Crombie F, Manton D, Kilpatrick N. Aetiology of molar–incisor hypomineralization: A critical review. *Int J Paediatr Dent*. 2009;19:73–83.
4. Wong HM. Aetiological factors for developmental defects of enamel. *Austin J Anat*. 2014;1:1003. http://austinpublishinggroup.com/anatomy/fulltext/Anatomy-v1-id1003.php. Accessed April 17, 2017.
5. Alaluusua S, Lukinmaa PL, Vartiainen T, Partanen M, Torppa J, Tuomisto J. Polychlorinated dibenzo-para-dioxins and dibenzofurans via mother's milk may cause developmental defects in the child's teeth. *Environ Toxicol Pharmacol*. 1996;1(3):193–197.

6. Gao Y, Sahlberg C, Kiukkonen A, et al. Lactational exposure of Han/Wistar rats to 2,3,7,8-tetrachlorodibenzo-*p*-dioxin interferes with enamel maturation and retards dentin mineralization. *J Dent Res*. 2004;83(2):139–144.
7. Seow WK, Ford D, Kazoullis S, Newman B, Holcombe T. Comparison of enamel defects in the primary and permanent dentitions of children from a low-fluoride district in Australia. *Pediatr Dent*. 2011;33 (3):207–212.
8. Arrow P. Risk factors in the occurrence of enamel defects of the first permanent molars among schoolchildren in Western Australia. *Community Dent Oral Epidemiol*. 2009;37(5):405–415.
9. Nelson S, Albert JM, Lombardi G, et al. Dental caries and enamel defects in very low birth weight adolescents. *Caries Res*. 2010;44(6): 509–518.
10. Broadbent JM, Thomson WM, Williams SM. Does caries in primary teeth predict enamel defects in permanent teeth? A longitudinal study. *J Dent Res*. 2005;84(3):260–264.
11. De Amorim LF, Estrela C, Da Costa LR. Effects of traumatic dental injuries to primary teeth on permanent teeth – a clinical follow-up study. *Dent Traumatol*. 2011;27(2):117–121.
12. Farsi N. Developmental enamel defects and their association with dental caries in preschoolers in Jeddah, Saudi Arabia. *Oral Health Prev Dent*. 2010;8(1):85–92.
13. Hong L, Levy SM, Warren JJ, Broffitt B. Association between enamel hypoplasia and dental caries in primary second molars: A cohort study. *Caries Res*. 2009;43(5):345–352.
14. Kazoullis S, Seow WK, Holcombe T, Newman B, Ford D. Common dental conditions associated with dental erosion in schoolchildren in Australia. *Pediatr Dent*. 2007;29(1):33–39**.**
15. Lunardelli SE, Pérez MA. Prevalence and distribution of developmental enamel defects in the primary dentition of pre-school children. *Braz Oral Res*. 2005;19(2):144–149.
16. Vargas-Ferreira F, Salas MMS, Nascimento GG, et al. Association between developmental defects of enamel and dental caries: A systematic review and meta-analysis. *J Dent*. 2015;43(6):619–628.
17. Angelillo IF, Romano F, Fortunato L, Montanaro D. Prevalence of dental caries and enamel defects in children living in areas with different water fluoride concentrations. *Community Dent Health*. 1990;7(3): 229–236.
18. Casanova-Rosado AJ, Medina-Solís CE, Casanova-Rosado JF, et al. Association between developmental enamel defects in the primary and permanent dentitions. *Eur J Paediatr Dent*. 2011;12(3):155–158.
19. Rugg-Gunn AJ, Al-Mohammadi SM, Butler TJ. Effects of fluoride level in drinking water, nutritional status, and socio-economic status on the prevalence of developmental defects of dental enamel in permanent teeth in Saudi 14-year-old boys. *Caries Res*. 1997;31(4):259–267.
20. Cochran JA, Ketley CE, Arnadottir IB, et al. A comparison of the prevalence of fluorosis in 8-year-old children from seven European study sites using a standardized methodology. *Community Dent Oral Epidemiol*. 2004;32(Suppl 1):28–33.
21. Opydo-Szymaczek J, Gerreth K. Developmental enamel defects of the permanent first molars and incisors and their association with dental caries in the region of Wielkopolska, Western Poland. *Oral Health Prev Dent*. 2015;13(5):461–469.
22. Dini EL, Holt RD, Bedi R. Prevalence of caries and developmental defects of enamel in 9–10-year-old children living in areas in Brazil with differing water fluoride histories. *Br Dent J*. 2000;188(3):146–149.
23. Wong HM, McGrath C, Lo EC, King NM. Association between developmental defects of enamel and different concentrations of fluoride in the public water supply. *Caries Res*. 2006;40(6):481–486.
24. Arrow P. Prevalence of developmental enamel defects of the permanent first molars among school children in Western Australia. *Aust Dent J*. 2008;53(3):250–259.
25. Milsom KM, Woodward M, Haran D, Lennon MA. Enamel defects in the deciduous dentition as a potential predictor of defects in the permanent dentition of 8- and 9-year-old children in fluoridated Cheshire, England. *J Dent Res*. 1996;75(4):1015–1018.
26. Borysewicz-Lewicka M, Opydo-Szymaczek J. Fluoride in Polish drinking water and the possible risk of dental fluorosis. *Pol J Environ Stud*. 2016;25(1):9–15.
27. WHO. Fluorides and Oral Health: Report of a WHO Expert Committee on oral health status and fluoride use. In: *WHO Technical Report Series No. 846*. Geneva, Switzerland: WHO;1994:18.
28. Kuscu OO, Caglar E, Aslan S, Durmusoglu E, Karademir A, Sandalli N. The prevalence of molar incisor hypomineralization (MIH) in a group of children in a highly polluted urban region and a windfarm-green energy island. *Int J Paediatr Dent*. 2009;19(3):176–185.
29. Jaraczewska K, Lulek J, Covaci A, et al. Distribution of polychlorinated biphenyls, organochlorine pesticides and polybrominated diphenyl ethers in human umbilical cord serum, maternal serum and milk from Wielkopolska region, Poland. *Sci Total Environ*. 2006;372(1):20–31.
30. Slayton RL, Warren JJ, Kanellis MJ, Levy SM, Islam M. Prevalence of enamel hypoplasia and isolated opacities in the primary dentition. *Pediatr Dent*. 2001;23(1):32–36.
31. Tapias-Ledesma MA, Jiménez R, Lamas F, et al. Factors associated with first molar dental enamel defects: A multivariate epidemiological approach. *J Dent Child (Chic)*. 2003;70(3):215–220.
32. Leppaniemi A, Lukinmaa PL, Alaluusua S. Nonfluoride hypomineralizations in the permanent first molars and their impact on the treatment need. *Caries Res*. 2001;35(1):36–40.
33. Anuradha B, Laxmi GS, Sudhakar P, et al. Prevalence of dental caries among 13 and 15-year-old school children in an endemic fluorosis area: A cross-sectional study. *J Contemp Dent Pract*. 2011;12:447–450.
34. Iida H, Kumar JV. The association between enamel fluorosis and dental caries in U.S. schoolchildren. *J Am Dent Assoc*. 2009;140(7):855–862.
35. McGrady MG, Ellwood RP, Maguire A, Goodwin M, Boothman N, Pretty IA. The association between social deprivation and the prevalence and severity of dental caries and fluorosis in populations with and without water fluoridation. *BMC Public Health*. 2012;12:1122. doi: 10.1186/1471-2458-12-1122. Accessed April 17, 2017.
36. Szpunar SM, Burt BA. Dental caries, fluorosis, and fluoride exposure in Michigan schoolchildren. *J Dent Res*. 1988;67(5):802–806.
37. Wondwossen F, Astrøm AN, Bjorvatn K, Bardsen A. The relationship between dental caries and dental fluorosis in areas with moderate- and high-fluoride drinking water in Ethiopia. *Community Dent Oral Epidemiol*. 2004;32(5):337–344.
38. Emerich K, Adamowicz-Klepalska B. Trends in dental caries experience among children and adolescents in northern Poland between 1995 and 2003. *Community Dent Health*. 2010;27(4):218–221.

Odontogenic effects of two calcium silicate-based biomaterials in human dental pulp cells

Emel Olga Önay[1,A–F], Erkan Yurtcu[2,B–D], Yunus Kasim Terzi[3,B–D], Mete Üngör[1,E], Yener Oguz[4,B], Feride Iffet Şahin[3,E]

[1] Department of Endodontics, School of Dentistry, Baskent University, Ankara, Turkey
[2] Department of Medical Biology, School of Medicine, Baskent University, Ankara, Turkey
[3] Department of Medical Genetics, School of Medicine, Baskent University, Ankara, Turkey
[4] Department of Oral Surgery and Implantology, Private practice (Drs Nicolas & Asp), Dubai, United Arab Emirates

A – research concept and design; B – collection and/or assembly of data; C – data analysis and interpretation;
D – writing the article; E – critical revision of the article; F – final approval of the article

Advances in Clinical and Experimental Medicine, ISSN 1899-5276 (print), ISSN 2451-2680 (online) *Adv Clin Exp Med*. 2018;27(11):1541–1547

Address for correspondence
Emel Olga Önay
E-mail: eonay@baskent.edu.tr

Funding sources
None declared

Conflict of interest
None declared

Acknowledgements
This study was supported by Research Grant No. D-KA13/06 from Baskent University Research Fund. The authors are grateful to Dr. Mustafa Agah Tekindal for providing assistance with the statistics.

Received on February 25, 2017
Reviewed on April 18, 2017
Accepted on May 30, 2017

Abstract

Background. The goal of treating exposed pulp with an appropriate pulp capping material is to promote the dentinogenic potential of the pulpal cells. There have been recent attempts to develop more effective pulp-capping materials.

Objectives. The aim of this study was to evaluate the effect of newly developed calcium silicate-based material on odontogenic differentiation of primary human dental pulp cells (HDPCs), in comparison with a contemporary calcium silicate-based material.

Material and methods. Human dental pulp cells isolated from dental pulps were cultured in standard culture conditions in Dulbecco's Modified Eagle's Medium (DMEM) and then the effects of Micro-Mega mineral trioxide aggregate (MM-MTA) (Micro-Mega, Besançon, France) and ProRoot MTA (MTA) (Dentsply Sirona, Tulsa, USA) (positive control) were evaluated on HDPCs at 1, 7 and 14 days. Untreated cells were used as a negative control. Odontoblastic differentiation was assessed by alkaline phosphatase (*ALP*) activity. Runt-related transcription factor 2 (*RUNX2*), alkaline phosphatase liver/bone/kidney (*ALPL*), bone morphogenetic protein 2 (*BMP2*), dentin sialophosphoprotein (*DSPP*), and Distal-less homeobox 3 (*DLX3*), as odontoblastic/osteoblastic expression markers, were evaluated by semi-quantitative real-time polymerase chain reaction (RT-PCR) analysis. Calcium levels of culture media were also determined.

Results. The MM-MTA group significantly increased the expression of *BMP2* compared with that of the MTA group at 3 different time periods ($p < 0.05$). The up-regulation of *ALPL* between day 1 and 14 and the up-regulation of *DSPP* between day 7 and 14 were significant in both groups ($p < 0.05$). Micro-Mega MTA and MTA exhibited similar messenger RNA (mRNA) expression levels of *ALPL*, *DSPP*, *RUNX2*, *DLX3*, and *ALP* activities, as well as calcium levels.

Conclusions. Based on the cell responses observed in this study, MM-MTA might be used efficiently in dental pulp therapy as a potential alternative to MTA.

Key words: alkaline phosphatase, calcium silicate, dentinogenesis, mineral trioxide aggregate, transcription factors

DOI
10.17219/acem/74197

Introduction

Mineral trioxide aggregate (MTA) was introduced in the early 1990s and has been the material of choice for endodontic therapies due to its high mineralization capacity and relatively few inflammatory reactions in clinical use.[1,2] A number of in vivo and in vitro studies concerning cell and tissue interactions with MTA have shown its favorable biological characteristics. Some in vivo studies showed that MTA allowed cemental regeneration over the root-end filling when used in dogs and monkeys, whereas in vitro studies reported osteoblasts, periodontal ligament cells, bone marrow stromal cells, and dental pulp cells attached to MTA, inducing proliferation.[3–12] Moreover, the placement of MTA on pulp tissue leads to the proliferation, migration and differentiation of odontoblast-like cells, which produce a collagen matrix.[1]

Despite many positive characteristics, MTA has a couple of disadvantages, such as its extended setting time, difficulty in handling due to its sandy consistency and high porosity, poor dispersion, and high cost.[13,14]

After the development of MTA, many types of endodontic cements were developed, with Micro-Mega MTA (MM-MTA; Micro-Mega, Besançon, France) being one of those materials. It has a similar content as MTA, which is composed of tricalcium silicate, dicalcium silicate, tricalcium aluminate, calcium sulfate dehydrate, bismuth oxide, magnesium oxide, calcium carbonate ($CaCO_3$), and chloride accelerator.[15,16] The shorter setting time of MM-MTA is thought to be a result of the addition of $CaCO_3$ and chloride accelerator to the formula.[16] The material has also shown to be safe with respect to acceptable levels of arsenic, lead and metal oxides.[15] Additionally, the evaluation of different physical properties of the material that mainly focused on the radiopacity and push-out bond strength has yielded favorable results.[17,18] The MM-MTA is pre-dosed and the activated capsule is mechanically mixed, thus ensuring correct proportioning and homogenous mixing.

A number of studies have reported that the dentin bridge formation ability, biocompatibility, odontogenic differentiation, inflammatory response, and angiogenic potential of MM-MTA were all similar to those of MTA.[19–21] However, the exact mechanism of dentin regeneration/dentinogenesis after exposure to MTA and MM-MTA has not yet been completely explicated. Thus, the aim of this study was to evaluate and compare the biologic effects of newly developed MM-MTA and MTA on odontogenic differentiation of primary human dental pulp cells (HDPCs). The null hypothesis was that MTA and MM-MTA have similar effects in promoting odontogenic differentiation.

Material and methods

Six human impacted 3rd molars without any pathology extracted for orthodontic and impacted reasons were collected from 6 donors aged 18–25 years with informed consent, under a protocol approved by the Institutional Review Board and Ethics Committee of Baskent University, Ankara, Turkey (Project No. D-KA13/06). All 3 female and 3 male donors were healthy, without any known disease, were not taking any medications, and were non-smokers and non-alcohol consumers. Immediately after extraction, the extracted molars were cut horizontally at 1 mm below the cementoenamel junction. The carefully extracted pulp tissue was transferred to the laboratory in Dulbecco's Modified Eagle's Medium (DMEM)-F12 (Biochrom AG, Berlin, Germany) containing 1 drop of 1% streptomycin, neomycin and penicillin mixture (Biological Industries, Kibbutz Beit-Haemek, Israel). Physical dissection of the specimens was carried out by a scalpel. Under sterile conditions, the specimens were enzymatically digested with type I collagenase and dispase (Biochrom AG). After centrifugation at 500 g for 9 min, the supernatant was removed and the cells were placed in cell-culture medium (DMEM-F12 containing 10% heat-inactivated fetal bovine serum [FBS]; Biochrom AG), 2% L-glutamine (Biochrom AG), and 1% penicillin-streptomycin mixture (Biological Industries). The cells were cultured at 37°C in a humidified incubator supplemented with 5% CO_2 (Heraeus, Hanau, Germany). The cell culture medium was changed every 2–3 days and cells were subcultured when confluence reached 80%. Fourth to 7th subculture of cells was used for experimental procedure. Viability of cells was evaluated using the trypan blue exclusion test and up to 95% viable cells containing cultures were included in the experiments.

Material preparation and application

Teflon tubes (10 mm internal diameter, 2 mm height) were sterilized with ethylene oxide gas. White MTA (ProRoot MTA; Dentsply Sirona, Tulsa, USA, Lot No. 12002493) (positive control) and MM-MTA (Lot No. 7302238) were prepared according to the manufacturer's instructions, put into the tubes and stored in an incubator at 95% ±5% relative humidity at 37°C for 1 day.

Dental pulp cells and the tubes were incubated in 9 cm^2 Petri dishes. To prevent direct contact of materials with cells, the tubes were placed in a permeable transwell inserts with a pore size of 0.4 µm (Greiner Bio-One GmbH, Frickenhausen, Germany). At the end of the 1, 7 and 14-day time periods, the cells were harvested for gene expression and alkaline phosphates (*ALP*) activity, and also cell culture media were collected for calcium levels. Untreated cells were used as a negative control. All cell culture experiments were repeated in triplicate.

Determination of alkaline phosphatase activity

Intracellular *ALP* activities were determined according to the manufacturer's protocol by a commercially available colorimetric kit (Abcam, Cambridge, UK). Briefly, the total

cell number was determined by using a Thoma cell counting chamber (Paul Marienfeld GmbH & Co. KG, Lauda-Königshofen, Germany) and subsequently 1×10^5 cells were used. Cells washed in phosphate buffered saline (PBS) were homogenized in an assay buffer and para-nitrophenyl phosphate (pNPP) solution was added on cells in a 96-well microplate. After 60 min of incubation at room temperature under dark conditions, the stop solution was added. Optical densities were measured at 405 nm in a microplate spectrophotometer (Epoch; BioTek, Swindon, UK). Data analyses were carried out according to the manufacturer's instruction and *ALP* activity was expressed as U/mL.

Determination of calcium levels

Calcium levels were determined according to the manufacturer's protocol by a commercially available colorimetric kit (Abcam). Then, a chromogenic reagent and an assay buffer were added on 20 µL of culture medium in a 96-well microplate. After incubating for 5–10 min at room temperature under dark conditions, optical densities were measured at 575 nm in a microplate spectrophotometer (Epoch). Optical density of normal medium was used as blank and subtracted from optical density of all samples. Calcium concentrations were calculated according to the manufacturer's instruction and expressed as mg/dL.

Real-time polymerase chain reaction analysis

Total RNA was isolated from MTA and MM-MTA applied cells of 6 patients with TriPure isolation reagent according to the manufacturer's instructions (Roche Diagnostics GmbH, Mannheim, Germany). One microgram of total RNA was reverse transcribed using Transcriptor High Fidelity cDNA Synthesis Kit (Roche Diagnostics GmbH). Real-time ready catalog assays, which are short FAM-labeled hydrolysis probes containing locked nucleic acid, were used for real-time polymerase chain reactions (RT-PCR) (Roche Diagnostics GmbH). Expression of runt-related transcription factor 2 (*RUNX2*; Assay ID: 113380), alkaline phosphatase liver/bone/kidney (*ALPL*; Assay ID: 103448), bone morphogenetic protein 2 (*BMP2*; Assay ID: 104558), dentin sialophosphoprotein (*DSPP*; Assay ID: 139816), and distal-less homeobox 3 (*DLX3*; Assay ID: 140745) were determined using semi-quantitative RT-PCR by Light Cycler 480 II system (Roche Diagnostics GmbH) according to the manufacturer's instructions with a pre-incubation step at 95°C for 10 min, followed by 45 cycles at 95°C for 10 s, 60°C for 30 s, and 72°C for 1 s. Semi-quantitative PCR reactions were run in duplicate, and the relative expression levels of *RUNX2*, *ALPL*, *BMP2*, *DSPP* and *DLX3* transcripts' were calculated by the threshold cycle (Ct) and the 2^{-ddCt} method.[22] Glyceraldehyde 3-phosphate dehydrogenase (GAPDH) (Assay ID: 141139) were used for normalization of the expression data.

Statistical analysis

The Shapiro-Wilk test was used to assess the normality of distributions of the variables, and Levene's test was used to assess the homogeneity of variances among groups. Parametric test assumptions were not available for some variables. Data transformation methods were applied to these variables and then the analysis was performed. Comparisons of group means were performed with the repeated measures analysis of variance (ANOVA).

Data analyses were performed using the Statistical Package for the Social Sciences, v. 17.0 (SPSS Inc., Chicago, USA). A p-value < 0.05 was considered statistically significant. The results of statistical analysis were expressed as number of observations (n), mean ± standard deviation (mean ± SD, median and minimum–maximum values (min–max)).

Results

Alkaline phosphatase activity

Alkaline phosphatase activities levels were increased with MTA and MM-MTA. The most intense *ALP* activity was exhibited by the MM-MTA group at day 14. However, there was no significant difference in *ALP* activity among the negative control, MTA-, and MM-MTA-treated groups for all time periods ($p > 0.05$) (Fig. 1).

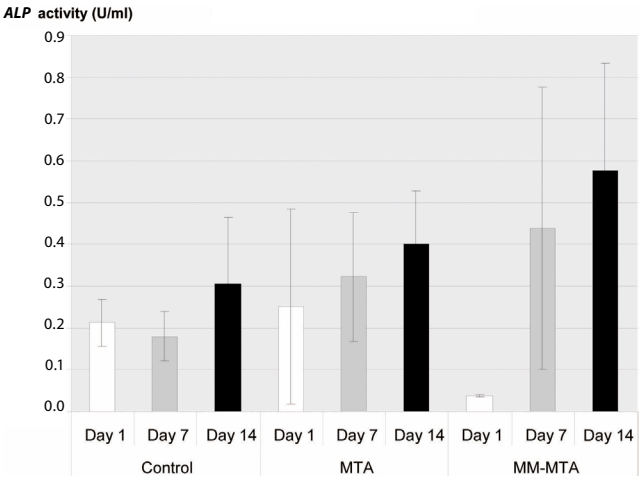

Fig. 1. The effects of MTA and MM-MTA on *ALP* activity in HDPCs ($p > 0.05$)

MTA –mineral trioxide aggregate; MM-MTA – Micro Mega MTA; *ALP* – alkaline phosphatase; HDPCs – human dental pulp cells.

Calcium levels

Observation from spectrophotometric analysis at day 7 revealed higher calcium level in HDPCs exposed of MTA and MM-MTA, whereas the calcium levels were not significantly different in negative control, MTA- and MM-MTA-treated groups for all time periods ($p > 0.05$) (Fig. 2).

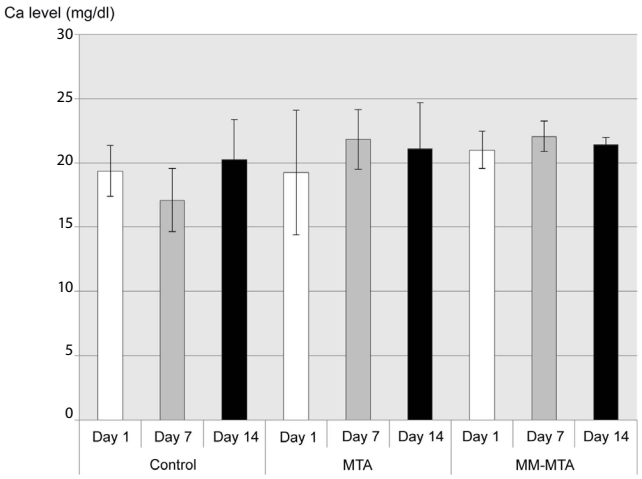

Fig. 2. The calcium levels of MTA and MM-MTA determined by spectrophotometric analysis at different time points (day 1, 7 and 14) ($p > 0.05$)

MTA – mineral trioxide aggregate; MM-MTA – Micro Mega MTA.

Real-time polymerase chain reaction gene expression analysis

The MM-MTA group significantly increased the expression of *BMP2* compared with that of the MTA group at 3 different time periods (day 1, 7 and 14) ($p < 0.05$) (Fig. 3). The up-regulation of *ALPL* between day 1 and 14 (Fig. 4), and the up-regulation of *DSPP* between day 7 and 14 (Fig. 5) were significant in both groups ($p < 0.05$). A down-regulation of *DSPP* between day 1 and day 7, and also between day 1 and day 14, were significant in both groups ($p < 0.01$) (Fig. 5). The MM-MTA and MTA groups exhibited similar messenger RNA (mRNA) expression levels of *ALPL* (Fig. 4), *DSPP* (Fig. 5), *RUNX2* (Fig. 6), and *DLX3* (Fig. 7) ($p > 0.05$).

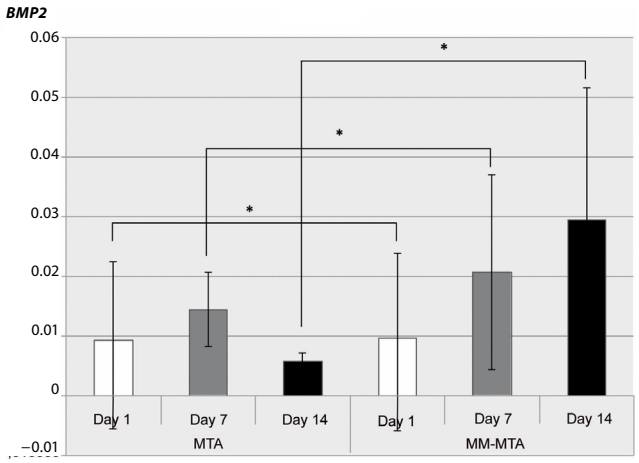

Fig. 3. The effects of MTA and MM-MTA on *BMP2* mRNA levels in HDPCs were determined by semi-quantitative RT-PCR at different time points (day 1, 7 and 14). Significant differences between test materials are indicated by asterisk and s (* $p < 0.05$)

MTA – mineral trioxide aggregate; MM-MTA – Micro Mega MTA; HDPCs – human dental pulp cells; *BMP2* – bone morphogenetic protein 2; RT-PCR – real-time polymerase chain reaction.

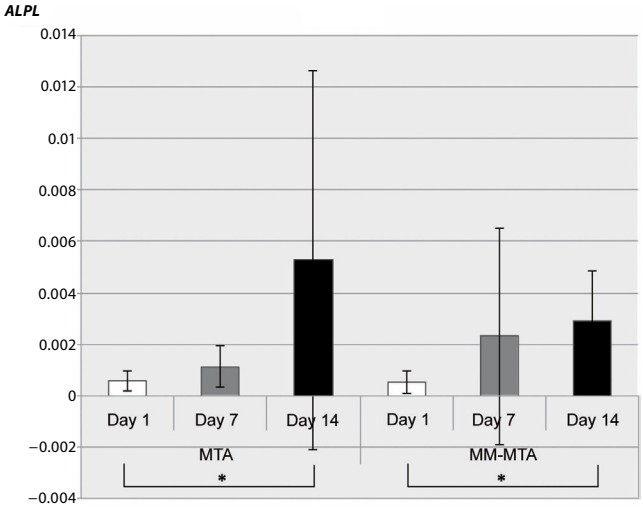

Fig. 4. The effects of MTA and MM-MTA on *ALPL* mRNA levels in HDPCs were determined by semi-quantitative RT-PCR at different time points (day 1, 7 and 14). Significant differences between test materials are indicated by asterisks (* $p < 0.05$)

MTA – mineral trioxide aggregate; MM-MTA – Micro Mega MTA; HDPCs – human dental pulp cells; *ALPL* – alkaline phosphatase liver/bone/kidney; RT-PCR – real-time polymerase chain reaction.

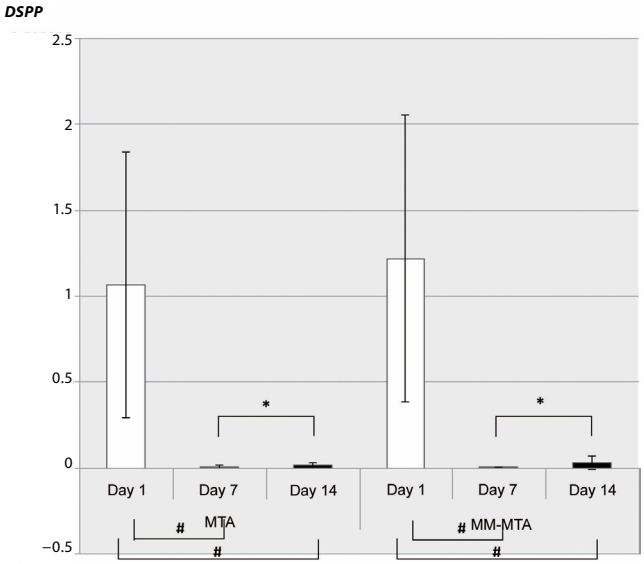

Fig. 5. The effects of MTA and MM-MTA on *DSPP* mRNA levels in HDPCs were determined by semi-quantitative RT-PCR at different time points (day 1, 7 and 14). Significant differences between test materials are indicated by asterisks (* $p < 0.05$) and number sign (# $p < 0.01$)

MTA – mineral trioxide aggregate; MM-MTA – Micro Mega MTA; HDPCs – human dental pulp cells; *DSPP* – dentin sialophosphoprotein; RT-PCR – real-time polymerase chain reaction.

Discussion

Dentinogenesis is the dentin formation process in which odontoblasts are responsible for the organic matrix synthesis and posterior mineral crystal deposition in this matrix. This pattern of formation is similar to that of bone, another mineralized connective tissue.[23] For both mineralized tissues, it is of fundamental importance to understand how

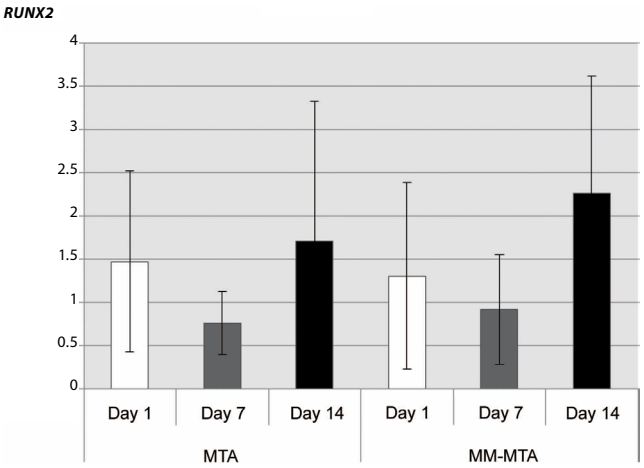

Fig. 6. The effects of MTA and MM-MTA on *RUNX2* mRNA levels in HDPCs were determined by semi-quantitative RT-PCR at different time points (day 1, 7 and 14). There were no significant differences ($p > 0.05$)

MTA – mineral trioxide aggregate; MM-MTA – Micro Mega MTA; HDPCs – human dental pulp cells; *RUNX2* – runt-related transcription factor 2; RT-PCR – real-time polymerase chain reaction.

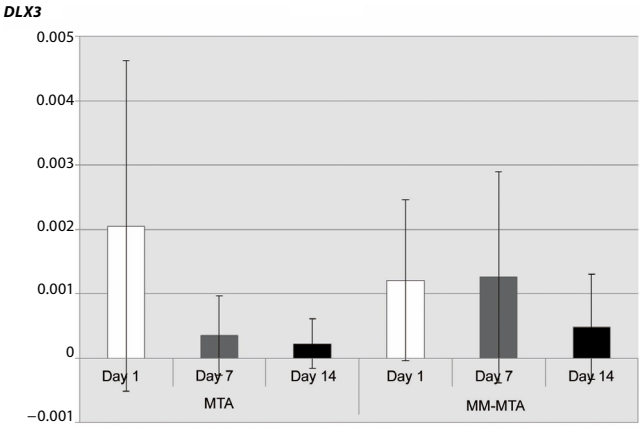

Fig. 7. The effects of MTA and MM-MTA on *DLX3* mRNA levels in HDPCs were determined by semi-quantitative RT-PCR at different time points (day 1, 7 and 14). There were no significant differences ($p > 0.05$)

MTA – mineral trioxide aggregate; MM-MTA – Micro Mega MTA; HDPCs – human dental pulp cells; *DLX3* – distal-less homeobox 3; RT-PCR – real-time polymerase chain reaction.

the different biomaterials are capable of promoting odontogenic differentiation.

In this study, the effect of MTA and MM-MTA on odontogenic differentiation of HDPCs is evaluated by measuring the mRNA levels of various differentiation markers genes and *ALP* activity. One of these specific markers is *DSPP*, which is believed to play a regulatory role in the mineralization of reparative dentin; it also serves as a specific marker for the odontoblastic phenotype.[24] Bone morphogenetic proteins are a group of cytokines that play an important role in stem cells' activity, adjusting the proliferation and differentiation of cells (e.g., osteoblast), and bone formation.[25] The up-regulation of *ALPL* (also known as tissue-nonspecific) has been associated with the onset of osteogenesis in vitro and its transcription can be up-regulated by *BMPs*.[26] Runt-related transcription factor 2 is a transcription factor that plays an essential role in bone and tooth development. The up-regulation of *RUNX2* in early odontoblasts followed by the down-regulation in differentiated and functional odontoblasts suggests that it is important for *RUNX2* to maintain the developmental stage-specific expression during odontogenic differentiation.[27] Homeodomain gene *DLX3* has been recently demonstrated as a potent regulator for proliferation and odontoblastic differentiation of HDPCs.[28] Alkaline phosphatase activity is frequently used for the evaluation of biologic mineralization.[29] This enzyme is crucial for the initiation (but not for the progression/maintenance) of the matrix mineralization process.[30]

In the present study, we aimed to reflect the clinical conditions of direct pulp capping in which the contact between pulp cells and biomaterials occurred indirectly through blood clots and physiologic fluids, which might not accurately model clinical setting. Seo et al. stated that the use of an interposed membrane only allows for the assessment of the effect of the diffusible components of MTA.[12] The results of the present study showed that *ALP* activity, calcium levels and mRNA expression levels of the dental pulp cells after treatment with elutes of MTA and MM-MTA were not significantly different compared with those of the untreated cells in the negative control group. This situation may be attributed to the permeable transwell inserts, which could act as a barrier and possibly decrease activation of the dental pulp cells.[31] Developing a model that would allow studying the effect of direct interaction between materials and dental pulp cells would be important for future studies.

In previous studies, MM-MTA has demonstrated similar characteristics to MTA when considering its ability to form a dentinal bridge, biocompatibility, osteo-/odontogenic differentiation capability, inflammatory response, and angiogenic potential.[19–21] The results of the present study agree with previous descriptions of these biomaterials in terms of odontogenic activity.[21] Our results were also consistent with the study carried out by Chang et al., who reported similar *ALP* activity and up-regulation of odontoblastic markers such as *ALP* and *DSPP* between MTA and MM-MTA at 7 and 14 days.[32] In the present study, *DSPP* gene was significantly down-regulated after day 1 and again significantly up-regulated after day 7 by both biomaterials. This could be attributed to a 14-day culture period, which might be the reason for unexpected differentiation results for both biomaterials.[33] Higher gene expression levels might be obtained in a longer period.

Extracellular proteins, particularly family of the transforming growth factor (*TGF*) proteins, including *BMPs*, have been explained in stem cell research as potent molecules to induce odontogenic differentiation. Micro-Mega MTA exhibited higher *BMP2* expression than MTA at all time periods of the present study. Despite similar calcium levels, the different effects of MM-MTA and MTA

on *BMP2* expression may be related to the differences in the speed of ion release in 2 biomaterials during the culture period. A study by Setbon et al., which, which investigated the composition of different tricalcium silicate cements, revealed that MM-MTA possessed a higher concentration of magnesium and sodium than MTA.[34] It has been demonstrated that these elements may represent an interest in terms of stimulation of osteodifferentiation.[35] Further pharmacokinetic studies on MM-MTA and MTA are, therefore, required to characterize and compare the ions released from these 2 biomaterials.

Expression patterns of homeobox genes of *DLX* family have been investigated during early stages of mouse odontogenesis. From that data, *DLX* genes have been proposed to contribute to odontogenic patterning.[36] It is also shown that *DLX3* supports the osteogenic differentiation in dental follicle cells via a *BMP2* positive feedback loop.[37] Moreover, Li et al. stated that *DLX3* expression progressively increased during odontoblast differentiation.[28] In contrast with those studies, the present study showed no significant up-regulation of *DLX3* marker at all time periods of the study. Further studies are required to reveal more details about the relationship between *DLX* transcription factors and the regulation of the odontogenic differentiation. These studies will also be available to disclose new information about the regulation of the *BMP2/DLX3* pathway.

Conclusions

Within the parameters of this study, MM-MTA exhibited higher *BMP2* expression than MTA at all time periods of the present study. Overall, MTA and MM-MTA showed similar osteo-/odontogenic-like phenotype differentiation of HDPCs with the mechanisms of up-regulation of the majority of osteo-/dentinogenesis-related genes. In this respect, our results suggest that MM-MTA is a potential alternative to MTA for use as an effective pulp capping material. More clinical studies are needed to assess if the expressions of these markers are clinically relevant.

References

1. Kuratate M, Yoshiba K, Shigetani Y, et al. Immunohistochemical analysis of nestin, osteopontin, and proliferating cells in the reparative process of exposed dental pulp capped with mineral trioxide aggregate. *J Endod*. 2008;34(8):970–974.
2. Nair PNR, Duncan HF, Pitt Ford TR, et al. Histological, ultrastructural and quantitative investigations on the response of healthy human pulps to experimental capping with mineral trioxide aggregate: A randomized controlled trial. *Int Endod J*. 2008;41(2):128–150.
3. Regan JD, Gutmann JL, Witherspoon DE. Comparison of Diaket and MTA when used as root-end filling materials to support regeneration of the periradicular tissues. *Int Endod J*. 2002;35(10):840–847.
4. Torabinejad M, Pitt Ford TR, Mckendry DJ, et al. Histologic assessment of mineral trioxide aggregate as a root-end filling in monkeys. *J Endod*. 1997;23(4):225–228.
5. Koh ET, Torabinejad M, Pitt Ford TR, et al. Mineral trioxide aggregate stimulates a biological response in human osteoblasts. *J Biomed Mater Res*. 1997;37(3):432–439.
6. Mitchell PJ, Pitt Ford TR, Torabinejad M, et al. Osteoblast biocompatibility of mineral trioxide aggregate. *Biomaterials*. 1999;20(2):167–173.
7. Balto HA. Attachment and morphological behavior of human periodontal ligament fibroblasts to mineral trioxide aggregate: A scanning electron microscope study. *J Endod*. 2004;30(1):25–29.
8. Bonson S, Jeansonne BG, Lallier TE. Root-end filling materials alter fibroblast differentiation. *J Dent Res*. 2004;83(5):408–413.
9. Gandolfi MG, Ciapetti G, Taddei P, et al. Apatite formation on bioactive calcium-silicate cements for dentistry affects surface topography and human marrow stromal cells proliferation. *Dent Mater*. 2010;26(10):974–992.
10. Gandolfi MG, Shah SN, Feng R, et al. Biomimetic calcium-silicate cements support differentiation of human orofacial mesenchymal stem cells. *J Endod*. 2011;37(8):1102–1108.
11. Min KS, Park HJ, Lee SK, et al. Effect of mineral trioxide aggregate on dentin bridge formation and expression of dentin sialoprotein and heme oxygenase-1 in human dental pulp. *J Endod*. 2008;34(6):666–670.
12. Seo MS, Hwang KG, Lee J, et al. The effect of mineral trioxide aggregate on odontogenic differentiation in dental pulp stem cells. *J Endod*. 2013;39(2):242–248.
13. Ber BS, Hatton JF, Stewart GP. Chemical modification of ProRoot MTA to improve handling characteristics and decrease setting time. *J Endod*. 2007;33(10):1231–1234.
14. Johnson BR. Considerations in the selection of a root-end filling material. *Oral Surg Oral Med Oral Pathol Oral Radiol Endod*. 1999;87(4):398–404.
15. Kum KY, Kim EC, Yoo YJ, et al. Trace metal contents of three tricalcium silicate materials: MTA Angelus, Micro Mega MTA and Bioaggregate. *Int Endod J*. 2014;47:704–710.
16. Khalil I, Naaman A, Camilleri J. Investigation of a novel mechanically mixed mineral trioxide aggregate (MM-MTA™). *Int Endod J*. 2015;48(8):757–767.
17. Tanalp J, Karapınar-Kazandağ M, Dölekoğlu S, et al. Comparison of the radiopacities of different root-end filling and repair materials. *The Scientific World Journal*. 2013;23:594950. doi: 10.1155/2013/594950
18. Celik D, Er K, Serper A, et al. Push-out bond strength of three calcium silicate cements to root canal dentine after two different irrigation regimes. *Clin Oral Investig*. 2014;18:1141–1146.
19. Khalil IT, Sarkis T, Naaman A. MM-MTA for direct pulp capping: A histologic comparison with ProRoot MTA in rat molars. *J Contemp Dent Pract*. 2013;14(6):1019–1023.
20. Margunato S, Taşlı PN, Aydın S, et al. In vitro evaluation of ProRoot MTA, Biodentine, and MM-MTA on human alveolar bone marrow stem cells in terms of biocompatibility and mineralization. *J Endod*. 2015;41(10):1646–1652.
21. Chang SW, Bae WJ, Yi JK, et al. Odontoblastic differentiation, inflammatory response, and angiogenic potential of 4 calcium silicate-based cements: Micromega MTA, ProRoot MTA, RetroMTA, and experimental calcium silicate cement. *J Endod*. 2015;41(9):1524–1529.
22. Livak KJ, Schmittgen TD. Analysis of relative gene expression data using real-time quantitative PCR and the 2(-Delta Delta C(T)) method. *Methods*. 2001;25(4):402–408.
23. Linde A. Dentin mineralization and role of odontoblasts in calcium transport. *Connect Tissue Res*. 1995;33(1–3):163–170.
24. Iohara K, Nakashima M, Ito M, et al. Dentin regeneration by dental pulp stem cell therapy with recombinant human bone morphogenetic protein 2. *J Dent Res*. 2004;83(8):590–595.
25. Kim JY, Kim MR, Kim SJ. Modulation of osteoblastic/odontoblastic differentiation of adult mesenchymal stem cells through gene introduction: A brief review. *J Korean Assoc Oral Maxillofac Surg*. 2013;39(2):55–62.
26. Tylzanowski P, Verschueren K, Huylebroeck D, et al. Smad-interacting protein 1 is a repressor of liver/bone/kidney alkaline phosphatase transcription in bone morphogenetic protein-induced osteogenic differentiation of C2C12 cells. *J Biol Chem*. 2001;276:40001–40007.
27. Yang F, Xu N, Li D, et al. A feedback loop between RUNX2 and the E3 ligase SMURF1 in regulation of differentiation of human dental pulp stem cells. *J Endod*. 2014;40:1579–1586.
28. Li X, Yang G, Fan M. Effects of homeobox gene distal-less 3 on proliferation and odontoblastic differentiation of human dental pulp cells. *J Endod*. 2012;38(11):1504–1510.

29. Wöltgens JH, Lyaruu DM, Bronckers AL, et al. Biomineralization during early stages of the developing tooth in vitro with special reference to secretory stage of amelogenesis. *Int J Dev Biol*. 1995;39: 203–212.
30. Bellows CG, Aubin JE, Heersche JN. Initiation and progression of mineralization of bone nodules formed in vitro: The role of alkaline phosphatase and organic phosphate. *Bone Miner*. 1991;14(1):27–40.
31. Paranjpe A, Smoot T, Zhang H, et al. Direct contact with mineral trioxide aggregate activates and differentiates human dental pulp cells. *J Endod*. 2011;37(12):1691–1695.
32. Chang SW, Lee SY, Kum KY, et al. Effects of ProRoot MTA, Bioaggregate, and Micromega MTA on odontoblastic differentiation in human dental pulp cells. *J Endod*. 2014;40(1):113–118.
33. Güven EP, Taşli PN, Yalvac ME, et al. In vitro comparison of induction capacity and biomineralization ability of mineral trioxide aggregate and a bioceramic root canal sealer. *Int Endod J*. 2013;46(12):1173–1182.
34. Setbon HM, Devaux J, Iserentant A, et al. Influence of composition on setting kinetics of new injectable and/or fast setting tricalcium silicate cements. *Dent Mater*. 2014;30(12):1291–1303.
35. Park KD, Lee BA, Piao XH, et al. Effect of magnesium and calcium phosphate coatings on osteoblastic responses to the titanium surface. *J Adv Prosthodont*. 2013;5:402–408.
36. Thomas B, Sharpe P. Patterning of the murine dentition by homeobox genes. *Eur J Oral Sci*. 1998;106:48–54.
37. Viale-Bouroncle S, Felthaus O, Schmalz G, et al. The transcription factor DLX3 regulates the osteogenic differentiation of human dental follicle precursor cells. *Stem Cells Dev*. 2012;21(11):1936–1947.

Homocysteine level in patients with obstructive sleep apnea/hypopnea syndrome and the impact of continuous positive airway pressure treatment

Jie Li[1,A–C,F], Li-Qiang Yu[1,A–C,F], Min Jiang[2,B–D,F], Ling Wang[1,A,D,F], Qi Fang[3,B,C,E,F]

[1] Department of Special Requirements, 1st Affiliated Hospital of Soochow University, Suzhou, China
[2] Clinical Laboratory, 1st Affiliated Hospital of Soochow University, Suzhou, China
[3] Department of Neurology, 1st Affiliated Hospital of Soochow University, Suzhou, China

A – research concept and design; B – collection and/or assembly of data; C – data analysis and interpretation; D – writing the article; E – critical revision of the article; F – final approval of the article

Advances in Clinical and Experimental Medicine, ISSN 1899-5276 (print), ISSN 2451-2680 (online) *Adv Clin Exp Med*. 2018;27(11):1549–1554

Address for correspondence
Ling Wang
E-mail: wwanglling@163.com

Funding sources
This project was supported by the National Natural Science Foundation of China (Grant No. 81500068 and Grant No. 81371387) and the Natural Science Foundation of Higher Education of Jiangsu Province of China (Grant No.14KJB320013).

Conflict of interest
None declared

Received on February 14, 2017
Reviewed on April 26, 2017
Accepted on May 29, 2017

Abstract

Background. Obstructive sleep apnea/hypopnea syndrome (OSAHS) is a common disorder in the general population.

Objectives. The aim of this study was to investigate the homocysteine (Hcy) level in the patients with OSAHS of varying degrees and the effect of continuous positive airway pressure (CPAP) treatment on OSAHS patients.

Material and methods. A total of 117 OSAHS patients were recruited and divided into 3 groups (mild OSAHS, moderate OSAHS and severe OSAHS), while 33 non-OSAHS people were selected as control group. For all cases, polysomnography (PSG) variables and the concentrations of Hcy, methane dicarboxylic aldehyde (MDA) and glutathione (GSH) were recorded. Serum Hcy was measured by cyclophorase. The values of MDA and GSH were measured by a spectrophotometer. In the severe OSAHS group, a total of 30 patients received CPAP for more than 4 h every night and were re-examined 6 months later.

Results. The serum levels of Hcy, MDA and GSH showed a significant difference in OSAHS patients and controls. The Hcy and GSH concentrations of OSAHS patients with CPAP treatment showed no apparent change compared with the prior treatment, but the MDA level was obviously lower after CPAP treatment. In controls and the mild/moderate OSAHS groups, multi-element linear regression analysis results indicated that there was a statistically significant relationship between the Hcy concentration and various independent variables (age, MDA, GSH, and the apnea-hypopnea index – AHI).

Conclusions. The change of the Hcy level was not proportional to the severity of the disease in different groups of OSAHS patients, and CPAP did not affect the Hcy levels.

Key words: continuous positive airway pressure, obstructive sleep apnea/hypopnea syndrome, homocysteine

DOI
10.17219/acem/74178

Introduction

Obstructive sleep apnea/hypopnea syndrome (OSAHS) is a common disorder in the general population, but often underestimated and underdiagnosed.[1] Accumulating evidence reveals that OSAHS is a significant risk factor for acute myocardial infarction and sudden cardiac death in patients with coronary heart disease.[2,3] The treatment of OSAHS includes continuous positive airway pressure (CPAP), orthodontic devices, weight loss in obese subjects, and positional therapy in episodes of obstructive apnea sleeping supine patients.[4] McDaid et al. reported that CPAP improved daytime and nighttime blood pressure in patients with moderate and severe OSAHS, highlighting the importance of the management and adherence to CPAP therapy, in particular to normalize the oxygen concentration.[5] Murri et al., Dorkova et al. and Hernández et al. all reported that treatment with CPAP could attenuate lipid peroxidation in OSAHS patients.[6–8]

Elevated plasma homocysteine (Hcy) levels have been considered an independent risk factor for cerebrocardiac vascular disease.[9] Niu et al. reported that the plasma Hcy levels were higher in obstructive sleep apnea (OSA) patients compared to control subjects.[10] Our previous study showed that the concentrations of Hcy were increased in elderly patients with OSAHS, but the levels of Hcy in patients with varying degrees of OSAHS remained disputed.[11] Therefore, this study aims to investigate the relationship between the Hcy levels and the severity of OSAHS, before and after 6 months of CPAP treatment.

Material and methods

Participants

Patients who submitted a full polysomnography (PSG) were selected from the Sleep Disorders Center patients in the 1st Affiliated Hospital of Soochow University (Suzhou, China) between June 2008 and December 2015. The participants (patients and controls) suffering from chronic disease, such as chronic obstructive pulmonary disease, liver cirrhosis, thyroid dysfunction, rheumatoid arthritis, chronic renal failure, and/or psychiatric disorders, were excluded from the study. The subjects who took drugs affecting the serum Hcy levels, such as vitamin B_6, vitamin B_{12} and folic acid, were not included, either. Before examination, information was collected about the general state of the participants, such as age, gender, body height and weight, as well as smoking history and hypertension, based on the final clinical diagnosis (Table 1).

The disease severity was assessed by the apnea-hypopnea index (AHI). For the purpose of analysis, the study population was classified into 4 groups: non-OSAHS (controls, n = 33) with AHI < 5; mild OSAHS (n = 41) with 5 ≤ AHI <15; moderate OSAHS (n = 40) with 15 ≤ AHI < 30; and severe OSAHS (n = 36) with AHI ≥ 30.

A total of 30 patients with severe OSAHS received CPAP for more than 4 h every night, and the Hcy levels and oxidative stress in patients with OSAHS under CPAP therapy, before and after 6 months of the therapy, were compared. The study was approved by the Ethics Committee of the 1st Affiliated Hospital of Soochow University. All the subjects gave their informed consent.

Polysomnography

A Respironics Alice 4 polysomnographer (Philips Respironics Inc., Murrysville, USA) was used to measure and record overnight PSG parameters, such as electroencephalogram (EEG), electrocardiogram (ECG), electrooculogram (EOG), chin and bilateral anterior tibials electromyogram (EMG), as well as chest and abdominal movements by strain gauges, nose air current, and pulse oxygen saturation (SaO_2). All the monitoring results analyzed by a computer were assessed by a specially assigned person. Apnea was defined as the cessation in airflow for at least 10 s, and hypopnea was defined as a decrease in the amplitude of the respiratory flow signal of at least 50% for a minimum of 10 s, followed by either a decrease in SaO_2 of 3% or signs of physiological arousal.

Biochemical analysis

Peripheral venous blood samples were obtained at 6 a.m. in the fasting state, after the diagnostic study night. Blood was centrifuged and serum was immediately separated in aliquots and stored at –80°C until assayed. The serum cholesterol, low-density lipoprotein cholesterol (LDL-C), total cholesterol (TC), triglyceride (TG), serum creatinine (SCr), and fasting plasma glucose (FPG) concentrations were tested by a full-automatic analyzer (AUS400 Olympus, First Chemical Ltd., Tokyo, Japan) on the same day. Creatinine clearance (CCr) was calculated according to the formula for SCr. The serum levels of Hcy were measured by cyclophorase (Jiuqiang Biological Technology Co., Ltd., Shanghai, China). The concentrations of methane dicarboxylic aldehyde (MDA) and glutathione (GSH) were measured by a spectrophotometer (Jiancheng Bioengineering Institute, Nanjing, China).

Statistical analysis

Data was expressed as mean ± standard deviation (SD) for continuous variables. The one-way analysis of variance (ANOVA) was used for the whole difference and the Student-Newman-Keuls test was used for differences between the groups. Correlation was calculated with Pearson's correlation coefficients. We used the χ^2 test to test the distributions of smoking history, hypertension and

gender among the 4 groups of patients. The multiple linear regression analysis was employed to determine variables that affected the Hcy levels. All statistical analyses were carried out using SPSS statistical software, v. 18.0 (IBM Corp., Armonk, USA). Differences were considered significant at $p < 0.05$.

Results

The survey data and basic parameters of all the cases

As shown in Table 1, there were no significant differences among OSAHS patients and controls, concerning gender, age, body mass index (BMI), smoking history, hypertension, and biochemical parameters, such as TC, TG, LDL-C, fasting blood glucose and CCr. The severity of OSAHS was graded according to AHI score, and the higher score indicated the more severe symptoms.[12] The change trend of the oxygen desaturation index (ODI) was consistent with AHI. In addition, the minimal and mean SaO_2 were both decreasing along with the increasing severity of the disease (Table 1).

The homocysteine, methane dicarboxylic aldehyde and glutathione levels

The Hcy, MDA and GSH levels in serum showed a significant difference in the OSAHS patients and controls ($p < 0.05$). Figure 1A shows that the serum concentrations of Hcy were significantly higher in mild and moderate OSAHS patients than in those from the control group, while they did not differ between severe OSAHS patients and the control group. Similar results were observed in the GSH levels; the serum concentrations of GSH rose noticeably in mild and moderate OSAHS patients, but did not differ between severe OSAHS patients and the control group (Fig. 1B). It is worth noting that the serum concentrations of MDA were higher in severe OSAHS patients than in other groups, and the MDA levels increased with the severity of the disease (Fig. 1C).

The relationship between the homocysteine levels and various independent variables

In the 3 OSASH groups and control group, the Pearson's correlation analysis identified that the serum Hcy level and age were correlated (r: 0.22, $p = 0.009$), and there was also a correlation between Hcy and MDA (r: 0.32, $p < 0.01$) and GSH (r: 0.74, $p < 0.01$), but no correlation between Hcy and AHI (r: 0.13, $p = 0.12$, data not shown). After the severe OSAHS group was removed, the Pearson's correlation analysis identified that the serum Hcy level was positively correlated with AHI (r: 0.81, $p < 0.01$) in the other 3 groups (mild/moderate OSAHS patients and the control group). Furthermore, the multiple linear regression analysis was performed with the changes of Hcy as the dependent variable and the abovementioned related parameters (age, MDA, GSH, and AHI) as the independent variables. There was a significant relation between the Hcy levels and the 4 variables – age, MDA, GSH, and AHI (Table 2) in the 3 groups (mild OSAHS, moderate OSAHS and non-OSAHS).

Table 1. The survey data and basic parameters of all the cases

Variable	Group			
	controls (n = 33)	mild OSAHS (n = 41)	moderate OSAHS (n = 40)	severe OSAHS (n = 36)
Age [years]	44.7 ±10.1	42.6 ±8.9	40.5 ±12.3	41.9 ±8.9
Sex (males/females)	29/4	37/4	33/3	35/5
BMI [kg/m^2]	25.08 ±3.35	24.36 ±3.61	26.49 ±2.78	27.34 ±2.82
Smokers [%]	21.21	26.83	22.50	22.22
Hypertension [%]	9.09	14.63	12.50	11.11
TC [mM/L]	4.34 ±1.17	4.91 ±0.69	4.48 ±1.24	4.55 ±1.81
TG [mM/L]	1.83 ±0.96	2.26 ±1.37	2.23 ±1.36	2.51 ±1.61
FBG [mM/L]	5.5 ±1.67	5.40 ±1.52	5.60 ±1.08	5.3 ±1.3
CCr [mL/min]	105.8 ±2.3	108.8 ±4.4	109.4 ±3.2	110.1 ±3.1
LDL-C [mM/L]	2.46 ±0.45	2.50 ±0.62	2.28 ±0.38	2.48 ±0.53
AHI [events/h]	3.57 ±0.55	10.63 ±2.19^a	22.90 ±3.82^{ab}	42.22 ±8.24^{abc}
Minimal SaO_2 [%]	91.0 ±4.0	87.0 ±5.0^a	86.0 ±6.0^a	69.0 ±12.0^{abc}
ODI [events/h]	3.6 ±2.2	9.7 ±2.5^a	20.3 ±4.8^{ab}	56.7 ±15.4^{abc}
Mean SaO_2 [%]	94.5 ±1.4	93.0 ±1.6^a	93.1 ±1.8^a	89.4 ±5.2^{abc}

BMI – body mass index; TC – total cholesterol; TG – triglyceride; FPG – fasting blood glucose; CCr – creatinine clearance; LDL-C – low-density lipoprotein cholesterol; AHI – the apnea-hypopnea index; ODI – oxygen desaturation index; ^{a} $p < 0.05$ compared to controls; ^{b} $p < 0.05$ compared to the mild OSAHS group; ^{c} $p < 0.05$ compared to the moderate OSAHS group; OSAHS – obstructive sleep apnea/hypopnea syndrome, SaO_2 – oxygen saturation.

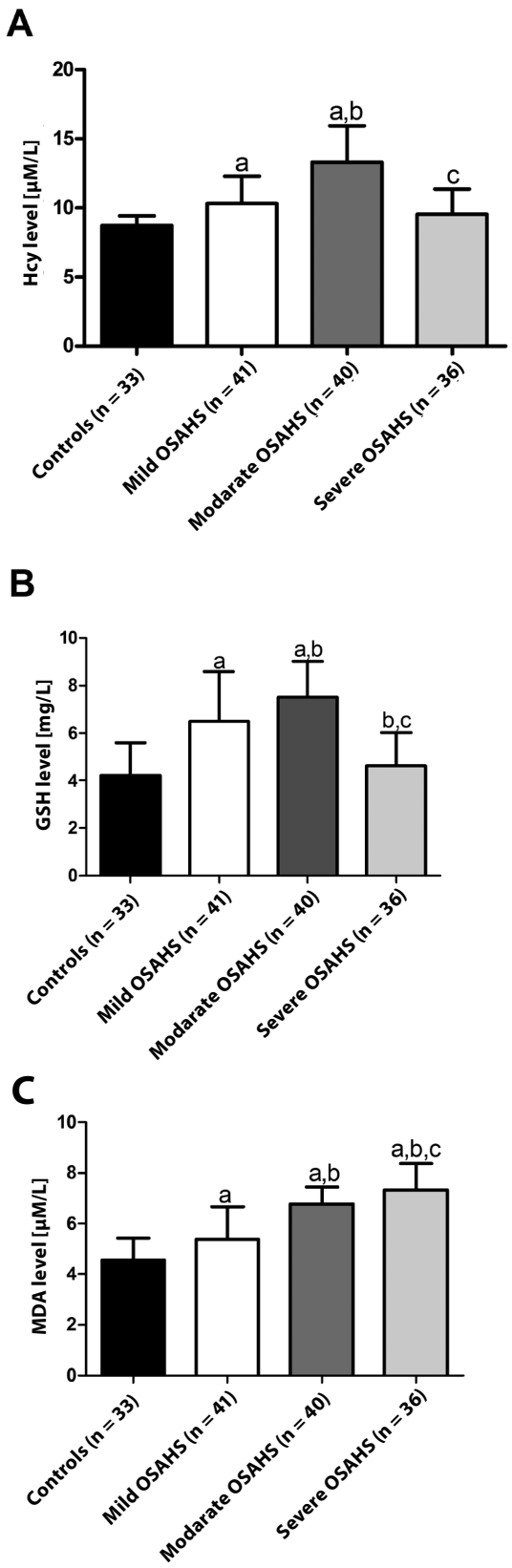

Fig. 1. The Hcy, GSH and MDA levels of all the cases

Hcy – homocysteine; GSH – glutathione; MDA – methane dicarboxylic aldehyde; OSAHS – obstructive sleep apnea/hypopnea syndrome; A – Hcy level; B – GSH level; C – MDA level; data are presented as mean ± standard deviation (SD); a – $p < 0.05$ compared to controls; b – $p < 0.05$ compared to the mild OSAHS group; c – $p < 0.05$ compared to the moderate OSAHS group.

Table 2. Multiple regression analysis of the relationship between the Hcy levels and various independent variables

Variables	β	p-value
Age	0.121	0.011
AHI	0.402	0.001
MDA	0.357	0.005
GSH	0.222	0.008

Hcy – homocysteine; β – standardized regression coefficient; AHI – the apnea-hyponea index; MDA – methane dicarboxylic aldehyde; GSH – glutathione.

The effects of continuous positive airway pressure treatment on severe obstructive sleep apnea/hypopnea syndrome patients

Continuous positive airway pressure therapy has become a reliable treatment procedure for OSAHS, which improves apnea-hypopnea during sleep as well as the sleep structure. A total of 30 patients with severe OSAHS received CPAP for 4 h every night, and the other 6 patients were not willing to participate in the treatment. During CPAP treatment, 4 patients dropped out due to the intolerance of CPAP. After 6 months of treatment, the Hcy, MDA and GSH levels were detected again in the remaining 26 patients. The Student-Newman-Keuls test results showed that only the MDA levels were significantly lower in severe OSAHS patients with CPAP treatment, while the Hcy and GSH levels were not significantly changed (Fig. 2). Decreased MDA levels were consistent with the reports showing that treatment with CPAP could reduce oxidative stress in OSAHS patients.[6–8] Thus, MDA may become an effective marker in OSAHS patients who received the CPAP treatment prognosis.

Discussion

This study evaluated the concentration of Hcy, MDA and GSH in patients with OSAHS, and the effect of CPAP on severe OSAHS patients. The Hcy level was higher in the plasma of the patients with OSAHS than in the control subjects, but not proportionally to the severity of OSAHS. Moreover, there was no obvious change in the Hcy plasma level of the patients with CPAP therapy.

Homocysteine is a well-studied marker of cardiovascular disease. Schnyder et al. evaluated the relationship between the Hcy plasma levels on admission and after a successful percutaneous coronary intervention, demonstrating that Hcy was an important independent predictor of future cardiovascular events and cerebrovascular disease.[13] However, the mechanisms of OSAHS related to cardiovascular disease remain to be investigated despite a vast amount of studies.

The relation between OSAHS and serum Hcy are still under debate. Accumulating evidence has revealed that in all OSAHS patients at different stages of the disease, the Hcy levels were elevated regardless of the presence

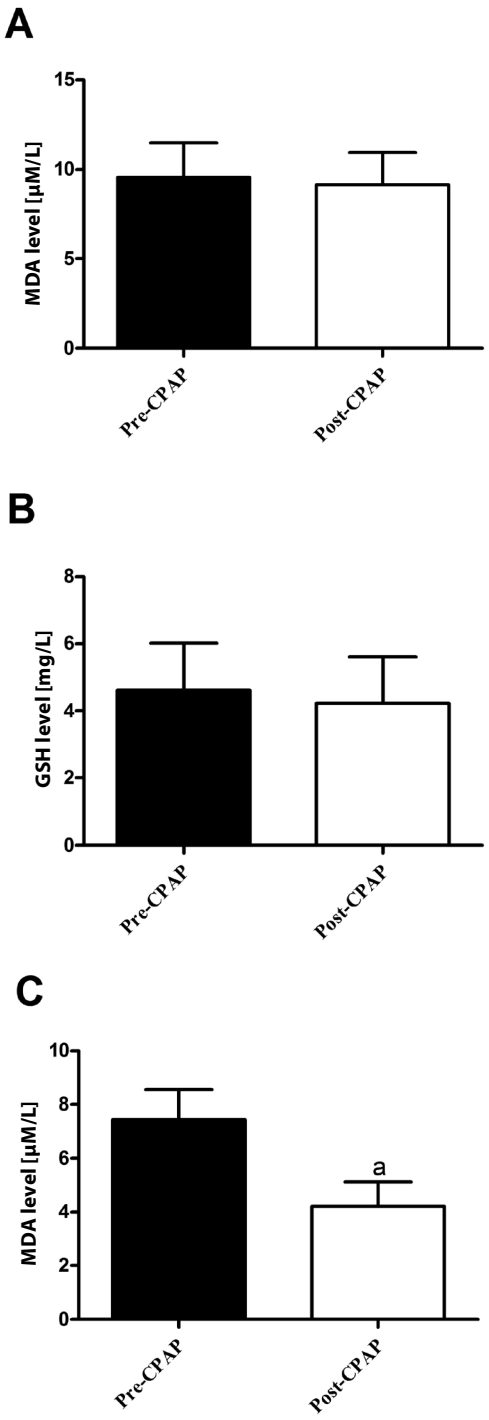

Fig. 2. The effects of CPAP treatment on the Hcy, GSH and MDA levels in severe OSAHS patients

Hcy – homocysteine; GSH – glutathione; MDA – methane dicarboxylic aldehyde; CPAP – continuous positive airway pressure; A – Hcy level; B – GSH level; C – MDA level; data are presented as mean ± standard deviation (SD); n = 26; a – $p < 0.05$: post-CPAP vs pre-CPAP.

of cardiovascular disease, and its levels were independently associated with the severity of OSAHS.[14–16] Meanwhile, Monneret et al. demonstrated that the serum Hcy levels were higher in OSAHS with metabolic syndrome compared to metabolic syndrome patients, and proportional to the severity of OSAHS.[17] However, Cintra et al. observed that the Hcy plasma levels did not differ between OSAHS patients and the control subjects that were matched for age and sex.[18] The results of those studies were consistent with part of our data showing that the Hcy levels did not differ between severe OSAHS patients and the control group, but were significantly higher in mild and moderate OSAHS patients than in those from the control group. Due to the increased generation of oxygen free radicals in OSAHS patients, GSH, as one of antioxidant defenses, correspondingly increased in order to resist the injury coming from oxidative stress. Furthermore, Hcy serves as an important producer for GSH, and the high levels of GSH will inhibit Hcy degradation in vivo. Hence, the accumulation of Hcy in vivo results in hyperhomocysteinemia (HHcy). Lipid peroxidation is more pronounced in severe OSAHS patients than in mild/moderate OSAHS patients; however, the ability of antioxidants is not enhanced accordingly.[11] Thereby, the Hcy level does not further increase in severe OSAHS patients. This mechanism provides further support for the present results and also offers a new clue to explain the conclusion that there was a clear association between slightly elevated blood Hcy levels and early-onset coronary artery disease, peripheral artery disease, cerebrovascular disease, stroke, etc.[19] Also, we noted that the Hcy level was positively correlated with age; this conclusion was similar to previous results.[20]

Recent studies have shown that oxidative stress exists in OSA patients.[21,22] As one of the cellular antioxidant defense systems, the amount of GSH is an important indicator of the anti-oxidation ability. Our results showed that the GSH levels rose noticeably in mild/moderate OSAHS patients. Ntalapascha et al. investigated whether systemic oxidative stress was increased in obstructive sleep apnea syndrome (OSAS) patients, and discovered that OSAS might be associated with an increased oxidative burden, possibly via the glutathione/oxidized glutathione (GSH/GSSG) pathway.[23] Being the main product of peroxidation in vivo, MDA is a biomarker of lipid peroxidation injury degree. Our results indicated that the MDA levels increased with the severity of OSAHS. Kilic et al. recently reported that the serum MDA levels are significantly higher in patients with OSAS than in control subjects, and both oxidative imbalance and vascular endothelial dysfunction lead to early development of atherosclerosis, which may cause health-threatening complications of OSAS.[24] Therefore, vascular endothelial dysfunction caused by oxidative stress is a predictive factor for the complications of OSAS. In addition, Mancuso et al. compared 3 well-known markers of oxidative stress – advanced oxidation protein products (AOPP), ferric reducing antioxidant power (FRAP) and total GSH – in a cohort of 41 untreated patients with OSAS, indicating that such oxidative stress markers may be useful to detect and monitor redox imbalance in OSAS.[25] The present study hinted that there were significant changes in oxidative stress marker levels, and the change of the MDA levels instead of the GSH levels was entirely

consistent with the antioxidant levels in OSAHS patients at different stages of the disease.

For patients with moderate or severe OSAHS, CPAP therapy can obviously alleviate excessive daytime sleepiness and improve the sleep quality, as well as patients' life quality and general well-being.[26] Continuous positive airway pressure therapy may decrease the risk of mortality and cardiovascular events in patients with OSA.[27] Chen et al. found that the Hcy levels were significantly reduced by CPAP therapy in patients with OSAHS and that the Hcy levels may be clinically recognized as a valuable indicator for the treatment of OSAHS.[28] However, we found that the Hcy levels were not noticeably changed in patients undergoing CPAP therapy, which was consistent with the research by Kumor et al., which showed that the Hcy levels did not decline after CPAP therapy for 3 months.[29] We also found that the MDA levels were significantly decreased after CPAP therapy, which was similar to a recent study that determined the effectiveness of CPAP therapy in reducing the MDA levels in OSA patients, proving that CPAP therapy yields clinical benefits by reducing oxidative stress in OSA patients.[30]

In conclusion, the Hcy levels were elevated in mild and moderate OSAHS patients, but not proportionally to the severity of OSAHS. The change of the Hcy level was not proportional to the severity of the disease in different OSAHS groups, and the reason was the increased lipid peroxidation without the accordingly enhanced ability of antioxidants in severe OSAHS patients. Although the CPAP did not affect the Hcy levels, the MDA level was significantly decreased after CPAP in severe OSAHS patients.

References

1. Jennum P, Riha RL. Epidemiology of sleep apnoea/hypopnoea syndrome and sleep-disordered breathing. *Eur Respir J*. 2009;33(4):907–914.
2. Destors M, Tamisier R, Baguet JP, Levy P, Pepin JL. Cardiovascular morbidity associated with obstructive sleep apnea syndrome [in French]. *Rev Mal Respir*. 2014;31(4):375–385.
3. Somers VK, White DP, Amin R, et al. Sleep apnea and cardiovascular disease: An American Heart Association/American College of Cardiology Foundation scientific statement from the American Heart Association Council for High Blood Pressure Research Professional Education Committee, Council on Clinical Cardiology, Stroke Council, and Council on Cardiovascular Nursing. In collaboration with the National Heart, Lung and Blood Institute National Center on Sleep Disorders Research (National Institutes of Health). *J Am Coll Cardiol*. 2008;52(8):686–717.
4. Lombardi C, Musicco E, Bettoncelli G, et al. The perception of obstructive sleep apnoea/hypopnoea syndrome (OSAHS) among Italian general practitioners. *Clin Mol Allergy*. 2015;13(1):1–7.
5. McDaid C, Durée KH, Griffin SC, et al. A systematic review of continuous positive airway pressure for obstructive sleep apnoea-hypopnoea syndrome. *Sleep Med Rev*. 2009;13(6):427–436.
6. Murri M, Alcazar-Ramirez J, Garrido-Sanchez L, et al. Oxidative stress and metabolic changes after continuous positive airway pressure treatment according to previous metabolic disorders in sleep apnea-hypopnea syndrome patients. *Transl Res*. 2009;154(3):111–121.
7. Dorkova Z, Petrasova D, Molcanyiova A, Popovnakova M, Tkacova R. Effects of continuous positive airway pressure on cardiovascular risk profile in patients with severe obstructive sleep apnea and metabolic syndrome. *Chest*. 2008;134(4):686–692.
8. Hernández C, Abreu J, Abreu P, Colino R, Jiménez A. Effects of nasal positive airway pressure treatment on oxidative stress in patients with sleep apnea-hypopnea syndrome. *Arch Bronconeumol*. 2006;42(3):125–129.
9. Djuric D, Jakovljevic V, Rasic-Markovic A, Djuric A, Stanojlovic O. Homocysteine, folic acid and coronary artery disease: Possible impact on prognosis and therapy. *Indian J Chest Dis Allied Sci*. 2008;50(1):39–48.
10. Niu X, Chen X, Xiao Y, et al. The differences in homocysteine level between obstructive sleep apnea patients and controls: A meta-analysis. *PLoS One*. 2014;9(4):e95794.
11. Wang L, Jie LI, Xie Y, Zhang XG. Association between serum homocysteine and oxidative stress in elderly patients with obstructive sleep apnea/hypopnea syndrome. *Biomed Environ Sci*. 2010;23(1):42–47.
12. Toshiaki S, Taniguchi AA, Ryujiro S, et al. Falling asleep while driving and automobile accidents among patients with obstructive sleep apnea-hypopnea syndrome. *Psychiatry Clin Neurosci*. 2002;56(3):333–334.
13. Schnyder G, Roffi M, Flammer Y, et al. Effect of homocysteine-lowering therapy on restenosis after percutaneous coronary intervention for narrowings in small coronary arteries. *Am J Cardiol*. 2003;91(10):1265–1269.
14. Sariman N, Levent E, Aksungar FB, Soylu AC, Bektaş O. Homocysteine levels and echocardiographic findings in obstructive sleep apnea syndrome. *Respiration*. 2009;79(1):38–45.
15. Thakre TP, Mamtani M, Ujaoney S, Kulkarni H. Association of plasma homocysteine with self-reported sleep apnea is confounded by age: Results from the National Health and Nutrition Examination Survey 2005–2006. *J Strategic Inf Syst*. 2015;16(4):324–352.
16. Niu X, Chen X, Xiao Y, et al. The differences in homocysteine level between obstructive sleep apnea patients and controls: A meta-analysis. *PLoS One*. 2013;9(4):e95794.
17. Monneret D, Tamisier R, Ducros V, et al. The impact of obstructive sleep apnea on homocysteine and carotid remodeling in metabolic syndrome. *Respir Physiol Neurobiol*. 2012;180(2–3):298–304.
18. Cintra F, Tufik S, D'Almeida V, et al. Cysteine: A potential biomarker for obstructive sleep apnea. *Chest*. 2011;139(2):246–252.
19. Sacco RL, Anand K, Lee HS, et al. Homocysteine and the risk of ischemic stroke in a triethnic cohort: The Northern Manhattan Study. *Stroke*. 2004;35(10):2263–2269.
20. Wang L, Li J, Xie Y, Zhang XG. Association between serum homocysteine and oxidative stress in elderly patients with obstructive sleep apnea/hypopnea syndrome. *Biomed Environ Sci*. 2010;23(1): 42–47.
21. Sánchez-Armengol A, Villalobos-López P, Caballero-Eraso C, et al. Gamma glutamyl transferase and oxidative stress in obstructive sleep apnea: A study in 1744 patients. *Sleep Breath*. 2015;19(3):1–8.
22. Alvarez RF, Cuadrado GR, Arias RA, et al. Snoring as a determinant factor of oxidative stress in the airway of patients with obstructive sleep apnea. *Lung*. 2016;194(3):1–5.
23. Ntalapascha M, Makris D, Kyparos A, et al. Oxidative stress in patients with obstructive sleep apnea syndrome. *Sleep Breath*. 2013;17(2):549–555.
24. Sardo L, Palange P, Di Mario F, et al. Intrarenal hemodynamic and oxidative stress in patients with obstructive sleep apnea syndrome. *Sleep Breath*. 2015;19(4):1205–1212.
25. Mancuso M, Bonanni E, Logerfo A, et al. Oxidative stress biomarkers in patients with untreated obstructive sleep apnea syndrome. *Sleep Med*. 2012;13(6):632–636.
26. Sato K, Umeno H, Chitose S, Nakashima T. Sleep-related deglutition in patients with OSAHS under CPAP therapy. *Acta Otolaryngol*. 2011;131(2):181–189.
27. Guo J, Sun Y, Xue LJ, et al. Effect of CPAP therapy on cardiovascular events and mortality in patients with obstructive sleep apnea: A meta-analysis. *Sleep Breath*. 2016;20(3):1–10.
28. Chen X, Niu X, Xiao Y, et al. Effect of continuous positive airway pressure on homocysteine levels in patients with obstructive sleep apnea: A meta-analysis. *Sleep Breath*. 2014;18(4):687–694.
29. Kumor M, Bielicki P, Przybyłowski T, Rubinsztajn R, Zieliński J, Chazan R. Three-month continuous positive airway pressure (CPAP) therapy decreases serum total and LDL cholesterol, but not homocysteine and leptin concentration in patients with obstructive sleep apnea syndrome (OSAS) [in Polish]. *Pneumonol Alergol Pol*. 2011;79(3):173–183.
30. Tichanon P, Wilaiwan K, Sopida S, Orapin P, Watchara B, Banjamas I. Effect of continuous positive airway pressure on airway inflammation and oxidative stress in patients with obstructive sleep apnea. *Can Respir J*. 2016;2016(4):1–7.

Vitamin D, cardiovascular and bone health in postmenopausal women with metabolic syndrome

Jolanta Dadoniene[1,2,A,C,D], Alma Čypienė[2,3,B,C], Egidija Rinkūnienė[2,3,B–D], Jolita Badariene[2,3,B,C], Aleksandras Laucevičius[2,3,A,E,F]

[1] Institute of Health Sciences, Faculty of Medicine, Vilnius University, Lithuania
[2] State Research Institute for Innovative Medicine, Vilnius, Lithuania
[3] Centre of Cardiology and Angiology, Vilnius University Hospital, Lithuania

A – research concept and design; B – collection and/or assembly of data; C – data analysis and interpretation; D – writing the article; E – critical revision of the article; F – final approval of the article

Advances in Clinical and Experimental Medicine, ISSN 1899-5276 (print), ISSN 2451-2680 (online) *Adv Clin Exp Med*. 2018;27(11):1555–1560

Address for correspondence
Jolanta Dadoniene
Email: jolanta.dadoniene@mf.vu.lt

Funding sources
None declared

Conflict of interest
None declared

Received on November 5, 2016
Reviewed on January 24, 2017
Accepted on June 20, 2017

Abstract

Background. The evidence highlights the importance of improving vitamin D levels in the general population for the prevention of adverse long-term health risks, including cardiovascular events, metabolic syndrome, cancer, anxiety and depression, and overall mortality, although controversies in the research are common.

Objectives. The purpose of this study was to investigate the relationship between vitamin D and vascular and bone health among postmenopausal metabolic women, controlling for traditional cardiovascular factors, and thus seeking to explore their plausible relation. The secondary aim was to look specifically for the relation between artery stiffness and bone health.

Material and methods. This is a cross-sectional study designed to evaluate the relation between vitamin D level and vascular and bone health among women with metabolic syndrome. Two hundred and ten women visiting a cardiologist were recruited consecutively into the study. The study variables included clinical examination, laboratory findings, measurements of vascular stiffness, and bone turnover markers.

Results. We found 126 (60%) metabolic women with a vitamin D deficiency (50 nmol/L) among the study group. We discovered no statistically significant correlation between vitamin D and vascular stiffness. Vitamin D was not associated neither with femoral neck bone mineral density (BMD) and T score, nor with lumbar spine BMD and T score. Nevertheless, there was an indirect weak correlation between vascular stiffness, in particular the augmentation index (AIx), and all bone health markers, including BMD and T score in both the femur head and lumbar spine.

Conclusions. We showed a high proportion of postmenopausal metabolic women with a vitamin D deficiency, but there was no relation between vitamin D and vascular health or vitamin D and bone health. Nevertheless, the relation between vascular health and bone health exists, although the role of vitamin D in this link has not yet been established.

Key words: metabolic syndrome, vitamin D, bone mineral density, vascular stiffness

DOI
10.17219/acem/75147

Introduction

There is sufficient evidence that vitamin D is related to bone health in children and the elderly, while the benefit for middle-aged people still needs to be proven.[1] The emerging evidence highlights the importance of normalizing vitamin D levels in the general population, as it may prevent long-term health problems, including cardiovascular events, metabolic syndrome, cancer, overall health, anxiety and depression, and overall mortality, although controversies in the literature are common and the data is inconclusive.[2,3] Our own previous experience from a cross-sectional study with 100 postmenopausal metabolic women revealed a favorable correlation between vitamin D concentrations and mean blood pressure and high density lipoproteins.[4] We showed that normalizing vitamin D level may lower the mean blood pressure. Similar evidence has mostly been based on cross-sectional studies, less in observational longitudinal studies, while randomized controlled studies in general have denied the beneficial effect of vitamin D.[5] In addition, studies with higher sample sizes, which is often the case in cross-sectional studies, are more powerful in proving the relation, while randomized controlled trials with small groups mostly fail. The aim of this cross-sectional analytic study was to investigate if there is a relationship between vitamin D (25(OH)D) and vascular health and bone health among postmenopausal metabolic women, taking into consideration traditional cardiovascular factors, and thus to explore their plausible relation. The secondary aim was to look specifically for the relation between artery stiffness and bone health.

Material and methods

Study design

A total of 210 women attending Vilnius University Hospital Santariskiu Klinikos, Lithuania, according to the Lithuanian high cardiovascular risk primary prevention program, signed the informed consent form and were enrolled into the study consecutively, after meeting the following inclusion criteria: age between 50 and 65 years, diagnosis of metabolic syndrome and being in menopausal period.[6] Metabolic syndrome was diagnosed if at least 3 out of 5 symptoms were present: waist circumflex >88 cm; systolic blood pressure (SBP) ≥130 mm Hg and/or diastolic blood pressure (DBP) ≥85 mm Hg; fasting glycemia >5.6 mmol/L or type 2 diabetes mellitus; triacylglyceride (TG) concentration >1.7 mmol/L or special treatment prescribed to reduce the TG concentration; high-density lipoprotein cholesterol (HDL-C) <1.2 mmol/L.[7] The exclusion criteria were: vitamin D supplements currently or at least half a year before the study, diagnosed coronary heart disease, malignant disease currently, kidney or liver failure, other advanced somatic or mental disease. The approval was obtained from the Lithuanian Bioethics Committee (158200-14-724-240). The enrollment period lasted 2 years, from March 2014 until March 2016.

Study variables

The clinical, laboratory and instrumental measurements were obtained during the 2nd visit to a cardiologist. These included clinical examination and measurements of laboratory markers: fasting cholesterol, glucose, C-reactive protein (CRP), creatinine, albumin, 25(OH) vitamin D, and ionized calcium. Vitamin D level was considered deficient when it was <50 nmol/L.[8] The physical activity index was obtained from the questionnaires containing information on intensity, duration and frequency of current exercise program, which was then entered into the equation (intensity × duration × frequency = total score).

Vascular health measurements

We applied 3 non-invasive techniques to examine the vascular health of 210 women enrolled in the study: pulse wave velocity (PWV), flow-mediated dilatation (FMD) and carotid artery intima-media thickness (IMT) measurements. All 3 measurements were carried out in the early morning hours and the participants were asked to refrain from drinking and eating for at least 12 h before the examination.

Pulse wave velocity was obtained by measuring the carotid-to-radial (PWVcr) and carotid-to-femoral (PWVcf) pulse wave flow. Mainly, the transit time of the wave from the sternal notch to the radial or femoral artery was used to estimate the path length between the carotid and radial or femoral arteries, using applanation tonometry with a high-fidelity micromanometer (SphygmoCor, Sydney, Australia). The augmentation index (AIx) adjusted for 75 beats/min was calculated from PWVcr, using an integrated software program. This technique was described by Kelly et al. in 1989 and later elaborated by Wilkinson et al. and O'Rourke and Gallagher.[9–11] A detailed description of the arterial stiffness measuring technique, as it was performed in a local clinical setting, was described in detail in the publication by our group.[12]

The endothelium-dependent FMD test in a brachial artery was measured on B-mode imaging by an ultrasound system (Logiq 7; GE Healthcare, Waukesha, USA) based on the recommendations by Celermajer et al.[13] Scans were taken twice, before the inflation and after deflation, and were carried out in the longitudinal plane, 1–8 cm above the antecubital fossa. The inflation of a pneumatic tourniquet to a suprasystolic pressure of 100 mm Hg was kept for 5 min, and the 2nd scan was taken within the first 15 s after the cuff release.

The intima-media thickness was measured in the common carotid artery, 1–2 cm from the bifurcation on the bottom wall, in a live 2-dimensional view, which comprised

4 cm automatic recognition, using a high-resolution ALOKA ultrasound system (Hitachi, Tokyo, Japan). The mean carotid IMT was calculated as the average from the means of the left and right common carotid artery IMT.

Bone health measurements

Bone mineral density (BMD) of the femoral neck and lumbar spine in region L1-L4 was measured by the dual-photon energy absorptiometry method (Hologic, Massachusetts, USA). T scores were calculated for each anatomical site. Osteopenia was defined when T score was below –1 but above –2.5, and osteoporosis was defined when T score was ≤–2.5.

Statistical analysis

Quantitative variables were presented as means and standard deviation (SD) or median and min–max, depending on normality. Qualitative variables were expressed as numbers and percentages. Quantitative comparisons were computed with an independent Student's t-test if they were normally distributed or the Mann-Whitney test if the normal distribution was violated. Pearson's or Spearman's correlation analyses were used for establishing the relations between the variables. Multivariate linear regression analysis (stepwise model) was performed separately for vitamin D (dependent variable) and vascular health measurements, and for vitamin D (dependent variable) and bone health measurements. The traditional cardiovascular factors were included into the multivariate analysis as important covariates: age, body mass index (BMI), waist circumflex, smoking, total cholesterol (TC), low-density lipoprotein cholesterol (LDL-C), HDL-C, TG, fasting glucose, CRP, and the albumin/creatinine ratio. The p-values <0.05 were considered statistically significant.

Results

Differences of health characteristics between women with and without a vitamin D deficiency

The average level of vitamin D was 48.01 nmol (±16.95) in the whole cohort (Table 1). We found 126 (60%) women with metabolic syndrome with a vitamin D deficiency and a minor proportion of them – 84 (40%) – had normal vitamin D levels. On average, the women were obese (BMI = 32.42 kg/m^2) with a low index of physical activity around 18. No clinically significant differences were observed when comparing the laboratory data between the 2 groups. Differences in early markers of atherosclerosis were unremarkable, except for PWVcr being higher in the group with normal vitamin D concentration. Almost a quarter of the women had osteoporosis or osteopenia. Bone health status, including BMD in the lumbar and femur area, was quite similar in different vitamin D level groups.

The relation between vitamin D and vascular health

We did not find a significant relation between vitamin D concentration and early atherosclerosis markers in a simple Spearman's correlation. However, after adjustment for age, mean blood pressure, BMI, waist circumflex, physical activity index, smoking, TC, LDL-C, HDL-C, TG, fasting glucose, CRP, and the albumin/creatinine ratio, the association between vitamin D levels and PWVcf became significant (p = 0.049) (Table 2). We consider it coincidental and it is doubtful whether it is clinically important.

The relation between vitamin D and bone health

In this study we failed to show an association between vitamin D and femoral neck BMD or its T score or with lumbar spine BMD and T score in a simple linear regression (Table 2). No association was found between vitamin D and bone health markers in multiple linear regression after adjusting for traditional markers for atherosclerosis.

Early atherosclerosis markers and bone health

Though an association between vitamin D and vascular health or bone health was not proven, we found an important link between AIx and bone health. There was an indirect weak correlation between AIx (adjusted for heart rate) and all bone health markers, including BMD and T score in both the femur head and lumbar spine (Table 3). We presume that when BMD decreases, the stiffening of the arteries becomes more pronounced. Therefore, keeping the bone structure healthy may prevent vascular stiffening. In other words, what is good for bone health is also good for blood vessels, though it is not that straightforward. We did not find vitamin D being somehow interrelated with this.

Discussion

We found 126 (60%) women with metabolic syndrome who had vitamin D deficiency (<50 nmol/L) and a minor proportion of 84 (40%) had normal vitamin D levels (>50 nmol/L). This cut-off was chosen following the recommendations developed by a consensus agreement of a Polish multidisciplinary group and it targeted the Central European population.[8] In this cross-sectional study, when applying multiple linear regression, we found no statistically significant relation between vitamin D and arterial stiffness. Furthermore, vitamin D was not associated with

Table 1. The characteristics of 210 metabolic women according to vitamin D levels

Characteristics	All (n = 210)	25 (OH) vitamin D (<50 nmol/L) (n = 126)	25 (OH) vitamin D (>50 nmol/L) (n = 84)	p-value
Age [years]	57.89 ±3.91	57.94 ±3.84	57.82 ±4.01	0.835
Current smokers, n (%)	33 (15.7)	20 (15.9)	13 (15.5)	0.938
BMI [kg/m^2]	32.42 ±4.12	32.58 ±4.37	32.19 (3.74)	0.498
Waist circumflex [cm]	103.83 ±9.39	104.08 ±9.25	103.46 ±9.66	0.645
Physical activity index (1–100; 100 – the highest)	18 (1–100)	16 (1–100)	20 (1–80)	0.348
TC [mmol/L]	6.54 ±1.37	6.58 ±1.37	6.49 ±1.36	0.619
LDL-C [mmol/L]	4.33 ±1.19	4.37 ±1.16	4.28 ±1.27	0.576
HDL-C [mmol/L]	1.31 ±0.30	1.29 ±0.30	1.35 ±0.29	0.146
TG [mmol/L]	1.75 (0.57–6.98)	1.8 (0.61–6.98)	1.78 (0.57–6.85)	0.777
Fasting glycemia [mmol/L]	5.91 (4.68–15.20)	5.75 (4.68–13.43)	5.97 (5.02–15.20)	0.064
CRP [mmol/L]	2.20 (0.30–23.80)	2.55 (0.40–15.50)	1.85 (0.30–23.80)	0.035
The albumin/creatinine ratio	0.58 (0.17–86.39)	0.60 (0.17–86.39)	0.56 (0.18–11.61)	0.411
FMD [%]	3.08 ±2.15	3.23 ±2.19	2.83 ±2.07	0.219
PWVcr [m/s]	8.80 (6–108)	8.65 (6–13)	8.95 (7–14)	0.049
PWVcf [m/s]	8.86 ±1.48	8.89 ±1.43	8.82 ±1.55	0.737
AIx (adjusted for 75 heart rate)	27.91 ±8.97	27.44 ±7.37	28.53 ±10.74	0.474
Mean arterial pressure [mm Hg]	105.59 ±12.61	106.74 ±13.70	103.88 ±10.64	0.109
IMF [μm]	685.64 ±95.82	673.70 ±83.41	703.98 ±110.30	0.026
25(OH) vitamin D [nmol/L]	48.01 ±16.95	37.72 ±8.70	63.81 ±14.13	–
Ionized calcium [mmol/L]	1.170 ±0.083	1.160 ±0.093	1.180 ±0.063	0.123
Total femur BMD [g/cm^2]	1.06 ±0.13	1.06 ±0.14	1.06 ±0.11	0.895
Total femur T score	0.48 ±1.07	0.49 ±1.16	0.47 ±0.94	0.866
Total lumbar spine BMD [g/cm^2]	1.14 ±0.16	1.14 ±0.17	1.16 ±0.15	0.475
Total lumbar spine T score	−0.28 ±1.35	−0.32 ±1.44	−0.21 ±1.21	0.574
Normal bone status, n (%)	152 (72.3)	87 (69.0)	81 (77.4)	0.290
Osteopenia, n (%)	52 (24.8)	34 (27.0)	18 (21.4)	
Osteoporosis, n (%)	6 (2.9)	5 (4.0)	1 (1.2)	

BMI – body mass index; TC – total cholesterol; LDL-C – low-density lipoprotein cholesterol; HDL-C – high-density lipoprotein cholesterol; TG – triacylglycerides; CRP – C-reactive protein; FMD – flow-mediated dilatation; PWVcr – pulse wave velocity (carotid-to-radial); PWVcf – pulse wave velocity (carotid-to-femoral); AIx – the augmentation index; IMF – intima-media thickness; BMD – bone mineral density.

femoral neck BMD and T score, nor with lumbar spine BMD and T score. In both models, the adjustment for age, mean blood pressure, BMI, waist circumflex, physical activity index, smoking, TC, LDL-C, HDL-C, TG, fasting glucose, CRP, and the albumin/creatinine ratio was made. This led to the conclusion that the association in simple or more sophisticated models between an independent factor – vitamin D – and vascular health markers or bone health markers cannot be proven.

It is known that vitamin D is predominantly synthetized in the skin or obtained with food or supplements, and these physiological functions go far beyond the regulation of calcium and phosphorus uptake, and extend to immunomodulatory effects, effects on the renin-angiotensin system, insulin secretion, and the apoptosis of malignant cell proliferation. Vitamin D deficiency (<50 nmol/L) is a worldwide epidemic with multiple implications on human health, due to its role in various physiological systems.[14] It is generally considered that vitamin D plays an important role in overall health and it is important to have adequate vitamin D.[2] The overall enthusiasm to search and to find links between disease and vitamin D deficiency has changed with the evolving paradox: the optimistic findings from observational studies were not supported by interventional studies.[5,15] This may be explained by the study duration, design and sample size, as it may take a longer time for the cardiovascular outcome to occur than the duration of a clinical trial. The classical observational Framingham Offspring Study showed an increase in the number of cardiovascular events when vitamin D was deficient.[16] A Norwegian study showed that all-cause mortality, as well as cardiovascular mortality, may be higher with vitamin D deficiency,and it is also applicable to a non-Caucasian population.[17,18] Clinical trials usually take under consideration the endothelial

Table 2. The relation between vitamin D, vascular health and bone health

Dependent variables	r	p-value	Beta	p-value (adjusted model)
Vascular health variables				
AIx (adjusted for 75 heart rate)	0.013	0.875	0.143	0.251
PWVcr [m/s]	0.087	0.314	–0.029	0.825
PWVcf [m/s]	–0.005	0.948	0.233	0.049
IMF [μm]	0.080	0.252	0.144	0.232
FMD [%]	–0.054	0.471	0.008	0.947
Bone health variables				
Total femur BMD [g/cm^2]	–0.024	0.746	–0.033	0.972
Total femur T score	–0.027	0.721	–0.005	0.956
Total lumbar spine BMD [g/cm^2]	0.96	0.195	0.035	0.716
Total lumbar spine T score	0.107	0.151	0.036	0.713
Ionized calcium [mmol/L]	0.130	0.062	0.124	0.199

Model adjusted for age, mean blood pressure, body mass index (BMI), waist circumflex, smoking, total cholesterol (TC), low-density lipoproteins, high-density lipoproteins, triacylglycerides (TG), fasting glucose, C-reactive protein, the albumin/creatinine ratio, and physical activity index; AIx – augmentation index; PWVcr – pulse wave velocity (carotid to radial); PWVcf – pulse wave velocity (carotid to femoral); IMF – intima-media thickness; FMD – flow-mediated dilatation; BMD – bone mineral density.

Table 3. The relation between the augmentation index (AIx) and bone health

Augmentation index/ bone health	r	p-value
Total femur BMD [g/cm^2]	–0.229	0.010
Total femur T score	–0.222	0.013
Total lumbar spine BMD [g/cm^2]	–0.287	0.001
Total lumbar spine T score	–0.301	0.001

*adjusted for 75 heart rate; BMD – bone mineral density.

functioning parameters as the main outcome rather than cardiovascular events, and it is due to the accepted agreement that the endothelial function itself may serve as an independent predictor of future cardiovascular events.[13] Several controlled clinical trials have shown that vitamin D supplementation improves the endothelial function, while others have not.[19–22] Therefore, there is not enough evidence to decide whether the substitution of low vitamin D would prevent cardiovascular events in the future. Our cross-sectional observational study did not show meaningful results concerning the endothelial functioning and vitamin D.

There is considerable evidence regarding the benefit of vitamin D in the prevention of rickets in children and osteomalacia in the senior population, but the benefit for the middle-aged population remains unclear and controlled clinical trials are needed in this setting of patients.[23] In a meta-analysis by Reid et al., 23 studies were included, and no evidence was gained suggesting that taking vitamin D prevents osteoporosis developing in the middle-aged population, with only a small effect on increasing BMD in the femoral neck.[24] These findings are in line with the systematic review by Cohrane collaboration, which came to the conclusion that vitamin D alone is unlikely to prevent fractures in older people when taken in the recommended daily dose. However, in combination with calcium, it may be helpful in preventing hip or any type of fracture in postmenopausal women or older men.[25] Our study did not show any link between vitamin D and BMD or T score, likewise other, more powerful studies.

On the other hand, by carrying out the main aim of this study, we examined the link between arterial stiffness and bone health in a simple linear regression model and it was obvious that there was an indirect weak correlation between AIx and bone health markers, including BMD and T score in the femur head and even more in the lumbar spine. Our data shows that higher arterial stiffness may be associated with a higher risk of osteopenia in postmenopausal women with metabolic syndrome, but it is not necessarily associated with vitamin D deficiency. A very recent study by Ye et al. looked into 25 studies and pooled data on 10,299 patients. The calcification of carotid arteries, the incidence of cardiovascular disease and coronary artery disease were taken into account and were significantly higher in numbers in low BMD patients compared to normal BMD patients. The same trend for BMD being related to arterial stiffness was observed in different settings of the population, including postmenopausal women, and persisted after the adjustments for gender, age, weight, and other vascular risk factors. In the quoted study, BMD was proven to be an independent risk factor that may increase the risk of arterial stiffness and atherosclerosis.[26] The results of our study are in line with the findings of this meta-analysis; however, the limitations of our study should be pointed out: cross-sectional study design and relatively small sample size. Both of them make this study less compelling when compared to other observational study designs.

Conclusions

In this cross-sectional study, we showed a high proportion of postmenopausal women with metabolic syndrome with vitamin D deficiency, but there was no relation between vitamin D and vascular health or vitamin D and bone health. Nevertheless, the relation between vascular health and bone health exists, but it is unlikely due to vitamin D.

References

1. Jorde R, Grimnes G. Vitamin D and metabolic health with special reference to the effect of vitamin D on serum lipids. *Prog Lipid Res*. 2011;50(4):303–312.
2. Lerchbaum E. Vitamin D and menopause: A narrative review. *Maturitas*. 2014;79(1):3–7.
3. Bjelakovic G, Gluud LL, Nikolova D, et al. Vitamin D supplementation for prevention of cancer in adults. *Cochrane Database Syst Rev*. 2014;(6):CD007469.
4. Dadonienė J, Čypienė A, Rinkūnienė E, et al. Vitamin D and functional arterial parameters in postmenopausal women with metabolic syndrome. *Adv Med Sci*. 2016;61(2):224–230.
5. Challoumas D. Vitamin D supplementation and lipid profile: What does the best available evidence show? *Atherosclerosis*. 2014;235(1):130–139.
6. Laucevičius A, Rinkūnienė E, Skujaitė A, et al. Prevalence of cardiovascular risk factors in Lithuanian middle-aged subjects participating in the primary prevention program: Analysis of the period 2009–2012. *Blood Press*. 2015;24(1):41–47.
7. National Cholesterol Education Program (NCEP) expert panel on detection, evaluation, and treatment of high blood cholesterol in adults (Adult Treatment Panel III). *Circulation*. 2002;106(25):3143–3421.
8. Płudowski P, Karczmarewicz E, Bayer M, et al. Practical guidelines for the supplementation of vitamin D and the treatment of deficits in Central Europe – recommended vitamin D intakes in the general population and groups at risk of vitamin D deficiency. *Endokrynol Pol*. 2013;64(4):319–327.
9. Kelly R, Hayward C, Avolio A, O'Rourke M. Noninvasive determination of age-related changes in the human arterial pulse. *Circulation*. 1989;80(6):1652–1659.
10. Wilkinson IB, Cockcroft JR, Webb DJ. Pulse wave analysis and arterial stiffness. *J Cardiovasc Pharmacol*. 1998;32(3):S33–37.
11. O'Rourke MF, Gallagher DE. Pulse wave analysis. *J Hypertens Suppl Off J Int Soc Hypertens*. 1996;14(5):S147–157.
12. Čypienė A, Laucevičius A, Venalis A, et al. The impact of systemic sclerosis on arterial wall stiffness parameters and endothelial function. *Clin Rheumatol*. 2008;27(12):1517–1522.
13. Celermajer DS, Sorensen KE, Gooch VM, et al. Non-invasive detection of endothelial dysfunction in children and adults at risk of atherosclerosis. *Lancet Lond Engl*. 1992;340(8828):1111–1115.
14. Galesanu C, Mocanu V. Vitamin D deficiency and the clinical consequences. *Rev Med Chir Soc Med Nat Iasi*. 2015;119(2):310–318.
15. Winckler K, Tarnow L, Lundby-Christensen L, et al. Vitamin D, carotid intima-media thickness and bone structure in patients with type 2 diabetes. *Endocr Connect*. 2015;4(2):128–135.
16. Wang TJ, Pencina MJ, Booth SL, et al. Vitamin D deficiency and risk of cardiovascular disease. *Circulation*. 2008;117(4):503–511.
17. Jorde R, Strand Hutchinson M, Kjærgaard M, Sneve M, Grimnes G. Supplementation with high doses of vitamin D to subjects without vitamin D deficiency may have negative effects: Pooled data from four intervention trials in Tromsø. *ISRN Endocrinol*. 2013;2013:348705.
18. Syal SK, Kapoor A, Bhatia E, et al. Vitamin D deficiency, coronary artery disease, and endothelial dysfunction: Observations from a coronary angiographic study in Indian patients. *J Invasive Cardiol*. 2012;24(8):385–389.
19. Tarcin O, Yavuz DG, Ozben B, et al. Effect of vitamin D deficiency and replacement on endothelial function in asymptomatic subjects. *J Clin Endocrinol Metab*. 2009;94(10):4023–4030.
20. Gurses KM, Tokgozoglu L, Yalcin MU, et al. Markers of subclinical atherosclerosis in premenopausal women with vitamin D deficiency and effect of vitamin D replacement. *Atherosclerosis*. 2014;237(2):784–789.
21. Moghassemi S, Marjani A. The effect of short-term vitamin D supplementation on lipid profile and blood pressure in post-menopausal women: A randomized controlled trial. *Iran J Nurs Midwifery Res*. 2014;19(5):517–521.
22. Ashraf AP, Alvarez JA, Dudenbostel T, et al. Associations between vascular health indices and serum total, free and bioavailable 25-hydroxyvitamin D in adolescents. *PloS One*. 2014;9(12):e114689.
23. Jorde R, Grimnes G. Vitamin D and health: The need for more randomized controlled trials. *J Steroid Biochem Mol Biol*. 2015;148:269–274.
24. Reid IR, Bolland MJ, Grey A. Effects of vitamin D supplements on bone mineral density: A systematic review and meta-analysis. *Lancet*. 2014;383(9912):146–155.
25. Avenell A, Mak JCS, O'Connell D. Vitamin D and vitamin D analogues for preventing fractures in post-menopausal women and older men. *Cochrane Database Syst Rev*. 2014;14(4):CD000227.
26. Ye C, Xu M, Wang S, et al. Decreased bone mineral density is an independent predictor for the development of atherosclerosis: A systematic review and meta-analysis. *PloS One*. 2016;11(5):e0154740.

The diagnostic potential of glutathione S-transferase (GST) polymorphisms in patients with colorectal cancer

Joanna Waś[1,B,C], Monika Karasiewicz[2,B,D], Anna Bogacz[3,4,A,C], Karolina Dziekan[3,B], Małgorzata Górska-Paukszta[3,B], Marek Kamiński[5,E], Grzegorz Stańko[6,B], Adam Kamiński[7,E], Marcin Ożarowski[8,E], Bogusław Czerny[9,F]

[1] Department of Medical Biology, Institute of Cardiology in Warsaw, Poland
[2] Laboratory of International Health, Department of Preventive Medicine, Poznan University of Medical Sciences, Poland
[3] Department of Stem Cells and Regenerative Medicine, Institute of Natural Fibres and Medicinal Plants, Poznań, Poland
[4] Department of Histocompatibility with Laboratory of Genetic Diagnostics, Regional Blood Center, Poznań, Poland
[5] Department of General Surgery and Gastroenterology, Independent Public Clinical Hospital No. 1, Pomeranian Medical University in Szczecin, Poland
[6] Department of General and Hand Surgery, Independent Public Clinical Hospital No. 1, Pomeranian Medical University in Szczecin, Poland
[7] Department of Orthopedics and Traumatology, Independent Public Clinical Hospital No. 1, Pomeranian Medical University in Szczecin, Poland
[8] Department of Biotechnology, Institute of Natural Fibres and Medicinal Plants, Poznań, Poland
[9] Department of Pharmacology and Pharmacoeconomics, Pomeranian Medical University in Szczecin, Poland

A – research concept and design; B – collection and/or assembly of data; C – data analysis and interpretation;
D – writing the article; E – critical revision of the article; F – final approval of the article

Advances in Clinical and Experimental Medicine, ISSN 1899–5276 (print), ISSN 2451–2680 (online) *Adv Clin Exp Med*. 2018;27(11):1561–1566

Address for correspondence
Anna Bogacz
E-mail: aniabogacz23@o2.pl

Funding sources
The study was supported by statutory projects from the Institute of Natural Fibres and Medicinal Plants and Pomeranian Medical University in Szczecin (Poland).

Conflict of interest
None declared

Received on January 16, 2017
Reviewed on February 15, 2017
Accepted on June 11, 2017

Abstract

Background. Colorectal cancer (CRC) is one of the most common cancers in the world. Despite improvements in screening for early diagnosis, CRC is one of the leading causes of cancer deaths.

Objectives. The aim of the study was to determine a potential association between the frequency of GSTM1 and GSTT1 null genotypes and the risk of CRC in the Polish population. Moreover, we analyzed the clinical parameters with the glutathione S-transferase (*GST*) gene polymorphisms in patients with CRC.

Material and methods. The study was conducted on 512 Caucasians, including 279 patients (105 women and 174 men) with CRC. DNA from peripheral blood was extracted and the multiplex polymerase chain reaction (PCR) technique was used for glutathione S-transferase theta (*GSTT1*) and mu (*GSTM1*) gene deletion genotyping.

Results. We found no statistically significant differences in the frequency of the *GST* gene polymorphisms in patients with CRC and controls. The prevalence of the GSTM1*0 variant in the test subjects was higher than in controls (45.9% vs 42.9%; $p > 0.05$). The frequency of the GSTT1*0 variant was also higher in patients with CRC compared to the control population (21.1% vs 18.9%; $p > 0.05$). In addition, the effect of the GSTM1 and GSTT1 polymorphisms on the incidence of CRC was also analyzed. There was a slight, but not statistically significant, increase of the risk of colon cancer for the GSTM1*0 and GSTT1*0 variants. Moreover, we examined the GST genotype due to the cancer TNM classification and the location of the primary tumor. Statistically significant differences in the distribution of the GSTT1*0 and GSTT1*1 genotypes in both the stage and the location of the primary tumor were observed.

Conclusions. It is suggested that the *GSTT1* polymorphism may have an impact on the severity of the tumor and its location.

Key words: colon cancer, gene polymorphism, GSTM1, GSTT1, multiplex polymerase chain reaction

DOI
10.17219/acem/74682

Introduction

Colorectal cancer (CRC) occurs most commonly in developed countries and it is the second most frequent tumor in Poland. The dynamic increase in the number of CRC cases makes Poland a leader among EU countries in the incidence of this disease entity. Europe shows the highest incidence of sporadic CRC worldwide.[1]

Colorectal tumors are often caused by many factors, both genetic and environmental. Several studies present the attempt to use the genotypes of phase II detoxification enzymes – glutathione S-transferase (GST), UDP-glucuronosyltransferase (UGT), sulfotransferase (SULT), and N-acetyltransferase (NAT) – as molecular markers of cancer risk. Due to its function, GST was the subject of a number of studies as a potential susceptibility gene for colon cancer.[2,3] Glutathione S-transferases (GSTs) are a superfamily of multifunctional proteins that play an important role in cellular detoxification. Cytosolic GSTs catalyze the coupling reactions between the nucleophilic reduced glutathione (GSH) and electrophilic forms of drugs, including chemotherapeutic agents (such as platin derivates), environmental pollution and a wide spectrum of xenobiotics. Moreover, GST enzymes are also involved in the detoxification of active metabolites generated during oxidative stress and provide protection against reactive oxygen species (ROS). On the other hand, it has been shown that the activity of GST in tumor cells may be associated with their resistance to chemotherapeutic drugs, because the level of the GST activity in cancer cells is probably significantly increased and may influence the outcome of the treated patients. Due to the limited efficacy of chemotherapy, including the case of gastrointestinal tract cancer, there is a high interest in the individualization of treatment. The GST polymorphisms primarily lead to the reduction of enzymatic activity compared to the wild-type homozygotes.[4] The glutathione S-transferase theta (*GSTT1*) and mu (*GSTM1*) polymorphisms are manifested by the absence of these genes, and the frequency of these variants in the population is dependent on the geographic location. Further, GST isoenzymes are present in most epithelial tissues of the gastrointestinal tract. In addition, clinical studies have shown that the loss of the *GSTM1* expression increases the risk of the digestive tract, bladder, lung and skin cancers. According to the European Prospective Investigation into Cancer and Nutrition, studies on the association between the level of polycyclic aromatic hydrocarbon-DNA adduct and dietary antioxidants may be important among GSTM1-null individuals.[5–8]

The aim of our study was to evaluate the prevalence of the *GSTT1* and *GSTM1* genes polymorphisms in patients with CRC and in the control group. Moreover, the clinical value of these findings for cancer therapy was also analyzed.

Material and methods

The study was conducted on a group of 512 Caucasians, including 279 patients (105 women, 174 men; mean age: 62.49 ±10.6 years) with CRC who were diagnosed and treated in the Clinic Hospital of the Pomeranian Medical University in Szczecin, Poland. In each case, histological studies were the basis for the diagnosis of cancer. The control group consisted of 233 cancer-free subjects (80 women, 153 men; mean age: 58.49 ±10.6 years) recruited from the same hospital. All patients were informed about the purpose of the study and submitted written informed consent. The research was conducted with the approval of the Pomeranian Medical University in Szczecin, Poland.

Genetic studies were conducted in the Department of Stem Cells and Regenerative Medicine at the Institute of Natural Fibers and Medicinal Plants in Poznań, Poland. Genomic DNA was obtained from 5 mL of whole blood using a Qiagen DNA isolation kit according to the manufacturer's protocol (Qiagen, Valencia, USA). DNA concentration was measured with the DeNovix DS-11 Spectrophotometer (DeNovix Inc., Wilmington, USA). Genotyping of the *GSTM1* and *GSTT1* variants was performed using the polymerase chain reaction (PCR) multiplex technique. For the detection of the *GSTM1* and *GSTT1* gene deletion, the amplification of *CYP1A1* was used as a positive reaction control. A 215 bp fragment for the *GSTM1* gene was amplified with the forward and reverse primers as follows: 5′GAACTCCCTGAAAAGCTAAAG-3′ and 5′GTTGGGCTCAAATATACGGTG-3′. Forward and reverse primers for the *GSTT1* gene amplification were 5′TTCCTTACTGGTCCTCACATC-3′ and 5′ TCACCGGATCATGGCCAGCA-3′, and the size of the PCR product was 480 bp. For the *CYP1A1* product amplification (312 bp), the forward primer 5'GAACTGCCACTTCAGCTGTCT-3' and reverse primer 5'CAGCTGCATTTGGAAGTGCTC-3' were used. All primers were synthesized at the Institute of Biochemistry and Biophysics, Polish Academy of Sciences, Warszawa, Poland. Polymerase chain reaction was performed in 20 µL reaction mixture containing 100 ng genomic DNA, 2 pmol each primer, 0.25 mM deoxynucleotides (dNTPs), 1× concentrate PCR buffer, 2mM MgCl2 and 1U Taq polymerase (Novazym, Poznań, Poland). Polymerase chain reaction was performed in a thermocycler PTC-200 (MJ Research, Inc., Waltham, USA) under the following conditions: initial denaturation at 94°C for 4 min and 35 cycles as follows – denaturation at 94°C for 30 s, annealing at 60°C for 30 s, elongation for 1 min at 72°C, and the final elongation step of 5 min at 72°C.

The PCR products were visualized on 3% agarose gel stained with ethidium bromide for 40 min at 100 V. The products of electrophoresis were evaluated using the system of documentation and computer analysis of the UVI image (KS 4000/Image PC; Syngen Biotech Molecular

Biology Instruments, Cromwell, USA). GSTT1*0 (null homozygous) and GSTM1*0 (null homozygous) were defined as the absence of the 480 bp or 215 bp PCR product, respectively. At the same time, the presence of the 312 bp fragment for *CYP1A1* indicated a successful PCR reaction. Then, SPSS Statistics 17.0 for Windows was utilized for statistical analysis (Chicago, USA). We used the Hardy-Weinberg equation to calculate the expected genotype frequencies for each polymorphism, which were compared with the observed values using the χ^2 test. The expected results are presented with 95% confidence intervals (CI). Additionally, the correlation analysis between the genotypes and clinical parameters was performed using one-way analysis of variance (ANOVA) test. The values of $p < 0.05$ were considered statistically significant.

Results

The following cases were observed based on the location of the tumor: sigmoid colon – 96 patients (34.4%), cecum and ascending colon – 78 patients (28%), rectum – 52 patients (18.6%), transverse colon – 39 patients (14%), and descending colon – 14 patients (5%). On the basis of histopathological examination, the following types of cancer were diagnosed: adenocarcinoma G2 in 73.4% of cases (205 patients), adenocarcinoma G1 in 14.3% of cases (40 patients), adenocarcinoma G3 in 5.7% of individuals (16 patients), carcinoma mucinosum in 4.3% of cases (12 patients), and carcinoma gelatinosum in 2.1% (6 patients). Moreover, according to the pathological TNM classification (pTNM), we identified preinvasive carcinoma (Tis) in 7 cases (2.5%), the tumor invading the muscularis propria (T2) in 40 patients (14.3%), while in 153 cases (54.8%), we found the features of T3, with the tumor invading through the muscularis propria into pericolorectal tissues. The infiltration of the tumor to the peritoneum (T4a) occurred in 68 cases (24.4%) and in 11 cases (3.9%), the cancer directly invaded or was adherent to other organs or structures (T4b). A total of 132 patients (47.3%) had no metastases in regional lymph nodes (N0) and in 89 cases (31.9%), we observed metastases in 1–3 lymph nodes (N1). Moreover, 58 cases (20.8%) had metastases in 4 or more regional lymph nodes (N2). At the time of diagnosis, metastases (M1) were found in 219 patients (78.5%), and 61 patients (21.9%) had no metastasis (M0). Moreover, in 44 cases, the tumor caused intestinal obstruction. In 35 patients, weight loss was a noticeable symptom of the disease, while in the majority (n = 244), weight loss was not observed. The control group consisted of 233 subjects (80 women and 153 men, mean age: 58.49 ±10.6 years) without CRC (symptom-free) and presented with no anemia.

Furthermore, the frequency of the *GSTM1* gene polymorphism in CRC patients and the control group was investigated. The analysis of the GSTM1*0 and GSTM1*1 variations was conducted among 279 patients with histologically diagnosed CRC and in 233 control cases. The χ^2 test showed no statistically significant differences between the values in the study group and in controls ($p = 0.22$). The prevalence of the GSTM1 null genotype variant in both groups was similar, and amounted to 45.9% in the study group and 42.9% in the control group. The frequency of GSTM1*1 was 54.1% in the study group and 57.1% in the control group (Table 1). Furthermore, we determined a risk of colon cancer depending on genotypes. In the case of the GSTM1 null variant, the odds ratio (OR) was slightly elevated (OR = 1.13, 95% CI = 0.78–1.63; $p = 0.28$). However, there was no significant impact of this polymorphism on the risk of developing colon cancer.

Additionally, the clinical data of patients diagnosed with CRC were compared with the *GSTM1* gene genotypes. We selected the clinical stage according to the TNM classification and the primary tumor location. The results are shown in Table 2. In the same group of patients and controls, the *GSTT1* gene polymorphism was determined. The χ^2 test showed no statistically significant difference between the study group and controls ($p = 0.30$) (Table 3).

The frequency of the GSTT1*0 variant was 21.1% compared to the control group (18.9%). The frequency of GSTT1*1 was 78.9% in the study group and 81.1% in controls. The effect of the GSTT1 polymorphism on the incidence of CRC was also analyzed. There was a slightly increased risk of CRC in the case of the GSTT1 null genotype (OR = 1.15, 95% CI = 0.73–1.83; $p = 0.30$), but not statistically significantly.

Additionally, the clinical data of patients diagnosed with CRC was compared with the *GSTT1* gene genotypes. We examined the cancer stage according to the TNM classification and the location of the primary tumor. Statistically significant differences in the distribution of the genotypes

Table 1. The frequency of the GSTM1 genotypes in patients with CRC and controls

Genotype	Patients	Controls	OR	95% CI	p-value
	observed value n (%)	observed value n (%)			
GSTM1*0	128 (45.9)	100 (42.9)	1.13	0.78–1.63	0.28
GSTM1*1	151 (54.1)	133 (57.1)	0.89	0.62–1.28	0.28
Total	279 (100)	233 (100)	–	–	–

CRC – colorectal cancer; OR – odds ratio; CI – confidence interval.

Table 2. Selected clinical parameters of patients with CRC and the GSTM1 genotype

Clinical parameters	Genotype n (%)		p-value
	GSTM1*0	GSTM1*1	
pT			
Tis	3 (1.08)	4 (1.43)	0.06
T1	–	–	
T2	19 (6.8)	21 (7.5)	
T3	68 (24.4)	85 (30.5)	
T4	38 (13.6)	41 (14.7)	
pN			
N0	60 (21.5)	72 (25.8)	0.12
N1	40 (14.3)	49 (17.6)	
N2	28 (10)	30 (10.8)	
M			
M0	23 (8.2)	38 (13.6)	0.15
M1	105 (37.6)	113 (40.5)	
Tumor location			
sigmoid colon	39 (14.0)	57 (20.4)	0.64
cecum and ascending colon	34 (12.2)	44 (15.7)	
rectum	30 (10.8)	22 (7.9)	
transverse colon	21 (7.5)	18 (6.5)	
descending colon	4 (1.4)	10 (3.6)	

CRC – colorectal cancer; pT, pN, M – pathological TNM classification of the tumor; Tis – carcinoma in situ; T1– tumor invades the submucosa; T2 – tumor invades the muscularis propria; T3 – tumor invades through the muscularis propria into pericolorectal tissues; T4 – tumor penetrates to the surface of the visceral peritoneum; N0 – no regional lymph node metastasis; N1 – metastasis in 1–3 regional lymph nodes; N2 – metastasis in 4 or more regional lymph nodes; M0 – no distant metastasis; M1 – metastasis to distant organs.

in both the stage and the location of the primary tumor were observed. There is a possibility that the GSTT1*0 and GSTT1*1 genotypes may have an impact on the severity of the tumor and its location. The results are shown in Table 4.

Discussion

It is well-known that GST isoenzymes are responsible for the detoxification of some mutagenic and carcinogenic chemical compounds. For this reason, it is possible that the deletion of the *GST* gene may be a risk factor in carcinogenesis. Some speculate that the GSTM1 null genotype can be associated with a predisposition to certain cancers, but these reports are inconclusive. On the other hand, predictive markers for the treatment of gastrointestinal cancer are needed. In our study, we assessed the possible role of the *GSTM1* and *GSTT1* polymorphisms in the development of CRC in the Polish population. We investigated the frequency of the GSTM1 and GSTT1 genotypes and their potential influence on the risk of CRC. Moreover, we also examined the GST genotype with regard to the cancer TNM classification and the location of the primary tumor.

The available data on the frequency of the *GSTM1* and *GSTT1* gene polymorphisms are quite diverse and depend on the ethnic origin of the analyzed population. Nevertheless, the frequencies of the GSTM1 and GSTT1 genotypes observed in our study are in accordance with those from other European Caucasian populations and consistent with previous studies.[2] Depending on the author, a lack of the GSTM1 enzymatic activity was observed in 40–60% of Caucasians, while the GSTT1 null genotype is less frequent and is present in 10–20% of this population.[9] In our study, the prevalence of the GSTM1*0 variant in the test subjects was 45.9% compared to 42.9% in controls. The frequency of the GSTT1*0 variant was 21.1% in total cancer cases compared to 18.9% in the control population. According to Arruda et al., the frequency of the *GSTM1* and *GSTT1* genes homozygous deletion is quite high among Caucasians and amounts to 55% for *GSTM1* (allele frequency: 0.74) and 18.5% for *GSTT1* (allele frequency: 0.43).[10] For comparison, in dark-skinned Brazilians, these values were 33% for the *GSTM1* (allele frequency: 0.57) and 19% for the *GSTT1* gene (allele frequency: 0.43), whereas in the Amazonian group these values were 20% for *GSTM1* (allele frequency: 0.45) and 11% for *GSTT1* (allele frequency: 0.34). Moreover, the frequency of the GSTM1 and GSTT1 both null genotypes in white- and dark-skinned patients was 11% (frequency of both alleles: 0.33) and 5% (allele frequency: 0.22), respectively. Importantly, Garte et al. suggest that the highest frequency of the GSTM1*0 homozygotes is in the Caucasian population (0.53), lower in Asians (0.52) and the lowest in Africans (0.26), depending on the origin of the study population.[11]

On the basis of the OR calculation, we found no statistically significant effect of the GSTM1 null (OR = 1.13, 95% CI = 0.78–1.63; p = 0.28) and GSTT1 null (OR = 1.15, 95% CI = 0.73–1.83, p = 0.30) genotypes on the risk of CRC development. Our findings are consistent with the results obtained by Hezova et al. and Chenevix-Trench et al., where neither of the *GSTM1* and *GSTT1* polymorphisms showed any associations with CRC.[2,12] Similarly, no increased risk of developing CRC for both the null variants in a British population study was found.[13] Most reports indicate that the increased risk is at a low level, approx. OR < 2.[14,15] Still, there are also those who suggest a much

Table 3. The frequency of the GSTT1 genotypes in patients with CRC and the controls

Genotype	Patients	Controls	OR	95% CI	p-value
	observed value n (%)	observed value n (%)			
GSTT1*0	59 (21.1)	44 (18.9)	1.15	0.73–1.83	0.30
GSTT1*1	220 (78.9)	189 (81.1)	0.87	0.55–1.37	0.30
Total	279 (100)	233 (100)	–	–	–

CRC – colorectal cancer; OD odds ratio; CI – confidence interval.

Table 4. Selected clinical parameters of patients with CRC and the GSTT1 genotype

Clinical parameters	Genotype n (%)		p-value
	GSTT1*0	GSTT1*1	
pT			
Tis	2 (0.7)	5 (1.8)	0.02
T1	–	–	
T2	7 (2.5)	33 (11.8)	
T3	35 (12.5)	118 (42.3)	
T4	15 (5.4)	64 (22.9)	
pN			
N0	27 (9.7)	105 (37.6)	0.04
N1	12 (4.3)	77 (27.6)	
N2	20 (7.2)	38 (13.6)	
M			
M0	16 (5.7)	45 (16.1)	0.03
M1	43 (15.4)	175 (62.7)	
Tumor location			
sigmoid colon	16 (5.7)	80 (28.7)	0.04
cecum and ascending colon	10 (3.6)	68 (24.4)	
rectum	11 (3.9)	41 (14.7)	
transverse colon	18 (6.5)	21 (7.5)	
descending colon	4 (1.4)	10 (3.6)	

CRC – colorectal cancer; pT, pN, M – pathological TNM classification of the tumor; Tis – carcinoma in situ; T1– tumor invades the submucosa; T2 – tumor invades the muscularis propria; T3 – tumor invades through the muscularis propria into pericolorectal tissues; T4 – tumor penetrates to the surface of the visceral peritoneum; N0 – no regional lymph node metastasis; N1 – metastasis in 1–3 regional lymph nodes; N2 – metastasis in 4 or more regional lymph nodes; M0 – no distant metastasis; M1 – metastasis to distant organs.

larger relationship between the GSTM1/GSTT1 double-null haplotype and the risk of gastrointestinal cancers.[16] Furthermore, in our research, no impact of the GSTM1 gene polymorphism on the location and stage of the tumor was noted. Similar results were presented by Gertig et al., Abdel-Rahman et al., Loktionov et al., and Zhu et al.[17–20] In contrast, Zhong et al. demonstrated an increased frequency of the GSTM1 null genotype in a population of 196 cases with CRC (56.1%) compared with the control group of 225 individuals (41.8%).[21] In their study, the increased evidence of proximal colon tumor in patients with the GSTM1 null genotype was noted. On the other hand, Katoh et al. suggested that the GSTM1 null genotype is a risk factor (OR = 2.03, 95% CI = 1.06–3.90) among patients with distal colorectal adenocarcinoma, while Wang et al. observed an increased rectal cancer risk (OR = 1.55, 95% CI = 1.05–2.30).[15,22] Furthermore, Katoh et al. indicated that the combined GSTM1 null and GSTT1 null genotypes frequency was similar in adenocarcinoma cases and in controls.[22] However, they observed a significant increase of the GSTM1 homozygous null genotype in patients with gastric adenocarcinoma (56.8%) compared to the control group (43.6%) (OR = 1.70, 95% CI = 1.05–2.76).

Moreover, in our study we investigated the effect of the *GSTT1* gene variants in relation to the tumor location and the pTNM characteristics. Statistically significant differences in the distribution of the GSTT1*0 and GSTT1*1 genotypes in both the stage and the location of the tumor were observed. We noted a high incidence of the GSTM1*1 genotype, especially in patients diagnosed as T3, M1 and N0. The highest percentage was reported in patients with sigmoid colon, cecum and ascending colon and rectum cancers. These relationships were not observed in the British population.[13] Other suggestions are derived from a meta-analysis where a statistically significant association between the GSTT1 null variant and rectal cancer was observed (OR = 1.28, 95% CI = 1.01–1.64).[23] There were no differences in the distribution of genotypes and the classification according to Duke's staging or histological differentiation, but a strong correlation between the increased risk of CRC and the combined GSTT1 and GSTM1 null genotypes was observed. Similar findings were obtained by Wan et al. for the correlation of the CRC sites and the *GSTT1* gene deletion in rectal tumors (OR = 1.50, 95% CI = 1.09–2.07; $p < 0.0001$), but in a lower level in CRC patients (OR = 1.33, 95% CI = 0.94–1.88).[24] Apart from that, no connection was found between the GSTT1 polymorphism and age, gender, tumor stage and differentiation. Otherwise, the results reported by Zhang et al. indicated that the prevalence of the GSTT1*0 variant was also higher in poorly differentiated cancers than in others.[25] According to them, the GSTM1*0 genotype was related to the cancer sites, and increased gradually from the right (37%) to the left colon (44%) and to the rectum (60%) ($p = 0.049$). Moreover, some authors indicated that the deletion of the *GSTT1* gene was more frequent among distal sporadic colorectal adenocarcinoma (SCRAC) cases compared to proximal ones (66.2% vs 44.4%; $\chi^2 = 3.97$; $p < 0.05$), and among the elderly compared to younger patients.[20] Moreover, there are some papers showing that the presence of the GSTT1 null genotype may increase the risk of tumor progression in patients below 70 years of age.[12] However, other authors do not agree with these proposals.[17,26] Furthermore, there was no evidence concerning the impact of smoking on the risk of CRC in patients with the GSTM1 null genotype (OR = 1.2, 95% CI = 0.3–4.2) and for GSTT1 null patients (OR = 1.1, 95% CI = 0.3–4.7).[17]

A review of the literature shows that the activity of phase II detoxification enzymes is generally important in the study of cancer epidemiology. Hence, it is worth noting that the polymorphisms of GST enzymes have been widely studied in other cancer cases. For example, a significant increase of the chronic myelogenous leukemia (CML) incidence in patients with the GSTT1 null genotype was observed.[27] Moreover, the increased toxicity of chemotherapy and reduced survival in children with acute lymphoblastic leukemia (ALL) and the *GSTT1* gene deletion was analyzed. There is also a thesis that the GST genes may be associated with the risk of an ALL relapse in childhood, the development of prostate cancer, bladder cancer, and skin malignances.[28] Moreover, based on meta-analyzes by Wang et al., there is some effect of the GSTT1 null variant on an increasing risk of lung cancer.[29]

Conclusions

In conclusion, it should be considered that the *GST* polymorphisms leading to reduced activity of the enzyme may be beneficial in the chemotherapy of patients with CRC. However, in our study we did not prove that the *GST* polymorphisms alone predispose to CRC. Overall, the homozygous GSTM1 null and GSTT1 null genotypes generate slight changes in the risk of developing colon cancer. However, the scale of the risk is greater when the genotype interactions with other factors are considered (e.g., diet, tobacco smoke exposure). It has been known that studies on the effect of the *GST* polymorphisms are limited by the insufficient amount of data on the phenotypic consequences of this gene deletion in the aspect of CRC. On the other hand, the combined incidence of multiple gene polymorphisms appeared to be important for CRC predispositions and survival. However, we observed differences in the location and stage of the tumor, depending on the GSTT1 genotype in randomly included patients. Due to different reports, there is a question whether the *GST* polymorphism may be of diagnostic use, and have an impact on the survival of patients and chemotherapy effectiveness.

References

1. Didkowska J, Wojciechowska U, Zatoński W. *Cancer in Poland in 2011* [in Polish]. Warszawa: Polish National Cancer Registry, Department of Epidemiology and Cancer Prevention; 2013.
2. Hezova R, Bienertova-Vasku J, Sachlova M, et al. Common polymorphisms in GSTM1, GSTT1, GSTP1, GSTA1 and susceptibility to colorectal cancer in the Central European population. *Eur J Med Res*. 2012;17:17.
3. Chirila DN, Popp RA, Balacescu O, et al. GST gene variants in synchronous colorectal cancers and synchronous association of colorectal cancers with other cancers. *Chirurgia (Bucur)*. 2013;108:365–371.
4. Gorukmez O, Yakut T, Gorukmez O, et al. Glutathione S-transferase T1, M1 and P1 genetic polymorphisms and susceptibility to colorectal cancer in Turkey. *Asian Pac J Cancer Prev*. 2016;17:3855–3859.
5. Sharma N, Singh A, Singh N, et al. Genetic polymorphisms in GSTM1, GSTT1 and GSTP1 genes and risk of lung cancer in a North Indian population. *Cancer Epidemiol*. 2015;39:947–955.
6. Zamora-Ros R, Barupal DK, Rothwell JA, et al. Dietary flavonoid intake and colorectal cancer risk in the European prospective investigation into cancer and nutrition (EPIC) cohort. *Int J Cancer*. 2017;140:1836–1844.
7. Economopoulos KP, Sergentanis TN. GSTM1, GSTT1, GSTP1, GSTA1 and colorectal cancer risk: A comprehensive meta-analysis. *Eur J Cancer*. 2010;46:1617–1631.
8. Beyerle J, Frei E, Stiborova M, et al. Biotransformation of xenobiotics in the human colon and rectum and its association with colorectal cancer. *Drug Metab Rev*. 2015;47:199–221.
9. Van Der Logt EM, Bergevoet SM, Roelofs HM, et al. Genetic polymorphisms in UDP-glucuronosyltransferases and glutathione S-transferases and colorectal cancer risk. *Carcinogenesis*. 2004;25:2407–2415.
10. Arruda VR, Grignolli CE, Goncalves MS, et al. Prevalence of homozygosity for the deleted alleles of glutathione S-transferase mu (GSTMI) and theta (GSTTI) among distinct ethnic groups from Brazil: Relevance to enviromental carcinogenesis. *Clin Genet*. 1998;54:210–214.
11. Garte S, Gaspari L, Alexandrie AK, et al. Metabolic gene polymorphism frequencies in control populations. *Cancer Epidemiol Biomarkers Prevent*. 2001;10:1239–1248.
12. Chenevix-Trench G, Young J, Coggan M, et al. Glutathione S-transferase M1 and T1 polymorphisms: Susceptibility to colon cancer and age of onset. *Carcinogenesis*. 1995;16:1655–1657.
13. Ye Z, Parry JM. Genetic polymorphisms in the cytochrome P450 1A1, glutathione S-transferase M1 and T1, and susceptibility to colon cancer. *Teratog Carcinog Mutagen*. 2002;22:385–392.
14. Ateş NA, Tamer L, Ateş C, et al. Glutathione S-transferase M1, T1, P1 genotypes and risk for development of colorectal cancer. *Biochem Genet*. 2005;43:149–163.
15. Wang J, Jiang J, Zhao Y, et al. Genetic polymorphisms of glutathione S-transferase genes and susceptibility to colorectal cancer: A case-control study in an Indian population. *Cancer Epidemiol*. 2011;35:66–72.
16. Martínez C, Martín F, Fernández JM, et al. Glutathione S-transferases mu 1, theta 1, pi 1, alpha 1 and mu 3 genetic polymorphisms and the risk of colorectal and gastric cancers in humans. *Pharmacogenomics*. 2006;7:711–718.
17. Gertig DM, Stampfer M, Haiman C, et al. Glutathione S-transferase GSTM1 and GSTT1 polymorphisms and colorectal cancer risk: A prospective study. *Cancer Epidemiol Biomarkers Prev*. 1998;7:1001–1005.
18. Abdel-Rahman SZ, Soliman AS, Bondy ML, et al. Polymorphism of glutathione S-transferase loci GSTM1 and GSTT1 and susceptibility to colorectal cancer in Egypt. *Cancer Lett*. 1999;142:97–104.
19. Loktionov A, Watson MA, Gunter M, et al. Glutathione-S-transferase gene polymorphisms in colorectal cancer patients: Interaction between GSTM1 and GSTM3 allele variants as a risk-modulating factor. *Carcinogenesis*. 2001;22:1053–1060.
20. Zhu Y, Deng C, Zhang Y, et al. The relationship between GSTM1, GSTT1 gene polymorphisms and susceptibility to sporadic colorectal adenocarcinoma. *Zhonghua Nei Ke Za Zhi*. 2002;41:538–540.
21. Zhong S, Wyllie AH, Barnes D, et al. Relationship between the GSTM1 genetic polymorphism and susceptibility to bladder, breast and colon cancer. *Carcinogenesis*. 1993;14:1821–1824.
22. Katoh T, Nagata N, Kuroda Y, et al. Glutathione S-transferase MI (GSTM1) and TI (GSTT1) genetic polymorphism and susceptibility to gastric and colorectal adenocarcinoma. *Carcinogenesis*. 1996;17:1855–1859.
23. Qin X, Zhou Y, Chen Y, et al. Glutathione S-transferase T1 gene polymorphism and colorectal cancer risk: An updated analysis. *Clin Res Hepatol Gastroenterol*. 2013;37:626–635.
24. Wan H, Zhou Y, Yang P, et al. Genetic polymorphism of glutathione S-transferase T1 and the risk of colorectal cancer: A meta-analysis. *Cancer Epidemiol*. 2010;34:66–72.
25. Zhang H, Ahmadi A, Arbman G, et al. Glutathione S-transferase T1 and M1 genotypes in normal mucosa, transitional mucosa and colorectal adenocarcinoma. *Int J Cancer*. 1999;84:135–138.
26. Butler WJ, Ryan P, Roberts-Thomson IC. Metabolic genotypes and risk for colorectal cancer. *J Gastroenterol Hepatol*. 2001;16:631–635.
27. Mondal BC, Paria N, Majumdar S, et al. Glutathione S-transferase M1 and T1 null genotype frequency in chronic myeloid leukaemia. *Eur J Cancer Prev*. 2005;14:281–284.
28. Davies SM, Robison LL, Buckley JD, et al. Glutathione S-transferase polymorphisms and outcome of chemotherapy in childhood acute myeloid leukemia. *J Clin Oncol*. 2001;19:1279–1287.
29. Wang Y, Yang H, Wang H. The association of GSTT1 deletion polymorphism with lung cancer risk among Chinese population: Evidence based on a cumulative meta-analysis. *Oncol Targets Ther*. 2015;12:2875–2882.

Circulating parameters of oxidative stress and hypoxia in normal pregnancy and HELLP syndrome

Ahmet Mentese[1,A–D,F], Süleyman Güven[2,A,D,F], Selim Demir[3,B–D], Ayşegül Sümer[4,B,C], Serap Özer Yaman[5,B,C], Ahmet Alver[5,A,E,F], Mehmet Sonmez[6,A,E,F], Süleyman Caner Karahan[5,A,E,F]

[1] Program of Medical Laboratory Techniques, Vocational School of Health Sciences, Karadeniz Technical University, Trabzon, Turkey
[2] Department of Obstetrics and Gynecology, Faculty of Medicine, Karadeniz Technical University, Trabzon, Turkey
[3] Department of Nutrition and Dietetics, Faculty of Health Sciences, Karadeniz Technical University, Trabzon, Turkey
[4] Department of Nursing, School of Health Services, Recep Tayyip Erdogan University, Rize, Turkey
[5] Department of Medical Biochemistry, Faculty of Medicine, Karadeniz Technical University, Trabzon, Turkey
[6] Department of Hematology, Faculty of Medicine, Karadeniz Technical University, Trabzon, Turkey

A – research concept and design; B – collection and/or assembly of data; C – data analysis and interpretation;
D – writing the article; E – critical revision of the article; F – final approval of the article

Advances in Clinical and Experimental Medicine, ISSN 1899-5276 (print), ISSN 2451-2680 (online) *Adv Clin Exp Med.* 2018;27(11):1567–1572

Address for correspondence
Ahmet Mentese
E-mail: amentese028@gmail.com

Funding sources
None declared

Conflict of interest
None declared

Received on August 2, 2016
Reviewed on January 22, 2017
Accepted on June 9, 2017

Abstract

Background. The HELLP syndrome (Hemolysis, Elevated Liver enzymes and Low Platelets) is a complication of severe pre-eclampsia, a condition characterized by oxidative stress elevation caused by disequilibrium between lipid peroxidation and antioxidant defense mechanisms, which, in turn, results in endothelial compromise and free radical-mediated cell damage. While several studies have examined the relationship between pre-eclampsia and oxidative stress, research investigating oxidative and hypoxic status in HELLP syndrome is limited.

Objectives. The aim of this study was to compare the levels of oxidative stress markers – total oxidant status (TOS), total antioxidant status (TAS), oxidative stress index (OSI), and malondialdehyde (MDA) – and a hypoxia marker – carbonic anhydrase IX (CA IX) – in patients with HELLP syndrome and in healthy pregnant women.

Material and methods. A total of 23 women with HELLP syndrome and 30 healthy pregnant women were included in the study. Serum levels of oxidative stress markers were determined using colorimetric methods, while serum levels of CA IX were measured using an enzyme-linked immunosorbent assay (ELISA) kit.

Results. The TOS, OSI, MDA, and CA IX levels were significantly higher in women with HELLP syndrome than in the controls ($p = 0.0001$, $p = 0.0001$, $p = 0.0001$, and $p = 0.008$, respectively).

Conclusions. Increased levels of oxidative stress and hypoxia markers in women with HELLP syndrome suggest that oxidative stress and hypoxia may be significantly involved in the pathophysiology of the disease. Further follow-up studies are now needed to investigate the prognostic roles of these parameters in patients with HELLP syndrome.

Key words: oxidative stress, carbonic anhydrases, hypoxia, HELLP syndrome

DOI
10.17219/acem/74653

Introduction

The HELLP (Hemolysis, Elevated Liver enzymes and Low Platelets) syndrome is a multi-systemic disease with a poor prognosis arising from endothelial dysfunction. It is characterized by multiple organ failure and widespread pregnancy symptoms, such as proteinuria, hypertension and generalized edema, as well as laboratory findings, such as microangiopathic hemolysis, increases in liver function tests and thrombocytopenia.[1–4] The condition occurs in 0.2–0.6% of all women during pregnancy and in 10–20% of cases of eclampsia or pre-eclampsia. The exact mechanism involved in HELLP syndrome, regarded as an extreme form of pre-eclampsia, is uncertain.[5] The disease occurs as a result of abnormal placental development or function and ischemia, as in severe pre-eclampsia. The 1st stage of the disease is characterized by defective placentation, in which trophoblasts in the decidua prevent complete conversion of the spiral arteries.[6] This leads to uneven blood perfusion, hypoxia and oxidative stress. Clinical symptoms, such as hypertension, proteinuria and edema, associated with maternal endothelial injury and systemic inflammation, subsequently appear.[7]

Oxidative stress is related to the deterioration of the pro-oxidant and antioxidant balance.[8] This results from both excessive reactive oxygen species (ROS) and/or inadequate antioxidant mechanisms.[9] Oxidative stress increases during uncomplicated pregnancy, due to increased metabolism and a rise in basal oxygen and energy consumption. The placenta, a highly vascular organ, rich in mitochondria and macrophages, is particularly responsible for the production of free radicals. These cell organelles manufacture significant quantities of oxidants, capable of causing injury to the placenta. However, at the same time, antioxidant levels also rise to protect against this injury. Under normal conditions, high levels of oxidants in pregnancy are compensated by antioxidant level elevation, thus averting significant oxidative damage. In contrast to normal pregnancy, when pre-eclampsia occurs, the existing antioxidant levels are incapable of preventing oxidative damage resulting from high levels of free radicals. Additionally, decreases in the levels and activities of a number of antioxidants are observed, including vitamin E, glutathione peroxidase (GPx) and superoxide dismutase (SOD). The combined impact of these factors results in increased lipid peroxidation, endothelial cell dysfunction and vasospasm.[10] However, the number of studies examining the relationship between oxidative stress and HELLP syndrome is limited. Decreased ferric reducing ability of plasma (FRAP) and increased protein carbonyl levels are reported in women with HELLP syndrome.[11] Increased levels of oxidative stress markers, such as malondialdehyde (MDA) and proinflammatory cytokines (interleukin-6 and -8) were also shown in infants of pre-eclamptic mothers with HELLP syndrome.[12] This prospective study of women with HELLP syndrome and normal pregnant women was intended to observe the relative changes in oxidative stress markers (MDA, total oxidant status [TOS], total antioxidant status [TAS], and oxidative stress index [OSI]) and a hypoxia marker (carbonic anhydrase IX [CA IX]).

Material and methods

Study design and patient settings

Once the approval had been received from the Karadeniz Technical University Medical Faculty Ethical Committee, Trabzon, Turkey, informed consent was obtained from all subjects. Pregnant women with HELLP syndrome (n = 23) and healthy pregnant women (n = 30) were enrolled as the study and control groups, respectively. Blood samples of the study and control groups were collected during the period January–June 2016. All women in the study group met all the criteria required for the diagnosis of HELLP syndrome: microangiopathic hemolytic anemia with characteristic schistocytes (helmet cells) on blood smear, platelet count (PLT) ≤100,000/mL, serum lactate dehydrogenase (LDH) >600 IU/L, and elevated liver enzymes (≥70 IU/L) – serum alanine aminotransferase (ALT) and aspartate aminotransferase (AST).[13] The control group consisted of healthy pregnant women attending the gynecology unit for a routine examination. The exclusion criteria were: a known history of deep vein thrombosis or pulmonary embolism, diabetes mellitus, antiphospholipid syndrome, chronic or acute renal disease, systemic lupus erythematosus, recurrent miscarriage, or thrombophilia; active smoker status; multi-fetal pregnancy; and the use of anticoagulant, non-steroidal anti-inflammatory, corticosteroid, or antiplatelet therapies. The study subjects were not receiving fetal lung maturation or HELLP syndrome treatment steroids at the time of the research.

Ethical approval

All procedures involving human participants were performed in accordance with the ethical standards of the institutional and/or national research committee and with the 1964 Helsinki Declaration and its later amendments, or comparable ethical standards.

Blood samples and laboratory methods

Five-milliliter blood samples from each subject were collected in separator gel containing Vacutainer tubes. After clotting, these were centrifuged at 1800 × g for 10 min. Serum samples were stored at −80°C until the analysis of all parameters. All routine biochemical parameter levels were determined using a Beckman Coulter autoanalyzer (Beckman Coulter, Brea, USA).

The concentrations of CA IX were measured using an enzyme-linked immunosorbent assay (ELISA) kit (R&D

Systems, Minneapolis, USA) according to the manufacturer's instructions. The absorbance of samples was measured at 450 nm, using a microplate reader (Molecular Devices, San Jose, USA). The results were expressed as pg/mL. The minimum detectable level of human CA IX is typically <2.3 pg/mL.

The MDA concentrations were determined using the method described by Yagi.[14] Tetramethoxypropane was used as a standard and the MDA levels were expressed as nmol/mL.

The levels of serum TOS and TAS were determined using a commercial colorimetric kit (Rel Assay Diagnostics, Gaziantep, Turkey) according to the manufacturer's instructions. The TOS results were expressed as μmol H_2O_2 equivalent/L and the TAS results as mmol trolox equivalent/L.

The TOS/TAS ratio was used as OSI. The units of TAS, expressed as mmol trolox equivalent/L, were converted into μmol trolox equivalent/L and OSI was calculated using the formula[15]:

$$\text{OSI} = [(\text{TOS, } \mu\text{mol } H_2O_2 \text{ equivalent/L})/ /(\text{TAS, } \mu\text{mol trolox equivalent/L}) \times 10].$$

Statistical analysis

Statistical analysis was performed using Statistical Package for Social Sciences (SPSS) software v. 23 (SPSS, Inc., Chicago, USA). The results are expressed as medians within the 25th and 75th percentile interquartile range (IQR). All variables were subjected to descriptive statistical analysis. Normal distribution of the concentrations of all parameters in the 2 groups was investigated using the Kolmogorov-Smirnov test. Differences between the groups were analyzed using the Mann-Whitney U test. The area beneath the receiver operating characteristic (ROC) curves was employed in order to calculate the discriminative power of all parameters in terms of the diagnosis or exclusion of HELLP. These ROC curves were used in the calculation of sensitivity, specificity, negative predictive values (NPV), and positive predictive values (PPV) for HELLP. Statistical significance was set at $p < 0.05$.

Results

The clinical characteristics of the 2 groups are presented in Table 1. The sociodemographic features of the patients were comparable, and no significant differences were observed between the clinical features in the HELLP and control groups.

Median (IQR) serum CA IX, MDA, TAS, TOS, and OSI levels in the groups are summarized in Table 2. Serum CA IX ($p = 0.008$), MDA, TOS, and OSI levels ($p = 0.0001$ for all) were significantly higher in women with HELLP syndrome compared to control subjects. However, although

Table 1. Demographic, clinical and laboratory characteristics of the groups

Clinical characteristics	Normal values	Control group (n = 30)	Study group (n = 23)	p-value
Age [years]	–	28 (24–32)	30 (25–34)	0.301
Gravida	–	2.00 (1.00–3.00)	2.00 (1.00–3.00)	0.244
Parity	–	1.00 (0.00–1.00)	1.00 (0.00–2.00)	0.491
Gestational day	–	238 (219–258)	222 (198–245)	0.123
Hemoglobin [g/dL]	12–17	11.75 (11.0–12.0)	11.7 (10.4–13.0)	0.732
PLT [number pf cells/mL]	150–400 × 10^3	210 × 10^3 (181,750–258,250)	71.5 × 10^3 (42,000–90,000)	0.0001*
LDH [IU/L]	<248	92.0 (69.0–111.0)	1,009 (789–1,642)	0.0001*
ALT [IU/L]	<40	18.0 (15.8–25.0)	125 (64–209)	0.0001*
AST [IU/L]	<40	23.0 (17.8–32.5)	159 (87–234)	0.0001*

PLT – platelet count; LDH – lactate dehydrogenase, ALT – alanine aminotransferase; AST – aspartate aminotransferase; * represents significant results ($p < 0.05$) compared to control group.

Table 2. Median values of oxidative stress and hypoxia markers in the groups

Parameters	Control group (n = 30)	Study group (n = 23)	p-value
CA IX [pg/mL]	1.10 (0.78–1.39)	1.590 (0.948–4.530)	0.008*
MDA [nmol/mL]	0.111 (0.082–0.196)	0.622 (0.351–1.30)	0.0001*
TAS [mmol trolox equivalent/L]	2.38 (2.22–2.60)	2.55 (2.30–2.87)	0.062
TOS [μmol H_2O_2 equivalent/L]	10.10 (8.89–12.10)	24.10 (13.20–28.10)	0.0001*
OSI	0.440 (0.365–0.505)	0.854 (0.580–1.940)	0.0001*

CA IX – carbonic anhydrase IX; MDA – malondialdehyde; TAS – total antioxidant status; TOS – total oxidant status; OSI – oxidative stress index; * represents significant results ($p < 0.05$) compared to control group.

Table 3. The ROC curve analysis of all parameters and their sensitivity, specificity, PPV, and NPV values

Parameters	Cut-off point	AUC (95% CI)	p-value	Sensitivity (%) (95% CI)	Specificity (%) (95% CI)	PPV (95% CI)	NPV (95% CI)
CA IX	>1.53	0.724 (0.585–0.837)	0.003	61 (32–77)	80 (66–93)	70 (45–89)	73 (55–86)
MDA	>0.21	0.924 (0.819–0.979)	0.0001	96 (75–100)	77 (59–90)	70 (49–87)	96 (81–100)
TAS	>2.71	0.658 (0.516–0.782)	0.051	40 (19–64)	94 (80–99)	80 (44–98)	73 (57–85)
TOS	>16.81	0.878 (0.760–0.951)	0.0001	70 (46–88)	97 (85–100)	93 (68–100)	85 (70–94)
OSI	>0.62	0.820 (0.691–0.911)	0.0001	65 (42–83)	97 (83–99)	93 (69–99)	78 (62–94)
ALT	>35	0.982 (0.900–0.997)	0.0001	91 (72–99)	93 (78–99)	91 (72–99)	93 (78–99)
AST	>36	0.987 (0.909–0.996)	0.0001	96 (78–99)	97 (83–99)	96 (78–99)	97 (83–99)
PLT	≤162,000	1.000 (0.932–1.000)	0.0001	100 (85–100)	100 (88–100)	100 (85–100)	100 (88–100)
LDH	>156	0.970 (0.881–0.996)	0.0001	96 (78–99)	97 (83–99)	96 (78–99)	97 (83–99)

AUC – area under the curve; CI – confidence interval; PPV – positive predictive value; NPV – negative predictive value; ROC – receiver operating characteristic; CA IX – carbonic anhydrase IX; MDA – malondialdehyde; TAS – total antioxidant status; TOS – total oxidant status; OSI – oxidative stress index; ALT – alanine aminotransferase; AST – aspartate aminotransferase; PLT – platelet count; LDH – lactate dehydrogenase.

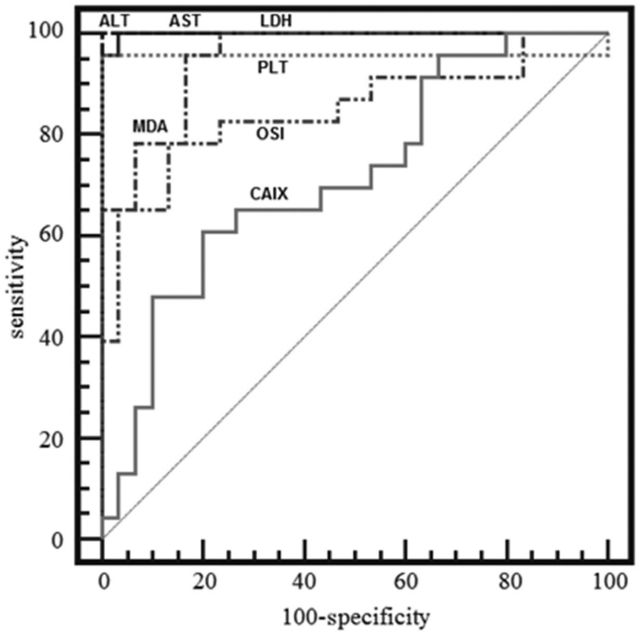

Fig. 1. The ROC curve analyses for all parameters

ROC – receiver operating characteristic; CA IX – carbonic anhydrase IX; MDA – malondialdehyde; OSI – oxidative stress index; ALT – alanine aminotransferase; AST – aspartate aminotransferase; PLT – platelet count; LDH – lactate dehydrogenase.

serum TAS levels were also higher in the study group compared to the control group, the difference was not statistically significant ($p > 0.05$).

The ROC curve analysis was also used to quantify serum PLT, ALT, AST, and LDH, and oxidative stress and hypoxia marker levels (Fig. 1). Values for cut-off points, the area under the curve (AUC), sensitivity, specificity, PPV, and NPV for individual parameters are shown in Table 3. In terms of measured oxidative stress and hypoxia parameters, the highest sensitivity was observed in MDA, while the highest specificity was observed in OSI and TOS.

Discussion

The HELLP syndrome constitutes a group of symptoms observed in pregnant women with either pre-eclampsia or eclampsia, who also exhibit signs of hepatic damage and coagulation anomalies. The disease originates in the placenta, although the pathogenesis is not clearly understood.[16] Oxidative stress is described as an excess of ROS compared to the buffering capacity of the existing antioxidants. The condition has been implicated in a range of diseases, including atherosclerosis, cancers and pre-eclampsia.[17] Good placental oxygenation is essential during pregnancy for cell replication, proliferation and maturation, embryo development, and pregnancy maintenance. In addition, the rises in oxygen concentrations lead to the emergence of oxidative stress markers. As all vascular diseases, pre-eclampsia is characterized by an inflammatory response following ischemia and reperfusion. In the case of pre-eclampsia, placental reperfusion injury leads to a pernicious inflammatory response, implicated in inflammation and oxidative damage mediated by oxidative stress.[18] Although numerous studies have examined the relationship between pre-eclampsia and oxidative stress, there are only limited studies of oxidative and hypoxic status in HELLP syndrome as an extreme form of pre-eclampsia.[11,12,17,19–22] The purpose of this study was, therefore, to assess the status of hypoxia and oxidative stress markers in HELLP syndrome. In this study, serum MDA, TOS and OSI levels were significantly higher in patients with HELLP syndrome compared to control groups ($p = 0.0001$ for all). In agreement with our results, Zusterzeel et al. reported decreased levels of FRAP and increased levels of protein carbonyl in women with HELLP syndrome compared to healthy pregnant women.[11] Mohanty et al. reported higher serum MDA levels in women with pre-eclampsia compared to healthy women. The increase in oxidative stress is further supported by the observation of a negative

correlation between MDA and antioxidants – vitamin E and vitamin C.[20] Sharma et al. reported increased levels of oxidative stress markers (GPx, SOD and MDA) and decreased levels of antioxidants (vitamin C and lycopene) in pre-eclamptic women compared to healthy controls.[17] Chamy et al. reported significantly decreased antioxidant enzyme activity and increased lipid peroxidation in pre-eclamptic groups compared to healthy pregnant women.[19] Vanitha Gowda et al. reported that lipid peroxidation and ceruloplasmin oxidase activity were significantly increased in pre-eclampsia compared to normotensive pregnant women.[21] Additionally, higher MDA and lower SOD levels were reported in women with pre-eclampsia women compared to the control group.[22] In our study, serum TAS levels were higher in the study group compared to the control group, but this was not statistically significant. We think that this may be attributed to the severity of the disease, the timing of sampling and methodological limitations, such as a relatively small study population.

Carbonic anhydrase IX is a membrane-associated glycoprotein and a member of the α-carbonic anhydrase family, responsible for catalyzing the reversible hydration of carbon dioxide to bicarbonate ions and protons. There are 16 known isoforms of CA in humans.[23] More than 50 genes can be induced by hypoxia, by means of hypoxia inducible factor 1 alpha (HIF-1α). Carbonic anhydrase IX is a particularly highly inducible and uniformly induced gene. Due to its stability and membrane location, it constitutes a reliable histochemical marker of hypoxia.[24] There is significant evidence that proves the existence of hypoxia in pre-eclampsia.[25] We, therefore, determined the CA IX levels as hypoxia markers in this study and observed significantly higher serum CA IX levels in patients with HELLP syndrome compared to healthy controls. Recent studies have shown the importance of pH in cell death under hypoxia, and the mechanisms of pH regulation are, therefore, likely to constitute vital pathways for survival. Northern blot analysis has revealed the CA IX expression in tissues, including the heart, liver, hair follicles, articular cartilage, placenta, choroid plexus, and salivary glands. The basal and lateral location of CA IX may similarly imply a role in the transport of bicarbonate or hydrogen ions. Bicarbonate or hydrogen ions in these areas are typically released into the luminal space and these cells may be exposed to extreme pH values.[24] Hence, there is a high probability that the activity of this membrane-associated carbonic anhydrase is involved in the preservation of intracellular pH in HELLP syndrome.

The exact pathobiology of HELLP syndrome is unclear, and no clinical gold standard biomarker for the evaluation of oxidative stress is yet available.[5,11] Similarly, effective and economical biochemical markers are needed for the early diagnosis of HELLP syndrome. We, therefore, prepared ROC curves for both studied parameters, and gold standards of HELLP syndrome. The results of this analysis are shown in Table 3 and Fig. 1. Although the sensitivity and specificity of the investigated markers were not comparable with those of ALT, AST, PLT, or LDH, we, nevertheless, think that these oxidative stress and hypoxia markers may assist physicians with the diagnosis of HELLP syndrome.

One limitation of our study was its low power. However, to the best of our knowledge, this study is the first to examine CA IX, TAS, TOS, and OSI as biochemical parameters in HELLP syndrome. Further follow-up studies are now needed to investigate the prognostic roles of these parameters in patients with HELLP syndrome.

References

1. Weinstein L. Syndrome of hemolysis, elevated liver enzymes and low platelet count: A severe consequence of hypertension in pregnancy. *Am J Obstet Gynecol*. 1982;142(2):159–167.
2. Pokharel SM, Chattopadhyay SK, Jaiswal R, Shakya P. HELLP syndrome: A pregnancy disorder with poor prognosis. *Nepal Med Coll J*. 2008;10(4):260–263.
3. Basturk M, Tokgoz O, Evsen MS, et al. Emergency approach in HELLP syndrome. *J Emerg Med*. 2009;8(1):9–12.
4. Benedetto C, Marozio L, Tancredi A, et al. Biochemistry of HELLP syndrome. *Adv Clin Chem*. 2011;53:85–104.
5. Guven S, Sonmez M, Karahan SC. The role of fibrinolytic and antifibrinolytic activities in the pathophysiology of HELLP syndrome. *Hypertens Pregnancy*. 2011;30(3):275–286.
6. Brosens JJ, Pijnenborg R, Brosens IA. The myometrial junctional zone spiral arteries in normal and abnormal pregnancies: A review of the literature. *Am J Obstet Gynecol*. 2002;187(5):1416–1423.
7. Hansson SR, Naav A, Erlandsson L. Oxidative stress in preeclampsia and the role of free fetal hemoglobin. *Front Physiol*. 2015;5:516.
8. Pisoschi AM, Pop A. The role of antioxidants in the chemistry of oxidative stress: A review. *Eur J Med Chem*. 2015;97:55–74.
9. Weidinger A, Kozlov AV. Biological activities of reactive oxygen and nitrogen species: Oxidative stress versus signal transduction. *Biomolecules*. 2015;5(2):472–484.
10. Siddiqui IA, Jaleel A, Tamimi W, Al Kadri HM. Role of oxidative stress in the pathogenesis of preeclampsia. *Arch Gynecol Obstet*. 2010;282:469–474.
11. Zusterzeel PL, Rutten H, Roelofs HM, Peters WH, Steegers EA. Protein carbonyls in decidua and placenta of pre-eclamptic women as markers for oxidative stress. *Placenta*. 2001;22(2–3):213–219.
12. Torrance HL, Krediet TG, Vreman HJ, Visser GH, van Bel F. Oxidative stress and proinflammatory cytokine levels are increased in premature neonates of preeclamptic mothers with HELLP syndrome. *Neonatology*. 2008;94(2):138–142.
13. Haram K, Svendsen E, Abildgaard U. The HELLP syndrome: Clinical issues and management: A review. *BMC Pregnancy Childbirth*. 2009;9:8.
14. Yagi K. Lipid peroxides and related radicals in clinical medicine. In: Armstrong D, ed. *Free Radicals in Diagnostic Medicine*. New York, NY: Plenum Press; 1994:1–15.
15. Turkmen S, Mentese S, Mentese A, et al. The value of signal peptide-CUB-EGF domain-containing protein 1 and oxidative stress parameters in the diagnosis of acute mesenteric ischemia. *Acad Emerg Med*. 2013;20(3):257–264.
16. Glanville T, Walker J. HELLP syndrome. *Obstet Gynecol*. 2003;5:149–154.
17. Sharma JB, Sharma A, Bahadur A, Vimala N, Satyam A, Mittal S. Oxidative stress markers and antioxidant levels in normal pregnancy and pre-eclampsia. *Int J Gynaecol Obstet*. 2006;94(1):23–27.
18. Sanchez-Aranguren LC, Prada CE, Riano-Medina CE, Lopez M. Endothelial dysfunction and preeclampsia: Role of oxidative stress. *Front Physiol*. 2014;5(372):1–11.
19. Chamy VM, Lepe J, Catalan A, Retamal D, Escobar JA, Madrid EM. Oxidative stress is closely related to clinical severity of pre-eclampsia. *Biol Res*. 2006;39(2):229–236.
20. Mohanty S, Sahu PK, Mandal MK, Mohapatra PC, Panda A. Evaluation of oxidative stress in pregnancy induced hypertension. *Indian J Clin Biochem*. 2006;21(1):101–105.

21. Vanitha Gowda MN, Aroor AR, Krishna L. Studies on oxidative stress in preeclampsia. *Biomed Res*. 2010;21(1):71–79.
22. Khatri M. Circulating biomarkers of oxidative stress in normal pregnancy and preeclampsia and efficacy of antioxidant supplementation. *Int J Reprod Contracept Obstet Gynecol*. 2013;2(3):304–310.
23. Ambrosio MR, Di Serio C, Danza G, et al. Carbonic anhydrase IX is a marker of hypoxia and correlates with higher Gleason scores and ISUP grading in prostate cancer. *Diagn Pathol*. 2016;11:45.
24. Potter C, Harris AL. Hypoxia inducible carbonic anhydrase IX, marker of tumour hypoxia, survival pathway and therapy target. *Cell Cycle*. 2004;3(2):164–167.
25. Tal R. The role of hypoxia and hypoxia-inducible factor-1 alpha in preeclampsia pathogenesis. *Biol Reprod*. 2012;87(6):134.

Relative value of serum pregnancy-associated plasma protein A (PAPP-A) and GRACE score for a 1-year prognostication: A complement to calculation in patients with suspected acute coronary syndrome

Marcin Ojrzanowski[1,A–F], Łukasz Figiel[1,A,B], Jan Z. Peruga[1,B], Sonu Sahni[2,3,B,D], Jarosław D. Kasprzak[1,A,E,F]

[1] Chair and Clinic of Cardiology, Medical University of Lodz, Poland
[2] Department of Pulmonary, Critical Care and Sleep Medicine, Long Island Jewish Medical Center, Northwell Health, New Hyde Park, USA
[3] Center for Heart and Lung Research, the Feinstein Institute for Medical Research, North Shore University Hospital, Northwell Health, Manhasset, USA

A – research concept and design; B – collection and/or assembly of data; C – data analysis and interpretation;
D – writing the article; E – critical revision of the article; F – final approval of the article

Advances in Clinical and Experimental Medicine, ISSN 1899-5276 (print), ISSN 2451-2680 (online) *Adv Clin Exp Med.* 2018;27(11):1573–1580

Address for correspondence
Marcin Ojrzanowski
E-mail: ojrzan@o2.pl

Funding sources
Club 30, Polish Cardiac Society (Announcement of Club 30 Young Investigator Grant).

Conflict of interest
None declared

Received on October 31, 2016
Reviewed on April 29, 2017
Accepted on July 4, 2017

Abstract

Background. The Global Registry of Acute Coronary Events (GRACE) study produced a scale for risk stratification in acute coronary syndromes (ACSs). Pregnancy-associated plasma protein A (PAPP-A) serum concentration was implicated as a marker of unstable atherosclerotic plaques.

Objectives. We hypothesized that the measurement of the concentration of PAPP-A on admission may improve the stratification of cardiovascular risk in suspected ACS patients.

Material and methods. We studied 70 patients with chest pain suggesting ACS diagnosis on admission. Serum cardiac biomarkers and PAPP-A were measured on top of the standard biochemical panel, and the GRACE risk score was calculated. A 12-month follow-up was completed to major adverse cardiac events (MACE): death, myocardial infarction (MI), need for percutaneous coronary intervention (PCI)/coronary artery bypass grafting (CABG), unplanned cardiovascular hospitalization.

Results. In hospital/6-month GRACE, low risk was found in 35 patients (50%)/37 patients (53%), intermediate risk in 23 patients (33%)/21 patients (30%) and high risk in 12 patients (17%)/12 patients (17%). Mean PAPP-A was 39.64 mIU/L (standard deviation – SD = 24.2), and median PAPP-A values for in hospital/6-month GRACE were 21.49 mIU/L (quartile 1st; 3rd – 13.41; 32.65) and 22.61 mIU/L (14.03; 34.1) for low risk patients, 51.76 mIU/L (35.18; 59.99) and 51.76 mIU/L (28.9; 62.1) for intermediate risk patients, and 68.82 mIU/L (58.54; 83.76) for high risk patients. The PAAP-A concentration with specific cut-off points had 66.7% positive predictive value (PPV) and 95.5% negative predictive value (NPV) for death, 33.3% PPV and 80.6% NPV for MI, and 71.4% PPV and 57.1% NPV for any event. Intermediate and high in hospital/6-months GRACE had 14.3%/15.2% PPV and 100%/100% NPV for death, 34.3%/33.3% PPV and 94.3%/91.9% NPV for MI, 74.3%/72.7% PPV and 65.7%/62.2% NPV for any event.

Conclusions. The PAPP-A serum concentration represents a promising prognostic biomarker with significantly improved PPV. The GRACE score is superior to stratification based on PAPP-A with regard to combined cut-off point for 1-year mortality.

Key words: biomarkers, acute coronary syndrome, pregnancy-associated plasma protein A, Global Registry of Acute Coronary Events risk score

DOI
10.17219/acem/75677

Introduction

Acute coronary syndromes (ACSs), which include myocardial infarction (MI), with or without ST elevation and unstable angina amongst others, are a substantial cause of morbidity and mortality. Presently, diagnosis of ACS is made on the basis of patient history, clinical examination, electrocardiographic findings, biochemical markers, and changes noted on cardiac imaging. Confirmation of diagnosis is often made using plasma biomarkers, such as troponins and myocardial fraction of creatine kinase. A critical clinical point is the effective prediction of ACS risk, which may help prevent these events and optimize pharmacologic therapy. Such a prognostication may involve novel biomarkers or imaging, preferably performed in an outpatient setting.

Global Registry of Acute Coronary Events risk score

The Global Registry of Acute Coronary Events (GRACE) risk score is the current standard for risk assessment in ACS. Global Registry of Acute Coronary Events created a risk stratification tool that may be useful in everyday cardiology practice.[1] It is used for evaluating risk of death during hospitalization and within 6 months from discharge in patients admitted to hospital with a diagnosis of ACS.[2] This kind of evaluation is important in order to implement adequate inpatient therapy and to sustain the best long-term treatment. The tool was created to make this evaluation quick and easy. The GRACE risk score calculator is an online calculator with free access, which analyzes 8 factors: age, pulse rate, systolic blood pressure, renal function, congestive heart failure, ST-segment deviation, cardiac arrest, and elevated biomarkers. The score is a percentage risk of death during hospitalization and within 6-months after discharge – such score was calculated for all subjects in the following study.

Management, accessibility and expeditious obtaining results of laboratory testing strongly facilitate ongoing research on biomarkers in cardiology, especially on those that may be utilized in acute situations. The overall aim is to identify a biomarker that conclusively has better sensitivity and specificity as compared to those that are currently in use. In lieu of investigating and determining novel biomarkers, some biomarkers commonly used in other specialties may be transposed and considered for new purposes. However, their clinical utility is yet to be determined, pending further studies.

Pregnancy-associated plasma protein A

Pregnancy-associated plasma protein A (PAPP-A) is a biomarker that is routinely, used in the field of obstetrics. It is often part of a screening test used to estimate the risk of congenital abnormalities such as Down (sensitivity 90%),[3] Edwards, and Patau syndromes. It may also help in assessing complications with the placenta or intrauterine growth restriction. The test is composed of blood sample analysis in conjugate with ultrasound examination to determine fetal measurements and parameters.[4] A positive test result warrants a subsequent amniocentesis to definitely exclude or confirm a diagnosis. The use of PAPP-A in the field of cardiology has been observed in a few small studies.[5,8] These studies have shown that elevated levels of PAPP-A correlate with the occurrence of ACSs. Due to the abovementioned findings, PAPP-A has become synonymous with a biomarker of vulnerable atheromatous plaque.[6,7]

It has been proven that PAPP-A is involved in the pathogenesis of atherosclerotic plaques and its blood concentration is elevated in the setting of MI or unstable angina.[8,9] However, there is no evidence that PAPP-A can provide any diagnostic utility in a group of patients with suspected ACS.[10]

The aim of this study was to evaluate whether the measurement of the serum concentration of PAPP-A on admission may improve the stratification of cardiovascular mortality risk (early and delayed) in patients with suspected ACS.

Material and methods

We studied 70 consecutive patients admitted to tertiary cardiology center due to a suspicion of ACS. Definition of ACS was typical, anginal chest pain lasting for a maximum of 12 h with electrocardiography (ECG) abnormalities characteristic of myocardial ischemia in accordance with European Society of Cardiology. All patients underwent coronary angiography and confirmation of coronary artery disease; including 59 patients who required percutaneous coronary intervention (PCI) or coronary artery bypass graft surgery (CABG). The demographic and clinical characteristics based on the interviews and hospital records are summarized in Table 1.

Cardiac biomarkers and PAPP-A were added to the standard biochemical panel on admission. Measurements of PAPP-A were made using Cobas Elecsys 2010 analyzer manufactured by Roche Diagnostics Ltd. (Basel, Switzerland) and with reagent PAPP-A manufactured by Roche Diagnostics Polska sp. z o.o. (Warszawa, Poland). The GRACE risk score was calculated using online tool available at www.gracecsore.org.

The follow-up consisted of outpatient office visit 4–8 weeks after discharge, phone interviews conducted at 6 months and another office visit after 12 months. Visits included a detailed medical interview focused on cardiovascular events (death, MI, need for PCI/CABG, and unplanned hospitalization from cardiovascular events), laboratory tests, cardiac stress testing, and echocardiography. The study endpoint was the occurrence of major

Table 1. Demographic and clinical characteristics of study subjects

Parameter	Value
Age [years], mean ±SD	60.90 ±9.4
Sex (male/female), n (%)	58 (82.9)/12 (17.1)
TnT [ng/mL], mean ±SD	0.148 ±0.139
Hypertension, n (%)*	29 (41.4)
Diabetes, n (%)**	12 (17.1)
Obesity (BMI >30), n (%)	24 (34.3)
Current smokers, n (%)***	49 (70.0)
Past smokers, n (%)****	12 (17.1)
Pain onset to open artery (average time) [min]	380.9
Admission to open artery (average time) [min]	38.9
Pharmacotherapy on admission/at discharge, n (%)	
Acetylsalicylic acid	20 (28.6)/70 (100)
Short-acting nitrates	8 (11.4)/61 (87.1)
Long-acting nitrates	2 (2.9)/0
β-adrenolytics	18 (25.7)/70 (100)
Converting enzyme inhibitor	19 (27.1)/70 (100)
Other antihypertensives	11 (15.7)/0
Statins	24 (34.3)/70 (100)
Oral antidiabetic medications	16 (22.9)/11 (15.7)
Insulin	2 (2.9)/6 (8.6)

TnT – troponin T; BMI – body mass index; * systolic blood pressure ≥140 mm Hg or diastolic blood pressure ≥90 mm Hg, or hypotensive therapy; ** by history/active treatment; *** patients who used any kind of tobacco within 1 year; **** patients who did not use any kind of tobacco for at least 1 year.

adverse cardiovascular events (MACE) defined as at least one of the following:

– cardiac death;
– (another) non-fatal MI;
– necessity of (another) revascularization (PCI in an ACS-related artery or CABG over 30 days from index hospitalization);
– necessity of CABG;
– (another) hospitalization from unstable angina/non-ST elevation MI (NSTEMI) or ST elevation MI (STEMI);
– non-fatal cardiac arrest.

Statistical analysis

Quantitative data was compared to the standardized bell curve with the Lilliefors test (based on the Kolmogorov-Smirnov test). When the data was compatible to normal distribution, a mean and standard deviation (SD) were used (mean ±SD). In other cases, we used a median with the presentation of the 1st and 3rd quartile (Me (Q_{25}; Q_{75})). In most cases, a variance analysis was made with the ANOVA test in the Kruskal-Wallis modification because of the inequality of groups and absence of normal distribution. Verification of the hypothesis and the evaluation of predictive values were made with contingency tables. The hypothesis was analyzed with Fisher's exact test, necessary because of significant differences in quantity of some groups. Cut-off points for serum concentration of biomarkers were assigned. The calculations were made with MedCalc V. 9.5.2.0 (MedCalc Software, Ostend, Belgium). Institutional Review Board approval was obtained for this study.

Results

A follow-up period that lasted 12 months was completed by 100% of patients – 38 (54.3%) of them required another hospitalization for cardiovascular reasons (ACS/PCI), 14 (20%) were diagnosed with MI and 5 (7.1%) died (all from cardiovascular reasons, including sudden cardiac death).

The occurrence of the events is specified in Table 2.

Table 2. Occurrence of events in specified time periods

Occurence of the event	Death (n = 5)	MI (n = 14)	MACE (n = 38)
During hospitalization	3	0	6
From discharge to 6 months	1	6	20
6–12 months	1	8	12

MI – myocardial infarction; MACE – major adverse cardiovascular event.

Pregnancy-associated plasma protein A concentration

The normal range of PAPP-A concentration is <7.15 mlU/L.[11] Mean PAPP-A concentration in our study group was 39.64 mlU/L and there was a significant difference of this parameter in subgroups of patients divided according to the hospital and 6-month GRACE score ($p < 0.001$). The median values were as follows: 21.49 mlU/L (quartile 1st; 3rd – 13.41; 32.65) and 22.61 mlU/L (14.03; 34.1) among patients with low risk in GRACE score, 51.76 mlU/L (35.18; 59.99) and 51.76 mlU/L (28.9; 62.1) among those with intermediate risk, and 68.82 mlU/L (58.54; 83.76) among those with high risk according to GRACE score. When the PAPP-A concentration was assessed in subgroups with 12-month events, the highest mean value was in the group of patients who died (Table 3).

The statistical analysis of PAPP-A concentrations in subgroups specified according to the occurrence of events with receiver operating characteristic (ROC) curve gave cut-off points: 88.63 mIU/L for death (risk of death: 4.5%, 66.7% for patients below and above the threshold, respectively), 88.63 mIU/L for MI (risk of MI: 19.4%, 33.3% for patients below and above the threshold, respectively) and 47.15 mlU/L for MACE (risk of MACE: 42.9%, 71.4% for patients below and above the threshold, respectively). A quantitative analysis of study subjects that exceeded the cut-off PAPP-A concentration and the division into

Table 3. Mean PAPP-A concentration in subgroups with 12-month events (death, infarction, combined endpoint)

Parameter	Dead (n = 5)	Alive (n = 65)	MI (n = 14)	No MI (n = 56)	MACE (n = 38)	No MACE (n = 32)
PAPP-A [mIU/L], mean ±SD	69.47 ±24.48	37.34 ±22.78	49.3 ±22.26	37.61 ±24.29	43.58 ±26.52	34.95 ±20.54
p-value (ANOVA K-W)	0.018		NS (0.073)		NS (0.234)	

MI – myocardial infarction; MACE – major adverse cardiovascular event; PAPP-A – pregnancy-associated plasma protein A; ANOVA K-W – Kruskal-Wallis ANOVA analysis; NS – not significant.

Table 4. Prognostic value of specific PAPP-A cut-off values for 12-month events (death, infarction, combined endpoint)

Event	Dead (n = 5)	Alive (n = 65)	MI (n = 14)	No MI (n = 56)	MACE (n = 38)	No MACE (n = 32)
≥PAPP-A cut-off	2	1	1	2	20	8
PAPP-A cut-off [mIU/L]	88.63		88.63		47.15	
p-value (Fisher's exact test)	0.01		NS (0.49)		0.03	
PPV [%]	66.7		33.3		71.4	
NPV [%]	95.5		80.6		57.1	
Accuracy [%]	94.3		78.6		62.9	

MI – myocardial infarction; MACE – major adverse cardiovascular event; PAPP-A – pregnancy-associated plasma protein A; ≥PAPP-A cut-off – number of patients that exceeded cut-off PAPP-A concentration; PPV – positive predictive value; NPV – negative predictive value; NS – not significant.

subgroups specified according to the occurrence of events are presented in Table 4. Additionally, predictive values have been shown.

The median values of troponin T (TnT) serum concentration tested on admission in subgroups with this uniform cut-off of PAPP-A serum concentration were specifically different (p = 0.01) – 0.15 ng/mL (0.1; 0.25) for PAPP-A ≥40 mIU/L and 0.09 ng/mL (0.06; 0.10) for PAPP-A <40 mIU/L.

We also tested the prognostic value of PAPP-A concentration 40 mIU/L (close to the mean value of PAPP-A serum concentration in our study group) as a universal prognostic threshold (Table 5).

Global Registry of Acute Coronary Events risk score

The median value of the estimated mortality risk during hospitalization in a whole study group according to GRACE scale was 1.15 (0.6; 2.0) and 3.5 (2.0; 5.8) in 6 months from discharge. The median values for categorized GRACE risk score are shown in Table 6.

The median values of the estimated mortality risk during hospitalization and in 6 months from discharge according to GRACE scale in subgroups are shown in Table 7. The highest calculated risks were found in a group of patients that died.

We combined patients with intermediate and high GRACE risk score in one group and compared them with patients with low GRACE risk score. The risk of death was 14.3% in the first group and 0% in the other one. The risk of MI was 34.3% and 5.7% and the risk of MACE was 74.3% and 34.3%, respectively. A quantitative analysis of study subjects with intermediate and high risk on GRACE scale in subgroups is shown in Table 8. Additionally, predictive values have been shown and they revealed a high NPV for death and MI.

Combined analysis of PAPP-A concentration and GRACE score

Based on the prognostic analysis of PAPP-A and GRACE score, we decided to test the composite approach to post-ACS risk stratification. A combined analysis of PAPP-A concentration with cut-off points for subgroups and GRACE score showed significant relations with the occurrence of death and MACE. In MACE group, PPV was 74.1% for in hospital GRACE risk score and 73.1% for 6-month

Table 5. Prognostic value of simplified, uniform PAPP-A cut-off value 40 mIU/L for death, infarction, combined endpoint

Event	Dead (n = 5)	Alive (n = 65)	MI (n = 14)	No MI (n = 56)	MACE (n = 38)	No MACE (n = 32)
PAPP-A ≥40 mIU/L	5	27	10	22	21	11
p-value (Fisher's exact test)	0.017		0.039		NS (0.096)	
PPV [%]	15.6		31.3		65.6	
NPV [%]	100.0		89.5		55.3	
Accuracy [%]	61.4		62.9		60.0	

MI – myocardial infarction; MACE – major adverse cardiovascular event; PAPP-A – pregnancy-associated plasma protein A; PAPP-A ≥ 40 mIU/L – number of patients with PAPP-A serum concentration ≥40 mIU/L; PPV – positive predictive value; NPV – negative predictive value; NS – not significant.

Table 6. Categorized probability of death during hospitalization and in 6 months from discharge according to GRACE scale

Parameter	Low (n = 35)	Intermediate (n = 23)	High (n = 12)
Medians of categorized mortality risk during hospitalization (Q_{25}; Q_{75})	0.6 (0.5; 0.7)	1.6 (1.5; 2.0)	4.9 (4.6; 5.7)
p-value	<0.001		
Parameter	**Low (n = 37)**	**Intermediate (n = 21)**	**High (n = 12)**
Medians of categorized mortality risk in 6 months from discharge (Q_{25}; Q_{75})	2.1 (1.4; 2.6)	5.3 (4.4; 5.8)	12.0 (9.7; 14.3)
p-value	<0.001		

GRACE – Global Registry of Acute Coronary Events.

Table 7. Probability of death during hospitalization and in 6 months from discharge according to GRACE scale in patients subgroups according to follow up events

Event	Dead (n = 5)	Alive (n = 65)	MI (n = 14)	No MI (n = 56)	MACE (n = 38)	No MACE (n = 32)
Probability of death during hospitalization, median (Q_{25}; Q_{75})	4.7 (4.6; 5.0)	1.0 (0.6; 1.6)	1.7 (1.43; 2.73)	1.0 (0.6; 1.63)	1.6 (0.85; 2.98)	0.7 (0.5; 0.33)
p-value (ANOVA K-W)	0.001		NS (0.052)		0.003	
Probability of death in 6 months from discharge, median (Q_{25}; Q_{75})	12.0 (9.7; 14.0)	2.6 (2.0; 5.3)	5.3 (4.4; 6.75)	2.6 (1.9; 5.35)	4.4 (2.6; 7.0)	2.6 (1.55; 3.73)
p-value (ANOVA K-W)	<0.001		0.046		0.004	

GRACE – Global Registry of Acute Coronary Events; MI – myocardial infarction; MACE – major adverse cardiovascular event; ANOVA K-W – Kruskal-Wallis ANOVA analysis; NS – not significant.

Table 8. Predictive value of intermediate/high GRACE score event probability for actual mortality, MI and MACE occurrence at 12-month follow-up

Event	Dead (n = 5)	Alive (n = 65)	MI (n = 14)	No MI (n = 56)	MACE (n = 38)	No MACE (n = 32)
Number of patients with intermediate and high risk of death during hospitalization (GRACE)	5	30	12	23	26	9
p-value (Fisher's exact test)	NS (0.054)		0.006		0.002	
PPV [%]	14.3		34.3		74.3	
NPV [%]	100		94.3		65.7	
Accuracy [%]	51.1		64.3		70	
Number of patients with intermediate and high risk of death in 6 months from discharge	5	28	11	22	24	9
p-value (Fisher's exact test)	0.019		0.014		0.004	
PPV [%]	15.2		33.3		72.7	
NPV [%]	100		91.9		62.2	
Accuracy [%]	60		64.3		67.1	

GRACE – Global Registry of Acute Coronary Events; MI – myocardial infarction; MACE – major adverse cardiovascular event; PPV – positive predictive value; NPV – negative predictive value; NS – not significant.

GRACE risk score. In a group of patients who died, NPV was 95.5% for both GRACE scores.

A combined analysis of PAPP-A concentration with a cut-off point ≥40 mIU/L for subgroups and GRACE score showed significant relations with the occurrence of death, MI and MACE. In a group of patients that died, NPV was 100% for both GRACE scores. In MI group, NPV was 90.2% for in hospital GRACE risk score and 88.4% for 6-month GRACE risk score. In MACE group, PPV was 72.4% for in hospital GRACE risk score and 70.4% for 6-month GRACE risk score.

The analysis of study subjects that exceeded cut-off PAPP-A concentration as well as those with intermediate and high GRACE risk scores with division into subgroups specified according to the occurrence of events are presented in Table 9 for variable cut-offs and in Table 10 for proposed unified cut-off.

Discussion

The assessment of the complications in ACS patients can strongly influence the therapeutic course and post-hospital management. To our knowledge, this is the first study that shows the correlation of plasma levels of PAPP-A and the risk of ACSs, complicated by cardiac death and/

Table 9. Prognostic value of specific PAPP-A cut-off values and intermediate/high GRACE score for 12-month events (death, infarction, combined endpoint)

Event	Dead (n = 5)	Alive (n = 65)	MI (n = 14)	No MI (n = 56)	MACE (n = 38)	No MACE (n = 32)
GRACE in hospital (intermediate and high risk) + ≥PAPP-A cut-off	2	1	1	2	20	7
PAPP-A cut-off [mIU/L]	88.63		88.63		47.15	
p-value (Fisher's exact test)	0.012		NS (0.494)		0.013	
PPV [%]	66.7		33.3		74.1	
NPV [%]	95.5		80.6		58.1	
Accuracy [%]	94.3		78.6		64.3	
GRACE 6 months (intermediate and high risk) + ≥PAPP-A cut-off	2	1	1	2	19	7
PAPP-A cut-off [mIU/L]	88.63		88.63		47.15	
p-value (Fisher's exact test)	0.012		NS (0.494)		0.025	
PPV [%]	66.7		33.3		73.1	
NPV [%]	95.5		78.6		62.9	
Accuracy [%]	94.3		78.6		62.9	

MI – myocardial infarction; MACE – major adverse cardiovascular event; GRACE – Global Registry of Acute Coronary Events; GRACE in hospital – patients with intermediate and high risk of death during hospitalization according to GRACE scale; PAPP-A – pregnancy-associated plasma protein A; ≥PAPP-A cut-off – number of patients that exceeded cut-off PAPP-A concentration; PPV – positive predictive value; NPV – negative predictive value; GRACE 6 months – patients with intermediate and high risk of death in 6 months from hospitalization according to GRACE scale; NS – not significant.

Table 10. Prognostic value of simplified, uniform PAPP-A cut-off value 40 mIU/L and intermediate/high GRACE score for death, infarction and combined endpoint

Event	Dead (n = 5)	Alive (n = 65)	MI (n = 14)	No MI (n = 56)	MACE (n = 38)	No MACE (n = 32)
GRACE in hospital (intermediate and high risk) + PAPP-A ≥40 mIU/L	5	24	10	19	21	8
p-value (Fisher's exact test)	0.001		0.016		0.015	
PPV [%]	17.2		34.5		72.4	
NPV [%]	100		90.2		58.5	
Accuracy [%]	65.7		67.1		64.3	
GRACE 6 months (intermediate and high risk) + PAPP-A >40 mIU/L	5	22	9	18	19	8
p-value (Fisher's exact test)	0.007		0.035		0.048	
PPV [%]	18.5		33.3		70.4	
NPV [%]	100		88.4		55.8	
Accuracy [%]	68.6		67.1		61.4	

MI – myocardial infarction; MACE – major adverse cardiovascular event; GRACE – Global Registry of Acute Coronary Events; GRACE in hospital – patients with intermediate and high risk of death during hospitalization according to GRACE scale; PAPP-A – pregnancy-associated plasma protein A; PAPP-A ≥40 mIU/L – number of patients with PAPP-A serum concentration ≥40 mIU/L; PPV – positive predictive value; NPV – negative predictive value; GRACE 6 months – patients with intermediate and high risk of death in 6 months from hospitalization according to GRACE scale.

or subsequent cardiac events, which can be treated as complementary to current GRACE risk score.

Pregnancy-associated plasma protein A serum concentration

Our study analyzed the relationship of PAPP-A and GRACE score. We were assessing PAPP-A blood concentration within the first 6 h from admission to hospital in a group of patients with symptoms of ACS. The concentration was compared to the risk of death in hospital and 6 months after ACS calculated with GRACE risk score, and to the concentrations of myocardial necrosis biomarkers. A comparison of these calculations to follow-up results helped to estimate predictive values of PAPP-A blood concentration, GRACE risk score and a combination of them. The necessity of identifying a prognostic biomarker that would help to estimate the probability of cardiac events has been postulated over the years.[12] Pregnancy-associated plasma protein A has promising attributes to fulfill the criteria of a new biomarker in the field of cardiology. It was observed that mean PAPP-A serum concentration was the highest in a subgroup of patients that died throughout

the duration of the study (Table 3). Assigning specific cut-off points for PAPP-A concentration (ROC analysis) in subgroups showed that it can provide a strong NPV for the occurrence of death (Table 4). Unified cut-off point (40 mIU/L) resulted in the loss of specificity of PAPP-A concentration for events in single and combined (with GRACE) analysis. However, exceeding this cut-off was tied in with elevated TnT serum concentration tested on admission. In opposite to our findings, some studies have shown that serum concentration of TnT can be in the normal range when PAPP-A serum concentration is increased,[9] but still correlates with cardiovascular risk and with absolute TnT serum concentration.[13]

Global Registry of Acute Coronary Events risk score

The GRACE study involved 250 sites in 30 countries and more than 100,000 patients were recruited. Nine independent risk factors have been identified[14] as those that help to assess the risk of death during hospitalization and in 6 months after discharge.[15] Management and modification in the calculation algorithm reduced the number of statistically significant risk factors to 8, and helped to create a widely available online calculator. It makes risk calculation very accessible and easily assigns risk categories: low, intermediate and high. The risk factors are: age, heart rate, Killip class, initial serum creatinine concentration, elevated initial cardiac markers, cardiac arrest on admission, and ST segment deviation.[14] Risk factors that have the strongest influence in the risk stratification are cardiac arrest on admission and age. Apart from that, the calculator widens a time spectrum of a potential endpoint occurrence to 1 and 3 years from the episode of ACS. In addition, it lets to assess the risk of death and MI 1 year from the episode. Several studies and registries confirmed the utility of GRACE risk score in the last few years, as it showed its dominance over other risk scores and proved that it could be a valid tool in assessing the risk of death even 5 years after discharge from hospital.[16–18] The assessment of GRACE score can help doctors decide the kind and urgency of medical intervention, intensity of chronic treatment and further medical care. All patients with a score >140 (>3% risk of death) should be subjected to coronary angiography within 24 h.[19] In the current analysis, the GRACE risk score showed its efficacy as a negative predictor of death, MI and MACE when divided into categories: low, intermediate and high (Table 8). The PPV of GRACE score was significant for the occurrence of MACE (Table 8).

When we analyzed the combined strategy for variable cut-offs, it resulted in highly specific criteria which might improve the risk stratification in selected populations. The NPV for the occurrence of death was also high. The use of unified cut-off for PAPP-A resulted in the loss of specificity.

Limitations

A relatively small number of hard events (5 deaths, 14 MIs, 32 composite events) was recorded in our small-sized group of 70 patients, which affected the strength of our statistical analysis. Stronger conclusions require a larger size study.

Conclusions

Our analysis revealed that in patients with suspected ACS, GRACE scale has modest accuracy due to low PPV. The PAPP-A serum concentration represents a promising prognostic biomarker with a significantly improved PPV. The GRACE score is superior to stratification based on PAPP-A with regard to combined cut-off point for 1-year mortality, and combining PAPP-A concentration with GRACE score does not improve overall prognostic value.

References

1. Fox KA, Goodman SG, Klein W, et al. Management of acute coronary syndromes. Variations in practice and outcome; findings from the Global Registry of Acute Coronary Events (GRACE). *Eur Heart J*. 2002; 23:1177–1189.
2. Stracke S, Dörr O, Heidt MC, et al. GRACE risk score as predictor of in-hospital mortality in patients with chest pain. *Clin Res Cardiol*. 2010; 99:627–631.
3. Wald NJ, George L, Smith D, et al.; International Prenatal Screening Research Group. Serum screening for Down's syndrome between 8 and 14 weeks of pregnancy. *Br J Obstet Gynaecol*. 1996;103(5):407–412.
4. Wald NJ, Hackshaw AK. Combining ultrasound and biochemistry in first-trimester screening for Down's syndrome. *Prenat Diagn*. 1997; 17:821–829.
5. Nichenametla G, Thomas VS. Evaluation of serum pregnancy associated plasma protein-A & plasma D-dimer in acute coronary syndrome. *J Clin Diagn Res*. 2016;10(1):BC01–BC03.
6. Heeschen C, Dimmeler S, Hamm CW, et al. Pregnancy-associated plasma protein-A levels in patients with acute coronary syndromes: Comparison with markers of systemic inflammation, platelet activation, and myocardial necrosis. *J Am Coll Cardiol*. 2005;45:229–237.
7. Wu XF, Yang M, Qu AJ, et al. Level of pregnancy-associated plasma protein-A correlates with coronary thin-cap fibroatheroma burden in patients with coronary artery disease: Novel findings from 3-vessel virtual histology intravascular ultrasound assessment. *Medicine (Baltimore)*. 2016;95:e2563.
8. Bayes-Genis A, Conover CA, Overgaard MT, et al. Pregnancy-associated plasma protein A as a marker of acute coronary syndromes. *N Engl J Med*. 2001;345:1022–1029.
9. Lund J, Qin QP, Ilva T, et al. Circulating pregnancy-associated plasma protein A predicts outcome in patients with acute coronary syndrome but no troponin I elevation. *Circulation*. 2003;108:1924–1926.
10. Qin QP, Laitinen P, Majamaa-Voltti K, et al. Release patterns of pregnancy associated plasma protein A (PAPP-A) in patients with acute coronary syndromes. *Scand Cardiovasc J*. 2002;36:358–361.
11. eLabDoc – Roche Dialog. https://dialog1.roche.com/pl/pl/elabdoc. Accessed August 24, 2016.
12. Iversen KK, Teisner B, Winkler P, et al. Pregnancy associated plasma protein-A as a marker for myocardial infarction and death in patients with stable coronary artery disease: A prognostic study within the CLARITOR Trial. *Atherosclerosis*. 2011;214:39–40.
13. Heeschen C, Dimmeler S, Hamm CW, et al. Pregnancy-associated plasma protein-A levels in patients with acute coronary syndromes: Comparison with markers of systemic inflammation, platelet activation, and myocardial necrosis. *J Am Coll Cardiol*. 2005;45:229–237.

14. Fox KA, Dabbous OH, Goldberg RJ, et al. Prediction of risk of death and myocardial infarction in the six months after presentation with acute coronary syndrome: Prospective multinational observational study (GRACE). *BMJ*. 2006;333:1091.
15. Bradshaw PJ, Ko DT, Newman AM, et al. Validity of the GRACE (Global Registry of Acute Coronary Events) acute coronary syndrome prediction model for six month post-discharge death in an independent data set. *Heart*. 2006;92:905–909.
16. Yan AT, Yan RT, Tan M, et al. In-hospital revascularization and one-year outcome of acute coronary syndrome patients stratified by the GRACE risk score. *Am J Cardiol*. 2005;96:913–916.
17. Ramsay G, Podogrodzka M, McClure C, et al. Risk prediction in patients presenting with suspected cardiac pain: the GRACE and TIMI risk scores versus clinical evaluation. *QJM*. 2007;100:11–18.
18. Fox KA, Carruthers KF, Dunbar DR, et al. Underestimated and underrecognized: The late consequences of acute coronary syndrome (GRACE UK–Belgian Study). *Eur Heart J*. 2010;31:2755–2764.
19. Roffi M, Patrono C, Collet JP, et al.; ESC Scientific Document Group. 2015 ESC Guidelines for the management of acute coronary syndromes in patients presenting without persistent ST-segment elevation: Task Force for the Management of Acute Coronary Syndromes in Patients Presenting without Persistent ST-Segment Elevation of the European Society of Cardiology (ESC). *Eur Heart J*. 2015;37(3):267–315.

Assessment of the *FTO* gene polymorphisms in male patients with metabolic syndrome

Ryszard Ślęzak[1,A–F], Przemysław Leszczyński[2,B–D,F], Magdalena Warzecha[1,B,C,F], Łukasz Łaczmański[3,C–F], Błażej Misiak[1,A,C–F]

[1] Department of Genetics, Wroclaw Medical University, Poland
[2] Department of Biology and Medical Parasitology, Wroclaw Medical University, Poland
[3] Ludwik Hirszfeld Institute of Immunology and Experimental Therapy, Polish Academy of Science, Wrocław, Poland

A – research concept and design; B – collection and/or assembly of data; C – data analysis and interpretation; D – writing the article; E – critical revision of the article; F – final approval of the article

Advances in Clinical and Experimental Medicine, ISSN 1899-5276 (print), ISSN 2451-2680 (online) *Adv Clin Exp Med.* 2018;27(11):1581–1585

Address for correspondence
Błażej Misiak
E-mail: mblazej@interia.eu

Funding sources
The study was performed within Wroclaw Medical University statutory activities (ST-815).

Conflict of interest
None declared

Received on November 7, 2016
Reviewed on March 23, 2017
Accepted on July 4, 2017

Abstract

Background. Accumulating evidence indicates the potential involvement of the *FTO* gene polymorphisms in the etiology of metabolic syndrome (MetS) and related disorders.

Objectives. In this study, we aimed to investigate whether the *FTO* gene polymorphisms are associated with the risk of MetS and its simple components in a homogeneous sample of males.

Material and methods. Anthropometric and biochemical parameters were assessed in 192 males. A total of 100 males met the National Cholesterol Education Program Adult Treatment Panel III (NCEP-ATPIII) criteria for a diagnosis of MetS. The following *FTO* gene polymorphisms were genotyped: rs1421085, rs17817449, rs1558902, and rs9939609.

Results. There were significant differences between participants with distinct rs9939609 genotypes with respect to waist-to-hip ratio (WHR) and the levels of total cholesterol. Individuals with the rs1421085 CC genotype had significantly higher levels of triglycerides compared to those with other corresponding genotypes. Participants with the rs1558902 AA genotype had significantly higher body mass index (BMI), WHR, as well as the levels of total cholesterol and triglycerides. There were no significant differences in genotype distribution allelic frequencies of all tested polymorphisms between individuals with MetS and control subjects.

Conclusions. Our results indicate that the genetic variation in the *FTO* gene might be related to single metabolic disturbances. However, the *FTO* gene polymorphisms are not associated with the risk of MetS.

Key words: metabolic syndrome, obesity, polymorphism, *FTO* gene

DOI
10.17219/acem/75676

Introduction

Obesity is increasingly being recognized as one of the major health problems and social burdens with a potential impact on future generations.[1] In 2014, the World Health Organization (WHO) revealed that more than 1.9 billion adults are overweight worldwide. Overweight and obesity can lead to a number of metabolic and cardiovascular adversities, such as dyslipidemia, insulin resistance and hypertension, which have been clustered into the condition called metabolic syndrome (MetS). It has been reported that MetS serves as the predictor of severe cardiovascular outcomes and type 2 diabetes. Indeed, it has been estimated that 2.8 million of deaths worldwide can be attributed to the consequences of being overweight or obese.

Several lines of evidence indicate the involvement of genetic and environmental factors, including cultural patterns of dietary habits and feeding behaviors, in the development of obesity and related conditions. In recent years, a special emphasis has been placed on the role of the *FTO* gene in the development of obesity. Indeed, a number of genome-wide association studies (GWASs) have revealed that single nucleotide polymorphisms (SNPs) located in intron 1 of the *FTO* gene confer the risk of obesity in European populations. On the basis of meta-analysis, Wang et al. also revealed that certain *FTO* SNPs (rs9939609, rs8050136 and rs1421085) were associated with the risk of MetS.[2] The majority of more recent studies confirmed these findings.[3–9] However, mechanisms mediating the impact of the *FTO* gene on the development of obesity and related phenotypes remain unclear. Given that these polymorphic variants are intronic, it has been postulated that the *FTO* SNPs act via interactions with genes located in their close proximity.[10] Other potential mechanisms linking the *FTO* gene function with obesity include interactions with dopaminergic neurotransmission within the brain reward circuitry and ghrelin-mediated signaling, as well as the possible role of the *FTO* gene in the regulation of epigenetic processes.[11]

Interestingly, some studies have reported gender effects in the association between the *FTO* gene SNPs and obesity-related phenotypes. For instance, in the study by Saldana-Alvarez et al., the rs1121980 polymorphism was associated with obesity in females only.[12] Another study revealed that the effects of the rs17817449 polymorphism on body weight might be limited to males and postmenopausal women.[13] Therefore, it might be hypothesized that studies investigating the relationship between the *FTO* SNPs and MetS indices should take into account possible gender effects. Thus, the aim of this study was to examine the effects of the *FTO* gene polymorphisms (rs1421085, rs17817449, rs1558902, and rs9939609) on the risk of MetS and its single components in a homogenous sample of male individuals.

Material and methods

Subjects

We recruited 192 males aged 39.7 ±10.2 years. A diagnosis of MetS was established in 100 males based on the National Cholesterol Education Program Adult Treatment Panel III (NCEP-ATPIII) criteria. Other participants, with body mass index (BMI) <25 kg/m^2, were included in the control group. Fasting levels of total cholesterol, low-density lipoproteins (LDL) and high-density lipoproteins (HDL), triglycerides, and glucose were determined using standard procedures. The following anthropometric parameters were measured: weight, height, BMI, waist circumference, hip circumference, and waist-to-hip ratio (WHR).

Genotyping

A multiplex polymerase chain reaction (PCR) assay was designed to amplify 4 fragments of *FTO* containing investigated SNPs (rs1421085, rs17817449, rs1558902, rs9939609). Multiplex PCR was performed with the Phire Hot Start II DNA Polymerase (Thermo Scientific, Waltham, USA). Briefly, the reaction mixture contained: 2 µL of ×5 reaction buffer (provides 1.5 mM $MgCl_2$ in the final ×1 concentration) (Thermo Scientific), 0.7 µL of deoxynucleotides (dNTPs) (40 mM) (Fermentas, Burlington, Canada), 0.5 µL of each primer (10 mM) (Generi Biotech s.r.o., Hradec Králové, Czech Republic), 0.2 µL of Phire Hot Start II DNA Polymerase, 1 µL DNA, in a total volume of 10 µL.

Table 1. Genotype distributions and allelic frequencies of the *FTO* gene polymorphisms

FTO gene polymorphism	Patients with MetS	Controls	χ^2	p-value
rs 1421085	n = 100	n = 91		
CC	27 (27.0)	33 (36.3)	1.91	0.386
CT	46 (46.0)	37 (40.6)		
TT	27 (27.0)	21 (23.1)		
C-allele	100 (50.0)	103 (56.6)	1.35	0.240
T-allele	100 (50.0)	79 (43.4)		
rs17817449	n = 100	n = 92		
GG	27 (27.0)	32 (34.8)	1.52	0.467
GT	52 (52.0)	40 (43.5)		
TT	21 (21.0)	20 (21.7)		
G-allele	106 (53.0)	104 (56.5)	0.28	0.590
T-allele	94 (47.0)	80 (43.5)		
rs1558902	n = 100	n = 90		
TT	29 (29.0)	36 (40.0)	2.69	0.261
TA	45 (45.0)	36 (40.0)		
AA	26 (26.0)	18 (20.0)		
T-allele	103 (51.5)	108 (60.0)	2.20	0.140
A-allele	97 (48.5)	72 (40.0)		
rs9939609	n = 100	n = 88		
TT	34 (34.0)	38 (43.2)	1.67	0.434
TA	45 (45.0)	34 (38.6)		
AA	21 (21.0)	16 (18.2)		
T-allele	113 (56.5)	110 (62.5)	0.89	0.350
A-allele	87 (43.5)	66 (37.5)		

Data expressed as the number of subjects (%); MetS – metabolic syndrome.

The reaction was performed in a PTC-200 thermal cycler (MJ Research Inc., St. Bruno, Canada) with the following reaction parameters: 95°C for 1 min 30 s, 35 cycles at 95°C for 20 s, 60°C for 20 s, 72°C for 15 s, and 72°C for 1 min 30 s final extension. Multiplex PCR products were checked for quality and yield by running 5 µL in 2% agarose–Tris-borate-EDTA gel, stained Sybr Green and visualized on a UV light transilluminator. Multiplex PCR products were purified using enzymatic digestion. In the study, 1 µL of multiplex PCR was treated with 1.5 µL of Clean-up enzyme mix (1 U of fast alkaline phosphatase and 10 U of Exo1) at 37°C for 15 min. SNaPshot analysis was performed using the SNaPshot Multiplex kit (Applied Biosystems, Woolston, Warrington, UK). Reactions were performed in a final volume of 5.5 µL, containing 2.5 µL of purified multiplex PCR product, 2.5 µL of SNaPshot Ready Multiplex Reaction Mix and 0.5 µL of equimolar probe mix (each probe at 2 mol/L final concentration). Multiplex single base extensions were carried out for 25 cycles with the following reaction parameters: 10 s at 96°C, 5 s at 50°C and 30 s at 60°C. SNaPshot products were then treated at 37°C for 1 h with 1 µL of fast alkaline phosphatase (1 U/µL) (Fermentas International Inc., Burlington, Canada). Fast alkaline phosphatase was inactivated for 15 min at 75°C. The labeled products were mixed with 9.5 µL of Hi-Di Formamide and 0.5 µL of Genescan-120LIZ size standard (Applied Biosystems). They were then separated using a 15-minute run on an ABI 310 DNA sequencer with POP-4 matrix (Applied Biosystems) and 10-second injection time. Fragment analyzes were performed on the Gene Marker software v. 1.85 (SoftGenetics, Centre County, State College, USA).

Statistical analysis

The Hardy-Weinberg (HWE) equilibrium was evaluated by comparing observed and expected genotype distributions using the χ^2 test. The χ^2 test was also used to compare the distribution of genotypes and allelic frequencies between patients with MetS and control subjects. Effects of distinct FTO genotypes on biochemical and anthropometric parameters were tested using the Kruskal-Wallis test. Adjustment for multiple testing was performed using Bonferroni correction, taking into account the number of tested polymorphisms. All tests were two-tailed with a 0.05 level of significance. Statistical analysis was performed using the STATISTICA software v. 12.5 (SPSS Inc., Chicago, USA).

Results

Genotype distributions for all polymorphisms genotyped in this study were in agreement with the HWE. There were no significant differences in genotype distributions and allelic frequencies between patients with MetS and healthy controls (Table 1). The analysis of the *FTO* gene polymorphisms with respect to anthropometric and biochemical parameters in both groups (patients with MetS and healthy controls) is presented in Table 2. In both groups, the rs9939609 AA genotype was associated with a significantly higher WHR and total cholesterol levels compared to other corresponding genotypes. Additionally, this genotype was related to higher BMI at the trend level significance. The level of triglycerides was significantly higher in individuals with the rs1421085 CC genotype in comparison with those with other rs1421085 genotypes. Finally, the rs1558902 AA homozygotes had significantly higher BMI, WHR, total cholesterol, and triglycerides than subjects with other corresponding genotypes. However, none of these differences were significant after Bonferroni correction ($p > 0.0125$). The *FTO* rs17817449 polymorphism was not significantly associated with biochemical and anthropometric parameters.

Discussion

The *FTO* gene is located on chromosome 16 and it consists of 9 exons; however, SNPs analyzed in our study are located in intron 1. The expression of the *FTO* gene has been described in the brain and adrenal glands. It has been demonstrated that the *FTO* gene exerts biological activity via the effects on DNA methylation of genes encoding transcription factors.[14] Upregulated *FTO* gene expression has been reported mainly within hypothalamic nuclei, which accounts for energy expenditure.[15] In addition, the expression of the *FTO* gene might be regulated by starvation and satiety signals. The *FTO* gene might also be involved in the regulation of hypothalamic-pituitary-adrenal axis functioning and lipolysis.[15] It also has been found that it might impact the sympathetic nervous system regulating the cardiovascular system and blood pressure.[16] Interestingly, the *FTO* gene expression might be regulated by estrogens, pointing to the widely-reported sex differences in obesity phenotypes.[17]

In this study, we found that neither of the tested *FTO* gene polymorphisms was associated with the risk of MetS development. However, we demonstrated that the *FTO* gene polymorphisms, except for the rs17817449 polymorphic variant, might impact certain metabolic parameters, including BMI and WHR, as well as the levels of total cholesterol and triglycerides. Although recent meta-analyses revealed that the *FTO* gene polymorphisms (rs9939609, rs8050136 and rs1421085) might be associated with the risk of MetS, authors indicated that ethnic differences and the use of various MetS criteria might impact effect sizes.[2,9] Therefore, the association of the *FTO* gene polymorphisms might hold true only in certain populations, depending also on MetS conceptualization.

Our findings are in agreement with previous GWASs, showing that the *FTO* gene polymorphisms might confer the risk of MetS. Importantly, in the majority of previous

Table 2. Effects of the *FTO* gene polymorphisms on metabolic parameters in the whole group of participants

Parameter	rs9939609 mean ±SD			p-value	rs 1421085 mean ±SD			p-value	rs17817449 mean ±SD			p-value	rs1558902 mean±SD			p-value
	TT	AT	AA		TT	TC	CC		TT	TG	GG		TT	TA	AA	
Height [cm]	179 ±6.18	177 ±6.18	177 ±6.22	0.212	179 ± 6.53	177 ± 6.15	177 ± 5.68	0.520	179 ± 5.96	178 ± 6.29	177 ±6.10	0.222	179 ± 5.79	177 ± 6.51	177 ± 5.87	0.061
Weight [kg]	82.5 ±11.2	85.7 ±12.6	88.0 ±18.4	0.238	82.1 ±10.6	85.8 ±14.6	86.4 ±14.5	0291	82.7 ±10.7	85.9 ±14.0	84.9 ±15.6	0.408	82.4 ±12.2	85.7 ±13.5	96.7 ±15.0	0.184
BMI [kg/m^2]	25.9 ±3.99	27.4 ±4.21	28.1 ±5.66	0.077	25.9 ±0.86	27.4 ±4.73	27.5 ±4.72	0.139	26 ±3.47	27.3 ±4.76	27.2 ±5.13	0.210	25.8 ±4.14	27.4 ±4.48	27.7 ±4.87	0.046*
Waist circumference [cm]	92.4 ±8.7	94.7 ±9.8	97.1 ±13.0	0.148	92.1 ±8.2	95.0 ±10.8	95.6 ±11.1	0.223	92.1 ±8.1	95.2 ±10.4	94.8 ±12.0	0.127	91.9 ±8.8	95.0 ±10.4	96.2 ±11.4	0.109
Hip circumference [cm]	103 ±5.11	103 ±5.61	104 ±8.0	0.918	103 ± 4.62	104 ± 6.48	104 ± 6.42	0.716	103 ±5.04	104 ±5.90	103 ±7.18	0.486	103 ±5.27	104 ±6.05	104 ±6.75	0.862
WHR	0.90 ±0.06	0.91 ±0.07	0.93 ±0.06	0.032*	0.9 ± 0.08	0.91 ±0.07	0.92 ±0.06	0.08	090 ±0.05	0.92 ±0.07	0.92 ±0.06	0.067	0.89 ±0.05	0.91 ±0.07	0.93 ±0.06	0.013*
LDL [mmol/L]	3.05 ±0.77	3.31 ±0.91	3.38 ±0.94	0.122	3.11 ±0.79	3.25 ±0.94	3.29 ±0.88	0.607	3.13 ±0.8	3.29 ±0.92	3.17 ±0.89	0.475	3.04 ±0.71	3.27 ±0.97	3.36 ±0.87	0.173
HDL [mmol/L]	1.4 ±0.33	1.47 ±0.44	1.39 ±0.28	0.393	1.39 ±0.33	1.43 ±0.41	1.51 ±0.4	0.275	1.4 ±0.33	1.43 ±0.4	1.50 ±0.42	0.549	1.44 ±0.39	1.44 ±0.43	1.44 ±0.30	0.887
Total cholesterol [mmol/L]	5.12 ±0.94	5.5 ±0.97	5.47 ±0.92	0.035*	5.09 ±0.87	5.41 ±1.05	5.55 ±0.90	0.065	5.17 ±0.99	5.40 ±1.0	5.44 ±0.88	0.259	5.1 ±0.82	5.41 ±1.04	5.59 ±0.93	0.026*
Triglycerides [mmol/L]	1.48 ±0.91	1.67 ±1.09	2.1 ±1.48	0.067	1.40 ±0.93	1.76 ±1.19	1.85 ±1.21	0.034*	1.44 ±0.94	1.70 ±1.13	1.61 ±1.32	0.096	1.36 ±0.76	1.77 ±1.22	1.96 ±1.31	0.019*
Glucose [mmol/L]	5.74 ±069	5.86 ±1.03	5.84 ±0.61	0.632	5.83 ±0.76	5.88 ±1.01	5.71 ±0.63	0.870	5.76 ±0.75	5.85 ±0.98	5.79 ±0.6	0.760	5.87 ±0.71	5.85 ±1.02	5.78 ±0.65	0.953

SD – standard deviation; BMI – body mass index; WHR – waist-to-hip ratio; LDL – low-density lipoproteins; HDL – high-density lipoproteins; * significant differences ($p < 0.05$).

studies, the *FTO* gene polymorphisms were related to single metabolic parameters, including anthropometric measures and the levels of glucose, HDL or triglycerides, highlighting the potential involvement of this gene in the etiology of obesity.[18–20] In agreement with our results, previous studies have repeatedly reported the association between the *FTO* rs9939609 polymorphism and BMI.[19–21] More specifically, the A allele within this polymorphic site has been related to higher BMI. Similar results were also obtained by Al-Attar et al., who found the association between the *FTO* rs9939609 AA genotype and higher BMI (at the trend level significance) and WHR (significant association).[22] In addition, there are studies showing the impact of this polymorphism on the risk of cardiovascular diseases and type 2 diabetes.[18,23,24] Finally, in a study by Freathy et al., this polymorphism was associated with higher levels of glucose and triglycerides as well as lower levels of HDL that appeared due to the effect on BMI.[25]

Similar results have been reported with respect to other SNPs analyzed in this study. Regarding rs1558902, no significant effects on MetS risk have been demonstrated. However, this SNP has been related to higher BMI and fasting levels of glucose.[6,26] Other SNPs tested in our study (rs1421085 and rs17817449) have been found to impact BMI and WHR. Interestingly, in the study by Harbron et al., risk alleles of the rs1421085 and rs17817449 SNPs predicted poor eating behaviors (higher hunger, internal locus of hunger and emotional disinhibition) and a higher intake of high fat foods and refined starches.[27]

Our study has some limitations that should be taken into account. Firstly, our sample size was relatively low and thus it cannot be excluded that negative results with respect to the impact of the *FTO* gene SNPs on MetS risk or other metabolic parameters are simply due to a lack of statistical power. Another point is that a number of variables connected to lifestyle factors and eating behaviors have not been included in this study. Therefore, more precise conclusions on causality cannot be established. Another point is that our analysis was confined to the assessment of a limited number of metabolic parameters, restricting the conclusions regarding the biological mechanisms that might mediate the effects of the *FTO* gene SNPs on obesity and related outcomes. Finally, caution should be taken in interpreting the association between the *FTO* SNPs and anthropometric or biochemical parameters in the whole group of participants, since significant results of the statistical analysis that was unadjusted for multiple testing were not significant after Bonferroni correction.

In conclusion, the results of our study indicate that the *FTO* gene might impact single metabolic parameters, rather than a clustering of cardio-metabolic disturbances conceptualized as MetS. Future studies should investigate the effects of the *FTO* SNPs on obesity and related conditions in bigger samples with comprehensive assessment of cardio-metabolic parameters, environmental factors and eating behaviors.

References

1. Hanson M, Gluckman P, Bustreo F. Obesity and the health of future generations. *Lancet Diabetes Endocrinol*. 2016;4(12):966–967.
2. Wang H, Dong S, Xu H, Qian J, Yang J. Genetic variants in *FTO* associated with metabolic syndrome: A meta- and gene-based analysis. *Mol Biol Rep*. 2012;39:5691–5698.
3. de Luis DA, Aller R, Conde R, Izaola O, de la Fuente B, Sagrado MG. Relation of the rs9939609 gene variant in *FTO* with metabolic syndrome in obese female patients. *J Diabetes Complications*. 2013;27: 346–350.
4. Elouej S, Nagara M, Attaoua R, et al. Association of genetic variants in the *FTO* gene with metabolic syndrome: A case-control study in the Tunisian population. *J Diabetes Complications*. 2016;30:206–211.
5. Hu YH, Liu JM, Zhang M, et al. Association between polymorphisms of fat mass and obesity-associated gene and metabolic syndrome in Kazakh adults of Xinjiang, China. *Genet Mol Res*. 2015;14:14597–14606.
6. Kawajiri T, Osaki Y, Kishimoto T. Association of gene polymorphism of the fat mass and obesity associated gene with metabolic syndrome: A retrospective cohort study in Japanese workers. *Yonago Acta Med*. 2012;55:29–40.
7. Liguori R, Labruna G, Alfieri A, Martone D, Farinaro E, Contaldo F. The *FTO* gene polymorphism (rs9939609) is associated with metabolic syndrome in morbidly obese subjects from southern Italy. *Mol Cell Probes*. 2014;28:195–199.
8. Yang J, Liu J, Li W, Li X, He Y, Ye L. Genetic association study with metabolic syndrome and metabolic-related traits in a cross-sectional sample and a 10-year longitudinal sample of Chinese elderly population. *PLoS ONE*. 2014;9:e100548.
9. Zhou D, Liu H, Zhou M, et al. Common variant (rs9939609) in the *FTO* gene is associated with metabolic syndrome. *Mol Biol Rep*. 2012;39: 6555–6561.
10. Merkestein M, Sellayah D. Role of *FTO* in adipocyte development and function: Recent insights. *Int J Endocrinol*. 2015; Article ID 521381.
11. Tung YC, Yeo GS, O'Rahilly S, Coll AP. Obesity and *FTO*: Changing focus at a complex locus. *Cell Metab*. 2014;20:710–718.
12. Saldana-Alvarez Y, Salas-Martinez MG, Garcia-Ortiz H, et al. Gender-dependent association of *FTO* polymorphisms with body mass index in Mexicans. *PLoS ONE*. 2016;11:e0145984.
13. Hubacek JA, Pitha J, Adamkova V, Lanska V, Poledne R. A common variant in the *FTO* gene is associated with body mass index in males and postmenopausal females but not in premenopausal females. Czech post-MONICA and 3PMFs studies. *Clin Chem Lab Med*. 2009;47: 387–390.
14. Wu Q, Saunders RA, Szkudlarek-Mikho M, Serna Ide L, Chin KV. The obesity-associated *FTO* gene is a transcriptional coactivator. *Biochem Biophys Res Commun*. 2010;401:390–395.
15. Yeo GS, O'Rahilly S. Uncovering the biology of *FTO*. *Mol Metab*. 2012; 1(1–2):32–36.
16. Fawcett KA, Barroso I. The genetics of obesity: *FTO* leads the way. *Trends Genet*. 2010;26(6):266–274.
17. Zhang Z, Zhou D, Lai Y, Liu Y, Tao X, Wang Q. Estrogen induces endometrial cancer cell proliferation and invasion by regulating the fat mass and obesity-associated gene via PI3K/AKT and MAPK signaling pathways. *Cancer Lett*. 2012;319:89–97.
18. Binh TQ, Phuong PT, Nhung BT, Thoang DD, Lien HT, Thanh DV. Association of the common *FTO*-rs9939609 polymorphism with type 2 diabetes, independent of obesity-related traits in a Vietnamese population. *Gene*. 2013;513(1):31–35.
19. Dusatkova L, Zamrazilova H, Sedlackova B, Vcelak J, Hlavaty P, Aldhoon Hainerova I. Association of obesity susceptibility gene variants with metabolic syndrome and related traits in 1,443 Czech adolescents. *Folia Biol (Praha)*. 2013;59(3):123–133.
20. Hunt SC, Stone S, Xin Y, Scherer CA, Magness CL, Iadonato SP. Association of the *FTO* gene with BMI. *Obesity (Silver Spring)*. 2008;16: 902–904.
21. Scuteri A, Sanna S, Chen WM, Uda M, Albai G, Strait J. Genome-wide association scan shows genetic variants in the *FTO* gene are associated with obesity-related traits. *PLoS Genetics*. 2007;3:e115.
22. Al-Attar SA, Pollex RL, Ban MR, et al. Association between the *FTO* rs9939609 polymorphism and the metabolic syndrome in a non-Caucasian multi-ethnic sample. *Cardiovasc Diabetol*. 2008;7:5.
23. Karaderi T, Drong AW, Lindgren CM. Insights into the genetic susceptibility to type 2 diabetes from genome-wide association studies of obesity-related traits. *Curr Diab Rep*. 2015;15:83.
24. Liu C, Mou S, Pan C. The *FTO* gene rs9939609 polymorphism predicts risk of cardiovascular disease: A systematic review and meta-analysis. *PLoS ONE*. 2013;8:e71901.
25. Freathy RM, Timpson NJ, Lawlor DA, et al. Common variation in the *FTO* gene alters diabetes-related metabolic traits to the extent expected given its effect on BMI. *Diabetes*. 2008;57:1419–1426.
26. Hotta, K, Nakata Y, Matsuo T, et al. Variations in the *FTO* gene are associated with severe obesity in the Japanese. *J Hum Genet*. 2008;53: 546–553.
27. Harbron J, van der Merwe L, Zaahl MG, Kotze MJ, Senekal M. Fat mass and obesity-associated (*FTO*) gene polymorphisms are associated with physical activity, food intake, eating behaviors, psychological health, and modeled change in body mass index in oveweight/obese Caucasian adults. *Nutrients*. 2014;6(8):3130–3152.

Analysis of peripheral nerve and autonomic nervous system function and the stage of microangiopathy in patients with secondary Raynaud's phenomenon in the course of connective tissue diseases

Izabela Gosk-Bierska[1,A], Maria Misterska-Skóra[2,B], Marta Wasilewska[1,B], Małgorzata Bilińska[3,C], Jerzy Gosk[4,D], Rajmund Adamiec[1,E], Magdalena Koszewicz[3,A,C]

[1] Department of Angiology, Hypertension and Diabetology, Wroclaw Medical University, Poland
[2] Department and Clinic of Rheumatology and Internal Medicine, Wroclaw Medical University, Poland
[3] Department and Clinic of Neurology, Wroclaw Medical University, Poland
[4] Clinical Department of Traumatology and Hand Surgery, Wroclaw Medical University, Poland

A – research concept and design; B – collection and/or assembly of data; C – data analysis and interpretation; D – writing the article; E – critical revision of the article; F – final approval of the article

Advances in Clinical and Experimental Medicine, ISSN 1899-5276 (print), ISSN 2451-2680 (online) *Adv Clin Exp Med.* 2018;27(11):1587–1592

Address for correspondence
Magdalena Koszewicz
E-mail: magdalena.koszewicz@umed.wroc.pl

Funding sources
None declared

Conflict of interest
None declared

Received on April 14, 2017
Reviewed on May 7, 2017
Accepted on July 1, 2017

Abstract

Background. The pathogenesis of secondary Raynaud's phenomenon (SRP) associated with connective tissue diseases (CTD) is not entirely understood. Nervous system dysfunction and microangiopathy are considered to be causes of this pathology.

Objectives. Peripheral and autonomic nervous system function, the stage of microangiopathy, and the relationships between these in patients with SRP were analyzed.

Material and methods. In the study, 20 patients with CTD-related SRP and 30 healthy controls were subject to capillaroscopy, standard conduction velocity tests and conduction velocity distribution (CVD) tests in ulnar and peroneal nerves, heart rate variability (HRV), and sympathetic skin response (SSR) tests.

Results. There were no significant differences in the standard motor and sensory conduction velocity tests, or in CVD tests in the ulnar and peroneal nerves in SRP patients compared with the controls. The patients with SRP had a significantly lower SSR amplitude and longer latency in hands and feet. The patients with CTD-related SRP had a significantly lower mean HRV with higher low frequency (LF) values in the spectral analysis and expiration/inspiration ratio (E/I) during deep breathing. There was no correlation between the stage of microangiopathy and neurophysiological test results.

Conclusions. Correct standard conduction velocity and CVD testing in patients with SPR suggest that vasomotor disturbances may occur in CTD regardless of peripheral neuropathy. The lack of relationship between SSR and microangiopathy could confirm that these 2 processes occur independently in patients with CTD-related SRP. Autonomic nervous system impairment together with normal peripheral nerve function suggest the central origin of CTD-related SRP.

Key words: microangiopathy, connective tissue diseases, secondary Raynaud's syndrome, peripheral nerves, autonomic nervous system

DOI
10.17219/acem/75618

Introduction

Raynaud's phenomenon (RP) occurs as recurrent episodes of the discoloration of fingers and/or toes in the course of reversible vasospasm in response to cold or to emotional stress.[1] Primary Raynaud's phenomenon (PRP) is diagnosed if the symptoms are idiopathic. Secondary Raynaud's phenomenon (SRP) is associated with different underlying diseases. SRP is a characteristic – although not specific – symptom of connective tissue diseases (CTD). SRP can overtake the development of the underlying disease by as much as several years, and, therefore, requires special observation. SRP occurs in 80% of patients with scleroderma, 10–35% of those with systemic lupus erythematosus, and 30% of dermatomyositis patients; it is the 1st symptom of the disease in about 33% of systemic connective tissue diseases (CTD).[2–6]

Microangiopathy and nervous system dysfunctions are considered to be the causes of SRP in patients with CTD. Clinical symptoms in PRP are only a consequence of vasomotor disturbances without anatomical changes of the microcirculation; thus, in capillaroscopy the correct shape and number of loops arranged in parallel series are seen. SRP in the course of CTD, after periods of vasomotor disturbances of varying length, appears as organic microvascular changes, which lead to skin ulceration and/or necrosis of the fingers. Microangiopathy observed in nailfold capillaroscopy is a harbinger of digital necrosis and ulcers.[3] The Maricq's et al. classification assesses the degree of microvascular damage, including morphological evaluation of the loops and their environment, and can be used in predicting the severity of vascular lesions.[6]

Peripheral nerve damage is observed in the course of CTD. The presence of specific antibodies, the deposition of immune complexes in peripheral nerves, and ischemic nerve injury secondary to vasculitis (vasa perineurium and vasa nervorum) are thought to be the main causes of neuropathy.[7–10] In systemic lupus erythematosus (SLE), nervous system dysfunction is present in 19–38% of cases, and the most common forms are multiple mononeuropathy, subacute or chronic axonal polyneuropathy, predominantly sensory, cranial neuropathy, and autonomic dysfunction.[11] Mixed axonal polyneuropathy, multiple mononeuropathy, cranial neuropathy (nerves V and VIII with sudden bilateral hearing loss, and mild paroxysmal positional vertigo), compression syndromes, and myositis might occur in about 36% of patients with systemic scleroderma. Multiple mononeuropathies are particularly common in CREST syndrome – calcinosis, Raynaud's syndrome, esophageal dysmotility, sclerodactyly, teleangiectasia.[7] Distal sensory neuropathy, carpal tunnel syndrome and other entrapment syndromes, and root syndrome as a result of the destruction of vertebral subluxation of the cervical spine are observed in rheumatoid arthritis.[12] Thus, both microvascular disorder and peripheral nerve changes may influence the occurrence of SRP in patients with CTD.

The aim of our study was to analyze the peripheral nerve and autonomic nervous system function, the stage of microangiopathy and possible relationships between these in patients with Raynaud's phenomenon secondary to CTD.

Material and methods

The studies were approved by the Ethics Committee of Wroclaw Medical University, Poland. All patients gave their informed consent.

We investigated 20 patients (3 men, 17 women; mean age 49.1 ±11.8 years old) with CTD-related SRP, and 30 healthy, age- and sex-matched controls. The following patients were excluded from the study: those with neurological disorders, primarily with neuropathy, compression syndrome (thoracic outlet syndrome, carpal tunnel syndrome), diabetes mellitus, malignancy, with exposure to neurotoxins and pharmacological treatment influencing the vascular and/or autonomic nervous system, alcohol addiction, tobacco addiction, with limb ischemia (atherosclerosis, thromboangiitis obliterans, Takayasu's arteritis, hammer mild syndrome, vibration disease) and other dermatological abnormalities. To identify patients with these diseases, we analyzed medical histories; detailed neurological, orthopedic, and vascular examinations were performed as well. All patients underwent chest and cervical spine X-rays.

The following laboratory tests were performed on all patients using standard methods: complete blood cell count, erythrocyte sedimentation rate (ESR), rheumatoid factor, serum protein electrophoresis, immunoglobulin assessment, thyroid-stimulating hormone (TSH), anti-neutrophil cytoplasmic antibody tests (ANCA), c-cytoplasmic, p-perinuclear pattern, antinuclear antibody (ANA), Scl-70, SS-A (Ro), SS-B (La) antibody tests, and standard chemical screening.

Neurophysiological tests were performed on all subjects using Viking Select and Viking Quest Nicolet Biomedical devices (Nicolet Biomedical Inc., Madison, USA). Nerve conduction velocity tests (sensory and motor with F-wave estimation) were performed in median (in order to exclude carpal tunnel syndrome), ulnar and peroneal (sural) nerves using standard methods together with conduction velocity distribution (CVD) tests in ulnar and peroneal nerves. In the CVD test, we analyzed motor velocity ranges as the 10th, 50th and 90th percentiles of the velocities.[13] Heart rate variability (HRV) was assessed at rest and during deep breathing. We analyzed R-R interval variability, shown as a percentage, and the expiration/inspiration ratio (E/I), when the subject breathed at a rate of 6 breaths per minute. We used spectral analysis of R-R intervals with an estimation of low-frequency (LF, range between 0.04 Hz and 0.15 Hz) and high-frequency (HF, range between 0.15 Hz and 0.4 Hz) bands together with the LF/HF ratio. The sympathetic skin response (SSR) test was performed

using the standard method (electrical stimulation of the right median nerve, recording from the left hand and foot).[14–17]

The subclavian, axillar, brachial, ulnar, and radial arteries were investigated via duplex ultrasound (GE Vivid 7, GE Healthcare, Little Chalfont, Great Britain) using a standard 9 MHZ imaging probe (UST5539). The standard protocol in the laboratory included cross-sectional and longitudinal gray-scale and color Doppler imaging.[18]

A nailfold capillaroscopy examination was performed via widefield capillary microscopy using a Nikon SMZ 800 stereomicroscope (Nicon Instruments, Tokyo, Japan). All fingers except the thumbs were examined. Immersion oil was used to improve the transparency of the skin. Capillaries were viewed under 40-fold magnification. Room temperature was between 20 and 22°C.

On the basis of the Maricq's classification, we identified 2 groups depending on the morphological changes in the capillaries (NC group – patients with normal capillaries; DC group – patients with enlarged and/or deformed capillary loops) and 2 groups depending on the presence of avascular areas (AZ group – patients with a reduced number of capillaries or avascular zones; NAZ group – patients without avascular zones and a normal number of capillaries).[6,19]

The statistical analyses were performed using STATISTICA v. 5.0 PL (StatSoft, Tulsa, USA). Statistical significance was set at $p < 0.05$. Differences in baseline demographic and clinical variables were tested for significant differences between groups with ANOVA for continuous variables and Pearson's χ^2 test for categorical variables. The Student's t-test and the Wilcoxon rank-sum test (when parameters were not distributed normally) were used to test for differences in the analyzed parameters between patients with Raynaud's phenomenon vs controls, and patients with microangiopathy vs patients without microangiopathy.

Results

In both groups, most of the patients were women (SRP – 85%, controls – 83%).

A total of 60% of patients manifested biphasic color changes (white and cyanotic phases without a red phase). The location of RP varied. RP was observed in 4 patients only in the hands.

All upper and lower extremities were the most common locations for RP. Only 15% of the patients presented additional locations of RP (earlobes, tip of the nose, penis).

The exact demographic and clinical characterization, including the etiology of SRP and the severity of microangiopathy, are presented in Table 1.

Standard neurophysiological test results (motor and sensory conduction in ulnar and peroneal nerves) were normal in all individuals. There were no significant statistical differences in the conduction velocity distribution in the ulnar and peroneal nerves in the group with SRP compared with the control group (Table 2).

In patients with SRP, a significantly lower SSR amplitude and a longer latency were shown in relation to the control group. Changes were more pronounced in the lower limbs (Table 3). The study showed a complete lack of SSR in upper and lower limbs in 2 patients (1 with scleroderma and 1 with SLE), and lack of SSR in the lower limbs in another 2 patients (1 individual with undifferentiated connective tissue disease and 1 individual with scleroderma). Lack of SSR was found in patients with varying severities

Table 1. Demographic and clinical data for patients with SRP

Variables	Data
Age [years]	49.1 ±11.8
Female/male	17/3
Mean duration of SRP [years]	9.8 (range 5–19)
Underlying disease:	
scleroderma	12 (60%)
systemic lupus erythematosus	3 (15%)
rheumatoid arthritis	2 (10%)
undifferentiated connective tissue disease	3 (15%)
Microangiopathy in capillaroscopy:	
normal capillaries	4 (20%)
dilatation of capillaries (loops giants)	16 (80%)
normal numbers of capillaries	6 (30%)
the presence of avascular zone	14 (70%)
Color changes during SRP	
triphasic (pallor, cyanosis, redness)	8 (40%)
biphasic (pallor, cyanosis)	12 (60%)
Localization of SRP	
upper limbs only:	4 (20%)
– fingers II, IV and V of right hand and fingers II–IV of left hand,	1
– fingers II–V of both hands,	2
– fingers II–IV of both hands	1
upper and lowers limbs:	13 (65%)
– fingers II–V of both hands and all toes of both feet,	8
– fingers II, III, V of right hand, fingers III, IV of left hand and all toes of both feet,	1
– fingers II, III of right hand, fingers III, IV of left hand and all toes of both feet,	1
– all fingers of both hands and all toes of both feet	3
limbs and other localization:	3 (15%)
– whole hands and feet, earlobes, tip of the nose, penis,	1
– fingers II–V of both hands and all toes of both feet, earlobes, tip of the nose,	1
– all fingers of both hands and all toes of both feet, tip of the nose	1
Sclerodactylia	6 (30%)
Tingling, numbness, stinging, burning of fingers:	
– at the time of the RP,	18 (90%)
– permanent	8 (40%)
Stiffness of the fingers or toes	6 (30%)
Subjective reduction of sensation in fingers or toes	6 (30%)
Pain in small joints of hands	10 (50%)

SRP – secondary Raynaud's phenomenon.

Table 2. Comparison of conduction velocity distribution in study groups and subgroups

SRP vs control CVD [m/sec]	SRP (n = 20)	Control (n = 30)	p-value
Ulnar nerve			
CVD 10%	45.5 ±7.1	47.5 ±5.5	ns
CVD 50%	51.2 ±7.1	54.3 ±5.4	ns
CVD 90%	57.1 ±6.6	59.1 ±6.1	ns
Peroneal nerve			
CVD 10%	39.9 ±2.1	40.7 ±2.5	ns
CVD 50%	43.9 ±2.5	45.1 ±2.8	ns
CVD 90%	46.9 ±2.4	48.4 ±2.6	ns
NC vs DC CVD [m/s]	**NC (n = 4)**	**DC (n = 16)**	**p-value**
Ulnar nerve			
CVD 10%	46.1 ±6.7	45.2 ±6.4	ns
CVD 50%	50.8 ±9.5	51.3 ±5.7	ns
CVD 90%	56.4 ±6.8	57.4 ±6.9	ns
Peroneal nerve			
CVD 10%	38.9 ±2.1	39.4 ±2.3	ns
CVD 50%	43.1 ±2.1	43.4 ±2.4	ns
CVD 90%	45.9 ±1.7	46.4 ±2.4	ns
NAZ vs AZ CVD [m/s]	**NAZ (n = 8)**	**AZ (n = 12)**	**p-value**
Ulnar nerve			
CVD 10%	46.5 ±6.4	44.1 ±6.5	ns
CVD 50%	51.7 ±8.1	50.5 ±5.7	ns
CVD 90%	57.6 ±7.4	56.2 ±5.7	ns
Peroneal nerve			
CVD 10%	39.3 ±2.1	39.3 ±2.6	ns
CVD 50%	43.6 ±2.1	42.7 ±2.4	ns
CVD 90%	46.5 ±2.3	45.7 ±2.1	ns

CVD – conduction velocity distribution; SRP – secondary Raynaud's phenomenon; NC – normal capillaries; DC – dilatation of capillaries (giant loops); NAZ – no avascular zone (normal numbers of capillaries); AZ – the presence of an avascular zone; ns – non-significant.

Table 3. Comparison of sympathetic skin response (SSR) between study groups and subgroups

SRP vs control	SRP (n = 20)	Controls (n = 30)	p-value
Palm latency [ms]	1,544 ±163	1,522 ±116	0.04393
Palm amplitude [mV]	2,155 ±1,809	3,122 ±1,815	0.00298
Foot latency [msec]	2,416 ±562	2,174 ±237	0.03798
Foot amplitude [mV]	944 ±847	2,230 ±1,221	0.00041
NC vs DC	**NC (n = 4)**	**DC (n = 16)**	**p-value**
Palm latency [ms]	1,496 ±227	1,492 ±208	ns
Palm amplitude [mV]	2,010 ±2,023	2,467 ±1,504	ns
Foot latency [ms]	2,310 ±256	2,355 ±526	ns
Foot amplitude [mV]	856 ±1,057	1,181 ±820	ns
NAZ vs AZ	**NAZ (n = 8)**	**AZ (n = 12)**	**p-value**
Palm latency [ms]	1,482 ±254	1,500 ±183	ns
Palm amplitude [mV]	2,120 ±2,197	2,754 ±1,304	ns
Foot latency [ms]	2,290 ±281	2,376 ±560	ns
Foot amplitude [mV]	1,161 ±1,030	990 ±814	ns

SSR – sympathetic skin response; SRP – secondary Raynaud's phenomenon; NC – normal capillaries; DC – dilatation of capillaries (giant loops); NAZ – no avascular zone (normal numbers of capillaries); AZ – the presence of avascular zone; ns – non-significant.

Table 4. Comparison of heart rate variability in study groups

Heart rate data	SRP (n = 20)	Control (n = 30)	p-value
HRV (%)	13.5 ±4.4	24.1 ±6.5	0.000000
LF (bpm)	53.1 ±22.3	40.92 ±9.2	0.018111
HF (bpm)	14.1 ±6.4	12.4 ±6.9	0.431469
LF/HF	3.9 ±0.5	3.4 ±0.6	0.027669
E/I	1.1 ±0.09	1.3 ±0.15	0.001424

HRV – heart rate variability; LF – low frequency; HF – high frequency; E/I – expiration/inspiration ratio.

of microvascular complications (2 patients without microangiopathy, 2 patients with microangiopathy). SSR showed no relationship with the severity of the microangiopathy (Fig. 1). There were no statistical differences in terms of SSR between patients with normal numbers of capillaries compared with the subgroup with avascular zones in capillaroscopy. There were also no differences in SSR results between patients with normal capillaries and individuals with dilatation of capillaries.

Statistical analysis showed a significantly lower mean HRV, and higher LF values, LF/HF ratio, and E/I ratio in patients with SRP than in the control group (Table 4).

There was no correlation between the stage of microangiopathy and neurophysiological tests (standard conduction velocity, CVD, SSR).

Discussion

This study is a continuation of our previous research on the pathogenesis of primary Raynaud's phenomenon.[15,20] In the present study, we analyze the role of the peripheral nervous system in patients with SRP in the course of CTD.

Typical peripheral nervous system lesions in the course of different connective tissue diseases mainly include axonal, ischemic peripheral nerve damage (distal sensory polyneuropathy, mononeuropathy/multiple mononeuropathy, cranial neuropathy), and myopathy. Therefore, Raynaud's phenomenon in CTD is thought to be secondary to the dysfunction of the peripheral nervous system. It would be interesting to answer the question as to whether patients with SRP without clinical evidence of peripheral neuropathy may have autonomic dysfunction.

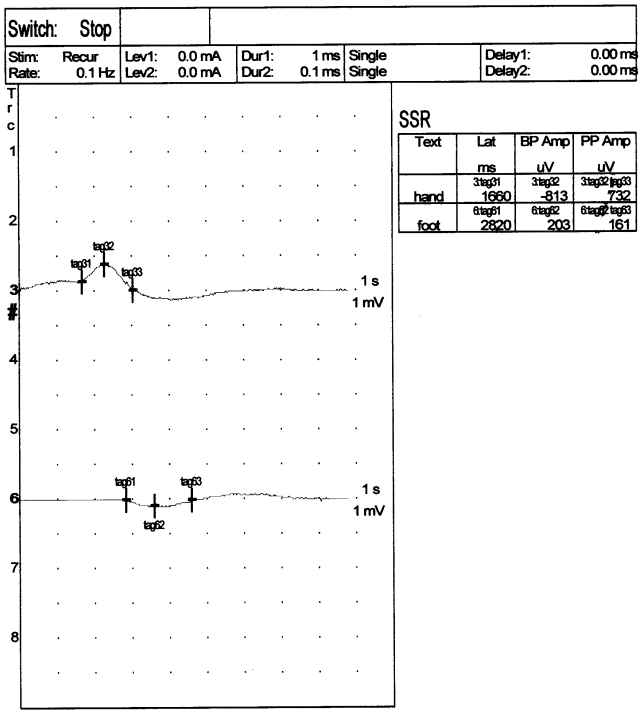

Fig. 1. K.M, woman, 48 years old, with rheumatoid arthritis, in capillaroscopy: capillaries without loops giants, no avascular zone. Abnormal sympathetic skin response (SSR): low amplitude, long latencies from hand and foot

Previous research into nervous system disorders in the pathogenesis of RP has been performed on patients with PRP, and these studies have shown that the pathogenesis of PRP is multifactorial and includes the sympathetic peripheral nervous system, central neural abnormalities and local defects.[15,20–22] Mondelli et al. showed dysregulation of cholinergic sympathetic fibers innervating the fingers in PRP. Abnormal SSR habituation has suggested that the central mechanism should also be considered.[22]

According to Charkoudian, the sympathetic nervous system is involved in the pathogenesis of both primary and secondary Raynaud's phenomenon, both in peripheral (local) and central system involvement mechanisms.[23]

In the opinion of Kaheleh et al., Raynaud's phenomenon is the result of dysregulated neuroendothelial control of vascular tone and circulating mediators.[24] These mechanisms are suggested as playing a major role in secondary Raynaud's phenomenon due to scleroderma.

In our study, detailed neurological and orthopedic examinations and standard neurophysiological tests, together with CVD and an analysis of different fibers in motor nerves (CVD test) were performed in order to exclude peripheral neuropathy. There were no significant statistical differences in these tests in the ulnar and peroneal nerves in the SRP group compared with the control group. Therefore, we assumed that vasomotor disturbances may occur in CTD regardless of peripheral neuropathy.

Central neural abnormalities are considered a cause of RP. Our study indicated sympathetic hyperactivity and the attenuation of the parasympathetic influence of heart rate. Similar abnormalities have previously been observed in patients with PRP.[15] According to Edwards et al.'s studies, patients with PRP present an abnormality of the central neuronal modulation of the brainstem with impaired habituations of vasodilator and vasoconstriction components of the warning system responsible for emotional stress.[25] The results of our study also suggest that SRP in the course of CTD, and without peripheral neuropathy, could be a consequence of central impairment of neuronal habituation.

In our study, similar to the previous one in PRP patients, we revealed the impairment of sympathetic sweat fibers, which could suggest that small autonomic fibers are damaged. The changes were more evident in lower limbs, which could be explained by their longer nerves, which are more susceptible to any disturbance to regenerative processes. In standard neurographic tests and CVD tests, we did not reveal any changes, so only very small fiber neuropathy (type C and unmyelinated fibers) could be found in SRP patients. The lack of correlation between SSR changes and microangiopathy indicates that SSR dysfunction in patients with SRP occurs regardless of structural changes in the capillaries. Further observations as to whether the SSR can be an independent predictor of skin necrosis must be conducted.

Conclusions

Correct standard conduction velocity and CVD tests in patients with SPR allow for the supposition that vasomotor disturbances may occur in CTD regardless of peripheral neuropathy.

The lack of a relationship between SSR and microangiopathy can confirm that these 2 processes occur independently in patients with CTD-related SRP.

Normal peripheral nerve function, together with revealed autonomic nervous system impairment, suggests the central origin of SRP in the course of CTD.

References

1. Raynaud M. On local asphyxia and symmetrical gangrene of the extremities 1862. New researches on the nature and treatment of local asphyxia of the extremities. In: Barlow T, trans. *Selected monographs*. London, UK: New Sydenham Society; 1874.
2. Harper FE, Maricq HR, Turner RE, et al. A prospective study of Raynaud's phenomenon and early CTD. A five-year report. *Am J Med*. 1982;72:883–888.
3. Herrick AL. Pathogenesis of Raynaud's phenomenon. *Rheumatology*. 2005;44:587–596.
4. Pavlov-Dolijanovic S, Damjanov NS, Stojanovic RM, et al. Scleroderma pattern of nailfold capillary changes as predictive value for the development of a connective tissue disease: A follow-up study of 3,029 patients with primary Raynaud's phenomenon. *Rheumatol Int*. 2012;32(10):3039–3045.
5. Wu PC, Huang MN, Kuo YM, Hsieh SC, Yu CL. Clinical applicability of quantitative nailfold capillaroscopy in differential diagnosis of connective tissue diseases with Raynaud's phenomenon. *J Formos Med Assoc*. 2013;112(8):482–488.

6. Maricq HR, Le Roy EC, D'Angelo WA, et al. Diagnostic potential of in vivo capillary microscopy in scleroderma and related disorders. *Arthritis Rheum*. 1980;23:183–189.
7. Andreadou E, Zouvelou V, Karandreas N, et al. Anti-myelin-associated glycoprotein polyneuropathy coexistent with CREST syndrome. *J Postgrad Med*. 2012;58:57–59.
8. Gunatilake SS, Wimalaratna H. Guillain-Barré syndrome presenting with Raynaud's syndrome. A case report. *BMC Neurol*. 2014;14:174.
9. Jasmin R, Sockalingam S, Ramanaidu LP, Goh KJ. Clinical and electrophysiological characteristics of symmetric polyneuropathy in a cohort of systemic lupus erythematosus patients. *Lupus*. 2015; 24(3):248–255.
10. Omdal R, Bekkelund SI, Meligren SI, et al. C-fibre function in systemic lupus erythematosus. *Lupus*. 1996;5:613–617.
11. Hanly JG, Urowitz MB, Sanchez-Guerrero J, et al. Systemic Lupus International Collaborating Clinics. Neuropsychiatric events at the time of diagnosis of systemic lupus erythematosus: An international inception cohort study. *Arthritis Rheum*. 2007;56:265–273.
12. Sim MK, Kim DY, Yoon J, et al. Assessment of peripheral neuropathy in patients with rheumatoid arthritis who complain of neurologic symptoms. *Ann Rehabil Med*. 2014;38:249–255.
13. Oh SJ. *Clinical Electromyography: Nerve Conduction Studies*. Lippincott, PA: Williams and Wilkins; 2003.
14. Kleiger RE, Stein PK, Bigger JT. Heart rate variability: Measurement and clinical utility. *Ann Noninvasive Electrocardiol*. 2005;10:88–101.
15. Koszewicz M, Gosk-Bierska I, Bilińska M, et al. Autonomic dysfunction in primary Raynaud's phenomenon. *Int Angiol*. 2009;28:127–131.
16. Elie B, Guiheneuc P. Sympathetic skin response: Normal results in different experimental conditions. *Electroencephalogr Clin Neurophysiol*. 1990;6:258–267.
17. Uncini A, Pullman SL, Lovelace RE, et al. The sympathetic skin response: Normal values, elucidation of afferent components and application limits. *J Neurol Sci*. 1988;87:299–306.
18. Gerhard-Herman M, Gardin JM, Jaff M, et al. Guidelines for noninvasive vascular laboratory testing: A Report from the American Society of Echocardiography and the Society of Vascular Medicine and Biology. *J Am Soc Echocardiogr*. 2006;19:955–972.
19. Maricq HR. Widefield capillary microscopy. Technique and rating scale for abnormalities seen in scleroderma and related disorders. *Arthritis Rheumatol*. 1981;24:1159–1166.
20. Koszewicz M, Gosk-Bierska I, Gosk J, et al. Peripheral nerve changes assessed by conduction velocity distribution in patients with primary Raynaud's phenomenon and dysautonomia. *Int Angiol*. 2011;30: 375–379.
21. Manek NJ, Holmgren AR, Sandroni P, et al. Primary Raynaud's phenomenon and small-fibre neuropathy: Is there a connection? A pilot neurophysiologic study. *Rheumatol Int*. 2011;31:577–585.
22. Mondelli M, Romano C, De Stefano R, et al. Nerve conduction velocity study of the upper limb in Raynaud's phenomenon. *Rheumatol Int*. 2000;19:165–169.
23. Charkoudian N. Skin blood flow in adult human thermoregulation: How it works, when it does not, and why. *Mayo Clin Proc*. 2003;78: 603–612.
24. Kaheleh B, Matucci-Cerinic M. Raynaud's phenomenon and scleroderma. Dysregulated neuroendothelial control of vascular tone. *Arthritis Rheumatol*. 1995;38:1–4.
25. Edwards CM, Marshall JM, Pugh M. Lack of habituation of the pattern of cardiovascular response evoked by sound in subject with primary Raynaud's disease. *Clin Sci*. 1998;95:249–260.

Significance of mutations in the region coding for NS3/4 protease in patients infected with HCV genotype 1b

Tadeusz W. Łapiński[1,A–F], Magdalena Rogalska-Płońska[1,B,F], Oksana Kowalczuk[2,B,C], Joanna Kiśluk[2,B,C], Joanna Zurnowska[2,B,C], Jacek Nikliński[2,F], Robert Flisiak[1,F]

[1] Department of Infectious Diseases and Hepatology, Medical University of Bialystok, Poland
[2] Department of Clinical Molecular Biology, Medical University of Bialystok, Poland

A – research concept and design; B – collection and/or assembly of data; C – data analysis and interpretation; D – writing the article; E – critical revision of the article; F – final approval of the article

Advances in Clinical and Experimental Medicine, ISSN 1899-5276 (print), ISSN 2451-2680 (online) *Adv Clin Exp Med*. 2018;27(11):1593–1600

Address for correspondence
Tadeusz Łapiński
E-mail: twlapinski@gmail.com

Funding sources
None declared

Conflict of interest
None declared

Received on January 27, 2016
Reviewed on May 24, 2016
Accepted on June 26, 2017

Abstract

Background. Fast hepatitis C virus (HCV) replication is one of the reasons for frequent changes in viral genome.

Objectives. The objective of this study was to evaluate the frequency and type of mutation in NS3/4 protease in patients with HCV genotype 1b and to determine the effect of the mutation on viral load, fibrosis stage, alanine aminotransferase (ALT) activity, and alpha-fetoprotein (AFP) level.

Material and methods. The study included 46 treatment-naïve patients, infected with HCV genotype 1b. Mutations were analyzed after isolating HCV RNA, and then evaluating the compliance of the amino acid sequence, using 3500 Genetic Analyzer (Applied Biosystems, Foster City, USA). RNA fragment from nucleotide 1–181 encoding NS3/4 protease was subjected to analysis.

Results. Mutations were demonstrated in 65% of subjects. Changes in the protease region affecting resistance to treatment (T54, Q80, V158, M175, D186) were detected in 10.8% of patients. Substitution mutation at T72 was found most frequently – in 49.9% of cases. In 13% of patients, mutation at G86 was demonstrated, including G86P in 5 patients and G86S in 1 patient. In the group of patients with T72 mutation, viral load was significantly higher (1.3 × 106 IU/mL vs 1.0 × 105 IU/mL; $p = 0.01$), AFP level was higher and fibrosis level was lower (1.26 vs 2.17; $p = 0.008$) compared to the patients without the mutation. Cryoglobulinemia was observed in 74% of patients with mutation at position T72.

Conclusions. Natural mutations of the region coding for NS3/4 protease are found frequently in patients infected with genotype 1b, but they may cause resistance to antiviral agents only in 11% of patients. Changes were most frequently found at position T72. Mutations at position T72 are correlated with the cryoglobulinemia occurrence. This is a substitution mutation, accompanied by a high viral load, high ALT activity and AFP level, which may point to a more unfavorable influence of such a modified virus, compared to wild-type virus, onto pathological processes in the liver.

Key words: mutations, cryoglobulinemia, hepatitis C virus genotype 1b, NS3/4 protease

DOI
10.17219/acem/75511

Introduction

Collectively, 6 hepatitis C virus (HCV) genotypes have been identified, differing in 30–35% of RNA sequence. In Poland, like in most European countries, genotype 1 subtype b (1b) is the most frequent HCV genotype, responsible for chronic infection. Hepatitis C virus replication is characterized by fast rate and frequent occurrence of modifications in the genome. The replication rate is connected with the activity of RNA-dependent RNA polymerase (RdRP). Except normal RNA synthesis, modified RNA strands are also produced during the HCV replication phase. They are characterized by point or multiple amino acid modifications, or even their loss. In the case of HCV, the correction of a modified RNA strand is not possible. Such modifications may be lethal and they may limit further replication, or lead to the appearance of a virus with different biological properties. Modified viral genome usually does not influence the change of biological properties, such as immunogenicity or tropism for hepatocytes; however, resistance to antiviral agents sometimes occurs as the result of such modifications.[1]

NS3 protease, having the properties of a helicase, is responsible for the initiation and unwinding of an RNA strand during the replication of the virus. It is encoded in the C-terminal viral RNA fragment, at positions 1–181. The protease has the properties of an adenosine triphosphatase (ATP) enzyme, nucleotide triphosphatase, necessary for the replication and transcription of RNA. Finding the loci coding for NS3 synthesis allows for designing agents inhibiting viral replication. Such agents are usually aptamers, short DNA or RNA fragments, or peptides binding specifically to a target molecule.[2] The most direct-acting antiviral agents (DDAs) used in HCV infections are aptamers. Replacement or loss of amino acids in NS3 significantly decreases the efficiency of HCV protease. Usually, this happens in the case of mutation at T36, T54, V55, A155, or V170 position. These positions are particularly prone to the resistance against protease ketoamide inhibitors. These compounds form a reversible covalent bond with a catalytic serine of NS3/4A protease. Such situation usually occurs during boceprevir or telaprevir therapy. Linear noncovalent protease inhibitors, such as faldaprevir tripeptide, simeprevir, asunaprevir, and vaniprevir, usually bind to position 168.[3,4] Currently, resistance associated with a single mutation within the HCV genome is not a serious problem, because high doses of antiviral agents or coadministration of several agents with different mechanisms of action guarantee successful therapy (Table 1).

Natural HCV mutations and their subsequent selection during the course of antiviral treatment are frequent. Hepatitis C virus mutants may acquire the ability for fast replication as well as competitiveness against wild-type viruses. Moreover, new mutations, unimportant from the point of view of therapy efficacy evaluation, may trigger the mechanisms of broader, unfavorable effect on the organism compared to the activity of a wild-type virus. In-depth analysis of new mutations seems to be inevitable in the monitoring of early oncogenesis, fibrosis or the activation of cryoglobulinemia. This may improve preliminary diagnosis and contribute to the prevention or significant delay of HCC development.[5] The problem is even more important, as patients after effective antiviral therapy still belong to the group with an increased risk for HCC development. Also, it is impossible to exclude geographical differences in the occurrence of mutations, resulting from epidemiological reasons and environmental factors. This justifies undertaking studies on the occurrence of mutations in the HCV genome in patients infected with this virus in different regions of the world.

Objectives

The study was performed in order to evaluate the frequency of mutations in the region coding for NS3/4 protease among people infected with HCV genotype 1b. The type of mutation was established in relation to resistance to antiviral treatment and other mutations, including substitutions. The effect of mutation on viral load as well as inflammation and fibrosis in the liver was studied.

Table 1. Changes in the protease NS3/4 region affecting resistance to protease inhibitor treatment[6–10]

Protease inhibitor	Position; changed amino acid												
	V36	F43	T54	V55	Q80	S122	I132	R155	A156	V158	D168	V170	M175
Boceprevir	M, A		A, S, C, G	A				K, T	S, T, V	I	N	A, T	L
Telaprevir	M, A, L, G, I		A, S				V	K, T, G, M	S, T, V, F, N		N		
Simeprevir					K, R	A, G, R		K, Q			V, E, A, H	T	
Faldaprevir								K, Q	T		V, E, A, N, T		
Paritaprevir			A	A				K, Q	S, T		A, E, H, T, V, Y	A	
Vaniprevir		S						K, G, T			V, Y G, A		
Grazoprevir								Q, K	S, T		A, V		
Danoprevir								R, K, Q			D, E	V, I	
Asunaprevir	M, R							K	T		A		

Material and methods

The study included 46 patients, 18 women and 28 men, aged 49 years on average (from 19 to 72 years), infected with HCV genotype 1b (Table 2). All the patients were treatment-naïve.

Hepatitis C virus infection was documented based on the presence of HCV RNA in the serum. The test was performed with the use of the reverse transcription polymerase chain reaction (RT-PCR) method, with reaction starters specific for viral noncoding 5'-terminal region (5'-UTR). The viral genotype was determined by direct sequencing of the PCR reaction product (Syngen Biotech, Tainan City, Taiwan).

Quantitative evaluation of HCV RNA was performed with the use of COBAS AmpliPrep (Roche, Mannheim, Germany). The procedure was automated, based on the amplification of nucleic acid by PCR. HCV virus RNA was determined quantitatively with the use of quantitative standard HCV QS. The method sensitivity was 11 IU/mL, linearity was 15 IU/mL.

Table 2. The patients' characteristics

Number of patients	46
Women/men	18/28
Age [years] mean range	 49 19–72
HCV-RNA [IU/mL] mean range	 1.1×10^6 4.1×10^4–5.5×10^6
Fibrosis mean range	 1.7 1–4
ALT [IU/mL] mean range	 78 20–360
AFP [ng/mL] mean range	 6.1 1.4–15.0
Cryoglobulinaemia n percentage [%]	 28 61

HCV – hepatitis C virus; ALT – alanine aminotransferase; AFP – alpha-fetoprotein.

Hepaptitis C virus mutation

Blood plasma was collected from the patients infected with a HCV genotype 1 virus. The total RNA was extracted from 500 µL of blood plasma using a devise for an automatic extraction of nucleic acids EasyMag (Biomerieux, Lyon, France). The fragment of the HCV genome covering NS3/4A was amplified in a nested-PCR with primers described by Paolucci et al.[11] The sequences of the primers were as follows: for the 1st PCR – *1-forward outer 5'-CGAGACCTTGCGGTGGCAGT-3'*, *1-reverse 5'-CAGCCGTYTCCGCTTGGTCC-3'*; for the 2nd PCR – *1-forward inner 5'-CATCACCTGGGGGGCAGACACC-3'*, *1-reverse inner 5'-GTCAGTTGAGTGGCACTCATCAC-3'*. The 1st PCR, prevented by complementary DNA (cDNA) synthesis, was performed with a OneStep RT-PCR kit (EURex Ltd., Gdańsk, Poland) in 25 µL of reaction mixture, containing 12.5 µL of 2 × Master Buffer Mix, 1 µL of both outer forward and reverse primer 10 µM solutions, 1 µL of Master Enzyme Mix solution, and 50–100 ng of RNA. The reaction conditions were as follows: 10 min denaturation at 94°C, followed by 50 cycles of 1 min at 94°C, 1 min at 55°C and 1 min at 72°C, with an extension at 72°C for 10 min. The 2nd PCR was carried out in 20 µL of reaction mixture, containing 1 × PCR buffer with $MgCl_2$, 0.8 mL of 20 mM deoxynucleotide (dNTP) solution, 1 µL of both inner forward and reverse primer 10 µM solutions, 0.1 µL of Taq DNA polymerase, and 1 µL of the 1st PCR solution (all reagents from EURex Ltd.). The 2nd PCR was performed with the following conditions: 5 min denaturation at 94°C, and then 30 cycles at 94°C for 1 min, 52°C for 1 min and 72°C for 1 min, with an extension at 72°C for 10 min.

The PCR products were checked and separated using an agarose gel electrophoresis, and then extracted from agarose slides, using a PCR clean-up Gel Extraction Kit (Macherey-Nagel, Duren, Germany). The extraction was performed automatically on a QIACUBE machine (Qiagen, Hilden, Germany).

Direct sequencing of cleaned PCR products was performed using an automatic DNA sequencer 3500 Genetic Analyzer (Applied Biosystems, Foster City, USA) and a BigDye Terminator v. 3.1 Cycle Sequencing kit (Applied Biosystems). Nucleotide sequences were compared with the HCV subtype 1b gene for polyprotein, NS3 protease region, partial cds, isolate:MS100913 (GenBank ID: AS709386.1). Particular sequences of codons 54, 55, 71, 72, 80, 86, 158, 168, and 175 of the gene were analyzed to search for the mutations resulting in HCV protease inhibitor resistance.[11]

In all the patients, tests for hepatitis B virus (HBV), detecting the presence of the antigen HBsAg in the serum, and for human immunodeficiency virus (HIV), looking for anti-HIV antibodies (Abbott Laboratories, Lake Bluff, USA) were performed. Moreover, the presence of alpha-fetoprotein (AFP), alanine aminotransferase (ALT) and cryoglobulinemia in the serum was evaluated.

In 20 patients, a liver biopsy was taken, and in 26, an elastography was performed. Sections from liver bioptates were subjected to hematoxylin and eosin staining in order to establish the intensity of the inflammatory process, and to Syrian red staining, evidencing the presence of connective tissue. The morphological state of the liver was described according to Scheuer's classification. In the case of patients with elastography, the liver fibrosis stage was transposed into the Metavir scale (the Metavir scale is comparable to Scheuer's classification).

After the study was approved by the Bioethical Committee at the Medical University of Bialystok, the patients expressed informed consent to participate in the research.

Statistical analysis

Statistical analysis was performed with the χ^2 and the Mann-Whitney U tests. The significance level was established at $p < 0.05$. Studies were performed using STATISTICA PL v. 10 (StatSoft Polska Sp. z o.o., Kraków, Poland) for Windows 10.

Results

In the group of patients with HCV genotype 1b, mutations were detected in 30 out of 46 (65%) patients (Table 3). Mutations potentially connected with resistance to NS3/4 inhibitors (T54 (1), Q80 (1), V158 (1), D168 (1), and M175 (1)) were detected in 5 (11%) patients. Only single mutations of this type were present in individual patients.

Most frequently, in 50% of cases, substitution at T72 not affecting the efficacy of antiviral therapy was detected. In 6 out of 46 (13%) patients, mutation at G86 was found, including 5 cases of G86P mutation; there was also 1 case of G86S. Other mutations were demonstrated sporadically (Table 4).

In the group of patients with a mutation at position T72, viral load was significantly higher than in patients without this mutation (1.3×10^6 IU/mL vs 1.0×10^5 IU/mL; $p = 0.01$) (Fig. 1).

Among the patients with T72 mutation, the average fibrosis stage in the hepatic tissue was significantly lower than in patients without this mutation (1.26 vs 2.17; $p = 0.008$) (Fig. 2).

Cryoglobulinemia was observed in 28 out of 46 (61%) patients. Among patients with a mutation at position

Table 3. Substitution mutations and cryoglobulinemia found in patients

No.	Patient	Position								Cryoglobulinemia
		T54	I71	T72	Q80	Q86	V158	D168	M175	
1	CA			X						X
2	WI			X		X				X
3	BM			X						
4	OW		X	X						X
5	JW						X			X
6	BB			X						
7	SR				X	X				X
8	ND			X						X
9	LM			X						X
10	PJ			X						X
11	KS			X						
12	BB								X	
13	GA					X				X
14	NA			X						X
15	WM					X				
16	KP					X				X
17	RJ			X						X
18	OM			X						X
19	AW			X						X
20	ZA			X						
21	SM			X						X
22	RL			X						X
23	WA			X						X
24	SS			X						X
25	KG					X				X
26	RW			X						X
27	GM			X				X		X
28	DW	X		X						
29	GH			X						
30	TR			X						X

Table 4. The substitution mutations (type and amount)

Position	n (%)	Type
T54	1 (2.17%)	Thr54Ser
I71	1 (2.17%)	Ile71Val
T72	23 (49.91%)	Thr72Ile
Q80	1 (2.17%)	Gln80Leu
Q86	5 (10.85%) 1 (2.17%)	Gln86Pro Gln86Ser
V158	1 (2.17%)	Val158Gly
D168	1 (2.17%)	Asp168Glu
M175	1 (2.17%)	Met175Asn

T72 (17/23), the incidence was significantly higher compared to those without the mutation (6/16), (74% vs 38%; p = 0.023).

Among the patients with T72 mutation, AFP level was significantly higher than in patients without this mutation (Fig. 3). In the same group of patients, higher ALT activities were documented compared to patients without this mutation (82 IU/mL vs 72 IU/mL); however, the difference was not statistically significant.

No patient was detected with HBs and anti-HIV.

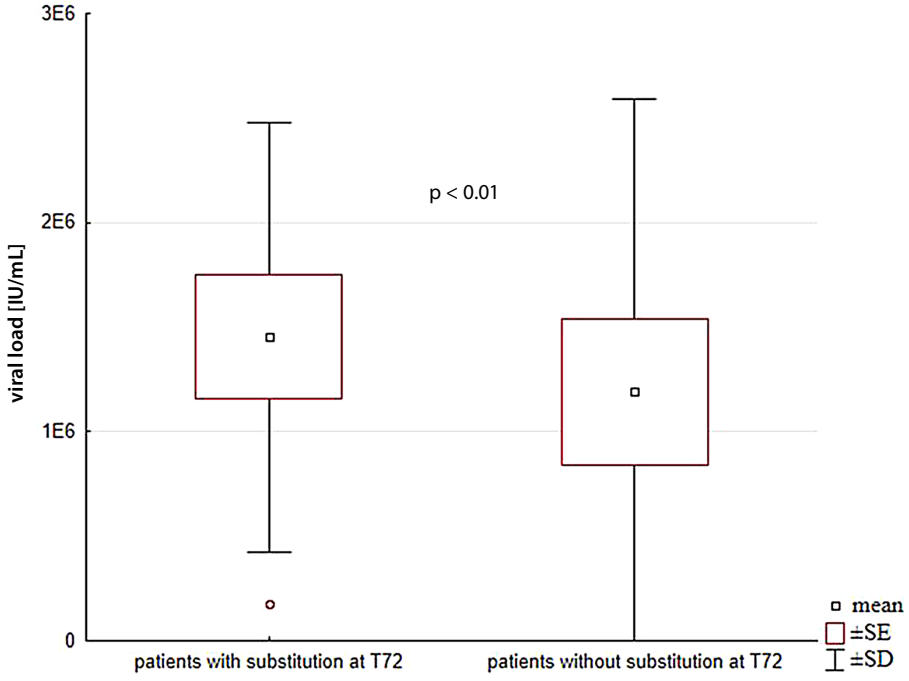

Fig. 1. Viral load in patients with and without substitution at T72 gene of HCV RNA

HCV – hepatitis C virus.

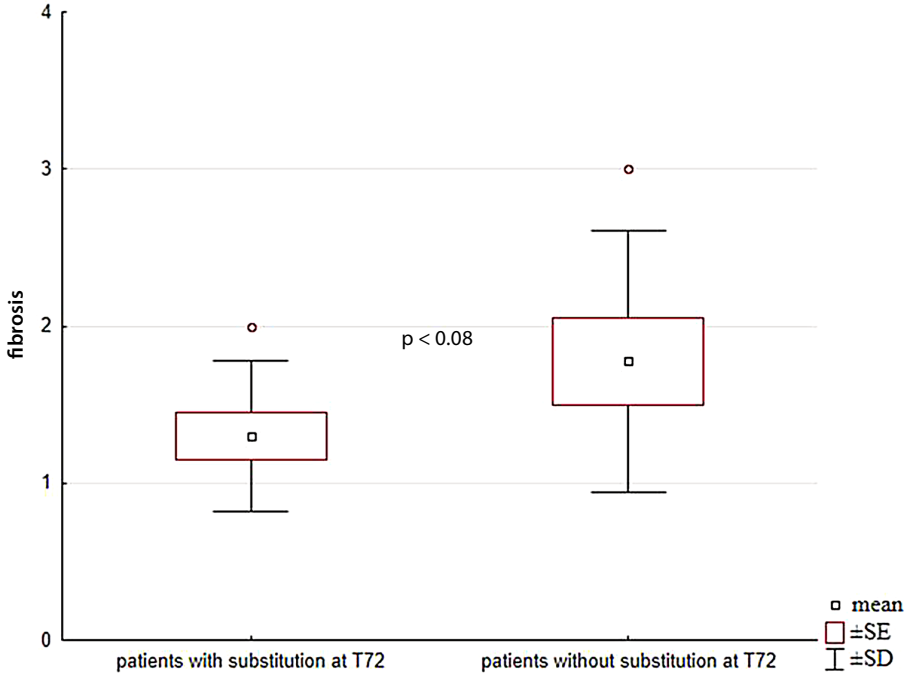

Fig. 2. Liver fibrosis in patients with and without substitution at T72 gene of HCV RNA

HCV – hepatitis C virus.

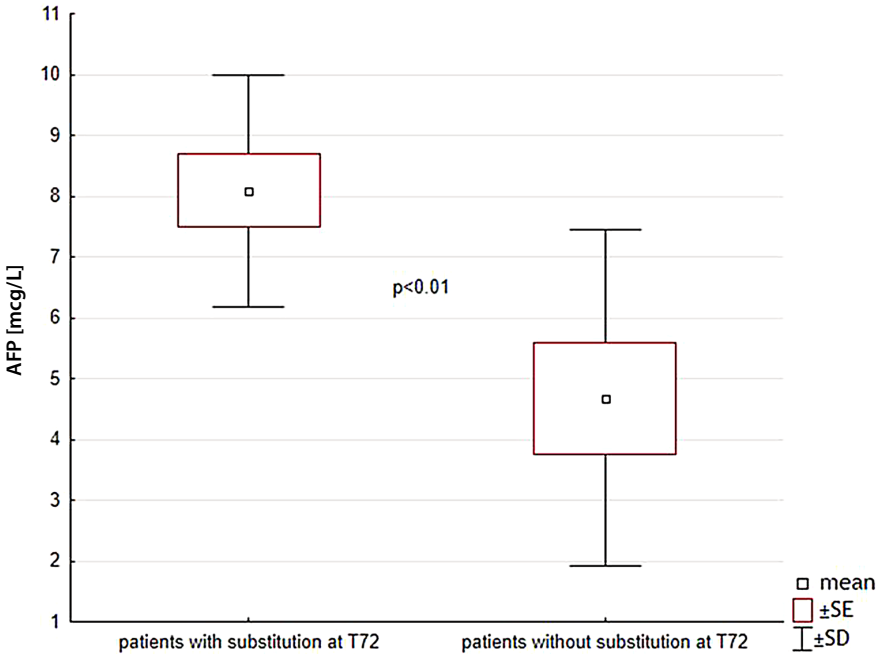

Fig. 3. The activity of AFP in the serum in patients with and without substitution at T72 gene of HCV RNA

AFP – alpha-fetoprotein; HCV – hepatitis C virus.

Discussion

Mutations in HCV genotype 1 are frequent. Jaspe et al. reported the possibility of such mutations in even 79% of patients infected with HCV genotype 1, before the start of therapy. Moreover, there are considerable differences in the prevalence of individual mutations, depending on the geographical region (Table 5).[12] A study by Miura et al., performed on patients infected with HCV genotype 1b, in 25 chronically infected patients without cirrhosis, 29 with cirrhosis and 25 with hepatocellular carcinoma (HCC) demonstrated the highest frequency of mutations in the part of the virus encoded in the region from position 61 to 100 (usually at positions 70, 75 and 91), in patients with liver cirrhosis and carcinogenesis.[13]

Equally frequently such mutations appear in patients treated with antiviral agents; however, these are different mutations. Danish Hepatological Group documented the occurrence of mutations in the HCV genome in 71%

Table 5. Frequency of amino acid substitution R7 0Q and L/C91M in patients with HCV genotype 1a and 1b infection with respect to different geographic regions[10]

Genotypes	n	Geographic regions	Substitution [%]	
			R70Q	L/C91M
1a	27	Venezuela	3.7	0
	27	USA	3.7	0
	0	Japan	0	0
1b	38	Venezuela	79	68
	34	USA	65	82
	80	Japan	40	31
	70	China	10	61

of patients unsuccessfully treated with telaprevir; however, many of these mutations do not affect the resistance to antiviral therapy.[14] In our research, the frequency of all mutations was 49%, but mutations in the region of NS3/4 protease, underlying the resistance to DAAs, were demonstrated in 11% of patients, which is in accord with the observations of other authors. Ferraro et al. detected such mutations in 14% patients infected with HCV genotype 1b at positions V36, F43, T54, I153, R1 55, and D168.[15] In similar studies, Paolucci et al., on the basis of a group of 39 treatment-naïve people infected with HCV genotype 1b, demonstrated the presence of mutations at positions V55, Q80 and M175 in 10% of the patients.[11] In the context of antiviral therapy, mutations decreasing the efficacy of boceprevir and telaprevir are most often detected, which, considering the frequent adverse reactions of these agents, justifies the recommendation to avoid their use in the treatment.[16,17] Most authors evaluating HCV mutations focus on determining their effect on the resistance to antiviral agents. This is certainly important, although the presence of other mutations not influencing the efficacy of antiviral therapies may play an important role in the biology of the virus and pathophysiological implications of the infection.

Hepatitis C virus RNA does not integrate with nucleic acids of humans. It seems that one of the most important pathways stimulating HCC development in the course of HCV infection is the influence of specific viral proteins synthesized on the basis of viral genome. Many reports suggest that mutations in the viral RNA may influence the synthesis of such proteins. Viral NS3 protein exerts a specific influence on the early stage of carcinogenesis in hepatocytes. It inhibits the activity of cellular p21 (WAF1) protein, while p21 remains in close cooperation

with p53, one of the main factors controlling the neoplastic process. Although the deficiency of p21 protein does not directly cause HCC development, the influence of this protein on a higher growth rate and proliferation of newly formed neoplastic cells has been confirmed.[18]

The occurrence of compensatory mutations in the course of HCV infection is a poorly studied process. Such mutations usually occur as a response to the loss of efficiency of nucleic acid, connected with the primary, unfavorable mutation. The new mutation may change the biological properties of the virus.[19] During the replication of HCV RNA, numerous mutations take place, resulting in the synthesis of new viral proteins, possibly showing different biological properties compared to normally synthesized proteins. Compensatory mutations occur at the same time as mutations conferring resistance to antiviral agents, but may also appear as independent mutations. This is particularly important in the case of the gene encoding protease NS3/4, responsible for the initiation and replication of the virus. At the moment, it is thought that mutations I71, T72 and Q86 are compensatory mutations in the HCV infection. Mutations I71 and T72 are compensatory for mutations V55 and M175, and compensatory mutation Q86 is present in the case of mutation at position Q80.[15] In our research, compensatory mutation T72 was observed in 1 patient in relation to substitution at position T54. Also, mutation Q86 was detected in a single patient, who also had a mutation at Q80.

In the group of patients infected with HCV genotype 1b, Paolucci et al. demonstrated the presence of a mutation at T72 in 28% and at I71 in 13% of patients.[11] In our studies, mutation at position T72 was found in 49.9% (23/46) of patients and at I71 in only 1 patient.

Our results point to a significantly higher viral load and AFP level among the patients with a mutation at position T72 compared to patients without this mutation. This may suggest a stimulatory effect of this mutation on viral replication, which is reflected in higher ALT activity and less advanced fibrosis (more inflammation) in the group of patients with observed mutations. Lee et al. demonstrated that the infection with genotype 1b in itself is a risk factor for HCC compared to other genotypes of the virus. Moreover, a significantly higher HCV viral load was detected in patients with genotype 1b in whom HCC was diagnosed (397 patients with the cancer, 410 without).[20]

The study by Hu et al. performed on 63 patients infected with HCV genotype 1b with coexisting HCC showed more frequent occurrence of mutations at positions A028C, G209A, C219U/A, U264C, A271C/U/A, C378U, G435A/C, and G481A (mutations affecting the resistance to antiviral agents), and compensatory mutations at positions K10Q, R70Q, M91L, and G161S in comparison to 188 patients infected with HCV, but without HCC.[21]

Vallet et al. demonstrated a high frequency of mutations at positions Y56F, I71F, T72I, Q86P, P89S, S101G/D, R117H, S122G/T/N, V132I, and V170I in the group of treatment-naïve patients infected with HCV genotype 1. These mutations may significantly affect the whole codon of NS3 protease. Authors postulate that these mutations may lead to more frequent HCC development and more advanced fibrosis stage.[22] It seems that this compensatory mutation at position T72, unimportant from the point of view of resistance to drugs, may lead to an increased rate of HCV replication. Increased HCV replication is one of the prediction factors for HCC development. Yoshimi et al. demonstrated that in the case of mutation at position Y93H in the fragment encoding NS3/4 protease of HCV genotype 1b, higher HCV replication, higher ALT activity and more frequent HCC development may be expected. However, the mutation itself does not influence the efficacy of antiviral treatment.[23] Verga-Gérard et al. pointed to unfavorable significance of transforming growth factor beta (TGF-β) activation in the stimulation of HCC development. Their studies on NS3/4 protease showed that modification at position S139A was accompanied by the stimulation of TGF-β synthesis, upregulating HCC development.[24] Mutations at position R70 and L/C91 are present in genotype 1b only, and are substitution mutations. Many studies show that they may result in higher frequency of HCC, liver steatosis and higher resistance to interferon (IFN). The results of the study by Jaspe et al. demonstrate big differences in mutation frequency at positions R70 and L/C91, depending on geographical distribution of the population (Venezuela vs United States R70: 79% vs 69%; L/C91: 68% vs 75%).[4] It seems that the studies evaluating mutations within the genome of HCV are not currently very important from the point of view of resistance to new antiviral agents. Such studies may contribute new data concerning HCC development and stimulation of histopathological changes in the liver.

Conclusions

Mutations in the region encoding NS3/4 protease were present in 65% of treatment-naïve patients infected with genotype 1b, but they might affect the resistance to antiviral agents only in 11% of cases. Compensatory mutation at position T72 was present in 49.9% of patients, who showed a higher viral load and AFP concentration than patients without this mutation. A mutation at position T72 was correlated with the cryoglobulinemia occurrence. This may point to an unfavorable role of this mutation in the stimulation of pathological processes in the liver, connected with the infection.

References

1. Domingo E, Sheldon J, Perales C. Viral quasispecies evolution. *Microbiol Mol Biol Rev.* 2012;76:159–216.
2. Gao Y, Yu X, Xue B, et al. Inhibition of hepatitis C virus infection by DNA aptamer against NS2 protein. *PLoS ONE.* 2014;9:e90333.
3. Izumi N, Hayashi N, Kumada H, et al. Once-daily simeprevir with peginterferon and ribavirin for treatment-experienced HCV genotype 1-infected patients in Japan: the CONCERTO-2 and CONCERTO-3 studies. *J Gastroenterol.* 2014;49:941–953.
4. Lenz O, de Bruijne J, Vijgen L, et al. Efficacy of re-treatment with TMC435 as combination therapy in hepatitis C virus-infected patients following TMC435 monotherapy. *Gastroenterology*. 2012;143: 1176–1178.
5. Phenotype Working Group, Drug Development Advisory Group. Clinically relevant HCV drug resistance mutations figure and tables (updated). *Ann Forum Collab HIV Res.* 2015;14:1–8.
6. Pilot-Matias T, Tripathi R, Cohen D, et al. In vitro and in vivo antiviral activity and resistance profile of the hepatitis C virus NS3/4A protease inhibitor ABT-450. *Antimicrob Agents Chemother.* 2015;59: 988–997.
7. Apelian D. Achillion Pharmaceuticals. http://www.informedhorizons.com/hepdart2013. Accessed on December 19, 2013.
8. Lim SR, Qin X, Susser S, et al. Virologic escape during danoprevir (ITMN-191/RG7227) monotherapy is hepatitis C virus subtype dependent and associated with R155K substitution. A*ntimicrob Agents Chemother.* 2012;56:271–279.
9. Ali A, Aydin C, Gildemeister R, et al. Evaluating the role of macrocycles in the susceptibility of hepatitis C virus NS3/4A protease inhibitors to drug resistance. *ACS Chem Biol.* 2013;8:1469–1478.
10. Ahmad J, Eng FJ, Branch AD. HCV and HCC: Clinical update and a review of HCC-associated viral mutations in the core gene. *Semin Liver Dis.* 2011;31:347–355.
11. Paolucci S, Fiorina L, Piralla A, et al. Naturally occurring mutations to HCV protease inhibitors in treatment-naïve patients. *J Virol.* 2012; 9:245.
12. Jaspe RC, Sulbarán YF, Sulbarán MZ, Loureiro CL, Rangel HR, Pujol FH. Prevalence of amino acid mutations in hepatitis C virus core and NS5B regions among Venezuelan viral isolates and comparison with worldwide isolates. *J Virol.* 2012;9:214.
13. Miura M, Maekawa S, Takano S, et al. Deep-sequencing analysis of the association between the quasispecies nature of the hepatitis C virus core region and disease progression. *J Virol.* 2013;87:12541–12551.
14. Sølund C, Krarup H, Ramirez S; DANHEP group. Nationwide experience of treatment with protease inhibitors in chronic hepatitis C patients in Denmark: Identification of viral resistance mutations. *PLoS ONE*. 2014;9:e113034.
15. Ferraro D, Urone N, Di Marco V, Craxì A. HCV-1b intra-subtype variability: Impact on genetic barrier to protease inhibitors. *Infect Genet Evol.* 2014;23:80–85.
16. Wu S, Kanda T, Nakamoto S, Imazeki F, Yokosuka O. Hepatitis C virus protease inhibitor-resistance mutations: Our experience and review. *World J Gastroenterol.* 2013;19:8940–8948.
17. De Meyer S, Ghys A, Foster GR, et al. Analysis of genotype 2 and 3 hepatitis C virus variants in patients treated with telaprevir demonstrates a consistent resistance profile across genotypes. *J Viral Hepat.* 2013;20:395–403.
18. Tsai WL, Chung RT. Viral hepatocarcinogenesis. *Oncogene.* 2010;29: 2309–2324.
19. Poon A, Chao L. The rate of compensatory mutation in the DNA bacteriophage phiX174. *Genetics.* 2005;170:989–999.
20. Lee MH, Yang HI, Lu SN; REVEAL-HCV Study Group. Hepatitis C virus genotype 1b increases cumulative lifetime risk of hepatocellular carcinoma. *Int J Cancer.* 2014;135:1119-1126.
21. Hu Z, Muroyama R, Kowatari N, Chang J, Omata M, Kato N. Characteristic mutations in hepatitis C virus core gene related to the occurrence of hepatocellular carcinoma. *Cancer Sci.* 2009;100:2465–2468.
22. Vallet S, Gouriou S, Nkontchou G, et al. Is hepatitis C virus NS3 protease quasispecies heterogeneity predictive of progression from cirrhosis to hepatocellular carcinoma? *J Viral Hepat.* 2007;14:96–106.
23. Yoshimi S, Ochi H, Murakami E, et al. Rapid, sensitive, and accurate evaluation of drug resistant mutant (NS5A-Y93H) strain frequency in genotype 1b HCV by invader assay. *PLoS ONE*. 2015;10:e0130022.
24. Verga-Gérard A, Porcherot M, Meyniel-Schicklin L, André P, Lotteau V, Perrin-Cocon L. Hepatitis C virus/human interactome identifies SMURF2 and the viral protease as critical elements for the control of TGF-β signa ling. *FASEB J.* 2013;27:4027–4040.

The application of capillary electrophoresis, mass spectrometry and Brdicka reaction in human and rabbit metallothioneins analysis

Marta Kepinska[1,A–F], Sona Krizkova[2,3,B,F], Ewelina Guszpit[1,B,F], Miguel A. Merlos Rodrigo[2,3,B,F], Halina Milnerowicz[1,E,F]

[1] Department of Biomedical and Environmental Analysis, Faculty of Pharmacy with Division of Laboratory Medicine, Wroclaw Medical University, Poland
[2] Department of Chemistry and Biochemistry, Faculty of Agronomy, Mendel University in Brno, Czech Republic
[3] Central European Institute of Technology, Brno University of Technology, Czech Republic

A – research concept and design; B – collection and/or assembly of data; C – data analysis and interpretation;
D – writing the article; E – critical revision of the article; F – final approval of the article

Advances in Clinical and Experimental Medicine, ISSN 1899-5276 (print), ISSN 2451-2680 (online) *Adv Clin Exp Med*. 2018;27(11):1601–1608

Address for correspondence
Marta Kepinska
E-mail: zalewska.m@gmail.com

Funding sources
Study was supported by grant No. Pbmn178 from Wroclaw Medical University and by the AZV (Czech Agency for Healthcare Research) AZV CR grant No. 14-28334a (Prague, Czech Republic).

Conflict of interest
None declared

Received on June 6, 2018
Reviewed on August 3, 2018
Accepted on October 11, 2018

Abstract

Background. Metallothioneins (MTs) constitute a family of evolutionary conserved low molecular weight proteins with small variations in their amino acid sequences. They play a role in the regulation of trace metals metabolism, in the detoxification of heavy metal ions and in mechanisms controlling growth, differentiation and proliferation of cells.

Objectives. The aim of this study was to evaluate the human and rabbit MTs purity and characterization using advanced analytical approaches. Due to the common use of MT from rabbit liver as a model protein, the properties of the rabbit and human MTs were compared.

Material and methods. Capillary electrophoresis (CE), matrix-assisted laser desorption and ionization time-of-flight mass spectrometry (MALDI-TOF-MS) and Brdicka reaction were used for human and rabbit MTs characterization.

Results. In chip CE analysis, changes in the range of 5–8 kDa corresponding to the MT monomer, as well as some peaks of 13–14 kDa corresponding to dimers in both species, were observed. Using MALDI-MS, rabbit (MT-2D) and human (MT-1A, MT-1G, MT-1G + Cd and MT-2A) MTs were identified. In the Brdicka reaction analysis, a lower concentration of MTs from both organisms coincided with a decrease in the signal corresponding to MT level (Cat2). However, human MT gave higher Cat2 peak than the same concentration (0.025 mg/mL) of rabbit MT.

Conclusions. The applied methods allowed for the characterization of MTs and gave complementary information about MT isoforms. Altered electrochemical activity of human and rabbit MTs, despite the same number of –sulfhydryl (–SH) groups, was observed, which may be due to different availability of MT cysteinyl groups.

Key words: metallothionein, mass spectrometry, capillary electrophoresis, Brdicka reaction

DOI
10.17219/acem/98916

Introduction

Metallothioneins (MTs) make up a large family of evolutionarily conserved low molecular weight, thermostable proteins, found in practically all life forms: in vertebrates, invertebrates, fungi, and even in plants. Their sizes range from 25 (fungal) to 84 (plant) amino acids.[1] A single polypeptide chain of mammalian MT is composed of 61–68 mostly non-aromatic amino acids and contains 20 cysteinyl residues in highly conserved locations along the peptide chain. High number of cysteines in MTs explains their high capacity for binding metal ions through sulfhydryl groups, forming metal–thiolate complexes. Thus, their main proposed functions were derived from their role in the homeostatic control of a number of essential metals (copper – Cu, zinc – Zn), in detoxification of toxic ones (e.g., cadmium – Cd, mercury – Hg), and in protective actions against oxidative stress conditions.[2–4] This known fact forms the basis of MTs being used as possible biomarkers for metal exposure.[5]

Four isoforms of mammalian MT (MT-1, MT-2, MT-3, and MT-4) have been identified. Isoforms with minor differences, such as amino acid residue, have been detected as subgroups of the 2 major isoforms (MT-1 and MT-2) and are termed subisoforms. These 2 main groups of MT isoforms have been classified according to human MT elution order by anionic-exchange chromatography: MT-1 and MT-2.[6] They are the most widely distributed MT isoforms, expressed in many cell types in different tissues and organs. They can be induced by the administration of metals such as Cd, Zn and Cu; by oxidative stress; by glucocorticoids; and by cytokines.[7] MT-1 and MT-2 are present in nearly all tissues and have been isolated from organs such as the liver, kidney and brain. MT-3 is expressed mostly in nervous tissue[8] and MT-4 has been detected in epithelial cells.[9] Since various subisoforms are biosynthesized differentially, they could play a specific biological role, but this aspect is still being investigated. The interesting properties of MTs are closely related to their structure. In addition to slight differences in amino acid sequences, MTs exist as a mixture of varying metallic content.[5] It is not a simple task to detect and quantify MT, also due to its high cysteine content and relatively low molecular mass. The characteristics of human MTs are not widely described because rabbit MTs are more often used in studies as a model protein; thus, it is so valuable to compare MTs from these organisms. To analyze MTs, many methods can be used that differ in the analytical approach, usually based on the metal ions detection, free thiol moieties or enzyme-linked immunosorbent assay (ELISA). Human and rabbit MTs have previously been analyzed by western blot, ELISA, capillary electrophoresis (CE), and high-performance liquid chromatography.[10–15]

Therefore, the purpose of the research was the comprehensive characterization of human and rabbit MTs. Modern electrochemical and advanced analytical approaches such as the Brdicka reaction, chip CE and matrix-assisted laser desorption and ionization time-of-flight mass spectrometry (MALDI-TOF-MS) were used to characterize and compare human and rabbit MTs.

Material and methods

Material

All chemicals used were commercially available. Rabbit liver MT-2 (M-5392), 2-mercaptoethanol, ammonia solution, ammonium bicarbonate, trifluoroacetic acid (TFA), and formic acid were purchased from Sigma–Aldrich (St. Louis, USA). Acetonitrile (ACN) and methanol were purchased from Fluka (Seelze, Germany). Acidic MALDI matrices α-cyano-4-hydroxycinnamic acid (HCCA), 2,5-dihydroxobenzoic acid (DHB) and peptide calibration standard mixture were purchased from Bruker Daltonics (Bremen, Germany). All reagents were of the highest available purity. Doubly distilled deionized water was used throughout all the experiments.

Preparation of metallothioneins from human liver

Isoforms MT-1 and MT-2 were purified from human liver earlier at the Department of Biomedical and Environmental Analysis, Faculty of Pharmacy with Division of Laboratory Medicine, Wroclaw Medical University, Poland, and the presence of MTs was confirmed by sodium dodecyl sulfate–polyacrylamide gel electrophoresis (SDS-PAGE) and western blot.[10]

Chip capillary electrophoresis

Capillary electrophoresis experiments were performed on an automated microfluidic Experion electrophoresis system (Bio-Rad, Hercules, USA), according to the manufacturer's instructions and with supplied chemicals (Experion Pro260 analysis kit, Cat. No. 700-7101, Bio-Rad). Metallothioneins in a quantity of 4 µL (0.1 or 0.18 µg/µl) were mixed with 2 µL of reducing sample buffer (30 µL of a nonreducing sample buffer and 1 µL of β-mercaptoethanol); after 4 min of boiling, 84 µL of water were added. The ladder was also prepared in reducing conditions. After the priming of the chip with the gel and gel-staining solution in the diluted priming station sample, 6 µL of the mixture were loaded into the sample wells. The Pro260 Ladder included in the kit was used as a standard. For operation and standard data analysis, Experion software v. 3.10 (Bio-Rad) was used.

Mass spectrometry analysis

Mass spectrometry analysis was performed using matrix-assisted laser desorption and ionization time-of-flight mass spectrometry (MALDI-TOF-MS). Working standard

solutions were prepared daily by diluting the stock solutions. A mixture of peptide calibration standard (Bruker Daltonics) was used to calibrate the instrument. All measurements were performed on the UltrafleXtreme MALDI-TOF/TOF mass spectrometer (Bruker Daltonics) equipped with a laser operating at a wavelength of 355 nm with an accelerating voltage of 25 kV, cooled with liquid nitrogen, at a maximum energy of 36 μJ with a repetition rate of 2000 Hz in reflector-positive ionization mode, and with software for data acquisition and processing of mass spectra flexControl v. 3.4 and flexAnalysis v. 2.2. The spectra were measured in the range of 0–20,000 mass-to-change ratio (m/z). Laser power intensity was set to 5% above the threshold, which determines the minimal intensity for suitable spectrum; it is set experimentally by measuring spectra with increasing laser power intensity. A MALDI MTP 384 target plate (polished steel) was used.

Before MT analysis, a cut-off filter (Amicon 3K; Merck Millipore, Burlington, USA) for desalinization of the MT sample and buffer exchange to water was used. Then, the samples were mixed with DHB or HCCA matrix solution in 1:1 volume ratio and then 1 μL of the mixture was deposited on the target plate (dried-droplet method) and dried under atmospheric pressure and ambient temperature. Saturated solutions of DHB or HCCA were prepared in TA30 (30% ACN and 0.1% TFA). Mass spectra were typically acquired by averaging 20 subspectra from a total of 500 shots of the laser (Smartbeam 2 v. 1_0_38.5; Bruker Daltonics).

Differential pulse voltammetry

Differential pulse voltammetry (DPV) measurements were performed with a 747 VA Stand instrument connected to a 746 VA Trace Analyzer and a 695 Autosampler (Metrohm, Herisau, Switzerland) using a standard cell with 3 electrodes and a cooled sample holder (4°C). A hanging mercury drop electrode (HMDE) with a drop area of 0.4 mm^2 was used as the working electrode. An Ag/AgCl/3M KCl was the reference electrode and a glassy carbon electrode was the auxiliary electrode. The GPES v. 4.9 software supplied by EcoChemie (Utrecht, the Netherlands) was employed for smoothing and baseline correction of the raw data. The Brdicka supporting electrolyte containing 1 mM $Co(NH_3)_6Cl_3$ and 1 M ammonia buffer (NH_3(aq) + NH_4Cl, pH = 9.6) was used. The parameters of the measurement were as follows: initial potential of –0.7 V, end potential of –1.75 V, modulation time 0.057 s, time interval 0.2 s, step potential 2 mV, and modulation amplitude –250 mV. All experiments were carried out at 4°C employing a Julabo F12 thermostat (Julabo Labortechnik GmbH, Seelbach, Germany).

Results and discussion

Sequence differences in human and rabbit metallothioneins

Most studies concerning mammalian MTs usually associate MT-1 with MT-2. These 2 isoforms are examined as equal peptides, mostly because they are the closest paralogs that have been found and purified together.[16] They are commonly referred as MT-1/MT-2. However, the availability of transcriptomic and proteomic techniques highlights differences in MT-1 and MT-2 that cannot be ignored, suggesting some degree of functional differentiation between these isoforms both within the same species as well as between humans and rabbits.

Amino acid sequences of rabbit MT isoforms show differences when compared to the sequences of human MTs (Fig. 1). Human MTs are controlled by 17 genes located on chromosome 16, 10 of which are functional. To date, 10 subisoforms of human liver MT-1/2 have been reported (MT-1A, MT-1B, MT-1E, MT-1F, MT-1G, MT-1H, MT-1M, MT-1L, MT-1X, and MT-2A)[2]; their amino acid sequences are shown in Fig. 1A. Subisoform MT-1G contains 62 amino acids, whereas the others display a structure of 61 amino acids.

Rabbit MT genes are located on chromosome 5. Six subisoforms of rabbit liver MT-1/2 have been reported so far (MT-1A, MT-2A, MT-2B, MT-2C, MT-2D, and MT-2E)[17]; their amino acid sequences are presented in Fig. 1B. Subisoforms MT-2A and MT-2C contain 62 amino acids, whereas the others display a structure of 61 amino acids. The reasons for the high diversity of MT isoforms and their specific functional roles are still unclear. The potential biological significance of each isoform should not be neglected but the analytical techniques available cannot easily separate them.[18]

By ion-exchange chromatography, human MTs were separated into 2 charge-separable isoforms, designated as MT fractions 1 and 2.[17] However, MT fractions from rabbit liver obtained with the same ion-exchange chromatography cannot be separated into MT-1 and MT-2 subfractions. This conventional nomenclature division based on charge differences refers to the absence (MT-1) or presence (MT-2) of an aspartic acid residue at position 11 or 12 (10 or 11) of the sequence (Fig. 1) and it is not based on their global charge.[19]

Amino acid sequences of 6 rabbit MT isoforms show some differences compared to the sequences of human MTs (Fig. 1). Owing to the insertion of an additional amino acid at position 10, MT-2A and MT-2C sequences have a total chain length of 62 amino acids. MT-1G, having the same length and the same insertion, has also been identified in human liver. The presence of differential expression of MT-1G1 (with an additional alanine) and MT-1G2 (without additional alanine) suggests tissue- and cell-specific alternative splicing for the MT-1G isoform.[20] The insertion of the alanine residue at position 10 of the sequence relates to the location of the connection of exons 1 and 2 of the rabbit

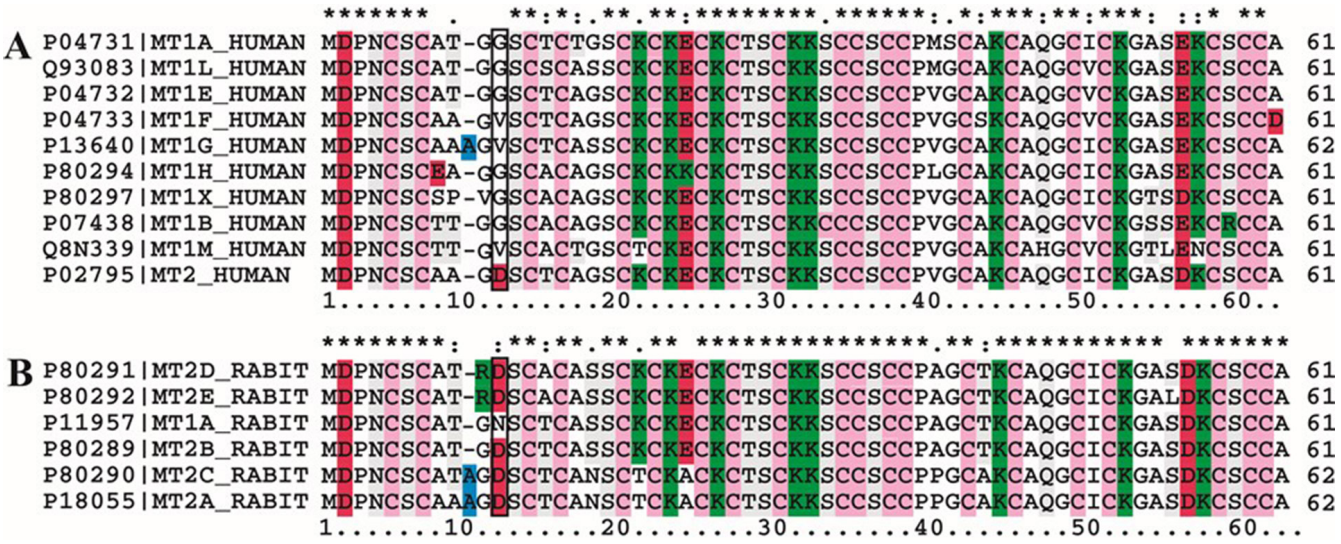

Fig. 1. Comparison of human and rabbit metallothionein (MT) isoforms 1 and 2 sequences (MT-1 and MT-2). Sequence comparison of MT-1/2 from human (MT-1A, MT-1B, MT-1E, MT-1F, MT-1G, MT-1H, MT-1M, MT-1L, and MT-1X, MT-2A) and from rabbit (MT-1A, MT-2A, MT-2B, MT-2C, MT-2D, and MT-2E) was performed using ClustulX program.[37] The sequences were derived from the database SWISS PROT (http://www.expasy.org/sprot/)

* indicates positions which have a single, fully conserved residue; : indicates conservation between groups of strongly similar properties – scoring > 0.5; indicates conservation between groups of weakly similar properties – scoring ≤0.5. The red color indicates negative amino acid residues; the color green indicates positive amino acid residues; the pink color indicates cysteine residues; the blue color marks alanine – an additional amino acid at position 10; substitution of an aspartic acid residue at position 11/12 is indicated by the frame.

MT-2A and 2C gene and human MT-1G gene. The presence of the additional alanine does not seem to influence neither the tertiary structure nor the metal-binding properties of the protein.[17,21] The biological consequence of that insertion remains undefined but its presence in more than 1 species suggests a common mechanism leading to the same phenotype.

In rabbit MT-2D and MT-2E, there is a substitution of arginine (R) residue in position 10/11 (Fig. 1B). The additional positive charge may be involved in compensating for the net negative charge of the 3-metal-cluster and thus can increase the stability of the β-cluster.[17]

Even minor changes in the sequence of MT may induce structural changes that can alter the metal-binding properties or stability of the 3-metal-cluster. The flexibility of the polypeptide chain as well as the charge environment of the coordinating sulfur atoms may greatly influence the feasibility and stability of the metal-thiolate bonds, and as a result, of the final metal–MT complex.

Aras et al. noticed a conserved PKC phosphorylation site at serine-32 (S32) of MT, which was important in modulating Zn^{2+}-regulated gene expression.[22] It is present in all rabbit and human MT isoforms shown in Fig. 1, except human MT-1B. The presence of cysteine in place of serine can change the tertiary structure of the protein as well as change the function of the protein dependent on phosphorylation.

Different expression patterns of MT subisoforms are observed in various types of human malignancies; this fact can be useful in the diagnosis and therapy of tumors.[3] The exact biological significance of the differences in amino acid sequences in human and rabbit MTs still remains unclear.

Detection of metallothioneins using capillary gel electrophoresis

Capillary electrophoresis is often used to analyze and separate MT isoforms from different organisms and tissues.[11,23] It can also be used for monitoring MT concentration in biological samples.[23] Křížková et al. were the first to propose a chip CE technique for the analysis of MT, i.e., of the effect of oxidation on the structure of MT and its ability to form aggregates and polymers.[24] Unfortunately, due to the presence of system peaks, an accurate analysis of the MT monomer is difficult.[12,25]

In this study, changes in the range of 5–8 kDa corresponding to the MT monomer were observed for both human and rabbit MTs. However, the monomers co-migrated with a system peak, which made it difficult to measure their correct size. In Fig. 2, the peak obtained for rabbit MT shifted to a bigger mass (8.2 kDa) in comparison to human MTs (6.0 and 7.7 kDa for human MT-1, and 5.3 and 6.1 kDa for human MT-2). An additional peak was observed at about 23–24 min, which may indicate the presence of 13.4 and 14.0 kDa oligomers. Peaks corresponding to MT dimers were observed both for human and rabbit MTs.

Mass spectrometry analysis

In the majority of MALDI-MS studies, DHB and HCCA were the constituents of the matrix used for the appropriate determination of MTs.[26] In our study, utilization of both matrixes resulted in different types of crystals. While HCCA produced uniform crystals, DHB produced

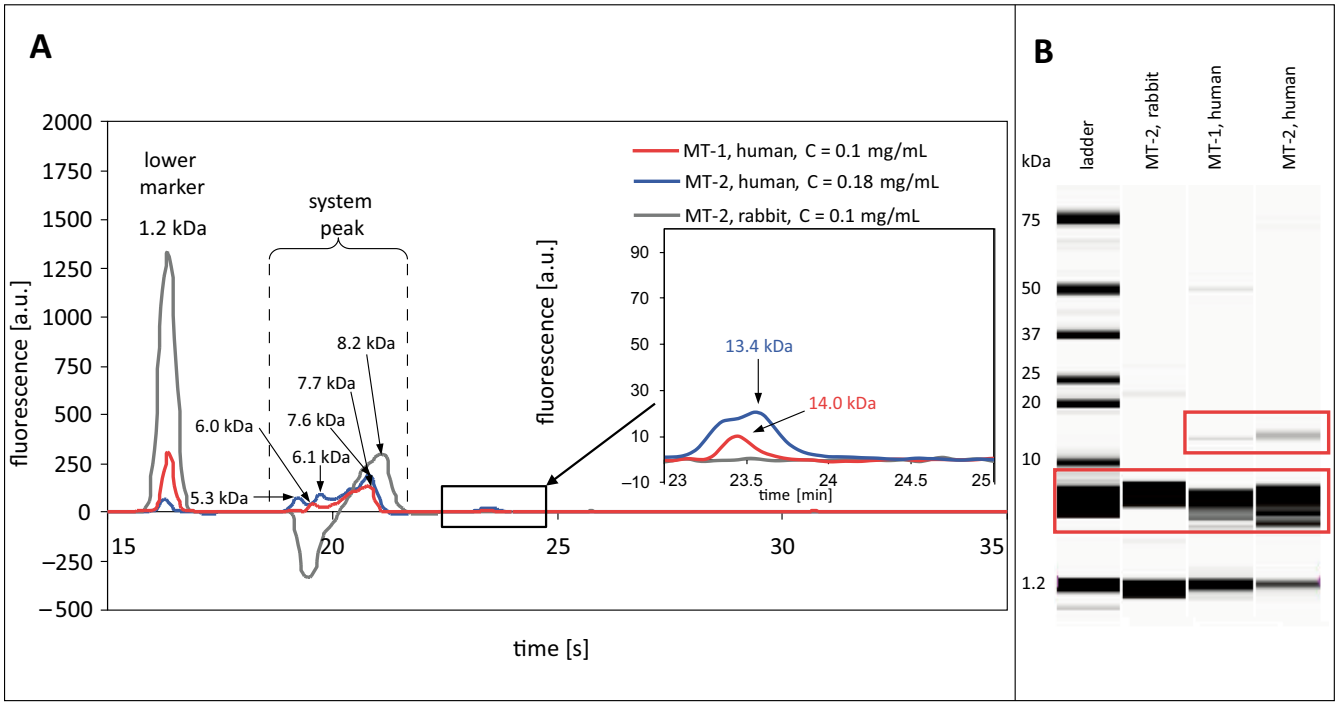

Fig. 2. Metallothionein (MT) separation using chip capillary gel electrophoresis (CE). Electropherograms of: A) in red, MT-1 from human liver; in blue, MT-2 from human liver; and in gray, MT-2 from rabbit liver are shown; B) chip CE virtual gel output of Pro260 ladder, MT-2 from rabbit liver, MT-1 and MT-2 from human liver

heterogeneous and robust crystals (Fig. 3A). Furthermore, DHB exhibited a significant rabbit MT-2 concentration-dependent increase in observed signal intensity (expressed in a.u.), higher when compared to that of HCCA (Fig. 3B). The main observed signal for rabbit MT-2 was 6211.07 m/z. Moreover, it was estimated that the isolated MT-2 was highly pure, because each spectrum showed only 1 peak of high intensity for the relevant protein. This peak showed a mass similar to rabbit MT-2D (6215.40 m/z).[27] The occurrence of the MT-2D form has been also observed in MT-2 from Sigma lots[27,28] and in MT-1 sample, as a remaining contaminant.[28] The size of 12342.11 Da corresponds to the MT-2 dimer (Fig. 3C inset).

The DHB was chosen as the most appropriate matrix in terms of sensitivity and reproducibility for human MTs; at given conditions (20 mg/mL of DHB in 30% ACN and 1% TFA), homogeneous spots applicable for automated MALDI-TOF-MS were formed. Further, to verify the proper isolation of MT-1 and MT-2 from humans, we analyzed their mass distribution. The main observed signals for human MTs (hMTs) shown in Fig. 4 were quasimolecular ions assigned as follows: $[hMT\text{-}1]^+$ (6145.23 m/z, 6176.46 m/z and 6220.12 m/z) (Fig. 4A), and $[hMT\text{-}2]^+$ (6066.24 m/z) (Fig. 4B). The sizes of 12523.89 Da and 12329.89 Da correspond to MT-1 and MT-2 dimers. The mass spectra of the human MT-1 sample yielded a main peak, the most intense at 6176.46 Da. Peaks observed in the spectra of these MT-1 samples can be attributed to potential subisoforms: MT-1A (6145.23 m/z), MT-1G (6176.46 m/z) and MT-1G+Cd (6240.12 m/z).[29,30] The theoretical mass of human MT-2A is 6042.16 m/z and our results showed main signals at 6066.24 m/z, corresponding to $[hMT\text{-}2A+Na]^+$.

The exposure of MTs to acidic pH values causes metal depletion and unfolding of the protein structure, generating apothioneins or metal-free forms. Using these matrixes caused the coordinated metals of the proteins to be removed, and the peaks obtained should be apothioneins, i.e., subisoforms without metal content.

Metallothionein dimers were first detected as transient intermediate species during interprotein metal exchange, and longer-lived dimers have been isolated that were stabilized by intermolecular disulfide bonds.[31] No transient intermediate dimers could be detected with mass spectrometry. However, a stable dimeric complex of MTs has been detected in this work by MALDI-TOF-MS and chip CE, and it appears to be stabilized by disulfide bridging. Metallothioneins can dimerize through the oxidation of their cysteinyl residues to form an interprotein Cys–Cys dithiol bridge; the experimental mass would decrease by 2 Da for every oxidative thiol bridge formation event.

Metallothionein analysis using the Brdicka reaction

Metallothionein exhibits significant electrochemical activity owing to its high content of sulfhydryl (SH) moieties. The method of determining proteins which contain –SH groups in an ammonia-buffered cobalt (III) solution was first described by Brdička.[32] Brdicka reaction is one of the most-often-used electrochemical methods for MT determination

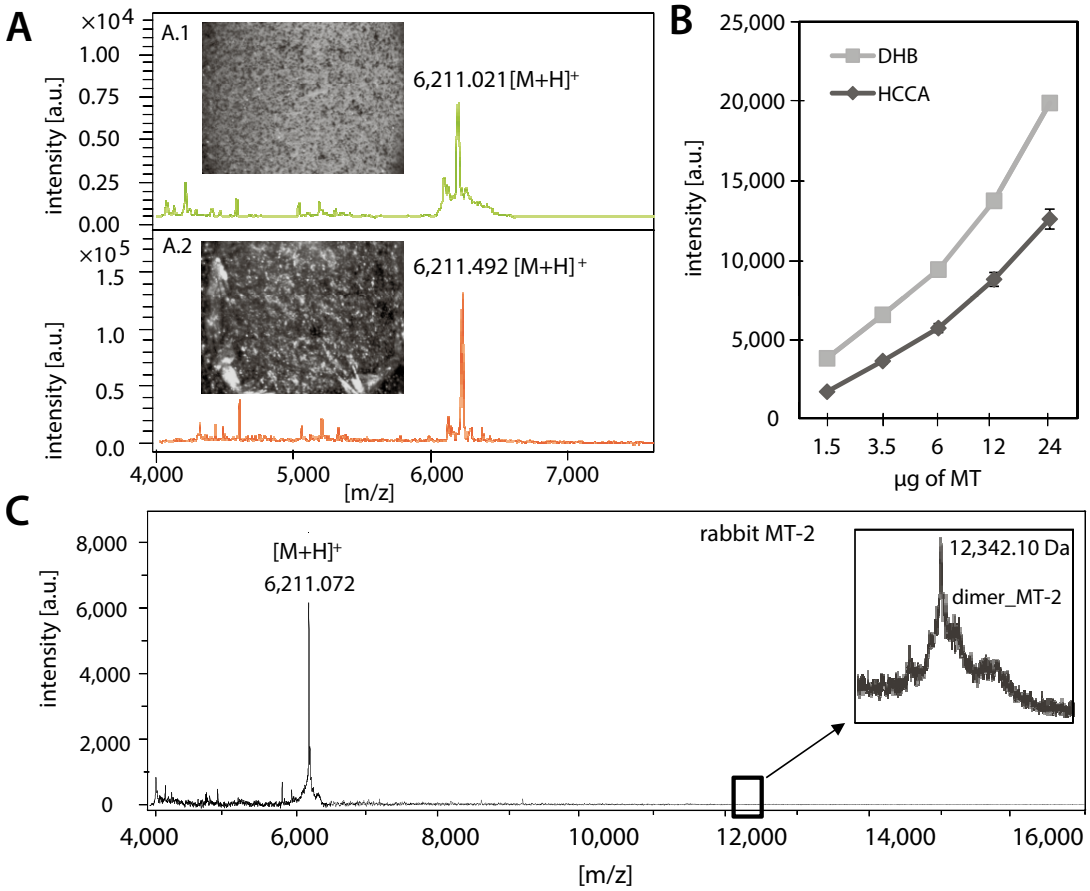

Fig. 3. Mass spectrum of rabbit metallothionein (MT). A) Spectrum of MT-2 from rabbit liver measured by matrix-assisted laser desorption and ionization time-of-flight mass spectrometry (MALDI-TOF-MS) with (A.1) α-cyano-4-hydroxycinnamic (HCCA) and (A.2) 2,5-dihydroxybenzoic acid (DHB) matrix. B) Graphs of signal intensity of different concentrations of rabbit MT-2 in DHB and HCCA matrices. 1–2 µL of sample/matrix mixture (1:1) deposited on MALDI plate and dried at room temperature (dried-droplet method). Analysis by a MALDI-TOF-MS mass spectrometer was performed in linear and reflector mode. Dimerization of MT analyzed by MALDI-TOF-MS is shown in the inset of Fig. C) Spectrum of rabbit MT-2 measured by MALDI-TOF-MS with the DHB matrix in linear positive mode in a mass range of 4–17 kDa prepared in TA30 with repetition rate of 2000 Hz

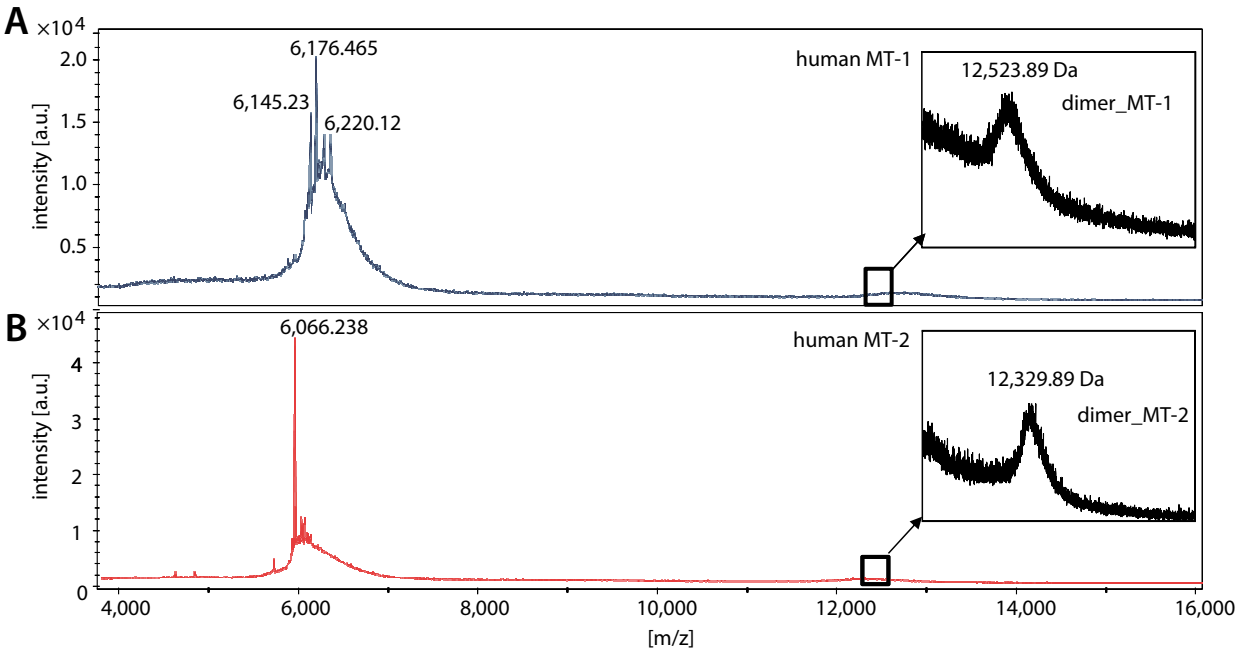

Fig. 4. Mass spectrum of human metallothionein (MT). Spectrum of MT-1 (A) and MT-2 (B) from human measured by matrix-assisted laser desorption and ionization time-of-flight mass spectrometry (MALDI-TOF-MS) with the 2,5-dihydroxybenzoic acid (DHB) matrix in linear positive mode in a mass range of 4–16 kDa prepared in TA30 with repetition rate of 2000 Hz

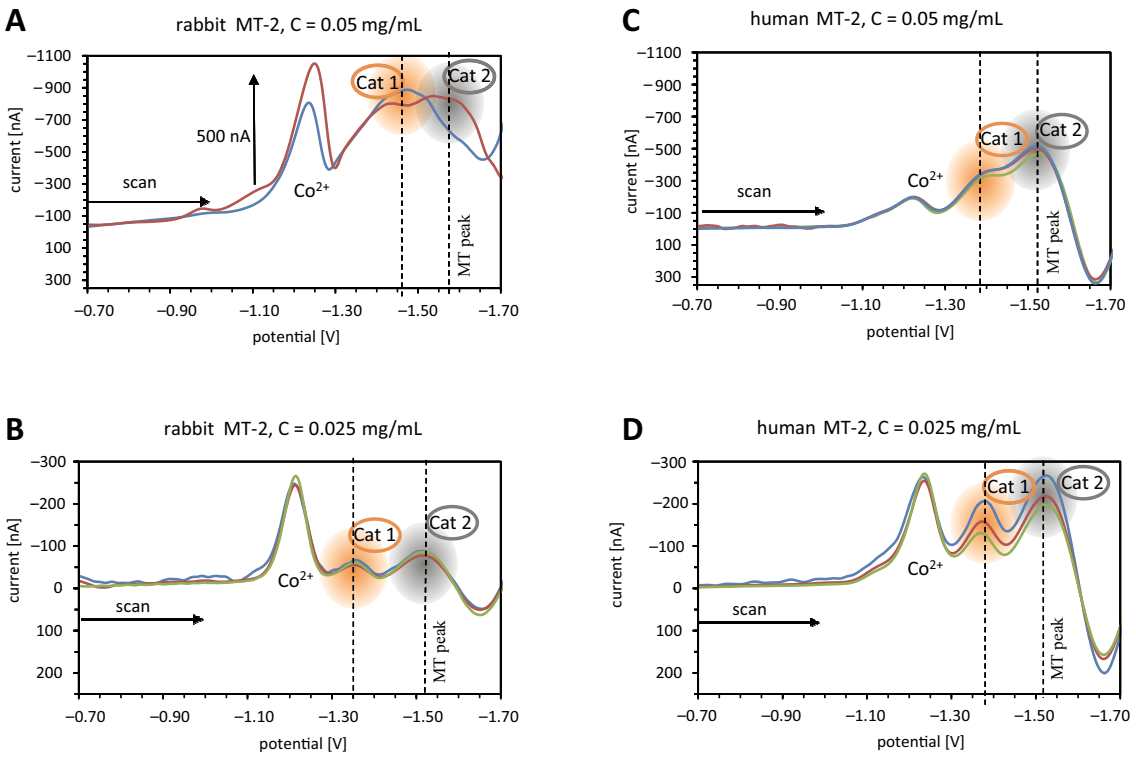

Fig. 5. Metallothioneins (MTs) from rabbit and human liver analysis using the Brdicka reaction. Different concentrations of MT were used: 0.025 mg/mL and 0.05 mg/mL.

in biological samples.[33] It is based on the reduction of hydrogen at the mercury electrode catalyzed by the –SH groups in the ammonia-buffered cobalt(III) solution.[34]

The Brdicka reaction has potential for monitoring the differences of various MT isoforms, both rabbit and human.[26] During MT analysis, changes in Cat2 signal (–1.55 V, which represents the current response of the MT complex with components of the Brdicka electrolyte), Co^{2+} (–1.25 V) and Cat1 (–1.40 V) corresponding to hydrogen evolution from the supporting electrolyte catalyzed by the MT were observed.[35] The presence of the Cat2 peak is closely connected with the quantification of –SH groups occurring in the Brdicka solution,[36] thus corresponding to the MT level. The voltammograms of human and rabbit MT are shown in Fig. 5. It can be observed that the character of the mentioned MT signals changes with different MT concentration both for rabbit and human MT (Fig. 5). Concentrations of MT 0.025 and 0.05 mg/mL were analyzed.

With a lower concentration of rabbit MT, the Co^{2+} signal decreases and shifts to a less negative potential, whereas it slightly increases with a decreasing concentration of human MT (Fig. 5). Cat1 and Cat2 signals are more exposed in a lower concentration of MTs. With a lower rabbit MT concentration, Cat1 and Cat2 signals decreased and shifted to a more positive potential. These signals in the lower concentration of human MT had a negligible potential shift. The character of the mentioned MT signals changed with MTs concentrations. A lower concentration of MTs from both organisms coincided with a decrease in the Cat2 signal. Lower, but more distinct signals were observed for human and rabbit MTs when a lower concentration was used (0.025 mg/mL). The same concentration of human MT gave higher Cat2 peak than rabbit MT. Metallothioneins isolated in both organisms behave differentially despite the same number of –SH groups.

Conclusions

The structure of MTs is constantly being studied due to their dynamic nature, lack of secondary structural features when metals are not present, and the absence of spectroscopically active aromatic residues. Thus, different methods have been used for the analysis of human MT-1 and MT-2 isoforms and rabbit MT-2 isoforms.

Both in rabbit and human MTs, mainly monomers were detected with chip CE and MALDI-TOF-MS. Additionally, distinctly lower signals from the dimers were observed. When MALDI-TOF-MS is employed, the main observed signal for rabbit MT-2 corresponds to the mass of MT-2D. In human, MT-1A, MT-1G, MT-1G+Cd and MT-2A were detected. Metallothionein subisoforms, except in the case of human MT-1G+Cd, have been identified without metals, which can be due to the use of acidic matrixes that cause a release of less bound metals.

In the Brdicka reaction, signals are different for MTs isolated from rabbit and human liver, meaning that they behave differentially in electrochemistry despite the same

number of –SH groups. This may be due to different availability of MT cysteinyl groups in different organisms.

These methods used together allow for the identification and characterization of MT and give complementary information about MT forms. Furthermore, MALDI-TOF-MS is capable of directly resolving more than just the main MT isoforms in the sample, which makes it the best of these techniques to identify isoforms of MT.

References

1. Osobová M, Urban V, Jedelský PL, et al. Three metallothionein isoforms and sequestration of intracellular silver in the hyperaccumulator *Amanita strobiliformis*. *New Phytol*. 2011;190(4):916–926.
2. Zalewska M, Trefon J, Milnerowicz H. The role of metallothionein interactions with other proteins. *Proteomics*. 2014;14(11):1343–1356.
3. Křížková S, Kepinska M, Emri G, et al. An insight into the complex roles of metallothioneins in malignant diseases with emphasis on (sub)isoforms/isoforms and epigenetics phenomena. *Pharmacol Ther*. 2017; 183:90–117.
4. Torreggiani A, Chatgilialoglu C, Ferreri C, Melchiorre M, Atrian S, Capdevila M. Non-enzymatic modifications in metallothioneins connected to lipid membrane damages: Structural and biomimetic studies under reductive radical stress. *J Proteomics*. 2013;92:204–215.
5. Macirella R, Brunelli E. Morphofunctional alterations in zebrafish (*Danio rerio*) gills after exposure to mercury chloride. *Int J Mol Sci*. 2017;18(4):824.
6. Sanz-Nebot V, Andón B, Barbosa J. Characterization of metallothionein isoforms from rabbit liver by liquid chromatography coupled to electrospray mass spectrometry. *J Chromatogr B Analyt Technol Biomed Life Sci*. 2003;796(2):379–393.
7. Ruttkay-Nedecky B, Nejdl L, Gumulec J, et al. The role of metallothionein in oxidative stress. *Int J Mol Sci*. 2013;14(3):6044–6066.
8. Artells E, Palacios O, Capdevila M, Atrian S. In vivo-folded metal-metallothionein 3 complexes reveal the Cu-thionein rather than Zn-thionein character of this brain-specific mammalian metallothionein. *FEBS J*. 2014;281(6):1659–1678.
9. Thirumoorthy N, Shyam Sunder A, Manisenthil Kumar K, Senthil Kumar M, Ganesh G, Chatterjee M. A review of metallothionein isoforms and their role in pathophysiology. *World J Surg Oncol*. 2011;9:54.
10. Milnerowicz H, Bizoń A. Determination of metallothionein in biological fluids using enzyme-linked immunoassay with commercial antibody. *Acta Biochim Pol*. 2010;57(1):99–104.
11. Zalewska M, Bizoń A, Milnerowicz H. Comparison of capillary electrophoretic techniques for analysis and characterization of metallothioneins. *J Sep Sci*. 2011;34(21):3061–3069.
12. Guszpit E, Křížková S, Kepinska M, et al. Fluorescence-tagged metallothionein with CdTe quantum dots analyzed by the chip-CE technique. *J Nanopart Res*. 2015;17(11):423.
13. Guszpit E, Krejčová L, Křížková S, et al. Kinetic analysis of human metallothionein and CdTe quantum dot complexes using fluorescence and voltammetry techniques. *Colloids Surf B Biointerfaces*. 2017; 160:381–389.
14. Dabrio M, Virtanen V, Bordin G, Rodriguez AR. Contribution to the study of complexing properties of Zn-metallothioneins by CZE-DAD. *Talanta*. 2000;53(3):587–598.
15. Mounicou S, Ouerdane L, L'Azou B, et al. Identification of metallothionein subisoforms in HPLC using accurate mass and online sequencing by electrospray hybrid linear ion trap-orbital ion trap mass spectrometry. *Anal Chem*. 2010;82(16):6947–6957.
16. Artells E, Palacios Ò, Capdevila M, Atrian S. Mammalian MT1 and MT2 metallothioneins differ in their metal binding abilities. *Metallomics*. 2013;5(10):1397–1410.
17. Hunziker PE, Kaur P, Wan M, Känzig A. Primary structures of seven metallothioneins from rabbit tissue. *Biochem J*. 1995;306(Pt 1): 265–270.
18. Beattie JH. Strategies for the qualitative and quantitative analysis of metallothionein isoforms by capillary electrophoresis. *Talanta*. 1998;46(2):255–270.
19. Kojima Y, Hunziker PE. Amino acid analysis of metallothionein. *Methods Enzymol*. 1991;205:419–421.
20. Mehus AA, Muhonen WW, Garrett SH, Somji S, Sens DA, Shabb JB. Quantitation of human metallothionein isoforms: A family of small, highly conserved, cysteine-rich proteins. *Mol Cell Proteomics*. 2014; 13(4):1020–1033.
21. Braun W, Vasák M, Robbins AH, et al. Comparison of the NMR solution structure and the x-ray crystal structure of rat metallothionein-2. *Proc Natl Acad Sci U S A*. 1992;89(21):10124–10128.
22. Aras MA, Hara H, Hartnett KA, Kandler K, Aizenman E. Protein kinase C regulation of neuronal zinc signaling mediates survival during preconditioning. *J Neurochem*. 2009;110(1):106–117.
23. Ryvolova M, Hynek D, Skutkova H, Adam V, Provaznik I, Kizek R. Structural changes in metallothionein isoforms revealed by capillary electrophoresis and Brdicka reaction. *Electrophoresis*. 2012;33(2):270–279.
24. Křížková S, Adam V, Kizek R. Study of metallothionein oxidation by using of chip CE. *Electrophoresis*. 2009;30(23):4029–4033.
25. Křížková S, Masařík M, Eckschlager T, Adam V, Kizek R. Effects of redox conditions and zinc(II) ions on metallothionein aggregation revealed by chip capillary electrophoresis. *J Chromatogr A*. 2010;1217(51): 7966–7971.
26. Merlos Rodrigo MA, Molina-López J, Jimenez Jimenez AM, et al. The application of curve fitting on the voltammograms of various isoforms of metallothioneins-metal complexes. *Int J Mol Sci*. 2017; 18(3):610.
27. van Vyncht G, Bordin G, Rodriguez AR. Rabbit liver metallothionein subisoform characterization using liquid chromatography hyphenated to diode array detection and electrospray ionization mass spectrometry. *Chromatographia*. 2000;52(11–12):745–752.
28. Chassaigne H, Lobinski R. Polymorphism and identification of metallothionein isoforms by reversed-phase HPLC with on-line ion-spray mass spectrometric detection. *Anal Chem*. 1998;70(13):2536–2543.
29. Tomalová I, Foltynová P, Kanický V, Preisler J. MALDI MS and ICP MS detection of a single CE separation record: A tool for metalloproteomics. *Anal Chem*. 2014;86(1):647–654.
30. Irvine GW, Pinter TBJ, Stillman MJ. Defining the metal binding pathways of human metallothionein 1a: Balancing zinc availability and cadmium seclusion. *Metallomics*. 2016;8(1):71–81.
31. Irvine GW, Heinlein L, Renaud JB, Sumarah MW, Stillman MJ. Formation of oxidative and non-oxidative dimers in metallothioneins: Implications for charge-state analysis for structural determination. *Rapid Commun Mass Spectrom*. 2017;31(24):2118–2124.
32. Brdička R. Polarographic studies with the dropping mercury electrode. Part IV. The influence of circuit resistance on maxima of current-voltage curves. *Collect Czechoslov Chem Commun*. 1936;8: 419–433.
33. Raspor B, Paić M, Erk M. Analysis of metallothioneins by the modified Brdicka procedure. *Talanta*. 2001;55(1):109–115.
34. Křížková S, Blahova P, Nakielna J, et al. Comparison of metallothionein detection by using Brdicka reaction and enzyme-linked immunosorbent assay employing chicken yolk antibodies. *Electroanalysis*. 2009;21(23):2575–2583.
35. Kruseova J, Hynek D, Adam V, et al. Serum metallothioneins in childhood tumors: A potential prognostic marker. *Int J Mol Sci*. 2013;14(6): 12170–12185.
36. Adam V, Chudobova D, Tmejova K, et al. An effect of cadmium and lead ions on *Escherichia coli* with the cloned gene for metallothionein (MT-3) revealed by electrochemistry. *Electrochimica Acta*. 2014;140: 11–19.
37. Thompson JD, Gibson TJ, Plewniak F, Jeanmougin F, Higgins DG. The CLUSTAL_X windows interface: Flexible strategies for multiple sequence alignment aided by quality analysis tools. *Nucleic Acids Res*. 1997;25(24):4876–4882.

Advances
in Clinical and Experimental
Medicine